CANADIAN THESES

THÈSES CANADIENNES

NOTICE

The quality of this microfiche is heavily dependent upon the quality of the original thesis submitted for microfilming. Every effort has been made to ensure the highest quality of reproduction possible.

If pages are missing, contact the university which granted the degree.

Some pages may have indistinct print especially if the original pages were typed with a poor typewriter ribbon or if the university sent us an inferior photocopy.

Previously copyrighted materials (journal articles, published tests, etc.) are not filmed.

Reproduction in full or in part of this film is governed by the Canadian Copyright Act, R.S.C. 1970, c. C-30.

AVIS

La qualité de cette microfiche dépend grandement de la qualité de la thèse soumise au microfilmage. Nous avons tout fait pour assurer une qualité supérieure de reproduction.

S'il manque des pages, veuillez communiquer avec l'université qui a conféré le grade.

La qualité d'impression de certaines pages peut laisser à désirer, surtout si les pages originales ont été dactylographiées à l'aide d'un ruban usé ou si l'université nous a fait parvenir une photocopie de qualité inférieure.

Les documents qui font déjà l'objet d'un droit d'auteur (articles de revue, examens publiés, etc.) ne sont pas microfilmés.

La reproduction, même partielle, de ce microfilm est soumise à la Loi canadienne sur le droit d'auteur, SRC 1970, c. C-30.

THIS DISSERTATION HAS BEEN MICROFILMED EXACTLY AS RECEIVED

LA THÈSE A ÉTÉ MICROFILMÉE TELLE QUE NOUS L'AVONS REÇUE

PHOSPHITE DERIVATIVES OF RUTHENIUM AND OSMIUM

by

Randy Frank Alex

B.Sc. First Class Hons., Simon Fraser University, 1982

THESIS SUBMITTED IN PARTIAL FULFILLMENT OF

THE REQUIREMENTS FOR THE DEGREE OF

DOCTOR OF PHILOSOPHY

in the Department

of

Chemistry

SIMON FRASER UNIVERSITY

January 1987

ISBN 0-315-36309-6

APPROVAL

Name: Randy Frank Alex

Degree: Doctor of Philosophy

Title of thesis: Phosphite Derivatives of Ruthenium and Osmium

Examining Committee:

Chairman: Dr. F.W.B. Einstein

Dr. ~~Roland~~ K. Pomeroy
~~Associate~~ Professor
Senior Supervisor

Dr. Derek Sutton
Professor

Dr. E.J. ~~Wells~~
Associate Professor

Dr. Josef Takats
Associate Professor
University of Alberta
External Examiner

Dr. Ross H. Hill
Assistant Professor
Internal Examiner

Date Approved: March 17, 1987

PARTIAL COPYRIGHT LICENSE

I hereby grant to Simon Fraser University the right to lend my thesis, project or extended essay (the title of which is shown below) to users of the Simon Fraser University Library, and to make partial or single copies only for such users or in response to a request from the library of any other university, or other educational institution, on its own behalf or for one of its users. I further agree that permission for multiple copying of this work for scholarly purposes may be granted by me or the Dean of Graduate Studies. It is understood that copying or publication of this work for financial gain shall not be allowed without my written permission.

Title of Thesis/Project/Extended Essay

PHOSPHITE DERIVATIVES OF RUBBER AND LIGNIN

Author: _____
(signature)

RANDY ALLEX
(name)

March 1/87
(date)

ABSTRACT

Phosphite Derivatives of Ruthenium and Osmium.

Several aspects of the chemistry of $Ru[P(OCH_3)_3]_5$ and related derivatives were investigated. The major technique used in this study was $^{31}P\{^1H\}$ NMR spectroscopy. Several complexes of the type $Ru[P(OR)_3]_3(\eta^4\text{-diene})$ (diene= C_4H_6, C_5H_8; R= CH_3, C_2H_5, $CH(CH_3)_2$) were prepared by the ultraviolet irradiation of $Ru[P(OCH_3)_3]_5$ or $Ru[P(OR)_3]_3(CO)_2$ and excess diene. These previously unknown complexes were found to undergo intramolecular phosphite exchange in solution (by $^{31}P\{^1H\}$ NMR spectroscopy). Reaction of $Ru[P(OCH_3)_3]_4(\eta^2\text{-}C_2H_4)$ with various two electron donor ligands gave the new complexes $Ru[P(OCH_3)_3]_4L$ (L= $P(OC_2H_5)_3$, $P(OCH(CH_3)_2)_3$, $P(OCH_2)_3CCH_3$, $P(OC_6H_5)_3$, PF_3, $P(CH_3)_3$, $P(CH_3)_2C_6H_5$, $PCH_3(C_6H_5)_2$, $P(C_2H_4CN)_3$, $Sb(CH_3)_3$). These derivatives all underwent rapid axial-equatorial phosphite exchange in solution. Both axial and equatorial forms of $Ru[P(OCH_3)_3]_4L$ (with trigonal bipyramidal structures) were observed at low temperatures, depending on L. Arguments based on steric and electronic considerations are used to rationalize the static solution structures for these compounds. Mechanistic studies suggested different fluxional mechanisms were operating for the axial and equatorial isomers. The X-ray structure of $Ru[P(OCH_3)_3]_4P(OCH_2)_3CCH_3$ is also discussed.

The cations $\{XRu[P(OCH_3)_3]_5\}^+$ (X= Cl, Br, I, H, CH_3) were prepared by reaction of $Ru[P(OCH_3)_3]_5$ with Cl_2, Br_2, I_2, NH_4^+,

and CH_3I, respectively. These cations, isolated as the PF_6 salts, all exhibited $^{31}P\{^1H\}$ NMR spectra due to an AB_4 spin system and were rigid in solution. The synthesis and characterization of $\{HRu[P(OCH_3)_3]_4P(OCH_2)_3CCH_3\}PF_6$ is also discussed. Also presented are the unsuccessful attempts to prepare the analogues of $Ru[P(OCH_3)_3]_5$ with $P(OR)_3$ (R= C_2H_5, $CH(CH_3)_2$, n-C_4H_9, $P(OCH_2)_3CCH_3$) and $Os[P(OCH_3)_3]_5$.

The clusters $Os_3[P(OCH_3)_3]_x(CO)_{12-x}$ (x= 1-6) were prepared from $Os_3(CO)_{12}$ and excess $P(OCH_3)_3$ by thermal and photolytic methods. The clusters with x= 5,6 are the most highly phosphite substituted derivatives of $Os_3(CO)_{12}$ yet synthesized. Isomers were observed for $Os_3[P(OCH_3)_3]_2(CO)_{10}$ and $Os_3[P(OCH_3)_3]_4(CO)_8$. Variable temperature ^{13}C and $^{31}P\{^1H\}$ NMR spectroscopy revealed that for x= 1-5, the complexes were stereochemically nonrigid in solution. The spectra were interpreted in terms of two types of mechanisms occurring within the clusters: axial-equatorial CO exchanges via intermediates with two carbonyl bridges, and trigonal twists at individual osmium atoms. The X-ray structure of $Os_3[P(OCH_3)_3]_6(CO)_6$ is also discussed.

DEDICATION

To Karen

ACKNOWLEDGEMENTS

The work contained in this thesis was performed in the laboratory of Dr. R. K. Pomeroy.

I would like to express my gratitude to Dr. Derek Sutton, Dr. Ted Wells, Dr. Colin Jones, and Dr. Fred Einstein; their support and encouragement were greatly appreciated.

I sincerely thank Dr. Richard Jones and Dr. Fred Einstein for the crystal structure determinations in this thesis and Dr. Al Tracey for helpful discussions about NMR spectroscopy.

The skilled technical assistance of Mr. Miki Yang, Mr. Greg Owen, Mrs. Marcie Tracey, and Mr. Paul Saunders is gratefully acknowledged.

TABLE OF CONTENTS

LIST OF TABLES

LIST OF FIGURES

CHAPTER 1

INTRODUCTION

1.1 Research Proposal

The use of phosphorus donor ligands in organometallic chemistry has attracted wide interest over the past several decades. The incorporation of phosphines (i.e. PR_3; R= alkyl and aryl) and phosphites (i.e. $P(OR)_3$; R= alkyl and aryl) into transition metal carbonyls, for example, has been found to alter the electronic and steric properties of these complexes considerably. Transition metal complexes containing trivalent phosphorus ligands have been utilized extensively as homogeneous catalytic reagents in transformations such as hydroformylation, hydrogenation, and others [1,2,3].

Transition metal species containing only one type of ligand (homoleptic) comprise a relatively rare class of complexes. The archetypical example, of course, is the metal carbonyls. There has recently been considerable interest in homoleptic transition metal-phosphite complexes (see chapter 2 introduction). Many of these contain a central metal in a formal oxidation state of zero and have stoichiometries analogous to the corresponding binary carbonyl complexes. The difference in electronic and steric properties of the carbonyl and $P(OR)_3$ ligands, however, might be expected to confer different chemical properties on the two types of complexes. For example, the better σ-donor and

poorer π-acceptor properties of the phosphite ligand relative to CO should give the metal centre of a binary phosphite complex a relatively high accumulation of electron density. Considering the vast and varied chemistry associated with binary metal carbonyls, the potential breadth of chemistry for the analogous metal-phosphite complexes is large.

Our interest in phosphite complexes of the transition metals had its beginnings in 1979. It was found that the ultraviolet irradiation of $Ru_3(CO)_{12}$ and excess $P(OCH_3)_3$ in hexane for several days led to the isolation of $Ru[P(OCH_3)_3]_5$ in good yield [4,5]. Pentakis(trimethyl phosphite)ruthenium(0) had been previously prepared by a more tedious route [6]. It was felt that this homoleptic metal(0)-phosphite complex merited further study. Although a number of complexes of this type had been prepared (see introduction to chapter 2), little study of their chemistry had been undertaken. It was predicted that the electron rich metal centre of $Ru[P(OCH_3)_3]_5$ would lead to facile oxidative-addition reactions. In addition, it was thought that the steric pressure of five relatively large $P(OCH_3)_3$ ligands (see later discussion on steric effects for phosphites) would allow the straightforward preparation of substituted derivatives, e.g. $Ru[P(OCH_3)_3]_4L$ and $Ru[P(OCH_3)_3]_3L_2$ (L= 2 electron donor ligand). Stereochemical nonrigidity is a ubiquitous feature of pentacoordinate, transition metal complexes [7]. It was expected that derivatives of $Ru[P(OCH_3)_3]_5$ would exhibit such behaviour; $^{31}P\{^1H\}$ NMR spectroscopy

represented the ideal technique to examine such processes. As mentioned previously, transition metal complexes with phosphorus donor ligands have found extensive use in homogeneous catalysis. The potential use of highly phosphite-substituted complexes in this area provided an added incentive to the proposed study.

In addition, it was felt that the generality of the preliminary results concerning the preparation of $Ru[P(OCH_3)_3]_5$ from $Ru_3(CO)_{12}$ and $P(OCH_3)_3$ by photolytic activation needed examination. It appeared reasonable that the iron and osmium congeners of $Ru[P(OCH_3)_3]_5$ could be prepared by a similar route and that phosphite ligands other than $P(OCH_3)_3$ would also yield penta(phosphite)-metal complexes.

The research proposal may be summarized as follows. The reactivity of pentakis(trimethyl phosphite)ruthenium(0) as a nucleophilic reagent and the substitutional lability of the complex were examined. Substituted derivatives of $Ru[P(OCH_3)_3]_5$ were studied by variable temperature $^{31}P\{^1H\}$ NMR spectroscopy to determine the factors influencing site preference of the ligands and the barriers to nonrigidity. The generality of the preparation of $Ru[P(OCH_3)_3]_5$ was also studied, with repect to both the central metal and identity of the phosphite ligand.

As will be seen later, the results were not always as expected. In particular, attempts to prepare $Os[P(OCH_3)_3]_5$ were unsuccessful. Instead, phosphite-substituted derivatives of $Os_3(CO)_{12}$ were isolated. The study of the stereochemical

nonrigidity exhibited by these trinuclear complexes (mainly by variable temperature ^{13}C and $^{31}P\{^{1}H\}$ NMR techniques) allowed considerable insight into the exchange processes operating.

1.2 Steric and Electronic Effects in Metal-Phosphite Complexes

There are two components to the metal-phosphorus bond in a metal-phosphorus donor ligand complex. Both are qualitatively similar to the bonding in metal carbonyl compounds but differ quantitatively. Donation of the phosphorus lone pair to a metal σ-type orbital forms a P-M σ-bond. Synergic back-bonding, where a filled metal d-orbital (or a metal nd-(n+1)p hybrid orbital) overlaps with an empty phosphorus π-type orbital, forms a M-P π-bond. The nature of the phosphorus orbital used in this π bonding has been the topic of recent discussion. Previous contemporary thought supported the notion that the empty 3d orbitals of the phosphorus donor ligand were involved [8]. Recent work, however, has implicated the σ^* orbitals of the phosphorus donor ligand (e.g. the antibonding orbitals of the phosphorus-carbon bonds in $P(CH_3)_3$) as the major contributor to M-P π-bonding [9].

In general, phosphite ligands are considered better σ-donors and poorer π-acceptors than the carbonyl group. In turn, phosphine ligands are typically considered better σ-donors and poorer π-acceptors than the phosphites. The special case of PF_3 is worthy of mention. Electronegative substituents are thought

to substantially reduce the σ-donor character of the phosphorus donor ligand; at the same time the P π-acceptor orbitals are contracted, leading to better π overlap [8]. Carbon monoxide and PF_3 are thus thought to be comparable in their electronic properties.

An attempt to rank the overall electron donor-acceptor properties of triply connected phosphorus ligands (i.e. σ and π effects) has been undertaken [10,11]. The method consisted of measuring the A_1 carbonyl stretching frequency of $Ni(CO)_3L$ in CH_2Cl_2, for a wide variety of trivalent phosphorus ligands L. These values (in cm^{-1}) were used to order the ligands in terms of their total electronic effect. Ligands with good σ-donor properties caused increased electron donation from the Ni into the π^* orbitals of the CO ligands, reducing the ν(CO) value. Poor π-acceptor ligands forced more metal electron density into the carbon monoxide π^* orbitals, also resulting in a lower A_1 frequency. No attempt was made to partition this total electronic effect into component σ and π contributions.

Recent work has shown that some of these conclusions regarding the electronic parameters of P donor ligands are too simplistic. A more detailed analysis of the donor-acceptor properties of the substituents on the P atom (using 157 different phosphorus ligands) indicated several factors were involved [12].

At least as important as electronic effects in metal-phosphorus donor ligand complexes are steric effects. Molecular structures, rate and equilibrium constants, NMR chemical shifts, and even relative infrared intensities have been correlated with ligand cone angles [11a]. The cone angle, θ, has become the accepted measure of the steric effect of a particular trivalent phosphorus ligand. This steric parameter (for symmetric ligands) has been defined as the solid angle of a cylindrical cone, centred 2.28 angstroms (2.57 cm when scaled) from the centre of the P atom of a space-filling model, which just touches the van der Waals radii of the outermost atoms of the model [11]. Special techniques were used to define θ for unsymmetrical ligands $PX_1X_2X_3$ and those with internal degrees of freedom (e.g. rotation about P-C bonds). Ligands with large cone angles have been shown to cause extensive dissociation from metal-phosphine and -phosphite complexes [11a] and might be expected to affect barriers to nonrigidity in fluxional molecules.

1.3 Previous Results Included in this Thesis

Some of the results included in this thesis were obtained before the formal commencement of the author's Ph.D. program (January, 1982). These results formed part of an undergraduate research project undertaken by the author, under the supervision of Dr. R. K. Pomeroy. Most of these are previously unpublished results. They are included in this thesis for a variety of

reasons. The synthesis and properties of $Ru[P(OCH_3)_3]_5$ are included for obvious reasons: this is the major starting material for many of the new derivatives reported here. The results concerning $Ru[P(OCH_3)_3]_5$ have been previously published [4,5]. The rationale for reporting the synthesis and properties of $Ru[P(OCH_3)_3]_4(\eta^2\text{-}C_2H_4)$ is also clear: this is the precursor for all the $Ru[P(OCH_3)_3]_4L$ derivatives presented in this thesis (see chapter 2). Subsequent work on the ethylene complex was performed after January, 1982. This included further mass spectral analysis and the measurement of the ^1H NMR spectrum, in addition to several reaction studies monitored by $^{31}P\{^1H\}$ NMR spectroscopy (see chapter 2). Previous results concerning $Ru[P(OCH_3)_3]_3(\eta^4\text{-}C_4H_6)$ are also included in this thesis. This was done to help assess the electronic and steric effects on the fluxional barriers for the two series of complexes $Ru[P(OR)_3]_3(\eta^4\text{-}C_4H_6)$ (R= Me, Et, *i*-Pr) and $Ru[P(OR)_3]_3(\eta^4\text{-}C_5H_8)$ (R= Me, Et) (see chapter 2). The complexes $\{XRu[P(OCH_3)_3]_5\}PF_6$ (X= Cl, Br, I, H, CH_3) also formed part of the previously mentioned undergraduate project and are presented in this thesis. Subsequent studies on these complexes carried out during this thesis include fast atom bombardment mass spectrometry and more detailed $^{31}P\{^1H\}$ NMR computer simulations. The results for the methyl complex $\{CH_3Ru[P(OCH_3)_3]_5\}I$ have been published [4,5]. These cationic Ru species are included in this thesis to place the research reported in chapter 3 in the proper context. The ease with which these cations were formed from $Ru[P(OCH_3)_3]_5$ suggested that a number of related derivatives might be

prepared; a number of reactions (mostly unsuccessful) were attempted based on this assumption (see chapter 3).

1.4 Thesis Contents

Chapter 2 of this thesis presents the preparation of $Ru[P(OCH_3)_3]_5$ and the substitutionally labile $Ru[P(OCH_3)_3]_4(\eta^2\text{-}C_2H_4)$. The diene complexes $Ru[P(OR)_3]_3(\eta^4\text{-}C_4H_6)$ (R= Me, Et, *i*-Pr) and $Ru[P(OR)_3]_3(\eta^4\text{-}C_5H_8)$ (R= Me, Et), prepared from either $Ru[P(OCH_3)_3]_5$ or $Ru[P(OR)_3]_3(CO)_2$ (R= Et, *i*-Pr), are reported. The stereochemical nonrigidity of these diene complexes in solution is also discussed. The monosubstituted derivatives $Ru[P(OCH_3)_3]_4L$ (L= $P(OC_2H_5)_3$, $P(OCH(CH_3)_2)_3$, $P(OCH_2)_3CCH_3$, $P(OC_6H_5)_3$, PF_3, $P(CH_3)_3$, $P(CH_3)_2C_6H_5$, $PCH_3(C_6H_5)_2$, $P(C_2H_4CN)_3$, $SbMe_3$), prepared by the reaction of $Ru[P(OCH_3)_3]_4(\eta^2\text{-}C_2H_4)$ and L, are reported. The variable temperature $^{31}P\{^1H\}$ NMR spectra of these fluxional complexes were measured; arguments based on steric and electronic considerations are used to rationalize the site preference of L and the variation in barriers to nonrigidity displayed by the $Ru[P(OCH_3)_3]_4L$ complexes. The X-ray structure of $Ru[P(OCH_3)_3]_4P(OCH_2)_3CCH_3$ is also discussed.

The focus of chapter 3 is the reaction of $Ru[P(OCH_3)_3]_5$ as a nucleophile. The cationic Ru complexes $\{XRu[P(OCH_3)_3]_5\}^+$ (X= H, CH_3, Cl, Br, I), isolated as the PF_6 salts, are presented. The rigid nature of these species in solution is shown by $^{31}P\{^1H\}$

NMR spectroscopy. Attempts to prepare several analogous complexes are reported. In addition, the synthesis and characterization of $[HRu[P(OCH_3)_3]_4P(OCH_2)_3CCH_3]PF_6$ are reported.

Chapter 4 is concerned with attempts to prepare analogues of $Ru[P(OCH_3)_3]_5$, utilizing ligands other than $P(OCH_3)_3$ (i.e. $P(OC_2H_5)_3$, $P(OCH(CH_3)_2)_3$, $P(O\text{-}n\text{-}C_4H_9)_3$, and $P(OCH_2)_3CCH_3$). Also reported are attempts to synthesize $Os[P(OCH_3)_3]_5$.

The synthesis and characterization of $Os_3[P(OCH_3)_3]_x(CO)_{12-x}$ (x= 1-6), $Os_3[P(OCH_3)_3]_3[P(OC_2H_5)_3](CO)_6$, $Os_3[P(OCH_2)_3CCH_3]_x(CO)_{12-x}$ (x= 1,2), and $Os[P(OCH_3)_3]_x(CO)_{5-x}$ (x= 1,2) are the subject of chapter 5. Also included is the X-ray structure of $Os_3[P(OCH_3)_3]_6(CO)_6$.

Chapter 6 is concerned with the stereochemical nonrigidity of $Os_3[P(OCH_3)_3]_x(CO)_{12-x}$ (x= 1-5) in solution. Variable temperature ^{13}C and $^{31}P\{^1H\}$ NMR spectroscopy were used to probe the fluxional processes occurring in these molecules. Two specific types of mechanisms are used to rationalize the temperature dependent NMR data.

A short appendix (2) discussing techniques for calculating activation parameters for the nonrigid processes examined in this thesis is also included.

CHAPTER 2

Phosphite Derivatives of Ruthenium. Preparation of $Ru[P(OCH_3)_3]_5$ and $Ru[P(OCH_3)_3]_4(\eta^2-C_2H_4)$. Complexes Derived from Substitution of Various Ligands for $P(OCH_3)_3$ in $Ru[P(OCH_3)_3]_5$. X-ray Structure of $Ru[P(OCH_3)_3]_4[P(OCH_2)_3CCH_3]$.

2.1 Introduction

This chapter and the succeeding one deal with the preparation and some chemistry of $Ru[P(OCH_3)_3]_5$. Consequently, a brief survey of known homoleptic metal(0)-phosphite complexes and their chemistry will be presented.

The complexes shown in table 2.1 have been synthesized. A number of synthetic routes have been used in their preparation. Photolytic activation of $Mo(CO)_6$ and $Ru_3(CO)_{12}$ in the presence of excess phosphite gave $Mo[P(OCH_3)_3]_6$ [13] and $Ru[P(OCH_3)_3]_5$ [4,5], respectively. The reduction of transition metal halides with Na/Hg, K/Hg, and other reducing agents in the presence of excess phosphite has been frequently utilized; this route has allowed the preparation of $M[P(OCH_3)_3]_6$ (M= Mo, W) [14,15,16], $M[P(OCH_3)_3]_5$ (M= Fe, Ru, Os) [6], $Re_2[P(OCH_3)_3]_{10}$ [14], $Co[P(OR)_3]_4$ (R= Me, *i*-Pr) [17,18,19], and $Co_2[P(OR)_3]_8$ (R=Me, *i*-Pr) [17,18,19]. Metal vapour synthesis has led to the formation of $Cr[P(OCH_3)_3]_6$ [20,21], $Fe[P(OCH_3)_3]_5$, and $Fe[P(OCH_2)_3CEt]_5$ [22]. Ligand displacement from labile precursors has been used to synthesize $Rh_2[P(OCH_3)_3]_8$ [23] and

Compound	References
$Cr[P(OR)_3]_6$ (R= Me)	20, 21
$Mo[P(OR)_3]_6$ (R= Me)	13, 14, 15, 21
$W[P(OR)_3]_6$ (R= Me)	14, 16, 21
$Re_2[P(OR)_3]_{10}$ (R= Me, Ph†)	14
$Fe[P(OR)_3]_5$ (R= Me, Et, *i*-Pr; R_3= $(CH_2)_3CEt$)	6, 22, 26
$Ru[P(OR)_3]_5$ (R= Me)	4, 5, 6
$Os[P(OR)_3]_5$ (R= Me†)	6
$Co[P(OR)_3]_4$ (R= Me, Et, *i*-Pr, Ph)	17, 18, 27, 28
$Co_2[P(OR)_3]_8$ (R= Me, Et, *i*-Pr)	17, 18, 19
$Rh[P(OR)_3]_4$ (R= *i*-Pr)	29
$Rh_2[P(OR)_3]_6$ (R= Me)	23
$Ir_2[P(OR)_3]_8$ (R= Ph†)	24
$Ni[P(OR)_3]_4$ (R= alkyl and aryl)	25a
$Ni[P(OR)_3]_3$ (R= o-tolyl, 2,4-xylyl)	25a
$Pd[P(OR)_3]_4$ (R= alkyl and aryl)	25a, 30
$Pd[P(OR)_3]_3$ (R= Ph)	30, 31
$Pt[P(OR)_3]_3$ (R= alkyl and aryl)	25a, 30
$Pt[P(OR)_3]_3$ (R= Me, Ph)	30

†= poorly or incompletely characterized

Table 2.1 Known zerovalent, homoleptic, metal-phosphite complexes.

$Ir_2[P(OC_6H_5)_3]_8$ [24].

Although a number of binary metal(0)-phosphite complexes have been prepared, their chemistry has not been studied in any detail. The photochemical lability of $W[P(OCH_3)_3]_6$ was illustrated by ultraviolet irradiation of the complex with H_2 in hexane: the tungsten hydrides $H_2W[P(OCH_3)_3]_5$, $H_4W[P(OCH_3)_3]_4$, and $H_2W[P(OCH_3)_3]_3[(CH_3O)_2POP(OCH_3)_2]$ were rapidly formed [16]. The reactions of H_2, H^+, and CO with $M[P(OCH_3)_3]_6$ (M= Mo, W) and $Re_2[P(OCH_3)_3]_{10}$ were studied by ^1H and $^{31}P\{^1H\}$ NMR spectroscopy [25]. The UV irradiation of $Mo[P(OCH_3)_3]_6$ and H_2 in THF gave $H_2Mo[P(OCH_3)_3]_5$ and $H_4Mo[P(OCH_3)_3]_4$ while the analogous reaction with $Re_2[P(OCH_3)_3]_{10}$ afforded $H_3Re[P(OCH_3)_3]_4$ and smaller amounts of $HRe[P(OCH_3)_3]_5$ and $HRe[P(OCH_3)_3]_3[(CH_3O)_2POP(OCH_3)_2]$. The treatment of $W[P(OCH_3)_3]_6$ with excess CF_3COOH in ethylene glycol dimethyl ether led to formation of $HW[P(OCH_3)_3]_4(O_2CCF_3)$, although small amounts of $\{HW[P(OCH_3)_3]_6\}^+$ were also detected. The product from the reaction of $Re_2[P(OCH_3)_3]_{10}$ and excess CF_3COOH in CD_2Cl_2 was tentatively identified as $H_2Re[P(OCH_3)_3]_3(O_2CCF_3)$. The major product derived from the UV irradiation of $Re_2[P(OCH_3)_3]_{10}$ and ^{13}CO in THF was *trans*-$HRe[P(OCH_3)_3]_4(^{13}CO)$ while the corresponding reaction with $W[P(OCH_3)_3]_6$ gave *trans*-$W[P(OCH_3)_3]_4(^{13}CO)_2$ and $W[P(OCH_3)_3]_5(^{13}CO)$.

Only the chemistry of $Fe[P(OCH_3)_3]_5$ has been studied in any detail [26]. The reaction of this complex with H_2 in THF slowly gave $H_2Fe[P(OCH_3)_3]_4$ and $P(OCH_3)_3$; the reverse reaction did not

proceed, even at elevated temperatures. The reaction of $Fe[P(OCH_3)_3]_5$ with carbon monoxide in polar solvents yielded a mixture of $Fe[P(OCH_3)_3]_3(CO)_2$ and $Fe[P(OCH_3)_3]_4CO$, although there is some controversy regarding the latter complex [5]. The rates of CO substitution were solvent dependent. The treatment of $Fe[P(OCH_3)_3]_5$ with excess PF_3 in CH_2Cl_2 afforded $Fe[P(OCH_3)_3]_3(PF_3)_2$. A series of cationic Fe complexes of the type $\{XFe[P(OCH_3)_3]_5\}^+$ (X= H, CH_3, Cl, Br, I) were prepared; these are discussed in more detail in the introduction to chapter 3.

Stereochemical nonrigidity in solution is a ubiquitous feature of five coordinate complexes [7,32]. A series of papers investigating this phenomenon for d^8 complexes of the type ML_5^{n+} (n=0: M= Fe, Ru, Os; n=1: M= Co, Rh, Ir; n=2: M= Ni, Pd, Pt; L= phosphite) have appeared in the literature [6,33,34,35,36,]. These complexes were studied by variable temperature $^{31}P\{^1H\}$ NMR spectroscopy in conjunction with density matrix line shape calculations and group theoretical methods of permutational analysis. In the slow exchange limit all these complexes exhibited $^{31}P\{^1H\}$ NMR spectra due to A_2B_3 or A_2B_3X spin systems (X= metal atom). As the temperature was raised most of these spectra broadened, coalescing into single lines (A_5 spectrum) or doublets (A part of an A_5X spectrum). The invariance of this behaviour to added ligand showed that the rearrangements were intramolecular.

A detailed permutational analysis of this rearrangement (in conjunction with density matrix calculations) revealed several important points. The line shape changes (in all cases) were consistent with the simultaneous exchange of the axial ligands with a pair of the equatorial ligands in the trigonal bipyramidal ground state structure; a corresponding process, involving only a single axial and equatorial group, was shown to be inconsistent with the observed line shape changes. Several physical mechanisms which result in the pairwise exchange of two axial and two equatorial ligands for ML_5 species with D_{3h} equilibrium stereochemistry have been proposed. These include the Berry mechanism [37] and the turnstile process [38].

The Berry mechanism has become commonly accepted as the most physically reasonable process consistent with the previously described permutational behaviour. This mechanism is shown schematically in figure 2.1. The acceptance of this process is based on several arguments. It takes into account the close relationship between the two most common geometries of pentacoordination in the solid state: the trigonal bipyramid and the square-based pyramid. Molecular orbital calculations have shown that a potential surface connecting these D_{3h} and C_{4v} geometries (through C_{2v} structures) has a small energy barrier, with D_{3h} possessing the lowest energy [39,40]. The energies of alternate possibilities (with optimized C_s geometry) were found to be considerably higher than those of either the D_{3h} or C_{4v} structures.

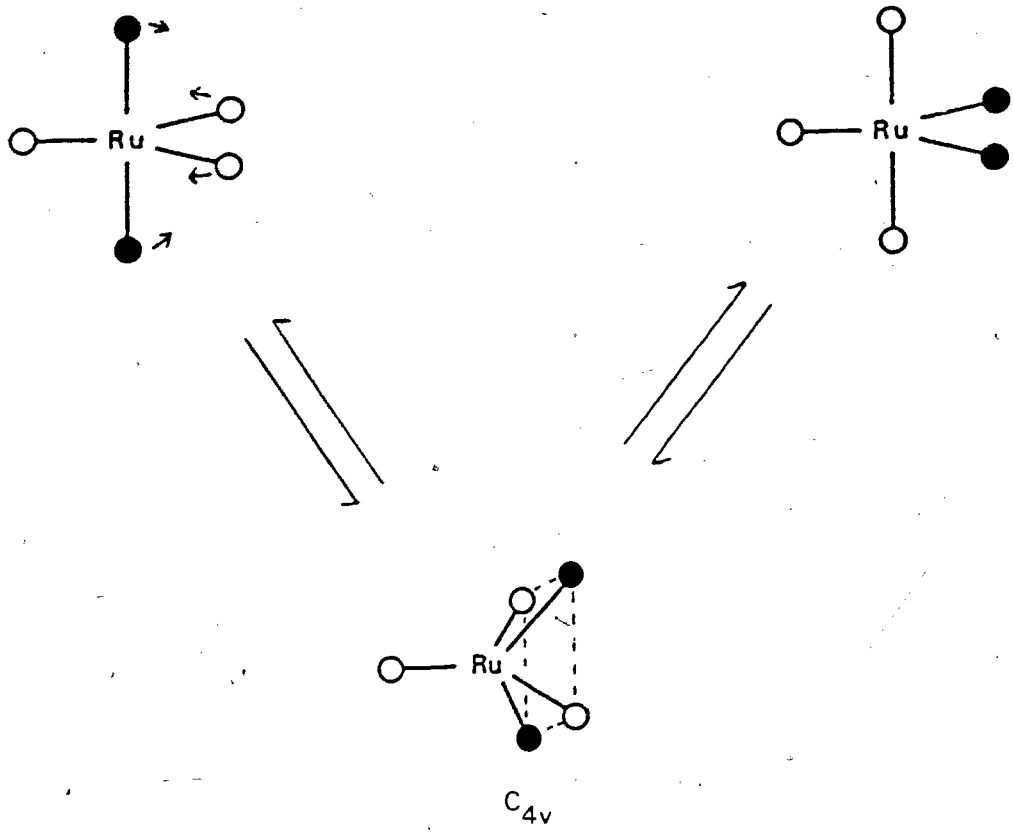

Figure 2.1 A schematic representation of the Berry mechanism.

In this chapter, the preparations of pentakis(trimethyl phosphite)ruthenium(0) and the substitutionally labile derivative $Ru[P(OCH_3)_3]_4(\eta^2\text{-}C_2H_4)$ are reported. Products of the general type $Ru[P(OR)_3]_3(\eta^4\text{-diene})$ (R= alkyl) and $Ru[P(OCH_3)_3]_4L$ (L= various phosphines and phosphites) are also presented. The diene complexes were prepared to compare their fluxional barriers to that of the previously studied $Ru[P(OCH_3)_3]_3(\eta^4\text{-}C_4H_6)$. In addition, the X-ray crystal structure of $Ru[P(OCH_3)_3]_4P(OCH_2)_3CCH_3$ is discussed. As previously mentioned, the results presented here for $Ru[P(OCH_3)_3]_5$ and $Ru[P(OCH_3)_3]_3(\eta^4\text{-}C_4H_6)$ and some of those relating to $Ru[P(OCH_3)_3]_4(\eta^2\text{-}C_2H_4)$ formed part of an undergraduate research

project (see chapter 1 for further details).

2.2 Results

The ultraviolet irradiation of $Ru_3(CO)_{12}$ and excess $P(OCH_3)_3$ in hexane (for 48 h) gave $Ru[P(OCH_3)_3]_5$. This air-sensitive product was isolated as a waxy, crystalline solid (yield: 66%) which was very soluble in common organic solids.

When a solution of $Ru[P(OCH_3)_3]_5$ in hexane was photolyzed in the presence of excess 1,3 butadiene, the complex $Ru[P(OCH_3)_3]_3(\eta^4\text{-}C_4H_6)$ was formed. The analogous reaction utilizing an excess of C_5H_8 (isoprene) led to the isolation of $Ru[P(OCH_3)_3]_3(\eta^4\text{-}C_5H_8)$.

The photolysis of $Ru_3(CO)_{12}$ and excess $P(OR)_3$ (R= Et, *i*-Pr) in hexane (for ~24 h) afforded $Ru[P(OR)_3]_3(CO)_2$. The corresponding reaction utilizing excess $P(O\text{-}n\text{-}C_4H_9)_3$ gave a mixture of products which were difficult to separate. The ultraviolet irradiation of $Ru[P(OR)_3]_3(CO)_2$ (R= Et, *i*-Pr) and excess C_4H_6 in hexane gave $Ru[P(OR)_3]_3(\eta^4\text{-}C_4H_6)$. The photolysis of $Ru[P(OC_2H_5)_3]_3(CO)_2$ and excess C_5H_8 in hexane (for 3.5 h) produced $Ru[P(OC_2H_5)_3]_3(\eta^4\text{-}C_5H_8)$. All of the tris(phosphite)-diene complexes just described were very soluble in common organic solvents; purification was accomplished by vacuum sublimation. These diene complexes were found to be stereochemically nonrigid in solution.

When a solution of $Ru[P(OCH_3)_3]_5$ and excess 2,5-norbornadiene in hexane was photolyzed, the expected tris(phosphite)-diene compound was not formed. Instead, the previously known $CH_3Ru[P(O)(OCH_3)_2](P(OCH_3)_3)_4$ was isolated and identified by $^{31}P\{^1H\}$ NMR spectroscopy [4,5]. An analogous reaction, using excess 1,5-cyclooctadiene, led to the isolation of the same product.

The ultraviolet irradiation of $Ru[P(OCH_3)_3]_5$ and excess C_2H_4 in hexane (for 4 h) afforded $Ru[P(OCH_3)_3]_4(\eta^2-C_2H_4)$; the yield was 83%. This air-sensitive complex was very soluble in common organic solvents. More importantly, the ethylene complex was thermally unstable and readily lost C_2H_4 in solution and under vacuum.

The thermal reaction of $Ru[P(OCH_3)_3]_4(\eta^2-C_2H_4)$ with various phosphite and phosphine ligands (L) led to formation of $Ru[P(OCH_3)_3]_4L$. The general synthetic route involved a 1-2 h reaction time at 50-60 °C, with a 1 to 3-fold excess of the ligand in toluene (see experimental section for details of individual cases). The complexes isolated and characterized were $Ru[P(OCH_3)_3]_4L$ (L= $P(OC_2H_5)_3$, $P(OCH(CH_3)_2)_3$, $P(OC_6H_5)_3$, $P(OCH_2)_3CCH_3$, $P(CH_3)_3$, $P(CH_3)_2C_6H_5$, $PCH_3(C_6H_5)_2$, $P(C_2H_4CN)_3$, PF_3); the trimethyl stibine complex $Ru[P(OCH_3)_3]_4Sb(CH_3)_3$ was prepared by a similar route. All of these monosubstituted derivatives of $Ru[P(OCH_3)_3]_5$ were found to be stereochemically nonrigid in solution by $^{31}P\{^1H\}$ NMR spectroscopy.

Efforts to prepare olefin complexes of the type $Ru[P(OCH_3)_3]_4(\eta^2\text{-alkene})$ were largely unsuccessful. The thermal reaction of $Ru[P(OCH_3)_3]_4(\eta^2\text{-}C_2H_4)$ with excess propene in hexane did not result in the isolation of the η^2-propene complex. The ultraviolet irradiation of $Ru[P(OCH_3)_3]_5$ and excess L (L= propene, 1-butene, cyclooctene, dimethyl fumurate) in hexane also did not give desired η^2-alkene species. There was, however, $^{31}P\{^1H\}$ NMR evidence for the formation of $Ru[P(OCH_3)_3]_4(\eta^2\text{-cyclooctene})$ from the thermal reaction of $Ru[P(OCH_3)_3]_4(\eta^2\text{-}C_2H_4)$ and excess cyclooctene in toluene. The details of these results are discussed in the text.

2.3 Characterization and Discussion.

2.3.1 Preparation and Properties of $Ru[P(OCH_3)_3]_5$.

The ultraviolet irradiation of $Ru_3(CO)_{12}$ and excess $P(OCH_3)_3$ in hexane gave $Ru[P(OCH_3)_3]_5$, a waxy solid which was extremely soluble in common organic solvents. This is not suprising since $Ru[P(OCH_3)_3]_5$ has a hydrocarbon exterior and is expected to have virtually no dipole moment. Pentakis(trimethyl phosphite)ruthenium(0) has previously been prepared by the Na/Hg reduction of $Ru[P(OCH_3)_3]_4Cl_2$ in the presence of excess phosphite in THF [6]. It was reported that the $^{31}P\{^1H\}$ NMR spectrum of $Ru[P(OCH_3)_3]_5$ (toluene-d_8/$CClF_2H$) (a singlet at room temperature) transformed into one due to an A_2B_3 spin system at

-125 °C. We have confirmed this result [5]. The chemical shifts and coupling constants for this spin system were reported: δ_A= 15.4, δ_B= 39.5, J_{AB}= 77.5 Hz [6]. These results indicate that in the slow exchange limit, $Ru[P(OCH_3)_3]_5$ has D_{3h} symmetry (i.e. is trigonal bipyramidal) in solution.

It is noted that throughout this thesis, ^{31}P NMR spectra are referenced to $P(OCH_3)_3$ at 0 ppm with the downfield direction positive.

Some points regarding the $^{31}P\{^1H\}$ NMR results for $Ru[P(OCH_3)_3]_5$ are important. In the slow exchange limit, the chemical shift of the resonances due to the equatorial $P(OCH_3)_3$ groups is downfield from that due to the axial phosphite ligands by ~24 ppm. This fact will later prove useful in determining the static solution structures of $Ru[P(OCH_3)_3]_4L$ (L= various phosphines and phosphites). Note also that the resonances due to both the axial and equatorial $P(OCH_3)_3$ groups of $Ru[P(OCH_3)_3]_5$ are shifted downfield with respect to the free ligand. This result is general for all the Ru(0) complexes presented in this thesis (see chapter 4 for a fuller discussion).

2.3.2 Preparation and Properties of $Ru[P(OR)_3]_3(\eta^4\text{-diene})$ (diene= C_4H_6: R= Me, Et, i-Pr; diene= C_5H_8: R= Me, Et). Attempted Reaction of $Ru[P(OCH_3)_3]_5$ with other dienes.

The ultraviolet irradiation of $Ru[P(OCH_3)_3]_5$ and excess 1,3-butadiene in hexane for 8 h afforded $Ru[P(OCH_3)_3]_3(\eta^4\text{-}C_4H_6)$. When the reaction was monitored by $^{31}P\{^1H\}$ NMR spectroscopy the following behaviour was observed: the resonance due to $Ru[P(OCH_3)_3]_5$ slowly disappeared, accompanied by the appearance of a free $P(OCH_3)_3$ signal and two broad resonances. The nature of the latter resonances resulted from the chemical exchange of the three phosphite ligands (vide infra). No signals due to intermediate products were observed. This reaction presumably proceeds via photochemically induced dissociation of a $P(OCH_3)_3$ ligand followed by coordination of C_4H_6 in an η^2 fashion.

$$Ru[P(OCH_3)_3]_5 \xrightarrow{h\nu} Ru[P(OCH_3)_3]_4 + P(OCH_3)_3$$

$$Ru[P(OCH_3)_3]_4 + C_4H_6 \longrightarrow Ru[P(OCH_3)_3]_4(\eta^2\text{-}C_4H_6)$$

Although the lack of spectroscopic evidence for the tetra(phosphite)/(η^2-diene) intermediate might suggest that it undergoes rapid loss of a second phosphite and subsequent η^4 coordination of the diene, this need not be the case. This η^2-diene species is expected to be stereochemically nonrigid in solution and its exchange broadened $^{31}P\{^1H\}$ NMR resonance(s)

could easily be lost in the baseline.

When the reaction was irradiated for periods longer than 8 h, the $^{31}P\{^{1}H\}$ NMR spectrum revealed the slow appearance of a pair of multiplets. These resonances were temperature invariant; this suggested the slow transformation of $Ru[P(OCH_3)_3]_3(\eta^4\text{-}C_4H_6)$ into a rigid, six coordinate species.

The photolysis of $Ru[P(OCH_3)_3]_5$ and excess C_5H_8 (isoprene) in hexane for 8 h gave $Ru[P(OCH_3)_3]_3(\eta^4\text{-}C_5H_8)$. This complex was likely formed via a mechanism similar to that just discussed for the butadiene analogue.

Attempts to generalize this synthetic route to produce tris(phosphite)/(η^4-diene) complexes with ligands other than $P(OCH_3)_3$ were frustrated by a lack of the appropriate starting materials. The penta(phosphite)ruthenium(0) complexes for ligands other than $P(OCH_3)_3$ are not known. The ultraviolet irradiation of $Ru_3(CO)_{12}$ and excess $P(OR)_3$ (R= Et, *i*-Pr, *n*-Bu) in hexane did not lead to $Ru[P(OR)_3]_5$ (see chapter 4 for further details).

Another potential starting material for the preparation of $Ru[P(OR)_3]_4(\eta^4\text{-diene})$ (R≠ Me) was available. Previous work had shown that the thermal reaction of $Ru_3(CO)_{12}$ and excess $P(OCH_3)_3$ in hexane gave high yields of $Ru[P(OCH_3)_3]_3(CO)_2$ [5]. It was found that this route gave the analogous products for other phosphites. Thus, when $Ru_3(CO)_{12}$ and excess $P(OC_2H_5)_3$ were heated in hexane at 120 °C for 30 h, $Ru[P(OC_2H_5)_3]_3(CO)_2$ was

formed and easily isolated in high yield. The corresponding reaction utilizing $P(OCH(CH_3)_2)_3$ gave $Ru[P(OCH(CH_3)_2)_3]_3(CO)_2$ as the major product; this complex was purified by fractional sublimation. The major product from the thermal reaction of $Ru_3(CO)_{12}$ and excess $P(O\text{-}n\text{-}C_4H_9)_3$ in hexane was $Ru[P(O\text{-}n\text{-}C_4H_9)_3]_3(CO)_2$, as determined by IR spectroscopy. However, efforts to separate this complex from associated impurities were unsuccessful.

For the reactions of $Ru_3(CO)_{12}$ with excess $P(OR)_3$ (R= Et, *i*-Pr, *n*-Bu) there was IR spectroscopic evidence for the stepwise formation of $Ru[P(OCH_3)_3]_x(CO)_{5-x}$ (x= 1,2). This was based on the close similarity of the IR spectra (carbonyl region) taken during these reactions to those of $Ru[P(OCH_3)_3](CO)_4$ and $Ru[P(OCH_3)_3]_2(CO)_3$ [5].

Small amounts of other products were isolated from the reactions of $Ru_3(CO)_{12}$ with excess $P(OR)_3$ (R= Et, *i*-Pr, *n*-Bu). Attempts to separate the final reaction mixtures by column chromatography on $P(OCH_3)_3$-deactivated Florisil led to the development of yellow bands which were collected. These yielded yellow-orange products which exhibited very similar IR $\nu(CO)$ spectra; the elemental analysis of the product from the reaction of $Ru_3(CO)_{12}$ and excess $P(O\text{-}n\text{-}C_4H_9)_3$ was consistent with a formulation of $Ru_3[P(O\text{-}n\text{-}C_4H_9)_3]_3(CO)_9$. In addition, each complex exhibited a temperature invariant singlet in the $^{31}P\{^1H\}$ NMR spectrum. Based on these observations, the yellow-orange products are tentatively identified as 1,2,3-$\{Ru_3[P(OR)_3]_3(CO)_9\}$

(R= Et, *i*-Pr, *n*-Bu).

The important result from the thermal reaction of $Ru_3(CO)_{12}$ and excess $P(OR)_3$ (R= Et, *i*-Pr) was the isolation of $Ru[P(OR)_3]_3(CO)_2$. These dicarbonyl species were found to be satisfactory starting materials for the preparation of tris(phosphite)-diene complexes. The ultraviolet irradiation of $Ru[P(OR)_3]_3(CO)_2$ (R= Et, *i*-Pr) and excess 1,3 butadiene in hexane led to the formation of $Ru[P(OR)_3]_3(\eta^4\text{-}C_4H_6)$; these complexes required tedious fractional sublimation to remove impurities. In addition, the photolysis of $Ru[P(OC_2H_5)_3]_3(CO)_2$ and excess isoprene in hexane afforded $Ru[P(OC_2H_5)_3]_3(\eta^4\text{-}C_5H_8)$.

The previously unknown complexes $Ru[P(OR)_3]_3(\eta^4\text{-diene})$ (diene= butadiene: R= Me, Et, *i*-Pr; diene= isoprene: R= Me, Et) and $Ru[P(OR)_3]_3(CO)_2$ (R= Et, *i*-Pr) were characterized by mass spectrometry and ^1H NMR spectroscopy; acceptable elemental analyses were obtained for all but $Ru[P(OCH(CH_3)_2)_3]_3(\eta^4\text{-}C_4H_6)$ (vide infra). The variable temperature $^{31}P\{^1H\}$ NMR spectra of the diene complexes were also measured.

The isolation of $Ru[P(OCH(CH_3)_2)_3]_3(\eta^4\text{-}C_4H_6)$ was hampered by tedious fractional sublimation for both the final product and the precursor (i.e. $Ru[P(OCH(CH_3)_2)_3]_3(CO)_2$). This led to a small yield (0.08 g) of $Ru[P(OCH(CH_3)_2)_3]_3(\eta^4\text{-}C_4H_6)$ which was used in its entirety for the variable temperature $^{31}P\{^1H\}$ NMR study. Further characterization was performed on the sample recovered from the NMR studies. The complex had suffered some

decomposition at higher temperatures and an acceptable elemental analysis was thus not obtained.

The ^1H NMR assignments for the 1,3-butadiene and isoprene ligands of $Ru[P(OR)_3]_3(\eta^4$-diene) (diene= butadiene: R= Me, Et, *i*-Pr; diene= isoprene: R= Me, Et) are shown in table 2.2. These are based on the ^1H NMR data for the free dienes. In general, coordination of the diene to the central metal causes an upfield shift of the proton resonances (relative to the free ligand). Of particular note is the large (~5 ppm) upfield shift of protons B and E/F (see table 2.2) upon coordination to the central metal. This may be ascribed to the proximity forced upon these protons by diene coordination, resulting in increased electron shielding relative to the free diene (see figure 2.4 and discussion later in this section). A number of the resonances in table 2.2 are broad; this is believed to be due to long range ^{31}P-^1H coupling. Comparable results have been found for similar systems (see references in the following paragraph).

The assignments in table 2.2 are generally consistent with those proposed for several related complexes: $Ru(CO)_3(\eta^4$-$C_4H_6)$ [41], $Fe[P(OR)_3]_3(\eta^4$-$C_4H_6)$ (R= Me, Et, *i*-Pr), $Fe[P(OR)_3]_3(\eta^4$-$C_5H_8)$ (R= *i*-Pr, Ph) [42], and $Ru[PPh_3]L_2(\eta^4$-$C_4H_6)$ (L= $P(OCH_3)_3$, $P(OCH_2)_3CCH_3$, PF_2NMe_2) [43].

The variable temperature $^{31}P\{^1H\}$ NMR spectra of $Ru[P(OR)_3]_3(\eta^4$-$C_4H_6)$ (R= Me, Et, *i*-Pr) and $Ru[P(OR)_3]_3(\eta^4$-$C_5H_8)$ (R= Me, Et) were temperature dependent. The variable temperature

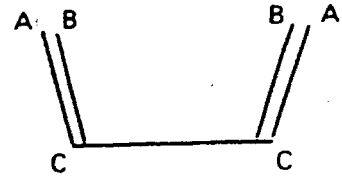

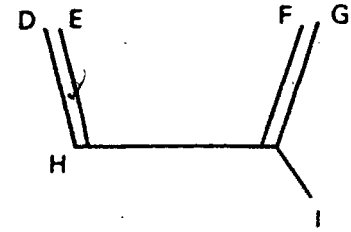

Complex	^{1}H NMR data[a, b]
$Ru[P(OCH_3)_3]_3(\eta^4\text{-}C_4H_6)$	C 4.90: broad triplet, $J_{AC}\simeq J_{BC}\simeq 6$ Hz, (1) A 1.38: broad doublet, $J_{AC}\simeq 6$ Hz, (1) B -0.42: broad, (1)
$Ru[P(OC_2H_5)_3]_3(\eta^4\text{-}C_4H_6)$	C 5.05: broad triplet, $J_{AC}\simeq J_{BC}\simeq 6$ Hz, (1) A 1.56: doublet with fine structure $J_{AC}\simeq 6$ Hz, (1) B -0.04: broad, (1)
$Ru[P(OCH(CH_3)_2)_3]_3(\eta^4\text{-}C_4H_6)$	C ~5.0: obscured by $P(OC\underline{H}(CH_3)_2)_3$ signal A ~1.5: obscured by $P(OCH(C\underline{H}_3)_2)_3$ signal B -0.4: broad
$Ru[P(OCH_3)_3]_3(\eta^4\text{-}C_5H_8)$	H 4.72: broad triplet, $J_{DH}\simeq J_{EH}\simeq 6$ Hz, (1) I ~1.9: obscured by residual protons of acetone-d_6 G 1.30: broad singlet, (1) D 1.14: doublet of doublets, J_{DH}= 6.4 Hz, J_{DE}= 1.7 Hz, (1) E -0.37: broad, (1) F -0.79: broad, (1)
$Ru[P(OC_2H_5)_3]_3(\eta^4\text{-}C_5H_8)$	H 4.61: broad triplet, $J_{DH}\simeq J_{EH}\simeq 6$ Hz, (1) I ~1.9: obscured by residual protons of acetone-d_6 G 1.30: broad doublet, (1) D ~1.1: obscured by $P(OCH_2C\underline{H}_3)_3$ signal E -0.39: broad, (1) F -0.78: broad, (1)

Table 2.2 ^{1}H NMR assignments for the 1,3 butadiene and isoprene ligands of the complexes $Ru[P(OR)_3]_3(\eta^4$-diene) (diene= C_4H_6: R= Me, Et, *i*-Pr; diene= C_5H_8: R= Me, Et). [a] in acetone-d_6 at 25 °C. [b] relative intensities in brackets.

$^{31}P\{^{1}H\}$ NMR spectra of $Ru[P(OCH_3)_3]_3(\eta^4\text{-}C_5H_8)$ in toluene-d_8/toluene (1:4) are shown in figure 2.2. The slow exchange limit spectra of these species were of two types. The 1,3-butadiene complexes exhibited a doublet and a triplet (with identical coupling constants) of relative intensity 2:1, respectively; this is indicative of an AB_2 spin system. The isoprene complexes had slow exchange limit $^{31}P\{^{1}H\}$ NMR spectra due to an ABC spin system. The experimental and computer simulated $^{31}P\{^{1}H\}$ NMR spectra of $Ru[P(OCH_3)_3]_3(\eta^4\text{-}C_5H_8)$ in toluene-d_8/toluene (1:4) at -37 °C are shown in figure 2.3. The spectral parameters are δ_A 39.9, δ_B 21.0, δ_C 15.9, J_{AB}=±30.1 Hz, J_{BC}= ±47.5 Hz, and J_{AC}= ±26.5 Hz.

It is generally considered that complexes of the type $ML_3(\eta^4\text{-diene})$ (M= Fe, Ru; L= phosphorus donor ligand) adopt a square pyramidal geometry in solution with the diene occupying two basal sites [42,43]. Supporting evidence comes from both variable temperature NMR data [42,43,44,45]. and X-ray studies [46,47]. The complexes $Ru[P(OR)_3]_3(\eta^4\text{-}C_4H_6)$ (R= Me, Et, *i*-Pr) and $Ru[P(OR)_3]_3(\eta^4\text{-}C_5H_8)$ (R= Me, Et) are thus assumed to adopt the static solution structure shown in figure 2.4. The slow exchange limit $^{31}P\{^{1}H\}$ NMR spectra of the butadiene (X= H) and isoprene (X= Me) complexes are consistent with this structure.

The changes in the variable temperature $^{31}P\{^{1}H\}$ NMR spectra of $Ru[P(OR)_3]_3(\eta^4\text{-}C_4H_6)$ (R= Me, Et, *i*-Pr) and $Ru[P(OR)_3]_3(\eta^4\text{-}C_5H_8)$ (R= Me, Et) were relatively uncomplicated. As the temperature was increased, all the resonances for the

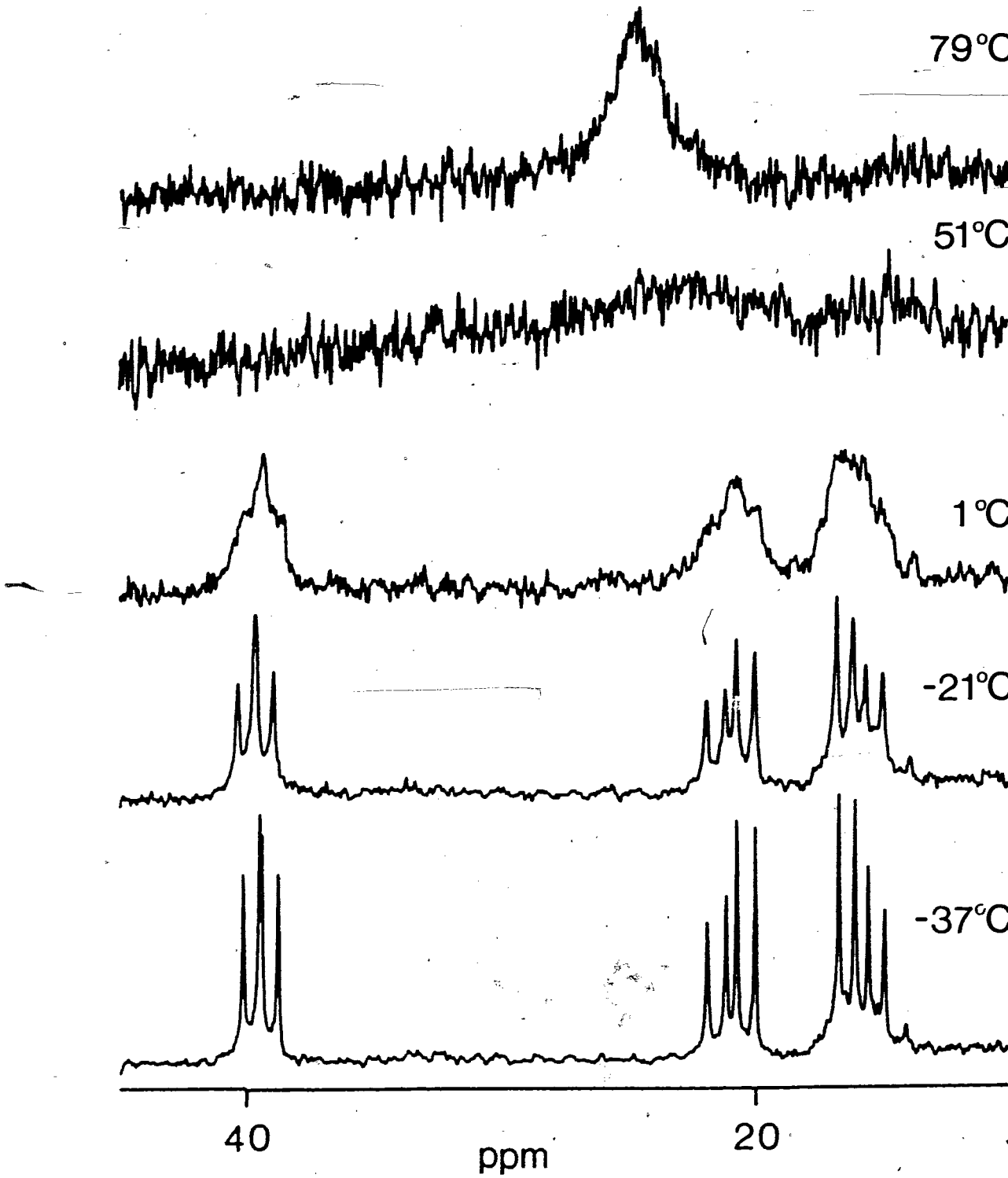

Figure 2.2 The variable temperature $^{31}P\{^{1}H\}$ NMR spectra of $Ru[P(OCH_3)_3]_3(\eta^4\text{-}C_5H_8)$ in toluene-d_8/toluene (1:4) measured at 40.54 MHz.

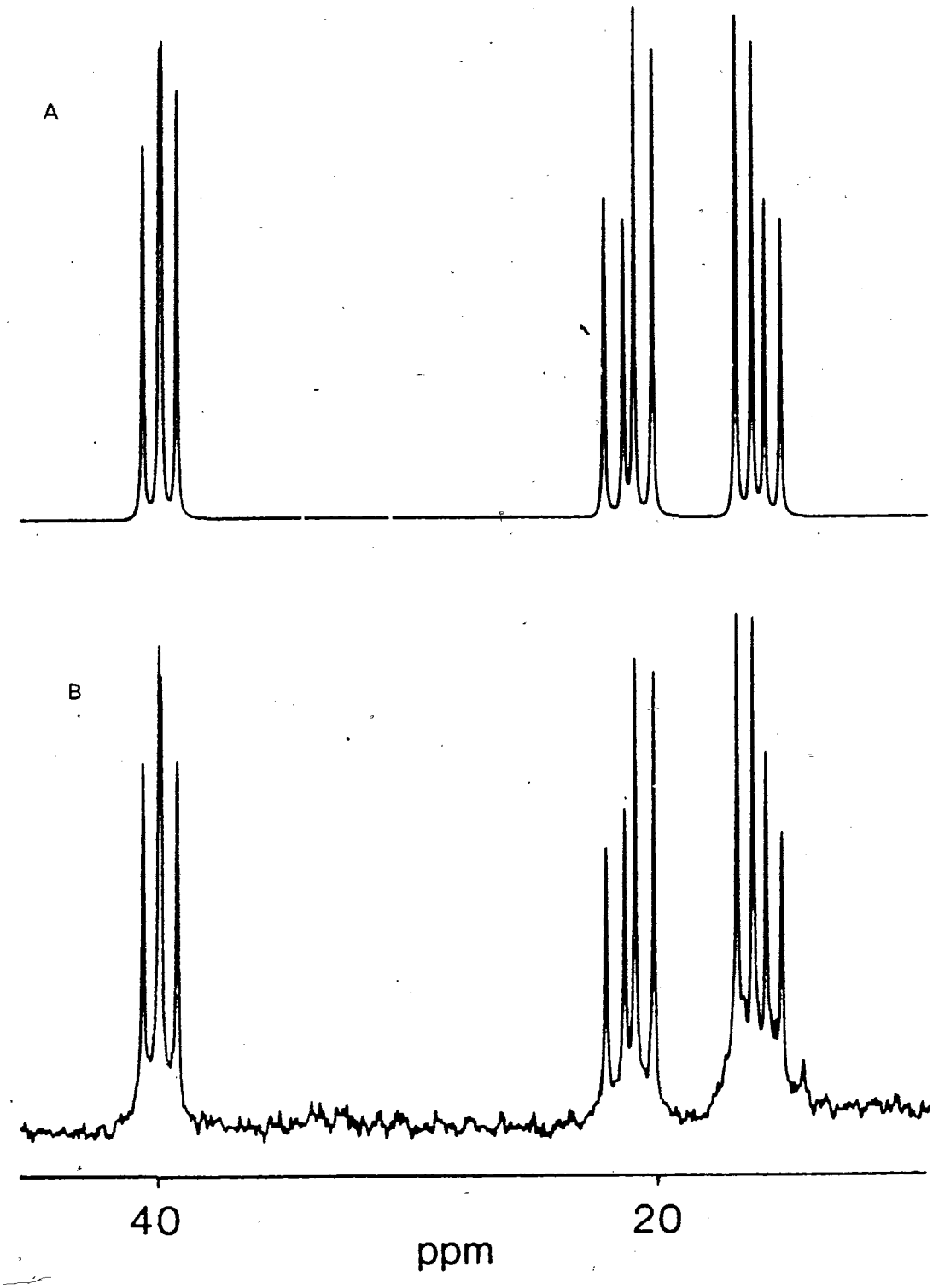

Figure 2.3 The experimental (B) and simulated (A) $^{31}P\{^{1}H\}$ NMR spectra of $Ru[P(OCH_3)_3]_3(\eta^4\text{-}C_5H_8)$ in toluene-d_8/toluene (1:4) at -37 °C. Spectral parameters given in text.

complex in question broadened at qualitatively the same rate and coalesced to a broad singlet (for example, see figure 2.2). The useful range of the solvent (toluene-d_8/toluene, 1:4, bp 111 °C) precluded the acquisition of fast exchange limit spectra. Resonances due to added $P(OR)_3$ (R= Me, Et, *i*-Pr) remained sharp over the measured temperature range for each complex, implying an intramolecular exchange process.

A number of studies concerning stereochemical nonrigidity in complexes of the type $ML_3(\eta^4$-diene) (M= Fe, Ru; L= phosphorus donor ligand or CO; diene= various cyclic and acyclic dienes) have appeared in the literature [42,43,44,45,48,49]. A detailed permutational analysis, in conjunction with density matrix line shape calculations, was undertaken with respect to the variable temperature $^{31}P\{^1H\}$ NMR data for $FeL_3(\eta^4$-diene) (L= various phosphines and phosphites; diene= cyclic and acyclic dienes) [42]. The results showed that the "turnstile" mechanism was the most reasonable physical process to associate with the observed

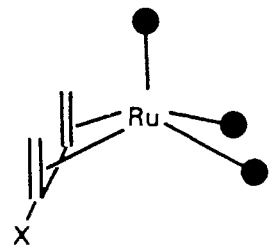

Figure 2.4 The assumed static solution structure of $Ru[P(OR)_3]_3(\eta^4$-$C_8H_6)$ (R= Me, Et, *i*-Pr) and $Ru[P(OR)_3]_3(\eta^4$-$C_5H_8)$ (R= Me, Et).

permutational behaviour. This process may be described as trigonal rotation of the FeL_3 moiety against the diene or diene rotation relative to the FeL_3 portion of the molecule (see figure 2.5). A distinction between the two descriptions does not appear to be meaningful. It is assumed that this process was responsible for the temperature dependent changes to the $^{31}P\{^1H\}$ NMR spectra of $Ru[P(OR)_3]_3(\eta^4\text{-}C_4H_6)$ (R= Me, Et, *i*-Pr) and $Ru[P(OR)_3]_3(\eta^4\text{-}C_5H_8)$ (R= Me, Et). It may be verified that the mechanism shown schematically in figure 2.5 would result in the averaging of the ^{31}P resonances (for each of the previously mentioned molecules) to a single signal in the fast exchange limit.

The activation barrier for this rearrangement was found to be sensitive to the identity of $P(OR)_3$ (R= Me, Et, *i*-Pr). A detailed line shape analysis of the variable temperature $^{31}P\{^1H\}$ NMR spectra for $Ru[P(OCH_3)_3]_3(\eta^4\text{-}C_4H_6)$ yielded the following activation parameters: $\Delta H^{\ddagger}$= 9.4±0.2 kcal mol^{-1}, $\Delta S^{\ddagger}$= -13.3±0.5 $cal(mol\text{-}^{\circ}K)^{-1}$, $\Delta G^{\ddagger}$(298 °K)= 13.4±0.2 kcal mol^{-1} [50]. The barrier to nonrigidity for the series $Ru[P(OR)_3]_3(\eta^4\text{-}C_4H_6)$ (R= Me, Et, *i*-Pr) was found to follow the order *i*-Pr > Et > Me. This ranking was based on coalescence temperatures of the $^{31}P\{^1H\}$ NMR spectra, taking into account chemical shift differences for each complex. A qualitative consideration of the temperatures at which line broadening became first apparent revealed that the rearrangement barrier for R= Et was greater than that for R= Me in $Ru[P(OR)_3]_3(\eta^4\text{-}C_5H_8)$.

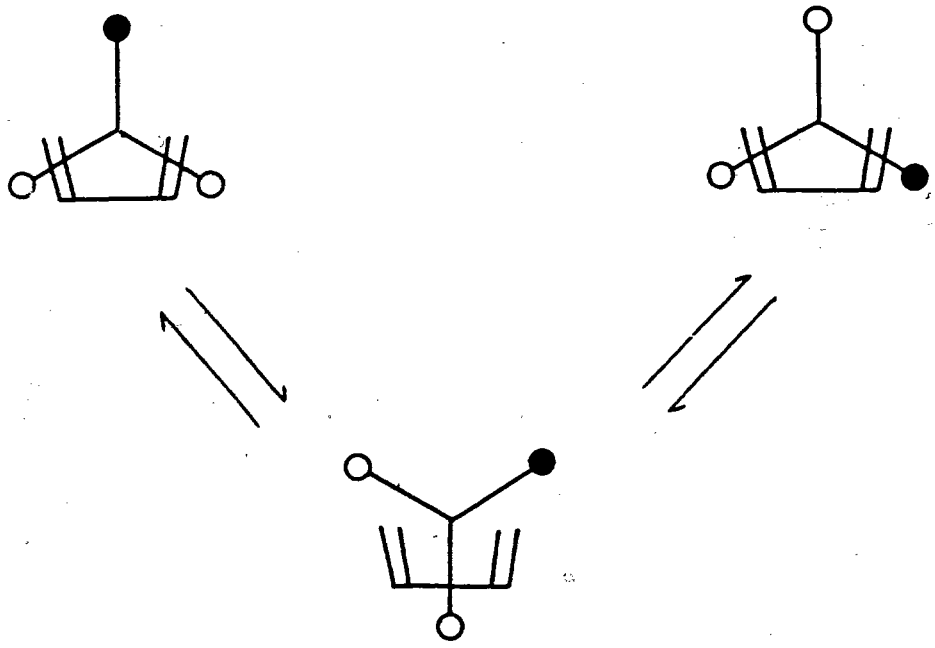

Figure 2.5 Schematic representation of the "turnstile" mechanism for a square pyramidal complex of the type $ML_3(\eta^4\text{-diene})$.

Both steric and electronic arguments may be advanced to explain these results. The ligand cone angles for $P(OCH_3)_3$, $P(OC_2H_5)_3$, and $P(OCH(CH_3)_2)_3$ are 107°, 109°, and 130°, respectively [10,51,11]. The increasing steric bulk of these ligands would be expected to raise the fluxional barrier for $Ru[P(OR)_3]_3(\eta^4\text{-}C_4H_6)$ (R= Me, Et, *i*-Pr) with respect to the process in figure 2.5. The Tolman ligand electronic effects for these three ligands are 2079.5, 2076.3, and 2075.9 cm^{-1}, respectively [10,11]. The trend in these values is also consonant with the observed order of the rearrangement barriers for $Ru[P(OR)_3]_3(\eta^4\text{-}C_4H_6)$, although the difference between the electronic parameters of $P(OC_2H_5)_3$ and $P(OCH(CH_3)_2)_3$ is small. Quantitative values of the fluxional barriers for $Ru[P(OR)_3]_3(\eta^4\text{-}C_4H_6)$ and $Ru[P(OR)_3]_3(\eta^4\text{-}C_5H_8)$ (i.e. $\Delta G^{\ddagger}$ values)

are required before more definitive conclusions may be drawn regarding steric and electronic effects on the barriers.

The results just presented may be compared to those from the related iron system, $FeL_3(\eta^4$-cyclooctadiene) (L= $P(OCH_3)_3$, $P(OC_2H_5)_3$, $P(OCH(CH_3)_2)_3$, $P(CH_3)_3$) [42]. The $\Delta G^{\ddagger}$(298 °K) values for the intramolecular rearrangement in these complexes are 10.7, 10.9, 12.3, and 14.8 kcal mol^{-1}, respectively. The ligand cone angle of $P(CH_3)_3$ is 118° [10,11,51] and the associated electronic parameter is 2064.1 cm^{-1} [10,11]. The authors stated that these results suggested a predominantly electronic effect on the barrier height, apparently based on the high barrier for the $P(CH_3)_3$ complex even though this ligand has a small cone angle. This interpretation of the data does not appear totally justified. The difference between the electronic characteristics of $P(CH_3)_3$ (a highly basic ligand with poor π-acceptor properties) and the phosphites is undeniably real. This is likely the cause of the anomalous behaviour of $P(CH_3)_3$. If the variation in $\Delta G^{\ddagger}$ is examined with respect to the phosphite ligands alone, one reasonably reaches the conclusion that steric effects are most important; the large difference in $\Delta G^{\ddagger}$ for L= $P(OC_2H_5)_3$ and $P(OCH(CH_3)_2)_3$ is better explained by the difference in ligand cone angles than the small variation in electronic parameters for these two ligands.

The photolytic activation of $Ru[P(OCH_3)_3]_5$ in the presence of other dienes did not result in the formation of of $Ru[P(OCH_3)_3]_3(\eta^4$-diene). The ultraviolet irradiation of

$Ru[P(OCH_3)_3]_5$ and excess 2,5-norbornadiene in hexane gave $CH_3Ru[P(O)(OCH_3)_2](P(OCH_3)_3)_4$ as the major product. The analogous reaction with 1,5-cyclooctadiene gave the same result. The formation of this product is not entirely unexpected. Recall that $Ru[P(OCH_3)_3]_5$ underwent methyl migration at 100 °C in hexane to yield $CH_3Ru[P(O)(OCH_3)_2](P(OCH_3)_3)_4$ [4,5]. The exhaustive photolysis of $Ru[P(OCH_3)_3]_5$ and excess $P(OCH_3)_3$ in hexane gave species with $^{31}P\{^1H\}$ NMR spectra similar (but not identical) to that of $CH_3Ru[P(O)(OCH_3)_2](P(OCH_3)_3)_4$ [5,52]. The likely cause of the difference between the latter result and that found for the UV irradiation of $Ru[P(OCH_3)_3]_5$ and excess norbornadiene or cyclooctadiene is the absence of $P(OCH_3)_3$. It is believed that the methyl migration proceeds via the 16 electron intermediate $Ru[P(OCH_3)_3]_4$ [5]. Excess $P(OCH_3)_3$ is expected to inhibit the formation of this species in solution, allowing a reaction by an alternative pathway.

The failure of $Ru[P(OCH_3)_3]_5$ and excess 2,5-norbornadiene or 1,5-cyclooctadiene to give $Ru[P(OCH_3)_3]_3(\eta^4\text{-diene})$ under photolytic conditions is puzzling in light of the relative ease of the reaction utilizing 1,3-butadiene or isoprene. The iron complex $Fe[P(OCH_3)_3]_3(\eta^4\text{-cyclooctadiene})$ was prepared by the metal atom evaporation technique [42]; it was noted, however, that the attempted preparation of this complex from $Fe[P(OCH_3)_3]_5$ gave unsatisfactory results. The inability of norbornadiene and cyclooctadiene to form η^4-diene complexes with the $Ru[P(OCH_3)_3]_3$ unit could be related to the reduced

flexibility of these cyclic dienes versus the acyclic C_4H_6 and C_5H_8. Detailed spectral analyses of J_{HH} and J_{CH} for $M(CO)_3(\eta^4$-butadiene) (M= Fe, Ru) have suggested that distortion of the C_4H_6 ligand occurs upon coordination [41,53]. The increased steric demands of a phosphite ligand relative to CO might be expected to cause an increase in this distortion for $Ru[P(OCH_3)_3]_3(\eta^4$-diene). Acyclic dienes could be capable of undergoing the required deformation more readily than their cyclic relatives.

2.3.3 Preparation and Properties of $Ru[P(OCH_3)_3]_4(\eta^2-C_2H_4)$ and $Ru[P(OCH_3)_3]_4L$ (L= $P(OC_2H_5)_3$, $P(OCH(CH_3)_2)_3$, $P(OCH_2)_3CCH_3$, $P(OC_6H_5)_3$, PF_3, $P(CH_3)_3$, $P(CH_3)_2C_6H_5$, $PCH_3(C_6H_5)_2$, $P(C_2H_4CN)_3$, $SbMe_3$). X-ray Structure of $Ru[P(OCH_3)_3]_4P(OCH_2)_3CCH_3$.

The preparation of $Ru[P(OCH_3)_3]_3(\eta^4$-diene) (diene= C_4H_6, C_5H_8) from $Ru[P(OCH_3)_3]_5$ suggested that monosubstituted derivatives of the type $Ru[P(OCH_3)_3]_4L$ (L= two electron donor ligands) were synthetically accessible. The use of $Ru[P(OCH_3)_3]_5$ as a precursor, however, suffered from a severe disadvantage. Previous results had shown that the chemical or photolytic activation of pentakis(trimethyl phosphite)ruthenium(0) in the presence of excess $P(OC_2H_5)_3$ (in hexane) gave both the mono- and disubstituted derivatives [52]. The low volatility and high solubility of these complexes made separation difficult. A more suitable starting material was required.

The ultraviolet irradiation of $Ru[P(OCH_3)_3]_5$ and excess C_2H_4 in hexane for 4 h gave $Ru[P(OCH_3)_3]_4(\eta^2\text{-}C_2H_4)$. When the reaction was monitored by $^{31}P\{^1H\}$ NMR spectroscopy, it was observed that the singlet due to $Ru[P(OCH_3)_3]_5$ lost intensity and was replaced by a free $P(OCH_3)_3$ signal plus two extremely broad resonances. The nature of the latter resonances resulted from chemical exchange of the phosphite ligands in $Ru[P(OCH_3)_3]_4(\eta^2\text{-}C_2H_4)$ (vide infra). The singlet due to $Ru[P(OCH_3)_3]_5$ did not completely disappear during the reaction; this suggested that $Ru[P(OCH_3)_3]_4(\eta^2\text{-}C_2H_4)$ easily lost C_2H_4 under photolytic conditions and recombined with free $P(OCH_3)_3$ to regenerate $Ru[P(OCH_3)_3]_5$. Prolonged irradiation of the reaction mixture led to the appearance of two unidentified multiplets.

The variable temperature $^{31}P\{^1H\}$ NMR spectra of $Ru[P(OCH_3)_3]_4(\eta^2\text{-}C_2H_4)$ in hexane (under an ethylene atmosphere) were measured. At -56 °C, a pair of triplets (δ_A 30.8, δ_B 15.8) of equal intensity and with identical coupling constants (J_{AB}= 64.7 Hz) were observed. This result is consonant with a static, trigonal bipyramidal structure with the alkene in an equatorial site. As the temperature was raised, the triplets broadened and coalesced into a singlet at 50 °C. An intermolecular, phosphite exchange process was ruled out by the observation that a signal due to added $P(OCH_3)_3$ remained sharp over this temperature range. The behaviour of the temperature dependent $^{31}P\{^1H\}$ NMR spectra of $Ru[P(OCH_3)_3]_4(\eta^2\text{-}C_2H_4)$ is consistent with the operation of the Berry mechanism (see figure 2.1); this process

would result in the averaging of the axial and equatorial phosphite signals to a single resonance. A detailed line shape analysis of the variable temperature ^{31}P data for $Ru[P(OCH_3)_3]_4(\eta^2\text{-}C_2H_4)$, based on this mechanism, yielded the following activation parameters: $\Delta H^{\ddagger}$= 9.9±0.2 kcal mol^{-1}, $\Delta S^{\ddagger}$= -9.2±0.4 cal$(mol\text{-}^{\circ}K)^{-1}$, and $\Delta G^{\ddagger}$(298 °K)= 12.7±0.2 kcal mol^{-1} [50]. However, the possibility of an intermolecular, C_2H_4 exchange process causing the observed variable temperature $^{31}P\{^1H\}$ NMR behaviour cannot be discounted (vide infra).

Solutions of $Ru[P(OCH_3)_3]_4(\eta^2\text{-}C_2H_4)$ in polar solvents and solid samples of the compound appeared thermally unstable. A $CDCl_3$ solution of the ethylene complex rapidly turned red at room temperature. Attempted sublimation of the solid at 25 °C gave the same result. These observations suggested that ethylene was easily lost from $Ru[P(OCH_3)_3]_4(\eta^2\text{-}C_2H_4)$; the parent $Ru[P(OCH_3)_3]_5$ was stable under these conditions. It was felt that $Ru[P(OCH_3)_3]_4(\eta^2\text{-}C_2H_4)$ could be the ideal precursor to species of the type $Ru[P(OCH_3)_3]_4L$ (L= two electron donor ligand).

A $^{31}P\{^1H\}$ NMR study was conducted to test this hypothesis. An NMR tube was charged with a solution of $Ru[P(OCH_3)_3]_4(\eta^2\text{-}C_2H_4)$ and $P(OCH_2)_3CCH_3$ (~1:4 molar ratio) in toluene-d_8/toluene (1:4). The $^{31}P\{^1H\}$ NMR spectrum after 1 h at room temperature revealed the onset of the desired reaction; in addition to the broad resonances of $Ru[P(OCH_3)_3]_4(\eta^2\text{-}C_2H_4)$ and the free $P(OCH_2)_3CCH_3$ singlet, a doublet and a quintet with

identical coupling constants (relative intensity 4:1, respectively) were observed. Based on the results for $Ru[P(OCH_3)_3]_5$, derivatives of the type $Ru[P(OCH_3)_3]_4L$ (L= phosphine and phosphite) were predicted to undergo rapid intramolecular ligand exchange in solution [5,6]. Depending on the chemical shift difference between the ^{31}P resonances of $P(OCH_3)_3$ and the unique ligand, the fast exchange limit $^{31}P\{^1H\}$ NMR spectra were expected to reflect either an A_4B or an A_4X spin system. The $^{31}P\{^1H\}$ NMR spectrum after 2 h at 65 °C showed the complete disappearance of $Ru[P(OCH_3)_3]_4(\eta^2\text{-}C_2H_4)$. In addition to the doublet and quintet, a weak singlet due to free $P(OCH_3)_3$ was observed. Subsequent heating at 80 °C for 24 h caused further changes to the $^{31}P\{^1H\}$ NMR spectrum: the free $P(OCH_3)_3$ resonance increased in height and signals due to $Ru[P(OCH_3)_3]_{5-x}[P(OCH_2)_3CCH_3]_x$ (x= 2,3) were observed.

The photolysis of $Ru[P(OCH_3)_3]_4(\eta^2\text{-}C_2H_4)$ in the presence of excess $P(OCH_2)_3CCH_3$ was also investigated. An NMR tube was charged with a solution of the ethylene complex and $P(OCH_2)_3CCH_3$ (~1:4 molar ratio) in CH_3CN. After 1 h at room temperature, a $^{31}P\{^1H\}$ NMR spectrum of the reaction solution again showed the onset of the desired reaction. The UV irradiation of the tube for 30 min resulted in complete disappearance of $Ru[P(OCH_3)_3]_4(\eta^2\text{-}C_2H_4)$; the $^{31}P\{^1H\}$ NMR spectrum revealed resonances due to $Ru[P(OCH_3)_3]_{5-x}[P(OCH_2)_3CCH_3]_x$ (x= 1,2) and free $P(OCH_3)_3$. After 2 h photolysis, signals representing $Ru[P(OCH_3)_3]_{5-x}[P(OCH_2)_3CCH_3]_x$ (x= 1,2,3) were present. These

results indicated that the thermal activation of $Ru[P(OCH_3)_3]_4(\eta^2\text{-}C_2H_4)$ and L was the route of choice to prepare $Ru[P(OCH_3)_3]_4L$ derivatives while minimizing the formation of more highly substituted products.

The scope of this reaction was studied with respect to the ligand L. In particular, there was a concern that phosphorus donor ligands with large cone angles might be sterically inhibited from coordinating to the metal. Toluene solutions of $Ru[P(OCH_3)_3]_4(\eta^2\text{-}C_2H_4)$ and L (~fivefold excess of L; L= PPh_3, $P(i\text{-}Pr)_3$, $P(n\text{-}Bu)_3$, $P(CH_3)_3$, $P(CH_3)_2C_6H_5$, $PCH_3(C_6H_5)_2$, $P(C_2H_4CN)_3$, $P(OC_6H_5)_3$, P(O-o-tolyl)$_3$) were placed in NMR tubes. These were heated to 50-60 °C and the reactions were monitored by $^{31}P\{^1H\}$ NMR spectroscopy. For L= PPh_3 and $P(i\text{-}Pr)_3$, the spectra showed that no $Ru[P(OCH_3)_3]_4L$ derivatives were formed; disappearance of the resonances due to the ethylene complex were accompanied by the emergence of a number of complex multiplets. The expected AX_4 pattern was not among these. For L= $P(n\text{-}Bu)_3$, P(O-o-tolyl)$_3$, and $PCH_3(C_6H_5)_2$, signals due to the $Ru[P(OCH_3)_3]_4L$ complex were observed early in the reaction. These were accompanied, however, by resonances due to free $P(OCH_3)_3$ and $Ru[P(OCH_3)_3]_5$. These latter signals grew in intensity at the expense of the AX_4 pattern as the reaction continued. The reactions with L= $P(CH_3)_3$, $P(C_2H_4CN)_3$, $P(CH_3)_2C_6H_5$, and $P(OC_6H_5)_3$ gave more satisfying results. After approximately 1 h at 55 °C, the $^{31}P\{^1H\}$ NMR spectra of these revealed the complete disappearance of $Ru[P(OCH_3)_3]_4(\eta^2\text{-}C_2H_4)$

and the presence of the $Ru[P(OCH_3)_3]_4L$ derivative; only minor impurity resonances were observed.

The thermal reaction of $Ru[P(OCH_3)_3]_4(\eta^2-C_2H_4)$ and L (one to fourfold excess) in toluene was used to prepare the following $Ru[P(OCH_3)_3]_4L$ derivatives: L= $P(OCH_2)_3CCH_3$, $P(OC_2H_5)_3$, $P(OCH(CH_3)_2)_3$, $P(OC_6H_5)_3$, $P(CH_3)_3$, $P(CH_3)_2C_6H_5$, $PCH_3(C_6H_5)_2$, $P(C_2H_4CN)_3$, PF_3, and $SbMe_3$. The details of temperature, reaction time, and ligand:$Ru[P(OCH_3)_3]_4(\eta^2-C_2H_4)$ ratio for specific cases are given in the experimental section of this chapter. The trifluorophosphine derivative was prepared under ~2 atmospheres of ligand pressure.

These monosubstituted derivatives were all air-sensitive and typically suffered extensive decomposition during several min exposure to air. Solid samples of $Ru[P(OCH_3)_3]_4Sb(CH_3)_3$ under N_2 suffered partial decomposition after 3 weeks at 25 °C. Except for $Ru[P(OCH_3)_3]_4P(OCH_2)_3CCH_3$ and $Ru[P(OCH_3)_3]_4P(C_2H_4CN)_3$, all of the $Ru[P(OCH_3)_3]_4L$ complexes were soluble in hexane and extremely soluble in both toluene and CH_2Cl_2. This made recrystallization impractical. None of these complexes sublimed under vacuum at 25 °C and higher temperatures usually caused decomposition. Column chromatography proved an ineffective separation technique; the $Ru[P(OCH_3)_3]_4L$ species bound irreversibly to even the mildest and most deactivated adsorbents. Purification was accomplished in a rather crude manner. Hexane or toluene solutions of the complex were filtered through a short (0.5-1.0x1.2 cm) column of alumina. This

procedure indiscriminantly removed both product and impurity. After one to three applications of this technique, the $Ru[P(OCH_3)_3]_4L$ derivatives were isolated as waxy solids which exhibited crystalline properties under the microscope. The $^{31}P\{^1H\}$ NMR spectra of these complexes, however, typically showed small amounts of impurities. These did cause minor difficulties with respect to interpretation of the slow exchange limit $^{31}P\{^1H\}$ NMR data, where the spectral intensity due to the $Ru[P(OCH_3)_3]_4L$ species was spread over a number of lines. Fortunately, this problem was not severe.

These monosubstituted derivatives and the parent $Ru[P(OCH_3)_3]_4(\eta^2\text{-}C_2H_4)$ were characterized by elemental analysis and ^1H NMR spectroscopy. Most of these complexes exhibited mass spectral parent ions although chemical ionization was required in several cases. The most effective technique for characterization was variable temperature $^{31}P\{^1H\}$ NMR spectroscopy and this will be the focus of the following discussion.

The variable temperature $^{31}P\{^1H\}$ NMR spectra (40.54 MHz) of $Ru[P(OCH_3)_3]_4P(OCH_2)_3CCH_3$ in $CD_2Cl_2/CHFCl_2$ (1:4) are shown in figure 2.6. The spectrum at -21 °C is in accord with the previous discussion: rapid phosphite exchange in solution causes magnetic equivalence of the $P(OCH_3)_3$ ligands and results in a spectrum due to an A_4X spin system. The observation that a signal due to added $P(OCH_3)_3$ remained sharp over the full temperature range of figure 2.6 argued against an intermolecular

exchange process.

As the temperature is decreased, the fast exchange limit resonances collapse and resolve to the slow exchange limit spectrum at -126 °C. The two major resonances (δ 42 and 13) of this spectrum were simulated. Based on an A_3BC spin system, two sets of spectral parameters gave simulated $^{31}P\{^1H\}$ NMR spectra which reasonably fit the experimental data. The experimental spectrum at -126 °C (B) and the two simulated spectra (A and C) for $Ru[P(OCH_3)_3]_4P(OCH_2)_3CCH_3$ are shown in figure 2.7. The spectral parameters for simulation A are δ_A 42.0, δ_B 14.6, δ_C 12.0, J_{AB}= ±75.7 Hz, J_{AC}= ±78.6 Hz, and J_{BC}= ∓108.3 Hz. The corresponding values for simulation C are δ_A 42.0, δ_B 15.8, δ_C 10.8, J_{AB}= ±77.0 Hz, J_{AC}= ±76.6 Hz, and J_{BC}= ∓472.3 Hz. Despite repeated attempts, a simulated spectrum based on an A_2B_2C spin system (using reasonable spectral parameters) could not be found which matched this experimental spectrum. These results are consistent with an axially substituted, trigonal bipyramidal structure for $Ru[P(OCH_3)_3]_4P(OCH_2)_3CCH_3$ in the slow exchange limit (see figure 2.8B). Reasonable alternative structures such as that shown in figure 2.8A or ones based on a square pyramid are clearly not in accord with the low temperature $^{31}P\{^1H\}$ NMR data. The question of the correct ^{31}P NMR spectral parameters for the slow exchange limit spectrum is discussed later in this section.

Recall that the slow exchange limit $^{31}P\{^1H\}$ NMR spectrum of $Ru[P(OCH_3)_3]_5$ (-137 °C) in pentane revealed an A_2B_3 pattern due

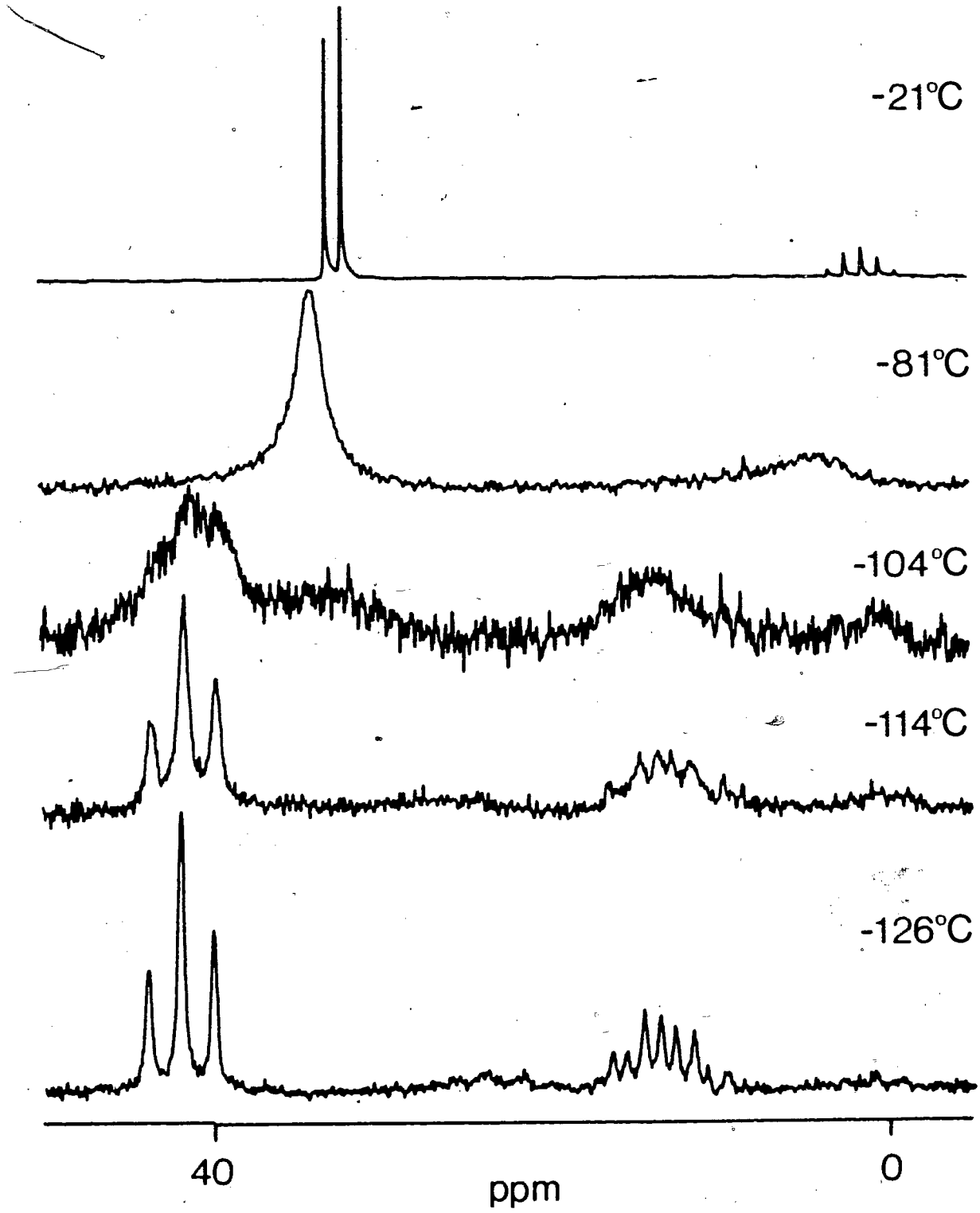

Figure 2.6 The variable temperature $^{31}P\{^{1}H\}$ NMR spectra of $Ru[P(OCH_3)_3]_4P(OCH_2)_3CCH_3$ in $CD_2Cl_2/CHFCl_2$ (1:4) measured at 40.54 MHz.

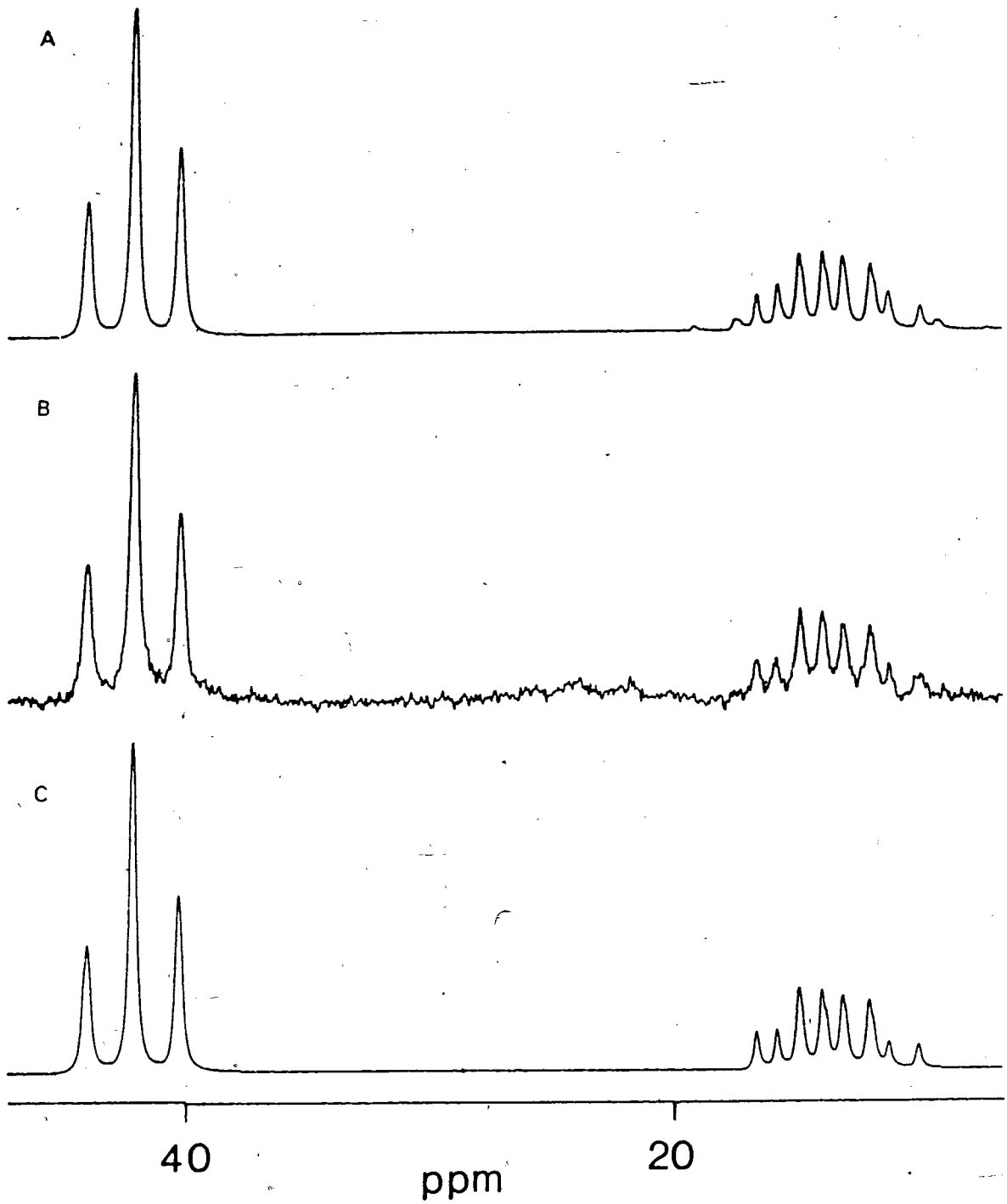

Figure 2.7 The experimental (B) and two computer simulated (A and C) $^{31}P\{^{1}H\}$ NMR spectra of $Ru[P(OCH_3)_3]_4P(OCH_2)_3CCH_3$ in $CD_2Cl_2/CHFCl_2$ (1:4) at -126 °C. Spectral parameters given in text.

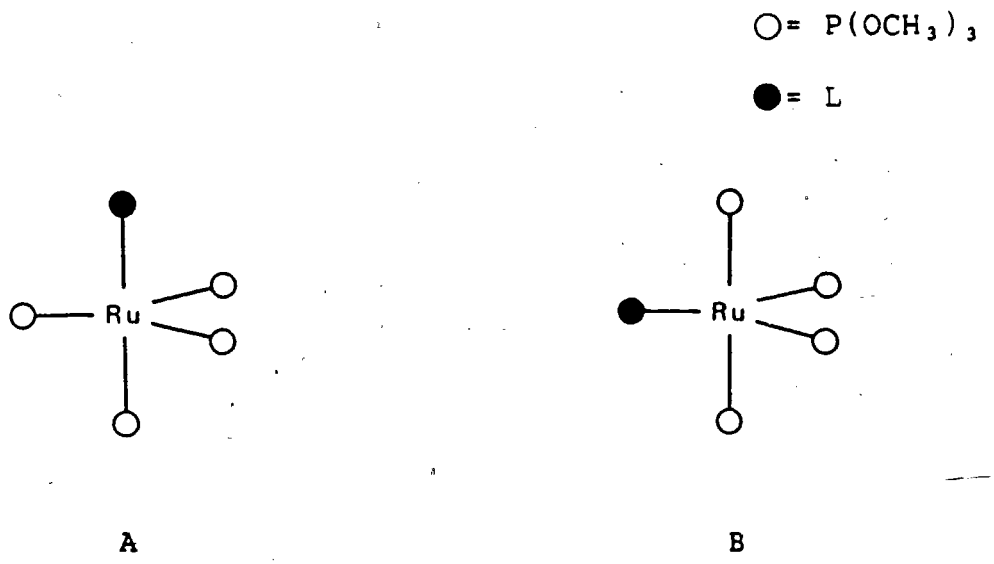

Figure 2.8 The two possible isomers for a trigonal bipyramidal $Ru[P(OCH_3)_3]_4L$ molecule.

---

to a trigonal bipyramidal arrangement of the ligands around the central metal [6]. The resonances due to the equatorial phosphites were at lower field (δ ~40) than those due to their axial counterparts (δ ~16). As these chemical shifts are referenced to that of free $P(OCH_3)_3$, it is noted that the equatorial ligands of $Ru[P(OCH_3)_3]_5$ undergo a larger ^{31}P downfield shift upon coordination than their axial counterparts. When these observations are examined in light of the present results for $Ru[P(OCH_3)_3]_4P(OCH_2)_3CCH_3$, the similarities are obvious. The coordination chemical shifts (i.e. the shift between the free and coordinated ligand) of the ^{31}P resonances in both complexes are similar for a given coordination site (i.e. axial or equatorial). The difference between the coordination chemical shifts of the axial and equatorial $P(OCH_3)_3$ ligands in $Ru[P(OCH_3)_3]_4P(OCH_2)_3CCH_3$, on the one hand,

and the analogous value for the caged phosphite ligand in $Ru[P(OCH_3)_3]_4P(OCH_2)_3CCH_3$ is noted (the ^{31}P signal for the free $P(OCH_2)_3CCH_3$ ligand falls at δ -49.0). This observation is consistent with an empirical relationship found for a wide range of transition metal complexes with phosphorus donor ligands: the further upfield the ^{31}P resonance of the free ligand, the larger the coordination chemical shift [55]. The coupling constants between the axial phosphite ligands of $Ru[P(OCH_3)_3]_4P(OCH_2)_3CCH_3$ and the equatorial $P(OCH_3)_3$ groups (75.7 to 78.6 Hz) are comparable to the analogous value for $Ru[P(OCH_3)_3]_5$ (77.5 Hz). The larger magnitude of J_{BC} (versus J_{AB} and J_{AC}) for $Ru[P(OCH_3)_3]_4P(OCH_2)_3CCH_3$, from either set of spectral parameters derived from figures 2.7A and C, is expected: the empirical observation that $trans\text{-}^2J_{PP}$ is usually larger than $cis\text{-}^2J_{PP}$ for a related pair of metal-phosphine or -phosphite complexes is based on a large volume of data [54]. The ^{31}P NMR spectral parameters associated with both the simulated, slow exchange limit spectra of $Ru[P(OCH_3)_3]_4P(OCH_2)_3CCH_3$ feature a $trans\text{-}^2J_{PP}$ of opposite sign to the two corresponding $cis\text{-}^2J_{PP}$ values. This behaviour is a general feature of the axially-substituted $Ru[P(OCH_3)_3]_4L$ derivatives discussed in this chapter (vide infra). The results and observations discussed in this paragraph were found to be very useful in the spectral analyses which follow.

The variable temperature $^{31}P\{^1H\}$ NMR data for $Ru[P(OCH_3)_3]_4P(OCH_2)_3CCH_3$ (figure 2.6) reveals additional

information. Consider the two weak multiplets (δ ~22 and ~1) in the spectrum at -126 °C. A careful examination of the three lowest temperature spectra reveals that these are not impurities but resolve from the same broadened resonances which give the A_3BC pattern. It is believed that these weak multiplets represent part of an A_2B_2C spin system due to the equatorially substituted isomer of $Ru[P(OCH_3)_3]_4P(OCH_2)_3CCH_3$ (i.e. figure 2.8B). The high field set of resonances are in the region expected for an equatorially coordinated $P(OCH_2)_3CCH_3$ ligand. The other multiplet (δ ~22) may be assigned to the axial $P(OCH_3)_3$ ligands of this minor isomer; the apparent triplet of the axial isomer could easily obscure the multiplet expected for the equatorial $P(OCH_3)_3$ ligands of the minor isomer. Unfortunately, the multiplets assigned to the equatorially substituted species have insufficient intensity to allow an accurate computer simulation. That the equatorial isomer was present in solution is indicated by the solid state structure of $Ru[P(OCH_3)_3]_4P(OCH_2)_3CCH_3$, which revealed that the caged phosphite was in an equatorial position. This structure is discussed in more detail later in this chapter.

The low temperature $^{31}P\{^1H\}$ NMR data for $Ru[P(OCH_3)_3]_4P(OCH_2)_3CCH_3$ measured at 40.54 MHz leaves two questions only partially answered. Although both the simulations in figure 2.7 are based on an A_3BC spin system, only one set of spectral parameters can be correct. Secondly, further evidence for the putative equatorial isomer of the caged phosphite

complex was precluded by an unfavourable equilibrium constant. In an effort to answer these questions, a low temperature $^{31}P\{^{1}H\}$ NMR spectrum of $Ru[P(OCH_3)_3]_4P(OCH_2)_3CCH_3$ in $CD_2Cl_2/CHFCl_2$ (1:4) was measured at 162.0 MHz. This spectrum (~-115 °C) is shown in figure 2.9 and clearly reveals that chemical exchange is still occurring; technical difficulties prevented measurement of the spectrum at a lower temperature on the Bruker WM-400 instrument. There is, however, still valuable information to be extracted from the data in question. The resonances due to the proposed minor (i.e. equatorial) isomer are clearly shown; the signal due to the equatorial $P(OCH_3)_3$ ligands of this species (unobserved at 40.54 MHz) is partially resolved from the low field triplet of the major isomer (see figure 2.9). The three resonances due to the equatorial molecule are observed to be broader than the signals of the dominant partner. This is an expected result if one considers the system in in terms of two isomers of unequal population undergoing chemical exchange: the resonances of the minor isomer are broadened and shifted more by the exchange than those due to the major counterpart [55a]. Another explanation for the broad nature of the resonances due to the minor isomer is advanced in a later section of this chapter (concerning mechanistic possibilities for the nonrigid process).

The experimental $^{31}P\{^{1}H\}$ NMR spectrum of $Ru[P(OCH_3)_3]_4P(OCH_2)_3CCH_3$ at ~-115 °C (162.0 MHz) in $CD_2Cl_2/CHFCl_2$ (1:4) is shown in figure 2.10B, along with two

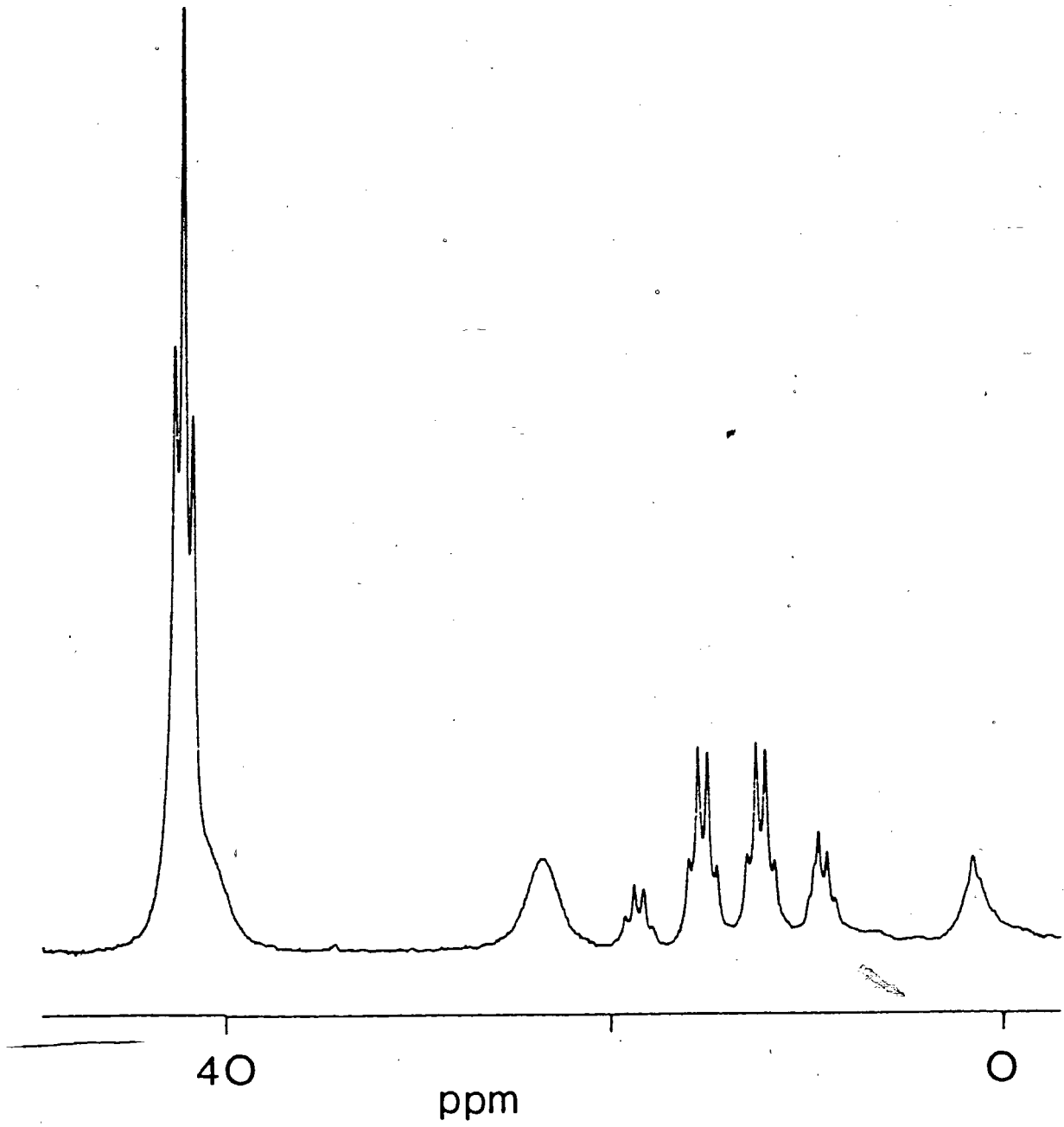

Figure 2.9 The $^{31}P\{^{1}H\}$ NMR spectrum of $Ru[P(OCH_3)_3]_4P(OCH_2)_3CCH_3$ in $CD_2Cl_2/CHFCl_2$ (1:4) at ~-115 °C measured at 162.0 MHz.

simulated spectra. The simulation shown in figure 2.10C is based on the A_3BC spectral parameters associated with figure 2.7A (i.e. at 40.54 MHz). The former simulation is clearly inconsistent with the experimental spectrum (figure 2.10B). The simulated spectrum shown in figure 2.10A, based on an A_3BC spin system, was calculated using the following spectral parameters: δ_A 42.1, δ_B 16.5, δ_C 11.2, J_{AB}= ±73.4 Hz, J_{AC}= ±76.2 Hz, and J_{BC}= ∓522.6 Hz. Given the exchange broadened nature of the experimental spectrum, simulation 2.10A gives an excellent fit. The spectral parameters for this calculated spectrum are in reasonable agreement with those associated with the simulated spectrum of figure 2.7C, which was based on 40.54 MHz data. The differences between the two are ascribed to the exchange broadened nature of the experimental spectrum at 162.0 MHz. The onset of chemical exchange causes significant chemical shift changes for the affected resonances. The iterative process used to derived the best fit to the experimental data is very sensitive to the proper chemical shift assignments in the experimental spectrum.

In summary, the low temperature $^{31}P\{^1H\}$ NMR results for $Ru[P(OCH_3)_3]_4P(OCH_2)_3CCH_3$ (40.54 and 162.0 MHz) strongly suggest that the complex has a trigonal bipyramidal structure with the $P(OCH_2)_3CCH_3$ ligand in an axial site (figure 2.8A). There is also considerable evidence for the presence of a small amount of the equatorial isomer (figure 2.8B). The variable temperature $^{31}P\{^1H\}$ NMR data for $Ru[P(OCH_3)_3]_4P(OCH_2)_3CCH_3$ are consonant

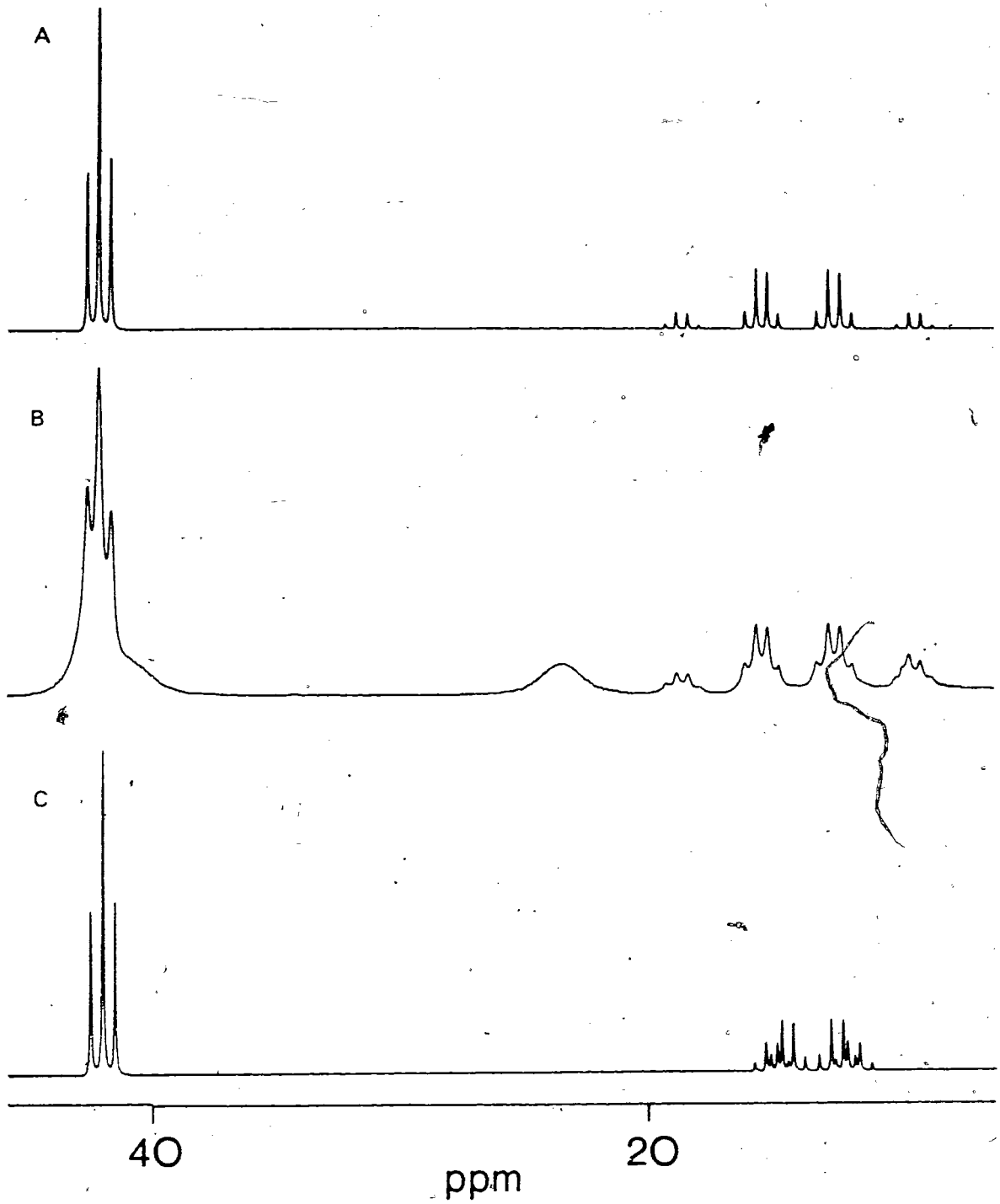

Figure 2.10 The experimental $^{31}P\{^{1}H\}$ NMR spectrum of $Ru[P(OCH_3)_3]_4P(OCH_2)_3CCH_3$ in $CD_2Cl_2/CHFCl_2$ (1:4) (~-115 °C) at 162.0 MHz (B), and two simulated spectra (A and C) based on an A_3BC spin system. Spectral parameters given in text.

with an intramolecular phosphite exchange process; a consideration of several possible mechanisms appears later in this chapter.

The variable temperature $^{31}P\{^{1}H\}$ NMR spectra (40.54 MHz) of $Ru[P(OCH_3)_3]_4P(OC_2H_5)_3$ in $CD_2Cl_2/CHFCl_2$ (1:4) are shown in figure 2.11. The weak multiplet at δ ~16 in the 24 °C spectra is due to an impurity. The fast exchange limit spectrum (24 °C) is due to an A_4B spin system, consistent with rapid scrambling of the phosphite ligands. The experimental (B) and simulated (A) $^{31}P\{^{1}H\}$ NMR spectra of $Ru[P(OCH_3)_3]_4P(OC_2H_5)_3$ in $CD_2Cl_2/CHFCl_2$ (1:4) at 24 °C are shown in figure 2.12. The spectral parameters as determined from the computer simulation are δ_B 20.7, δ_A 26.5, and J_{AB} = 52.4 Hz.

The slow exchange limit $^{31}P\{^{1}H\}$ NMR spectrum of $Ru[P(OCH_3)_3]_4P(OC_2H_5)_3$ was obtained at -121 °C (see figure 2.11). It may be observed that the impurity multiplet is coincident with the high field set of resonances due to the triethyl phosphite complex. Computer simulations based on both an A_3BC and an A_2B_2C spin system were found to give reasonable fits to this low temperature spectrum.

In an effort to unambiguously determine the site preference of the triethyl phosphite ligand, the low temperature $^{31}P\{^{1}H\}$ NMR spectrum of $Ru[P(OCH_3)_3]_4P(OC_2H_5)_3$ in $CD_2Cl_2/CHFCl_2$ (1:4) was measured at 162.0 MHz. This spectrum (at ~-115 °C) is shown in figure 2.13A. Again the effects of chemical exchange are

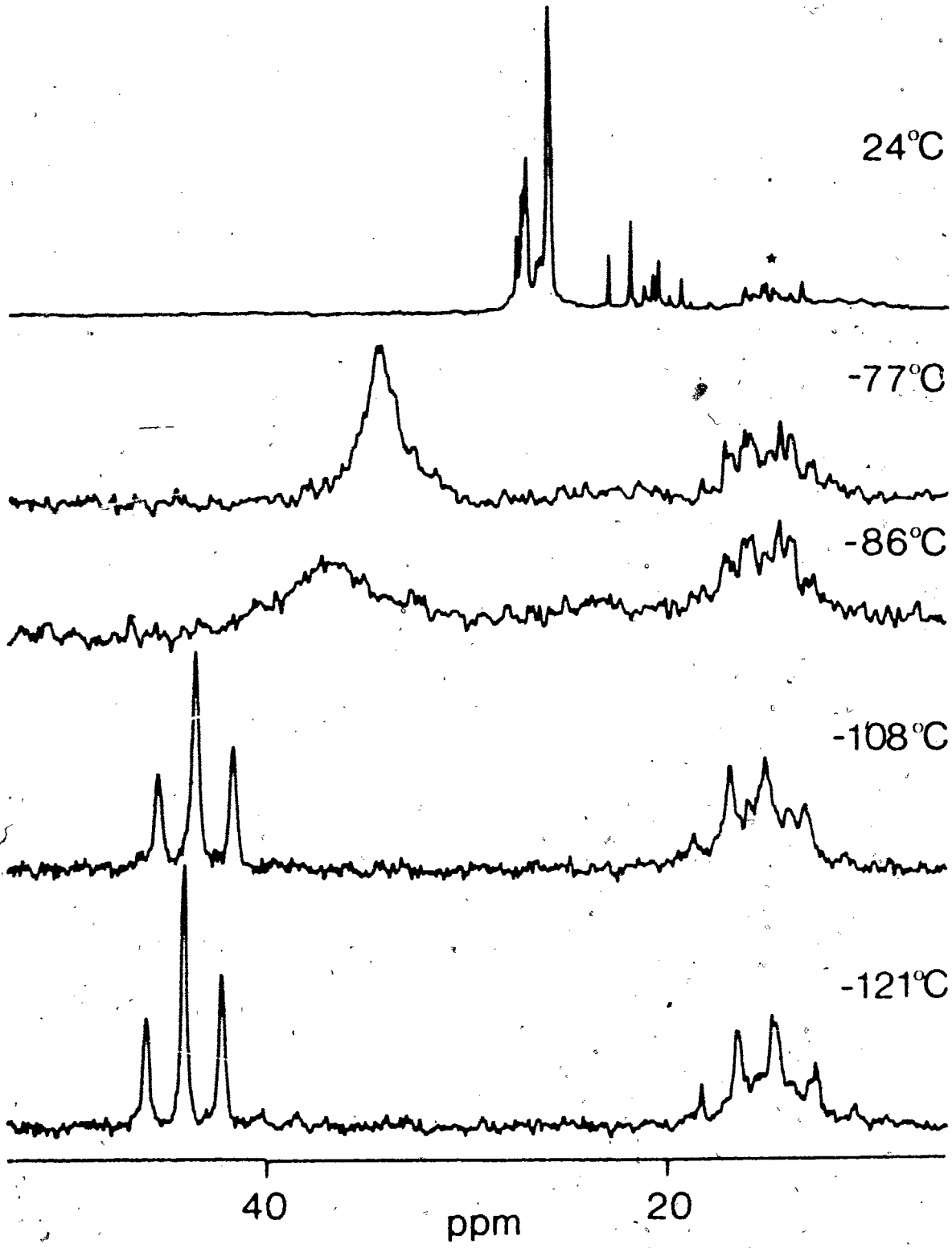

Figure 2.11 The variable temperature $^{31}P\{^{1}H\}$ NMR spectra of $Ru[P(OCH_3)_3]_4P(OC_2H_5)_3$ in $CD_2Cl_2/CHFCl_2$ (1:4) measured at 40.54 MHz. Multiplet marked with an asterisk is an impurity.

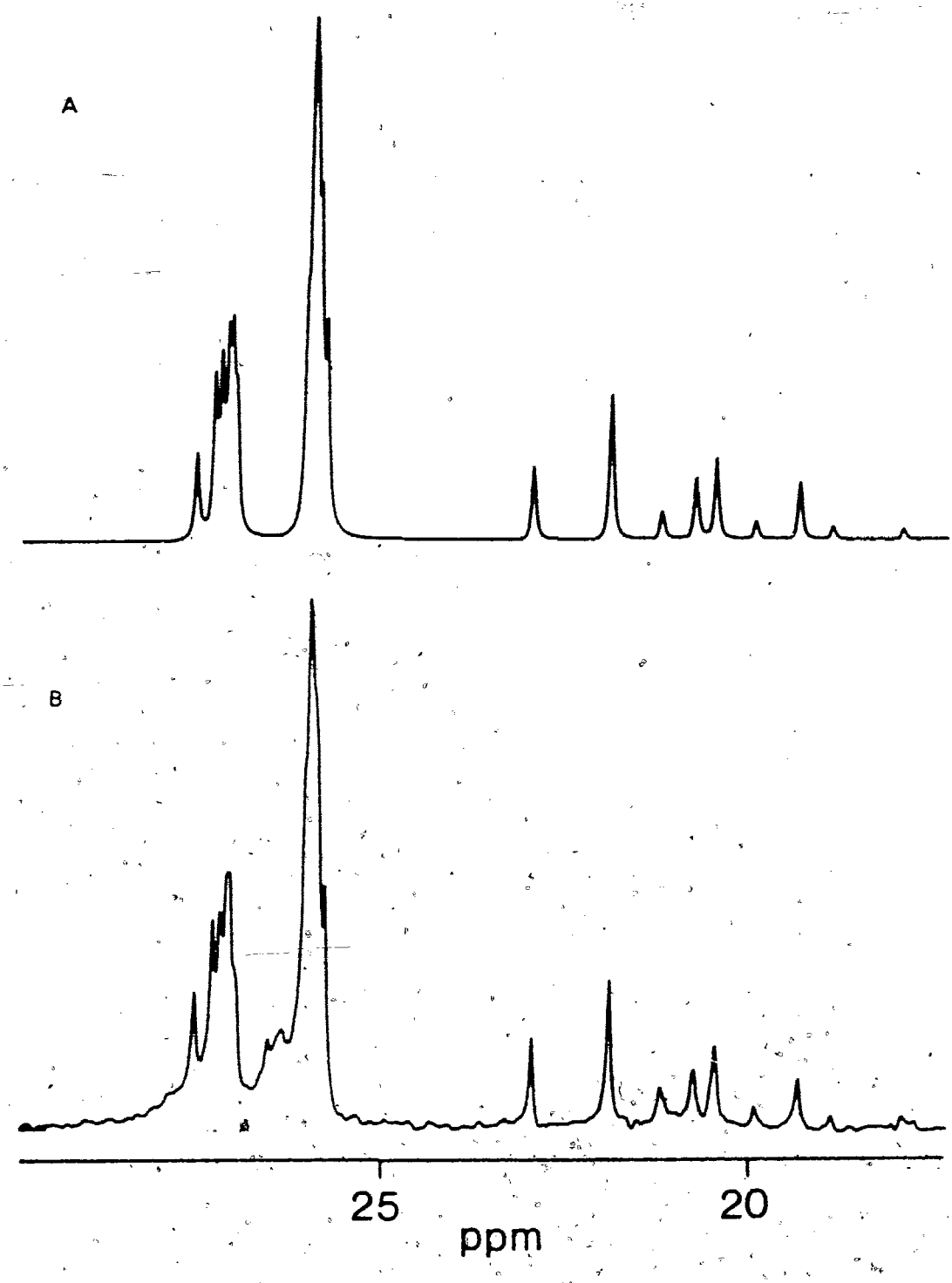

Figure 2.12 The experimental (B) and computer simulated (A) $^{31}P\{^{1}H\}$ NMR spectra of $Ru[P(OCH_3)_3]_4P(OC_2H_5)_3$ in $CD_2Cl_2/CHFCl_2$ (1:4) at 24 °C. Spectral parameters given in text.

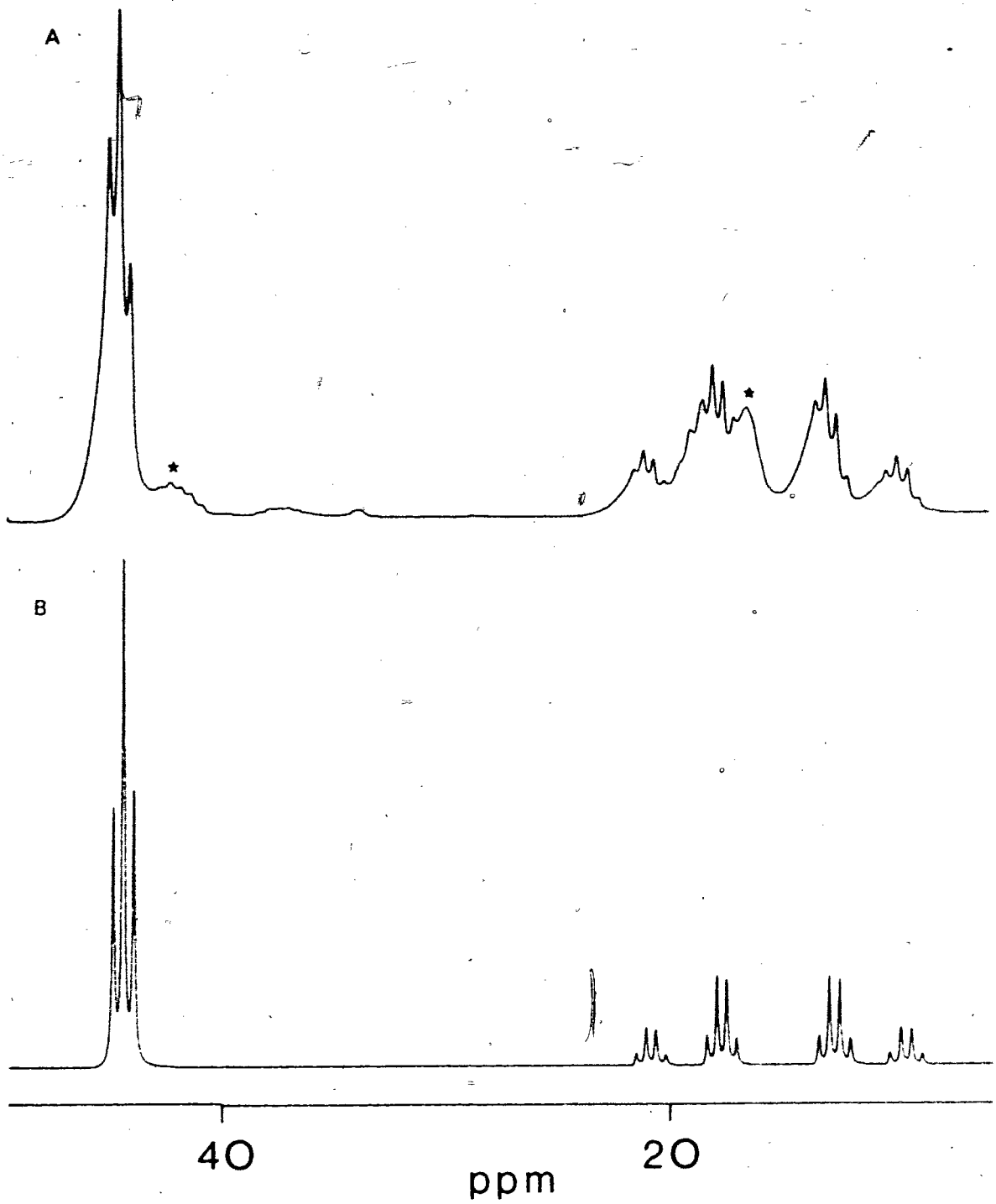

Figure 2.13 The experimental $^{31}P\{^{1}H\}$ NMR spectrum (162.0 MHz) of $Ru[P(OCH_3)_3]_4P(OC_2H_5)_3$ in $CD_2Cl_2/CHFCl_2$ (1:4) at ~-115 °C (A) and a simulation based on an A_3BC spin system (B). Spectral parameters given in text.

observed in the spectrum; this temperature was the lowest attainable on the WM-400 NMR instrument. The two resonances marked with asterisks are believed not to be due to the major isomer of $Ru[P(OCH_3)_3]_4P(OC_2H_5)_3$. Although these signals are in the frequency regions where the resonances of a minor isomer of $Ru[P(OCH_3)_3]_4P(OC_2H_5)_3$ would be expected to occur, there is no ancillary evidence to support this assignment. The simulated spectrum in figure 2.13B is based on an A_3BC spin system with the following spectral parameters: δ_A 44.3, δ_B 18.9, δ_C 11.2, J_{AB}= ±72.5 Hz, J_{AC}= ±76.9 Hz, J_{BC}= ∓514.4 Hz. Given the exchange broadened nature of the experimental spectrum and the unidentified resonances (marked with asterisks), this simulation gives a reasonably good fit. Despite numerous attempts, a calculated spectrum based on an A_2B_2C spin system (using reasonable spectral parameters) could not be found which matched the experimental spectrum (figure 2.13A). The parameters associated with the simulated spectrum in figure 2.13B are very similar to those found for the calculated 162.0 MHz spectrum of $Ru[P(OCH_3)_3]_4P(OCH_2)_3CCH_3$ (see figure 2.10A); the latter was based on an A_3BC spin system as well.

The spectral parameters associated with the simulation in figure 2.13B (i.e. 162.0 MHz data) were used to calculate the slow exchange limit $^{31}P\{^1H\}$ NMR spectrum of $Ru[P(OCH_3)_3]_4P(OC_2H_5)_3$ measured at 40.54 MHz. These are shown in figure 2.14. Considering the impurity resonances coincident with the high field multiplet of the experimental data (2.14A), the

simulated (2.14B) and experimental spectra are in close agreement.

Based on these results, the static solution structure of $Ru[P(OCH_3)_3]_4P(OC_2H_5)_3$ may be assigned as trigonal bipyramidal with the unique ligand occupying an axial coordination site. The high and low temperature limiting $^{31}P\{^1H\}$ NMR spectra of the $P(OC_2H_5)_3$ derivative (in conjunction with the corresponding variable temperature behaviour shown in figure 2.11) are consonant with axial-equatorial ligand scrambling. The temperature invariance of resonances due to added $P(OCH_3)_3$ and $P(OC_2H_5)_3$ argued against an intermolecular exchange process.

The variable temperature $^{31}P\{^1H\}$ NMR results (40.54 MHz) for $Ru[P(OCH_3)_3]_4P(OCH(CH_3)_2)_3$ were similar to those observed for the $P(OC_2H_5)_3$ analogue at the same field strength. The fast exchange limit spectrum (in toluene-d_8 at 25 °C) was due to an A_4B spin system. The spectral parameters as derived from a computer simulation were δ_B 20.0, δ_A 25.3, and J_{AB}= 52.1 Hz. An impurity multiplet similar to (and more intense than) the one described for $Ru[P(OCH_3)_3]_4P(OC_2H_5)_3$ (see figure 2.11) was also present in the $^{31}P\{^1H\}$ NMR spectrum of $Ru[P(OCH_3)_3]_4P(OCH(CH_3)_2)_3$. As the temperature was reduced, the $^{31}P\{^1H\}$ NMR spectrum of the triisopropyl phosphite derivative underwent collapse and resolution. The slow exchange limit spectrum of this sample was reached at -130 °C. As for the case of the $P(OC_2H_5)_3$ derivative, the impurity made accurate spectral simulation of the high field resonances (δ ~15) due to

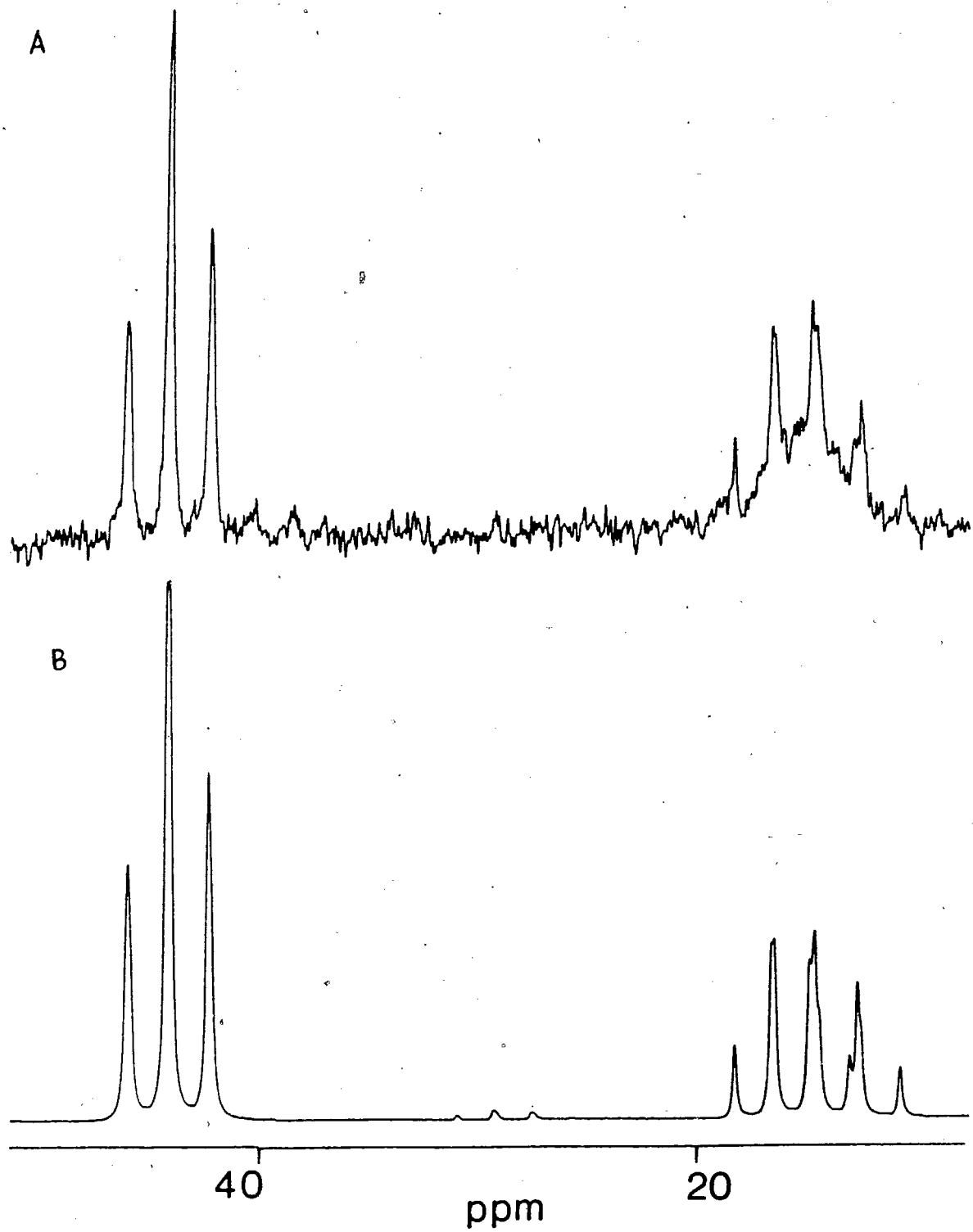

Figure 2.14 The experimental $^{31}P\{^{1}H\}$ NMR spectrum (A) of $Ru[P(OCH_3)_3]_4P(OC_2H_5)_3$ at -121 °C (40.54 MHz) and a computer simulated spectrum (B) based on an A_3BC spin system. Spectral parameters given in text.

$Ru[P(OCH_3)_3]_4P(OCH(CH_3)_2)_3$ difficult. The low field resonances in this spectrum of $Ru[P(OCH_3)_3]_4P(OCH(CH_3)_2)_3$, however, were very similar to those in the slow exchange, $^{31}P\{^1H\}$ NMR spectrum of the $P(OC_2H_5)_3$ analogue: a broad, apparent triplet was observed at δ 37.1 (see figure 2.11).

The low temperature $^{31}P\{^1H\}$ NMR spectrum of $Ru[P(OCH_3)_3]_4P(OCH(CH_3)_2)_3$ (in $CD_2Cl_2/CHFCl_2$ (1:4)) was measured at 162.0 MHz in an effort to elucidate the static solution structure of the complex. This spectrum (at ~-115 °C) was of little use in this regard. The resonances were even more exchange broadened than those of the corresponding spectra for $Ru[P(OCH_3)_3]_4L$ (L= $P(OCH_2)_3CCH_3$, $P(OC_2H_5)_3$). The spectrum of the $P(OCH(CH_3)_2)_3$ analogue did, however, share several qualitative features with the corresponding data for the $P(OC_2H_5)_3$ and $P(OCH_2)_3CCH_3$ derivatives (both with axial substitution): the former spectrum revealed a triplet (broad and ill-resolved) at δ ~37 and a quartet of very broad multiplets at δ ~15. The broad nature of these resonances made a spectral simulation impractical.

The available data does not allow a confident assignment of the static solution structure for $Ru[P(OCH_3)_3]_4P(OCH(CH_3)_2)_3$. There was, however, a qualitative similarity between the $^{31}P\{^1H\}$ NMR spectra (40.54 and 162.0 MHz) of the triisopropyl phosphite derivative and the corresponding data for the $P(OC_2H_5)_3$ congener. This provides some evidence for a tentative assignment: a trigonal bipyramidal structure is most likely for

$Ru[P(OCH_3)_3]_4P(OCH(CH_3)_2)_3$ at low temperatures, with the $P(OCH(CH_3)_2)_3$ ligand in an axial position. The variable temperature $^{31}P\{^1H\}$ NMR spectra of this complex appear to be in accord with the transformation of the slow exchange limit spin system into an A_4B spin system via an axial-equatorial ligand scrambling process.

The variable temperature $^{31}P\{^1H\}$ NMR spectra of $Ru[P(OCH_3)_3]_4P(OC_6H_5)_3$ in $CD_2Cl_2/CHFCl_2$ (1:4) (measured at 40.54 MHz) are shown in figure 2.15. Note the broad, ill-resolved multiplet at δ ~12 of the -124 °C spectrum; despite several alumina filtrations, the impurity causing this resonance could not be removed. The weak, high field singlet in the -12 °C spectrum is due to a small amount of free $P(OC_6H_5)_3$. Several purification attempts also failed to remove the last traces of this excess ligand from the reaction mixture. In the fast exchange limit, the $^{31}P\{^1H\}$ NMR spectrum (-12 °C) of $Ru[P(OCH_3)_3]_4P(OC_6H_5)_3$ reveals resonances due to an A_4X spin system. The spectral parameters are δ_X -6.1, δ_A 24.6, and J_{AX}= 49 Hz. The slow exchange limit $^{31}P\{^1H\}$ NMR data (-124 °C) reveals a spectrum considerably different from the analogous spectra for $Ru[P(OCH_3)_3]_4L$ (L= $P(OCH_2)_3CCH_3$ and $P(OC_2H_5)_3$). This experimental $^{31}P\{^1H\}$ NMR spectrum of $Ru[P(OCH_3)_3]_4P(OC_6H_5)_3$ at -124 °C was successfully simulated based on an A_2B_2C spin system; the results are shown in figure 2.16. The associated spectral parameters are δ_A 31.5, δ_B 20.8, δ_C -4.2, J_{AB}= ±74.7 Hz, J_{AC}= ∓179.1 Hz, and J_{BC}= ±81.4 Hz. The fact that both J_{AB}

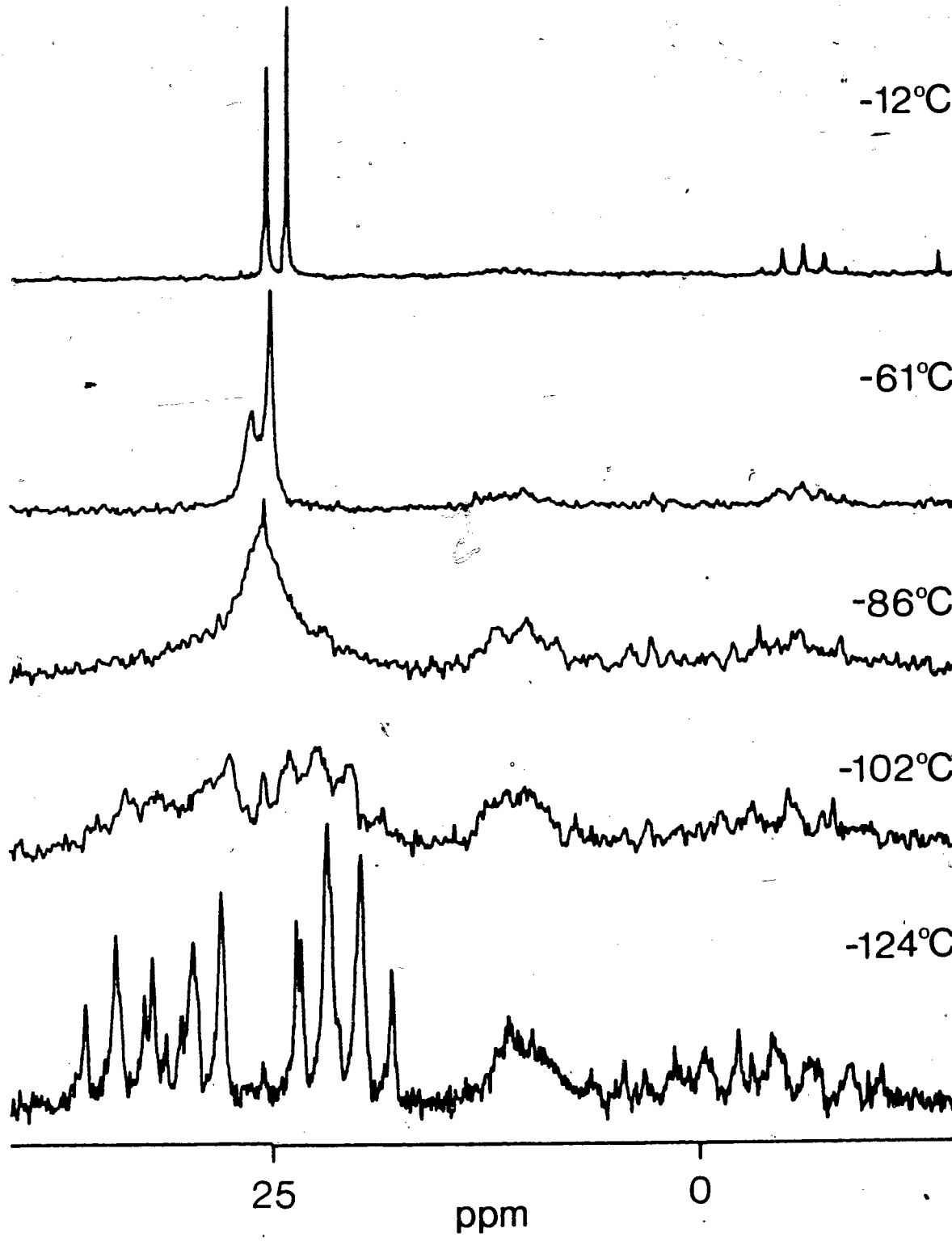

Figure 2.15 The variable temperature $^{31}P\{^{1}H\}$ NMR spectra of $Ru[P(OCH_3)_3]_4P(OC_6H_5)_3$ in $CD_2Cl_2/CHFCl_2$ (1:4) measured at 40.54 MHz. The broad, ill-resolved multiplet at δ ~12 is an impurity.

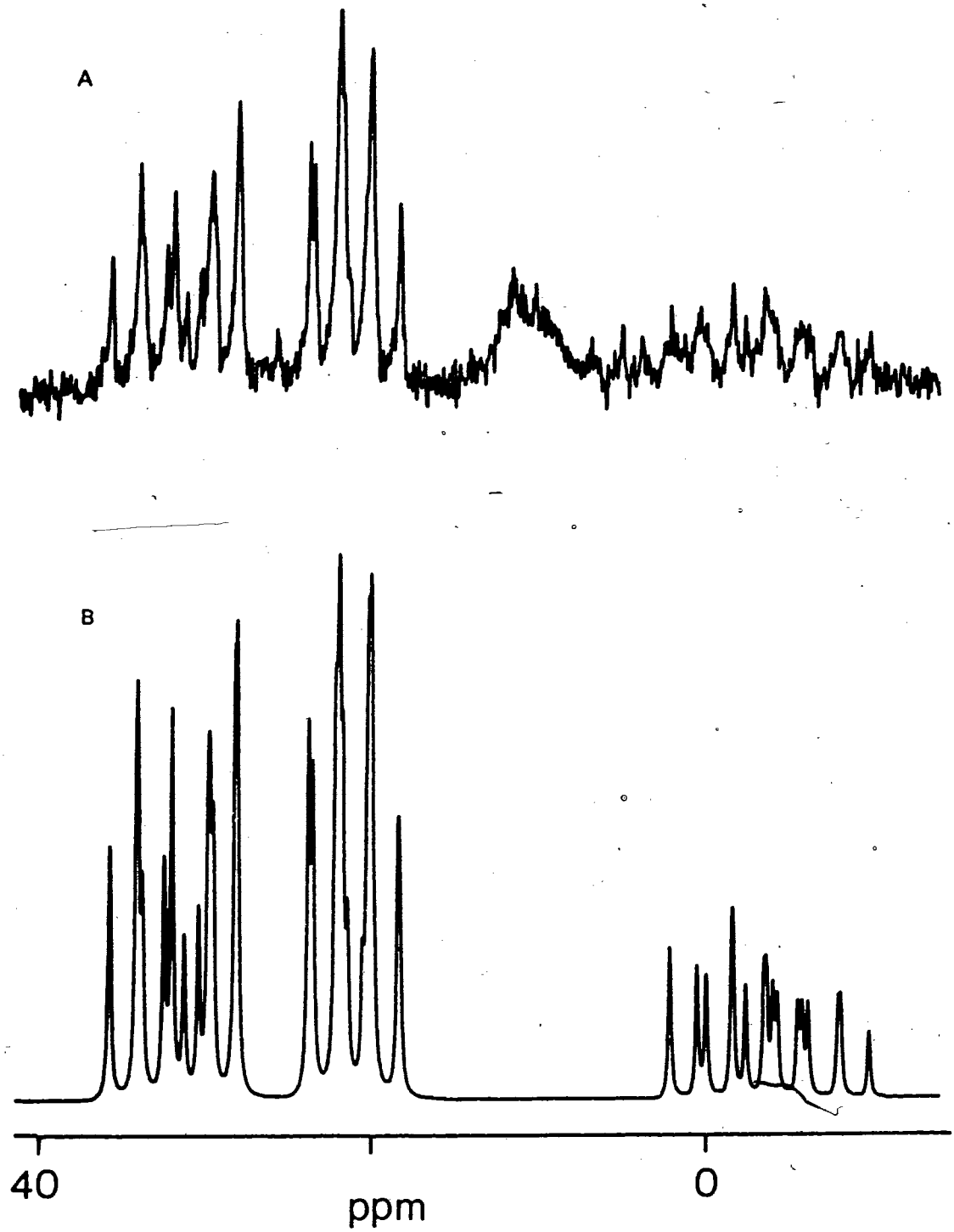

Figure 2.16 The experimental $^{31}P\{^{1}H\}$ NMR spectrum of $Ru[P(OCH_3)_3]_4P(OC_6H_5)_3$ in $CD_2Cl_2/CHFCl_2$ (1:4) at -124 °C (A) and a computer simulation based on an A_2B_2C spin system. Spectral parameters given in text.

and J_{BC} are of opposite sign to J_{AC} is noted. Numerous attempts to simulate the experimental spectrum based on an A_3BC spin system were unsuccessful. The evidence is consistent with $Ru[P(OCH_3)_3]_4P(OC_6H_5)_3$ adopting a static, trigonal bipyramidal structure in solution with the aryl phosphite in an equatorial position (figure 2.8B). The possibility of the impurity multiplet (δ ~12, see figure 2.15) being due to a minor isomer of $Ru[P(OCH_3)_3]_4P(OC_6H_5)_3$ is discounted. The resonances of such an isomer would be expected to clearly collapse into the baseline as a result of the intramolecular exchange process; it may be observed that this is not the case. Further support for the contention that the slow exchange limit $^{31}P\{^1H\}$ NMR spectrum of $Ru[P(OCH_3)_3]_4P(OC_6H_5)_3$ reflects an A_2B_2C spin system may be obtained by examining averaged coupling constants due to the observed axial-equatorial phosphite exchange (see figure 2.15). The spectrum in question did not exhibit any resonances due to a minor isomer; this suggests that the concentration of such an isomer (if present) must be considerably less than that of the major (i.e. equatorial) species. Under these conditions the coupling constant in the fast exchange limit (i.e. J_{AX}) should approximately reflect the average of the appropriate coupling constants from the slow exchange limiting spectrum. The weighted average of J_{AC} and J_{BC} is 48.9 Hz, which compares very well with J_{AX} in the fast exchange limit (49.0 Hz).

In summary, the slow exchange limit $^{31}P\{^1H\}$ NMR spectrum of $Ru[P(OCH_3)_3]_4P(OC_6H_5)_3$ (figure 2.16) is in accord with a

trigonal bipyramidal static solution structure with the unique ligand in an equatorial site. The changes to the spectrum with increased temperature indicate the operation of an axial-equatorial phosphite exchange process.

The $^{31}P\{^{1}H\}$ NMR spectrum of $Ru[P(OCH_3)_3]_4PF_3$ in $CD_2Cl_2/CHFCl_2$ (1:4) at -23 °C is shown in figure 2.17. Two sets of impurity signals are marked with asterisks. This spectrum may be analyzed in terms of an A_4MX_3 spin system, where fast axial-equatorial phosphite exchange renders the four $P(OCH_3)_3$ ligands (i.e. A) equivalent. The resonances due to these groups appear as an overlapping doublet of quartets (δ_A 26.3, J_{PP}= 48.4 Hz, $J_{PF}\simeq$ 25 Hz). The resonances due to the PF_3 ligand (M) may be approximately described as a quartet of quintets (δ_M -1.4, J_{PF}= 1365 Hz, $J_{PP}\simeq$ 49 Hz), although second order effects are evident. The outer quintets of this resonance are also very weak.

The slow exchange limit $^{31}P\{^{1}H\}$ NMR spectrum of $Ru[P(OCH_3)_3]_4PF_3$ in $CD_2Cl_2/CHFCl_2$ (1:4) was obtained at -129 °C. The spectrum, as anticipated, was complex. Spectral analysis was further hampered by the two impurity signals (see figure 2.17) which obscured one of the inner PF_3 resonances. The portion of the slow exchange limit $^{31}P\{^{1}H\}$ NMR spectrum due to the $P(OCH_3)_3$ ligands (i.e. the A_2B_2 part) is shown in figure 2.18 (A) with a partial simulation based on an $A_2B_2CX_3$ spin system (B). The spectral parameters are δ_A 40.0, δ_B 24.8, δ_C 0, J_{AB}= ±75.5 Hz, J_{AC}= ∓182.4 Hz, J_{BC}= ±90.1 Hz, J_{AX}= ∓44 Hz, J_{BX}= ±10 Hz, and J_{CX}= ±1000 Hz. The fact that most of the major resonances in the

region spanned by figure 2.18 were composed of numerous component transitions made assignments difficult; the iterative capability of the PANIC simulation program (see chapter 2 experimental section) was of little use in obtaining a better fit.

Based on the previous results for $Ru[P(OCH_3)_3]_4L$ (L= $P(OCH_2)_3CCH_3$, $P(OC_2H_5)_3$, $P(OCH(CH_3)_2)_3$, $P(OC_6H_5)_3$), the two most likely structures for $Ru[P(OCH_3)_3]_4PF_3$ are those represented by A and B in figure 2.8. The former represents an A_3BCX_3 spin system while the latter reflects an $A_2B_2CX_3$ system. Despite extensive efforts the partial, slow exchange limit $^{31}P\{^1H\}$ NMR spectrum of $Ru[P(OCH_3)_3]_4PF_3$ could not be even qualitatively simulated based on an A_3BCX_3 spin system. In addition, the values of J_{AB}, J_{AC}, and J_{BC} derived from the $A_2B_2CX_3$ simulation for $Ru[P(OCH_3)_3]_4PF_3$ (±75.5, ∓182.4, and ±90.1 Hz, respectively) are very similar to the corresponding values for $Ru[P(OCH_3)_3]_4P(OC_6H_5)_3$ (±74.7, ∓179.1, and ±81.4 Hz, respectively); the slow exchange limit $^{31}P\{^1H\}$ NMR spectrum of the latter complex was convincingly shown to be due to an A_2B_2C spin system.

A consideration of averaged coupling constants reveals additional evidence in support of an $A_2B_2CX_3$ spin system for $Ru[P(OCH_3)_3]_4PF_3$. As was the case for $Ru[P(OCH_3)_3]_4P(OC_6H_5)_3$, the slow exchange limiting $^{31}P\{^1H\}$ NMR spectrum of $Ru[P(OCH_3)_3]_4PF_3$ exhibited no resonances assignable to a minor isomer; the weighted average of the appropriate static coupling

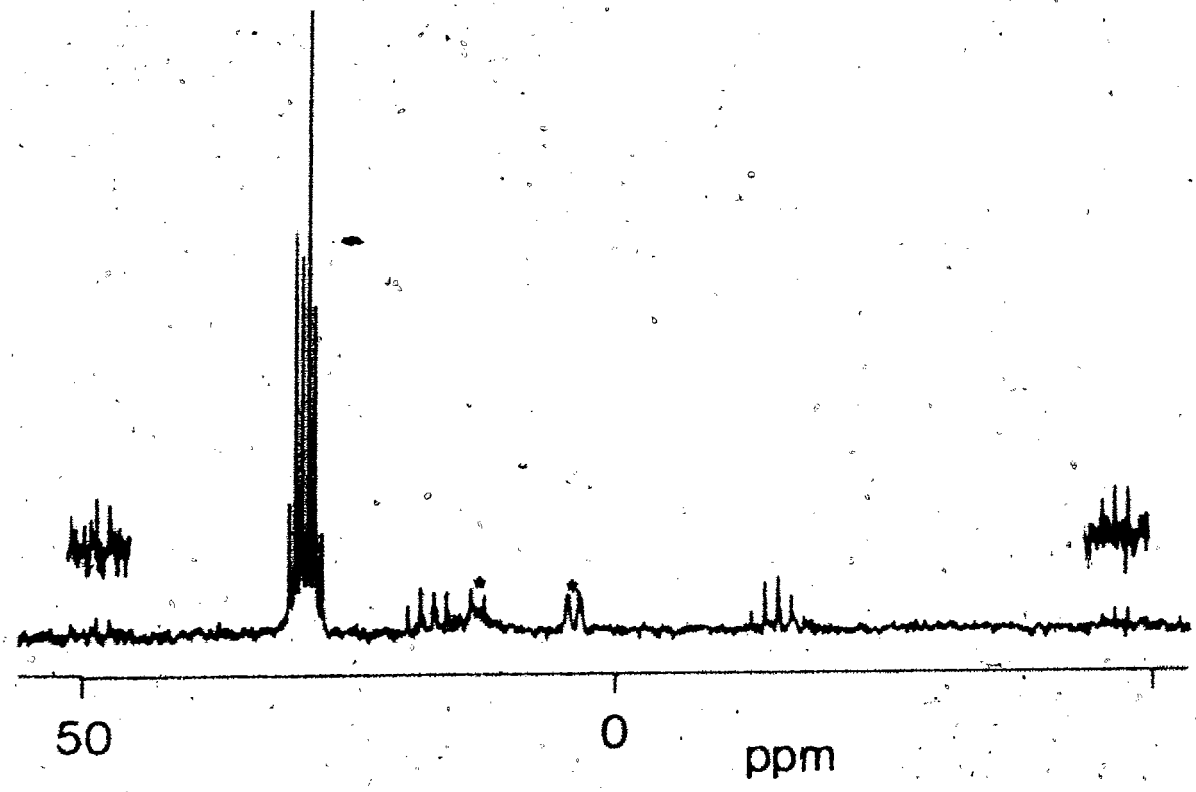

Figure 2.17 The $^{31}P\{^{1}H\}$ NMR spectrum of $Ru[P(OCH_3)_3]_4PF_3$ in $CD_2Cl_2/CHFCl_2$ (1:4) at -23 °C. The resonances marked with asterisks are due to impurities.

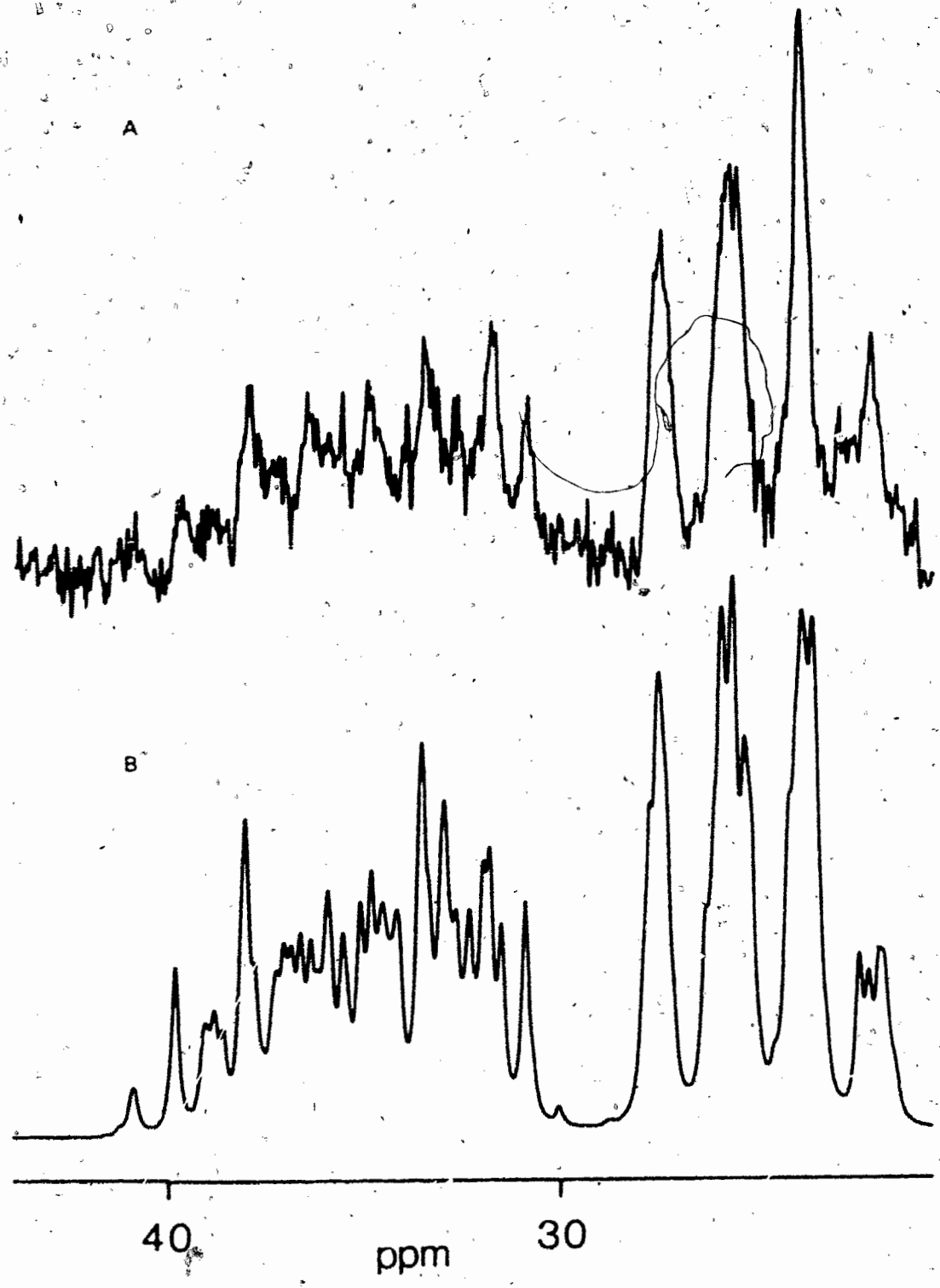

Figure 2.18 A partial $^{31}P\{^{1}H\}$ NMR spectrum of $Ru[P(OCH_3)_3]_4PF_3$ in $CD_2Cl_2/CHFCl_2$ (1:4) at -129 °C (40.54 MHz) (A) and a partial simulation (B) based on an $A_2B_2CX_3$ spin system. Spectral parameters given in text.

constants should therefore reflect the corresponding fast exchange limit value. The weighted average of J_{AX} and J_{BX} from the spectral parameters of the $A_2B_2CX_3$ simulation (27 Hz) agrees well with J_{AX} in the fast exchange limit (~25 Hz). The weighted average of J_{AC} and J_{BC} from the slow exchange limit spectrum is 46.2 Hz; this value is in good agreement with that of J_{AM} found from the high temperature limiting spectrum (48.4 Hz).

The available evidence thus supports the contention that the static solution structure of $Ru[P(OCH_3)_3]_4PF_3$ is trigonal bipyramidal with the unique ligand in an equatorial site (figure 2.8B). The variable temperature $^{31}P\{^1H\}$ NMR data for this complex is again consistent with scrambling of the ligands between axial and equatorial sites.

The variable temperature $^{31}P\{^1H\}$ NMR spectra of $Ru[P(OCH_3)_3]_4P(CH_3)_2C_6H_5$ in $CD_2Cl_2/CHFCl_2$ (1:4) (40.54 MHz) are shown in figure 2.20. The spectrum at 6 °C is near (but not in) the fast exchange limit and represents an A_4X spin system with δ_A 25.4, δ_X -127.9, and J_{AX}= 24.4 Hz.

The $^{31}P\{^1H\}$ NMR spectrum of $Ru[P(OCH_3)_3]_4P(CH_3)_2C_6H_5$ at -104 °C is in the slow exchange limit. This spectrum was successfully simulated on the basis of an A_3BX spin system; the experimental (B) and computer generated (A) spectra are shown in figure 2.19. The spectral parameters are δ_A 32.9, δ_B 17.0, δ_X -130.5, J_{AB}= ±74.7 Hz, J_{AX}= ±64.7 Hz, and J_{BX}= ∓292.4 Hz. Based on previous arguments, the weighted average of J_{AX} and J_{BX} (in the slow

exchange limit) should agree with J_{AX} in the fast exchange limit; these values are 24.6 and 24.4 Hz, respectively. These results are consonant with a trigonal bipyramidal structure for $Ru[P(OCH_3)_3]_4P(CH_3)_2C_6H_5$ in solution with the phosphine ligand occupying an axial site (figure 2.8A).

The variable temperature $^{31}P\{^1H\}$ NMR spectra of $Ru[P(OCH_3)_3]_4P(CH_3)_2C_6H_5$ (figure 2.20) reveal a novel feature. The inner two lines in the X part of the slow exchange limit spectrum (-104 °C) are temperature invariant; they remain sharp while the balance of the spectrum collapses as the temperature is increased. These two resonances eventually become the outer two lines of the X quintet in the fast exchange limit, A_4X spectrum.

Although a theoretical treatment of the general A_nBX_m has been undertaken [56], the exact nature of the eigenfunctions describing the system were not given; these are difficult to write in a closed form and contain linear combinations of symmetrized product functions. One may, however, speculate on the general form of the functions describing the spin states involved in the transitions for the two invariant lines. They must be of the form $|\alpha_A\alpha_A\alpha_A\alpha_B\alpha_X\rangle \longrightarrow |\alpha_A\alpha_A\alpha_A\alpha_B\beta_X\rangle$ and $|\beta_A\beta_A\beta_A\beta_B\beta_X\rangle \longrightarrow |\beta_A\beta_A\beta_A\beta_B\alpha_X\rangle$. This would explain the invariance of the two X transitions to the exchange process: the lower spin state is unaffected by nuclear permutation (i.e. a change in spin labels). The theoretical treatment yields some further information on an A_nBX_m spin system. The X transitions of such a

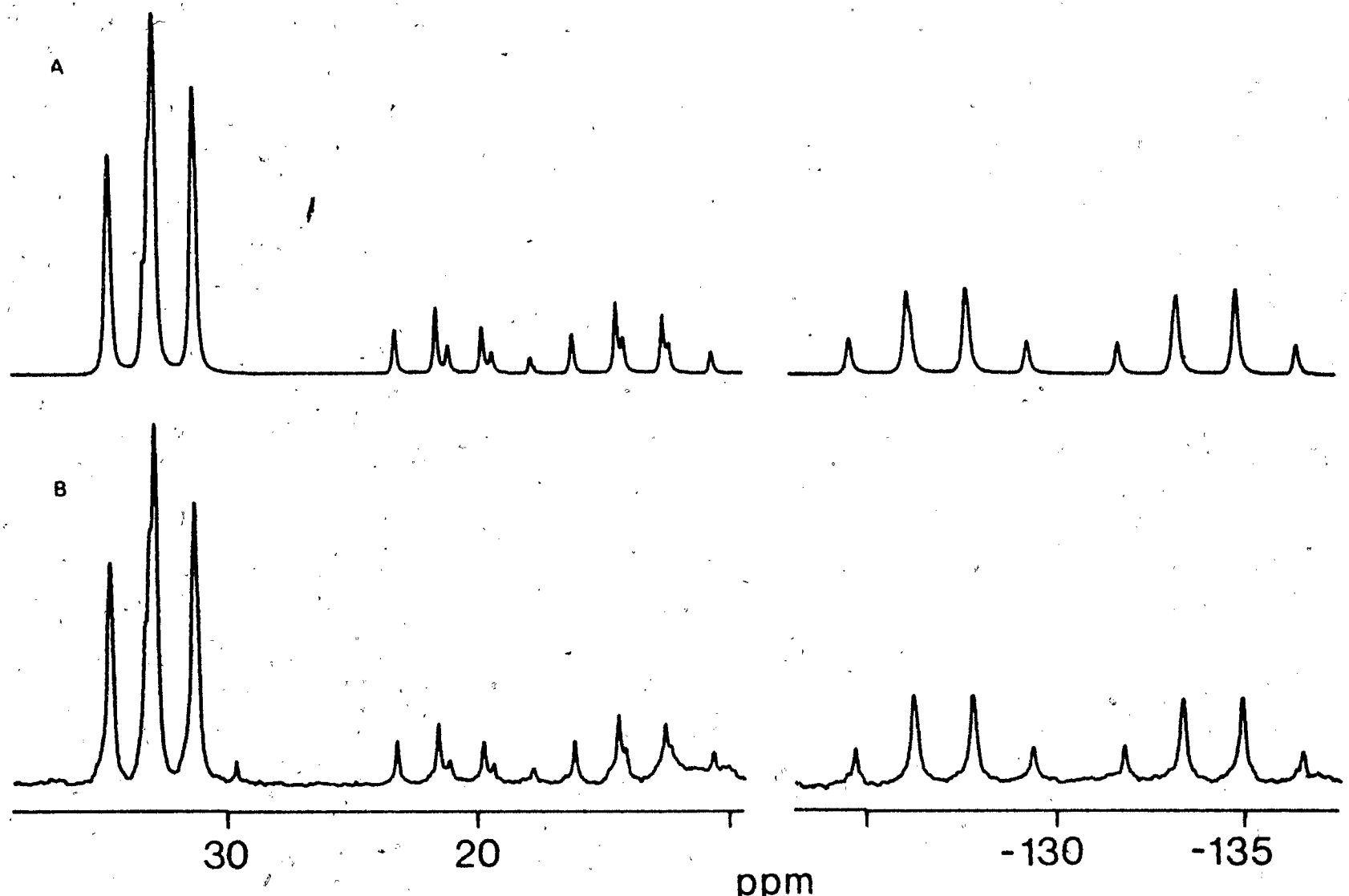

Figure 2.19 The experimental $^{31}P\{^{1}H\}$ NMR spectrum of $Ru[P(OCH_3)_3]_4P(CH_3)_2C_6H_5$ in $CD_2Cl_2/CHFCl_2$ (1:4) at -104 °C (B) and a computer simulation (A) based on an A_4BX spin system. Spectral parameters given in text.

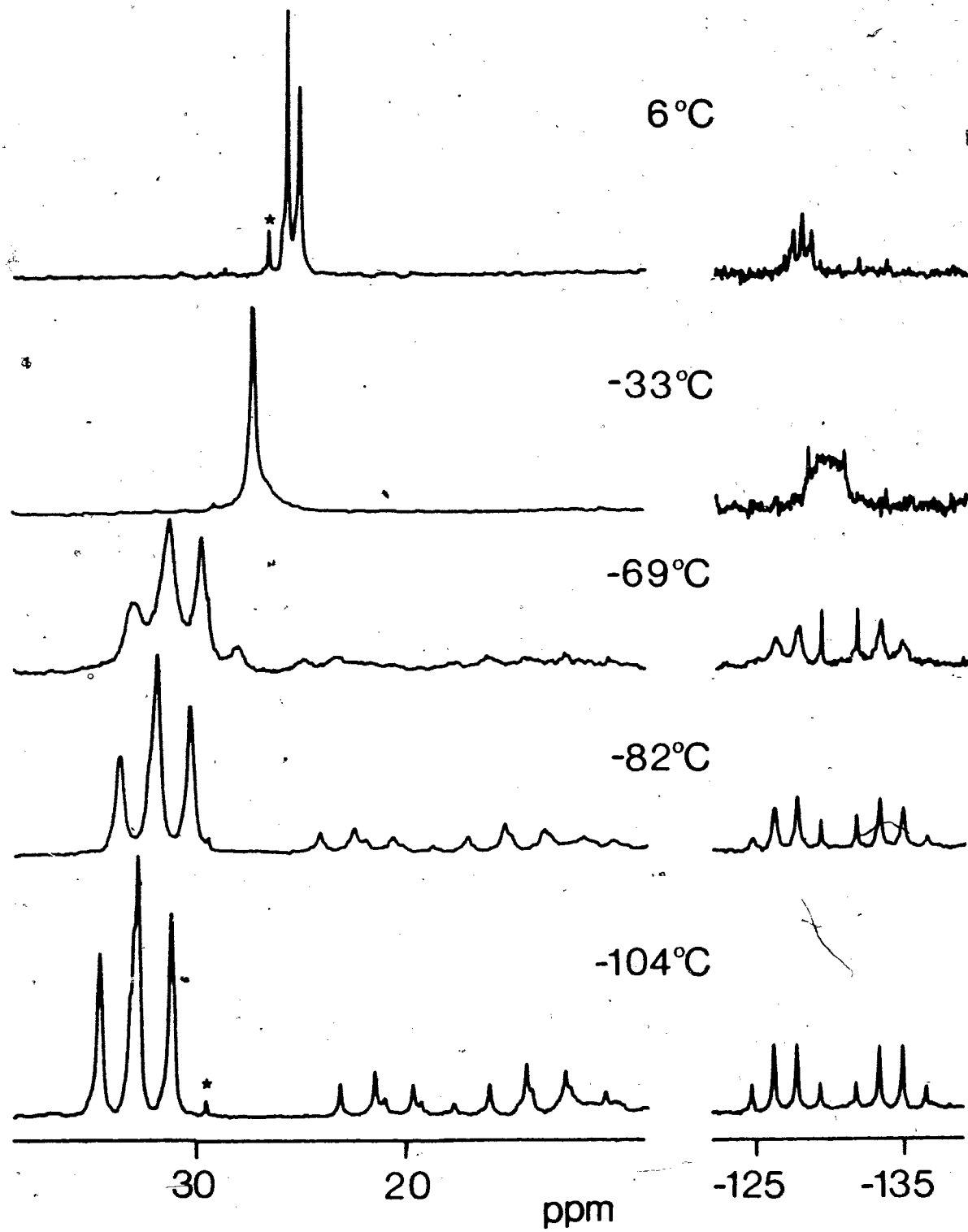

Figure 2.20 The variable temperature $^{31}P\{^{1}H\}$ NMR spectra of $Ru[P(OCH_3)_3]_4P(CH_3)_2C_6H_5$ in $CD_2Cl_2/CHFCl_2$ (1:4) measured at 40.54 MHz. The resonance marked with an asterisk is due to an $Ru[P(OCH_3)_3]_5$ impurity.

system are symmetrical about the frequency ν_X. In particular, the inner two lines are separated by a frequency of $2I_A J_{AX} + J_{BX}$ ($I_A = 3[1/2]$) and are independent of the applied field strength; the values of J_{AX} and J_{BX} from the spectral simulation and the frequency separation of the two inner lines from the experimental spectrum of $Ru[P(OCH_3)_3]_4P(CH_3)_2C_6H_5$ (at -104 °C) are consistent with the former requirement of this spin system.

In summary, the variable temperature $^{31}P\{^1H\}$ NMR data for $Ru[P(OCH_3)_3]_4P(CH_3)_2C_6H_5$ is consistent with an axially substituted, trigonal bipyramidal structure (in the slow exchange limit) undergoing phosphorus ligand scrambling as the temperature is increased.

The variable temperature $^{31}P\{^1H\}$ NMR spectra of $Ru[P(OCH_3)_3]_4P(CH_3)_3$ in toluene-d_8 measured at 162.0 MHz are shown in figure 2.22. The corresponding 40.54 MHz data for $Ru[P(OCH_3)_3]_4P(CH_3)_3$ was quite complex; small chemical shift differences in the slow exchange limit led to a tightly coupled spectrum which was difficult to analyze. A singlet due to an $Ru[P(OCH_3)_3]_5$ impurity is marked with an asterisk in figure 2.22. The fast exchange limit spectrum (76 °C) is consonant with previous findings for the $Ru[P(OCH_3)_3]_4L$ derivatives: rapid axial-equatorial ligand exchange results in a spectrum due to an A_4X spin system in this case (δ_A 24.8, δ_X -134.5, J_{AX} = 23 Hz).

The slow exchange limit $^{31}P\{^1H\}$ NMR spectrum was obtained at -75 °C. This was successfully simulated assuming an A_3BX spin

system. The experimental (A) and simulated (B) spectra are shown in figure 2.21. The spectral parameters derived from the simulated spectrum are as follows: δ_A 26.5, δ_B 31.0, δ_X -132.7, J_{AB} ±71.5 Hz, J_{AX}= ±67.9 Hz, and J_{BX}= ∓290.1 Hz. Based on previous arguments, the weighted average of J_{AX} and J_{BX} (in the slow exchange limit) should agree with J_{AX} in the fast exchange limit; these values are 21.6 and 23 Hz, respectively. The static solution structure of $Ru[P(OCH_3)_3]_4P(CH_3)_3$ is thus assigned as that shown in figure 2.8A, where the phosphine occupies an axial site.

The variable temperature $^{31}P\{^1H\}$ NMR behaviour of $Ru[P(OCH_3)_3]_4P(CH_3)_3$ is similar to that observed for $Ru[P(OCH_3)_3]_4P(CH_3)_2C_6H_5$. As the temperature is increased, the slow exchange A_3BX pattern collapses and coalesces to one due to an A_4X spin system. The inner lines of the X quartets are unbroadened during this process (as observed for the $P(CH_3)_2C_6H_5$ analogue) and become the outer lines of the high field quintet. In light of the previous discussion, these two resonances should be separated by a frequency of $3J_{AX} + J_{BX}$. The values of J_{AX} and J_{BX} obtained from the simulation and the experimental frequency separation of the lines in question are in agreement with this condition. The requirement that the frequency separation of these two resonances be independent of the applied field could not be tested precisely; the data measured at 40.54 MHz revealed a spin system where the X approximation was not totally valid. The frequency separation of the two lines from this spectrum

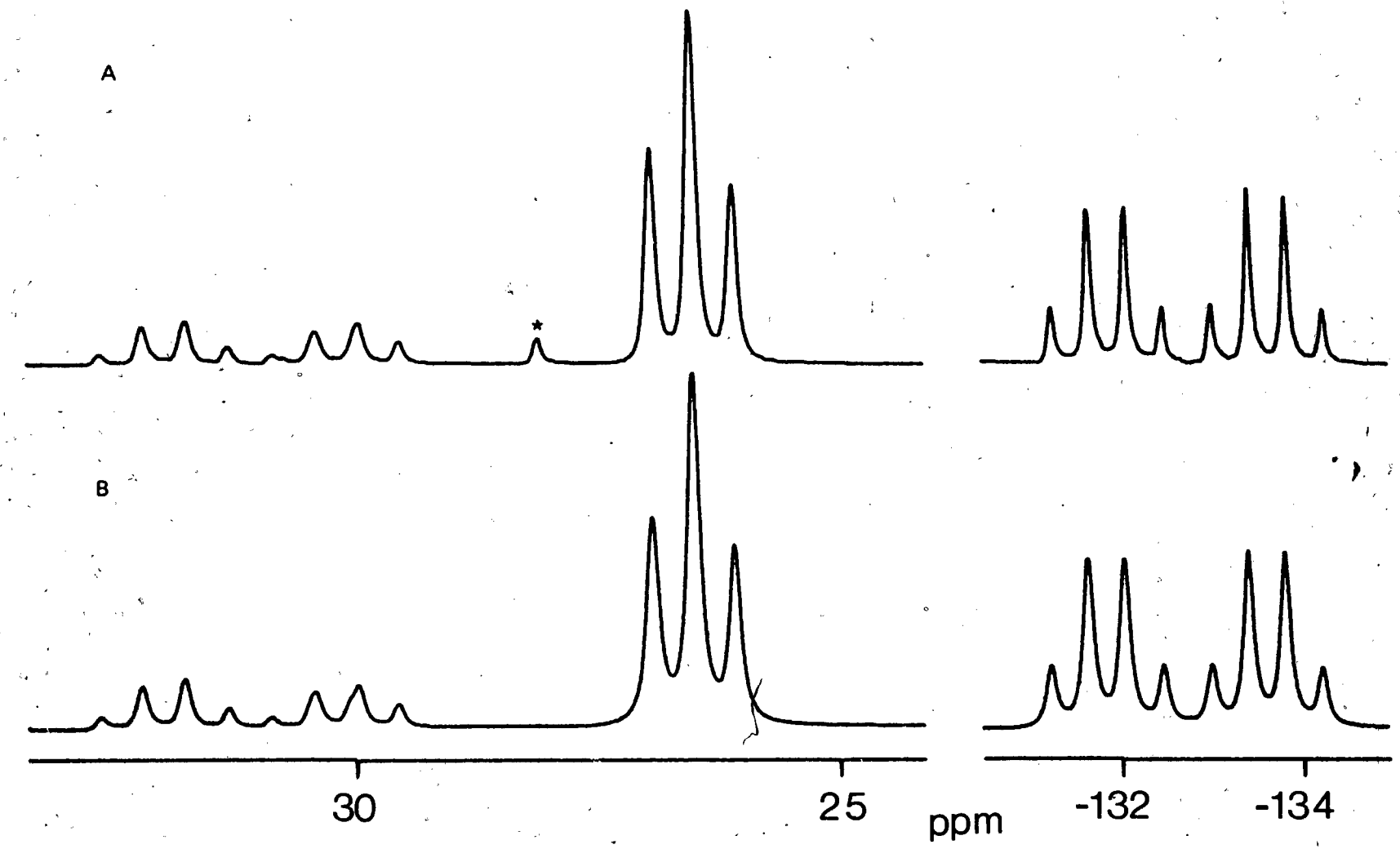

Figure 2.21 The experimental $^{31}P\{^{1}H\}$ NMR spectrum of $Ru[P(OCH_3)_3]_4P(CH_3)_3$ in toluene-d_8 at -75 °C (A) and a computer simulation (B) based on an A$_3$BX spin system. The experimental spectrum was measured at 162.0 MHz. Spectral parameters given in text.

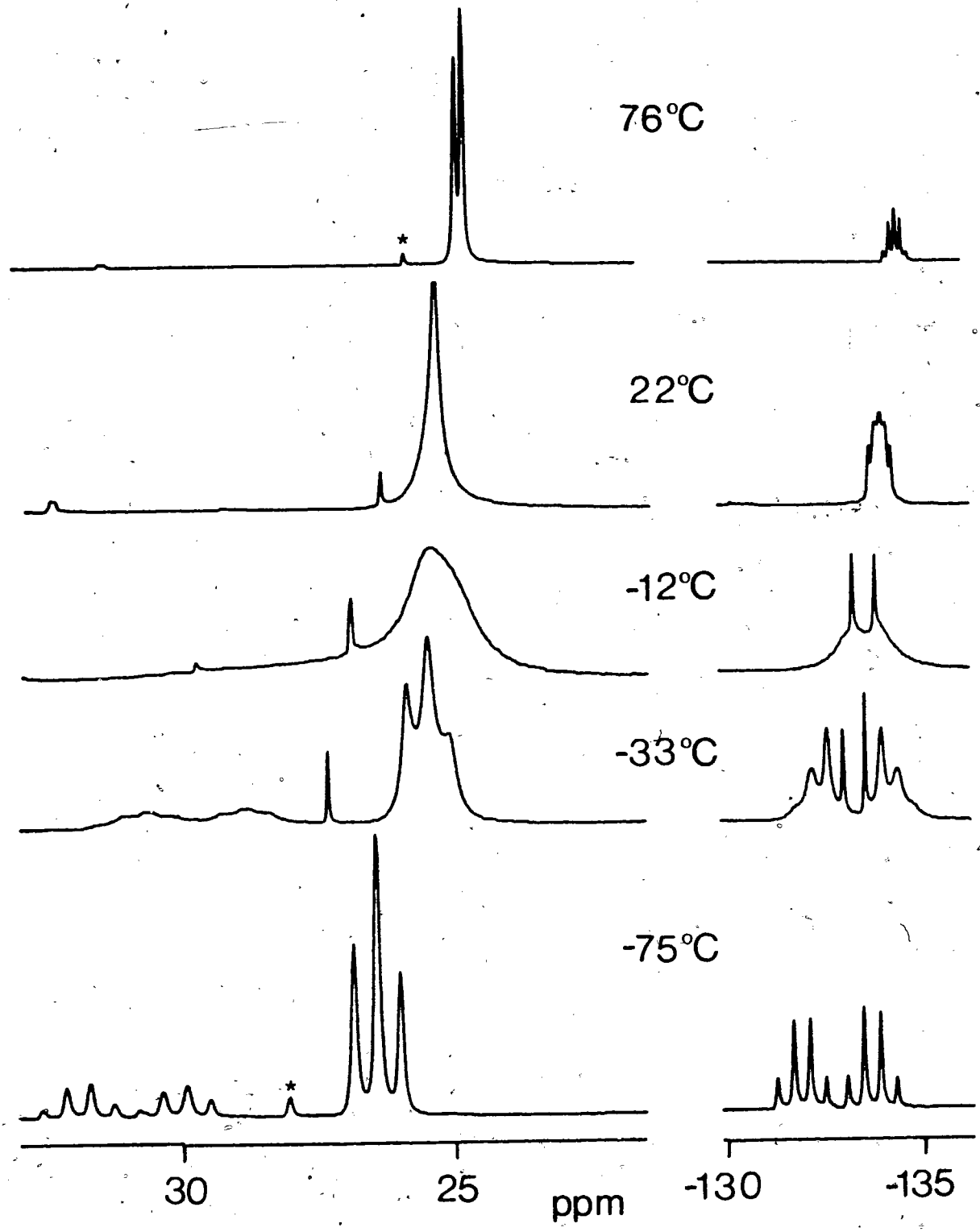

Figure 2.22 The variable temperature $^{31}P\{^{1}H\}$ NMR spectra of $Ru[P(OCH_3)_3]_4P(CH_3)_3$ in toluene-d_8 measured at 162.0 MHz. The signal marked with an asterisk is due to an $Ru[P(OCH_3)_3]_5$ impurity.

(85.8 Hz), however, was in reasonable agreement with the corresponding value obtained from the 162.0 MHz data (86.4 Hz).

One other aspect of the slow exchange limit $^{31}P\{^1H\}$ NMR spectrum of $Ru[P(OCH_3)_3]_4P(CH_3)_3$ is worthy of mention: the resonances due to the axial $P(OCH_3)_3$ ligands are at lower field than those due to their equatorial counterparts. All of the other $Ru[P(OCH_3)_3]_4L$ derivatives discussed in this thesis exhibit the opposite behaviour. The precise reason for this anomaly is unclear, although the electronic properties of the trimethyl phosphine ligand likely play a key role. Of the ligands L used in the $Ru[P(OCH_3)_3]_4L$ derivatives, $P(CH_3)_3$ has the smallest value of the electronic parameter (2064.1 cm^{-1} [11]). It is generally considered a very basic ligand with poor π-acceptor properties.

The variable temperature $^{31}P\{^1H\}$ NMR spectra of $Ru[P(OCH_3)_3]_4P(CH_3)_3$ are in accord with axial-equatorial ligand exchange. This process causes transformation of the slow exchange limit A_3BX pattern into a spectrum due to an A_4X spin system.

The variable temperature $^{31}P\{^1H\}$ NMR spectra of $Ru[P(OCH_3)_3]_4Sb(CH_3)_3$ in $CD_2Cl_2/CHFCl_2$ (1:4) (40.54 MHz) are shown in figure 2.23. The spectral analysis for the trimethyl stibine derivative was considerably more straightforward than for the other $Ru[P(OCH_3)_3]_4L$ complexes. Neither of the two stable isotopes of antimony have I= 1/2. The fast exchange limit

spectrum of $Ru[P(OCH_3)_3]_4Sb(CH_3)_3$ (-12 °C) reveals a single line, consistent with rapid axial-equatorial ligand exchange. The low temperature limiting $^{31}P\{^1H\}$ NMR spectrum of $Ru[P(OCH_3)_3]_4Sb(CH_3)_3$ (-113 °C) reveals a doublet and a partially second order quartet. This spectrum was successfully simulated based on an A_3B spin system. The experimental (A) and computer simulated (B) spectra are shown in figure 2.24. The spectral parameters are δ_A 38.2, δ_B 20.3, and J_{AB}= 66.5 Hz.

In summary, $Ru[P(OCH_3)_3]_4Sb(CH_3)_3$ adopts a trigonal bipyramidal geometry in solution at low temperatures with the $SbMe_3$ ligand in an axial position. The variable temperature $^{31}P\{^1H\}$ NMR data is consonant with rapid ligand scrambling at higher temperatures.

The $^{31}P\{^1H\}$ NMR spectrum of $Ru[P(OCH_3)_3]_4PCH_3(C_6H_5)_2$ in $CD_2Cl_2/CHFCl_2$ (1:4) at 3 °C exhibited at doublet (δ 21.3) and a quintet (δ -108.7) with identical coupling constants (J_{PP}= 28.7 Hz). The two resonances had relative intensities of 4:1, respectively. This is just the behaviour expected for $Ru[P(OCH_3)_3]_4PCH_3(C_6H_5)_2$ in the fast exchange limit. The complex underwent a slow but steady decomposition in this solvent mixture and a slow exchange limit spectrum was not obtained. Solutions of the $PCH_3(C_6H_5)_2$ derivative in hexane, toluene, and acetone-d_6 also underwent slow decomposition (at room temperature); the characteristic odours of both the free ligands were evident. The mass spectral analyses of $Ru[P(OCH_3)_3]_4PCH_3(C_6H_5)_2$ using the electron impact, chemical

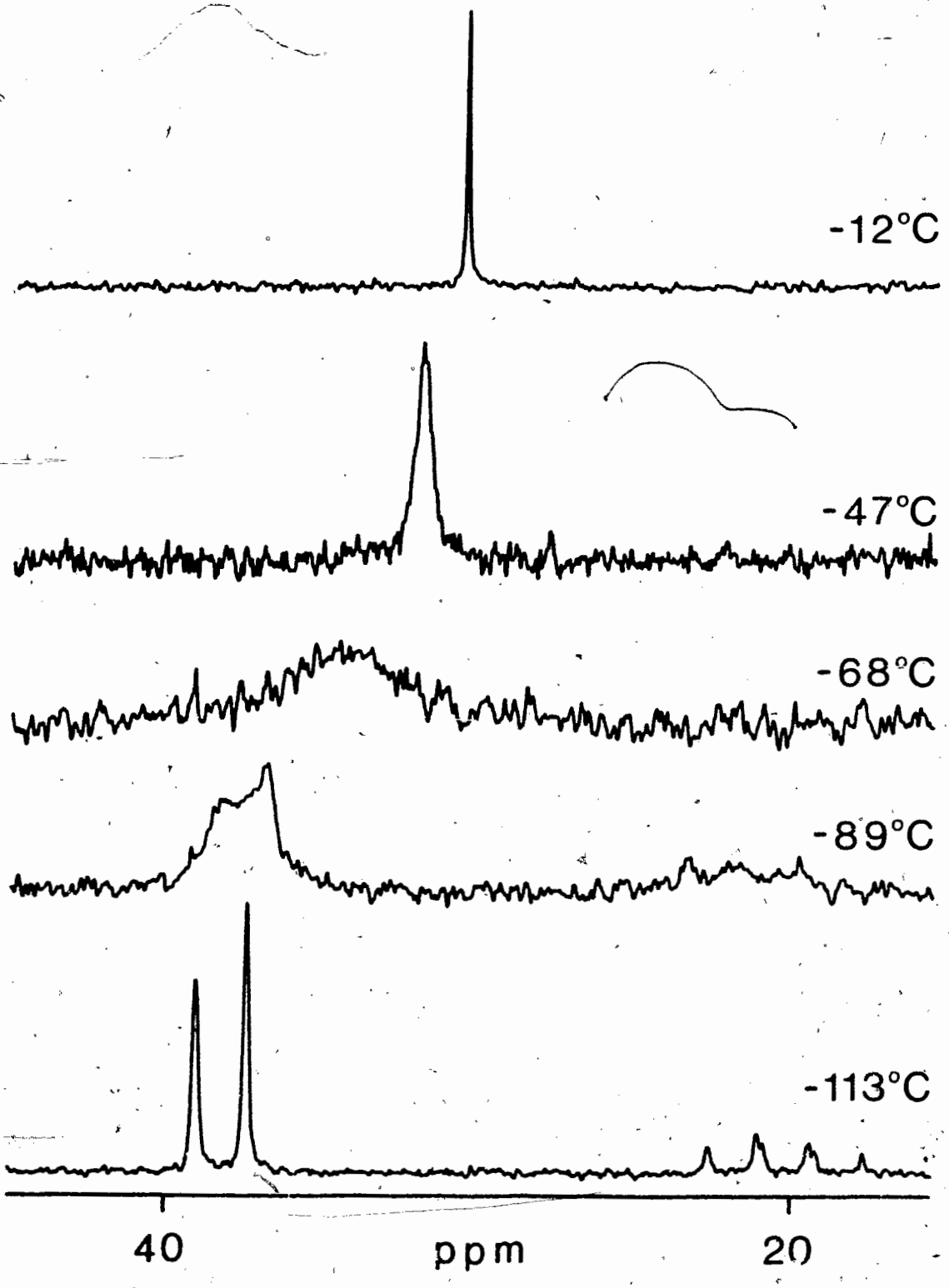

Figure 2.23 The variable temperature $^{31}P\{^{1}H\}$ NMR spectra of $Ru[P(OCH_3)_3]_4Sb(CH_3)_3$ in $CD_2Cl_2/CHFCl_2$ (1:4) measured at 40.54 MHz.

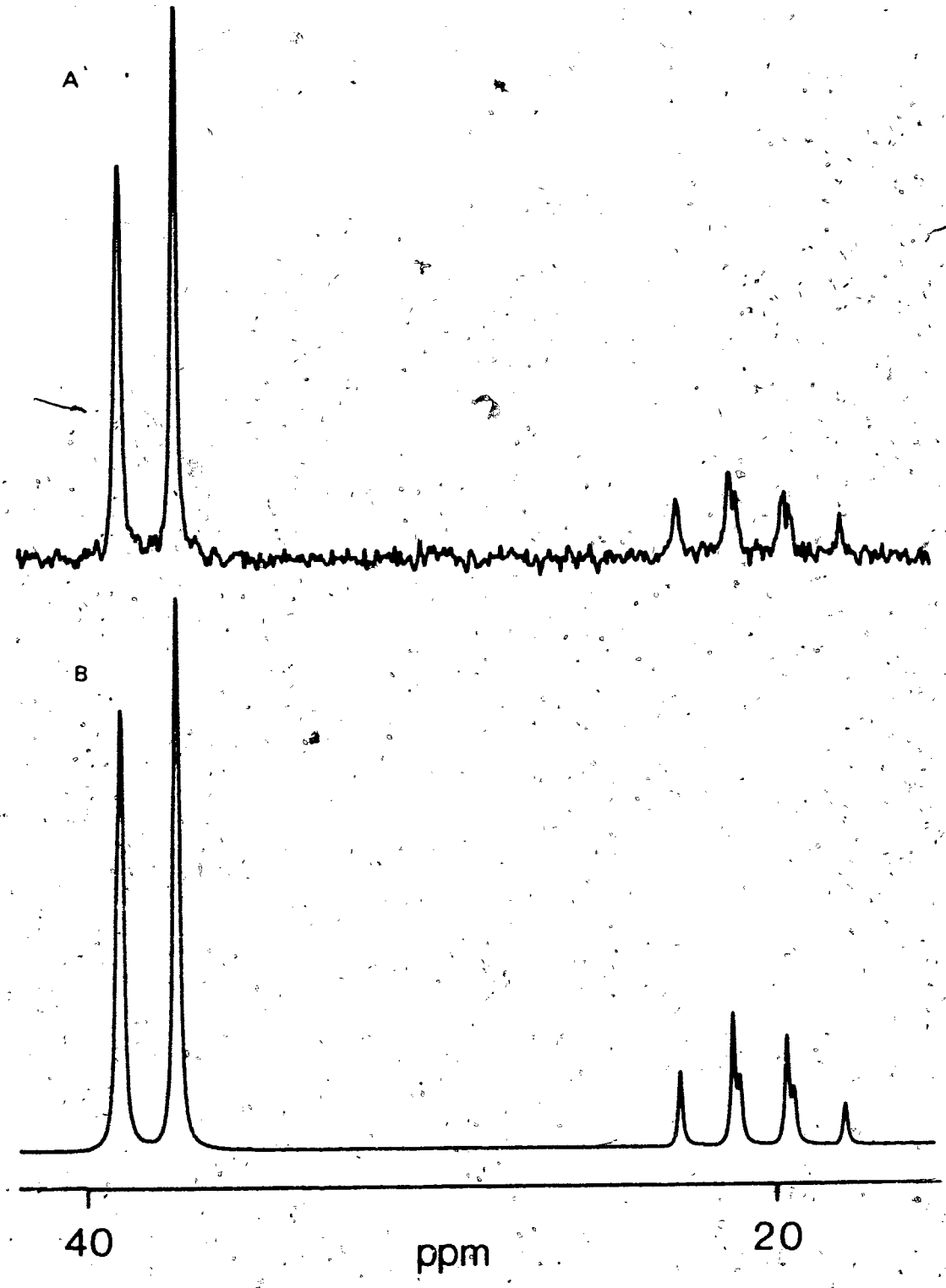

Figure 2.24 The experimental (A) and computer simulated (B) $^{31}P\{^{1}H\}$ NMR spectra of $Ru[P(OCH_3)_3]_4Sb(CH_3)_3$ at -113 °C. The experimental spectrum was obtained in $CD_2Cl_2/CHFCl_2$ (1:4) at 40.54 MHz. Spectral parameters given in text.

ionization, and fast atom bombardment techniques failed to reveal a parent ion (*m/e* 799). The electron impact mass spectrum exhibited ions due to $\{Ru[P(OCH_3)_3]_4\}^+$ and $\{Ru[P(OCH_3)_3]_3\}^+$ in addition to an unidentified species (very weak) at *m/e* 794. Given the fragile nature of the complex in solution, it is likely that thermal decomposition occurred under the conditions of the mass spectral analysis.

The $^{31}P\{^1H\}$ NMR spectrum of $Ru[P(OCH_3)_3]_4P(C_2H_4CN)_3$ in toluene-d_8 at 27 °C (40.54 MHz) revealed a doublet (δ 21.3) and a quintet (δ -108.7) of relative intensity 4:1, respectively. Both resonances had the same coupling constant (J_{PP} = 24.7 Hz). This NMR evidence is again consistent with a $Ru[P(OCH_3)_3]_4L$ derivative undergoing rapid ligand scrambling at room temperature. The $P(C_2H_4CN)_3$ complex suffered extensive decomposition in $CD_2Cl_2/CHFCl_2$ (1:4) and a slow exchange limit $^{31}P\{^1H\}$ NMR spectrum was not obtained. The mass spectrum of $Ru[P(OCH_3)_3]_4P(C_2H_4CN)_3$ also failed to exhibit a parent ion; the electron impact technique revealed fragments due to $\{Ru[P(OCH_3)_3]_4\}^+$ and $\{Ru[P(OCH_3)_3]_3\}^+$.

Both $Ru[P(OCH_3)_3]_4PCH_3(C_6H_5)_2$ and $Ru[P(OCH_3)_3]_4P(C_2H_4CN)_3$ were found to be quite air-sensitive. The complexes suffered extensive decomposition during 5 min exposure to air.

Before a fuller discussion of the previous results an additional piece of structural evidence will be presented. Recall that all of the $Ru[P(OCH_3)_3]_4L$ derivatives were quite

soluble in hexane except for $Ru[P(OCH_3)_3]_4P(OCH_2)_3CCH_3$ and $Ru[P(OCH_3)_3]_4P(C_2H_4CN)_3$. The former complex was recrystallized from hexane at -15 °C to yield colourless crystals suitable for structural analysis by X-ray diffraction. The structure was solved by Dr. Richard Jones and Professor F.W.B. Einstein (both of Simon Fraser University); their work is greatly appreciated.

The overall geometry of the molecule is shown in figure 2.25, which also features a partial numbering scheme. A number of selected bond angles and bond lengths are given in table 2.3.

The molecular structure of $Ru[P(OCH_3)_3]_4P(OCH_2)_3CCH_3$ reveals that the geometry about the Ru atom is approximately trigonal bipyramidal with the $P(OCH_2)_3CCH_3$ ligand occupying an equatorial site. The Ru-P distances for the axial $P(OCH_3)_3$ groups are not significantly different than those for the corresponding equatorial ligands. The average Ru-P distance (for the $P(OCH_3)_3$ ligands) is 2.282 Å. This value may be compared to Ru-P distances of 2.210(5), 2.233(7) Å in $Ru(\eta^3\text{-2-Me-allyl})_2[P(OCH_3)_3]_2$ [57] and 2.309(2) Å in $Ru[P(OCH_3)_3](CO)_4$ [58]. The three Ru-P bond distances in $Ru_3(\mu\text{-H})(\mu\text{-NO})(CO)_7[P(OCH_3)_3]_3$ are 2.283(2), 2.284(2), and 2.267(2) Å [59]. The Ru-P distance for the $P(OCH_2)_3CCH_3$ ligand in $Ru[P(OCH_3)_3]_4P(OCH_2)_3CCH_3$ (2.244(6) Å) is shorter than the average $Ru\text{-}P(OCH_3)_3$ distance in this complex, although the difference is not large. These results imply that the ruthenium-phosphorus bonding in $Ru[P(OCH_3)_3]_4P(OCH_2)_3CCH_3$ is slightly stronger for the $P(OCH_2)_3CCH_3$ ligand than for the

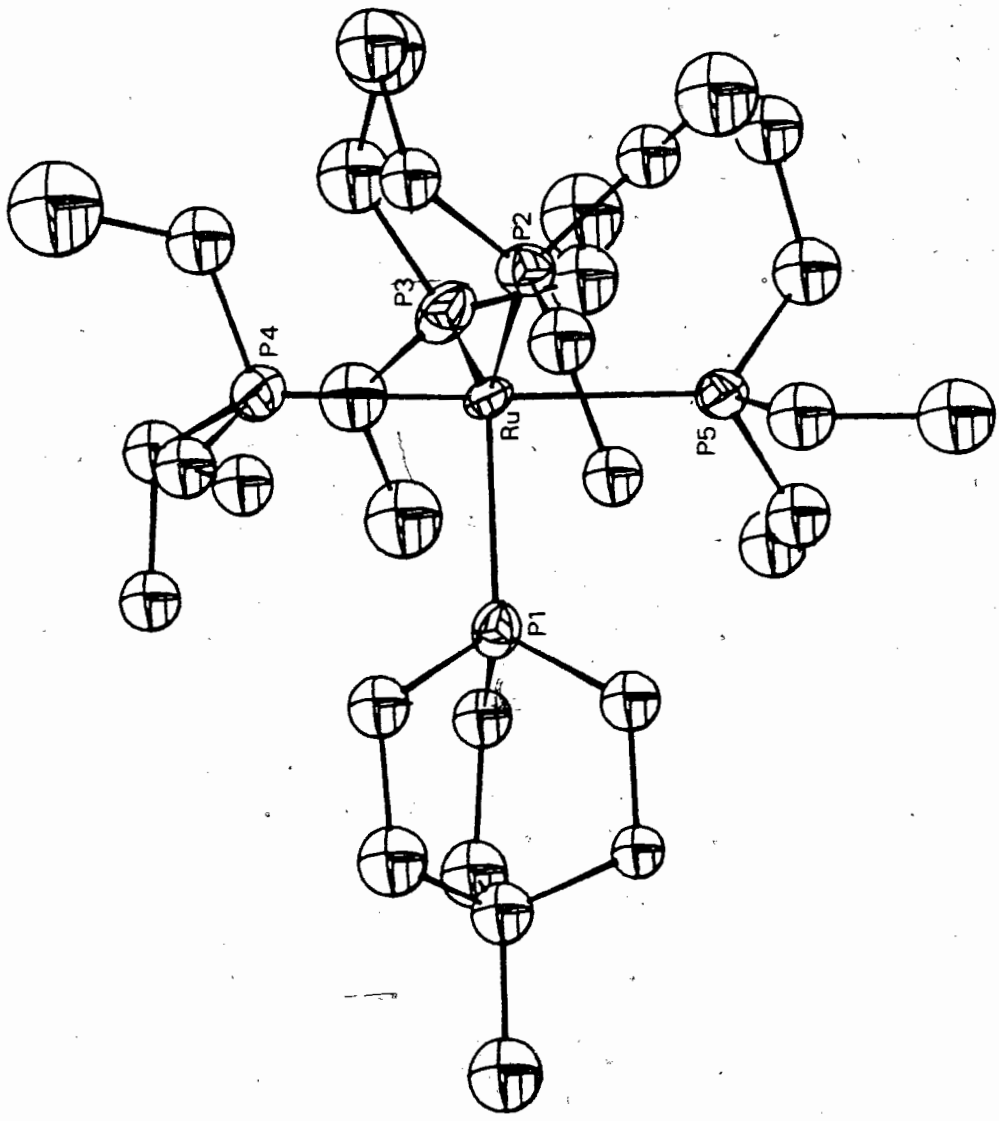

Figure 2.25 The molecular structure of $Ru[P(OCH_3)_3]_4P(OCH_2)_3CCH_3$.

Bond Angles (°)		Bond Distances (Å)	
P(2)-Ru-P(1)	118.2(2)	Ru-P(1)	2.244(6)
P(3)-Ru-P(1)	115.6(2)	Ru-P(2)	2.267(6)
P(3)-Ru-P(2)	126.2(3)	Ru-P(3)	2.278(6)
P(4)-Ru-P(1)	92.9(3)	Ru-P(4)	2.285(7)
P(4)-Ru-P(2)	91.1(2)	Ru-P(5)	2.297(6)
P(4)-Ru-P(3)	86.9(2)		
P(5)-Ru-P(1)	88.7(2)		
P(5)-Ru-P(2)	86.7(2)		
P(5)-Ru-P(3)	93.8(2)		
P(5)-Ru-P(4)	177.7(3)		

Table 2.3 Selected bond angles and bond distances for $Ru[P(OCH_3)_3]_4P(OCH_2)_3CCH_3$.

$P(OCH_3)_3$ groups. The electronic parameters for the $P(OCH_3)_3$ and $P(OCH_2)_3CCH_3$ ligands are 2079.5 and 2087.3 cm^{-1}, respectively [11]; these values suggest that the caged phosphite is a poorer σ-donor and/or a better π-acceptor than trimethyl phosphite. The shorter Ru-P bond for the $P(OCH_2)_3CCH_3$ ligand in $Ru[P(OCH_3)_3]_4P(OCH_2)_3CCH_3$ (relative to the Ru-$P(OCH_3)_3$ bonds) is consistent with better π-acceptor properties of the former ligand. Steric effects, however, may also be responsible for the observed ruthenium-phosphorus bond length difference in $Ru[P(OCH_3)_3]_4P(OCH_2)_3CCH_3$.

The Ru-P bond distance in $Ru(CO)_2(C_6H_8)(C_4F_6)[P(OCH_2)_3CCH_3]$ was found to be 2.314(4) Å [60]. That the Ru-$P(OCH_2)_3CCH_3$ bond in $Ru[P(OCH_3)_3]_4P(OCH_2)_3CCH_3$ is considerably shorter than this may be explained in terms of increased π back-bonding in the latter; this is consistent with the good σ-donor properties of the $P(OCH_3)_3$ ligand. The interligand bond distances and angles

for the caged phosphite in $Ru[P(OCH_3)_3]_4P(OCH_2)_3CCH_3$ agree well with the corresponding values in $Ru(CO)_2(C_6H_8)(C_4F_6)[P(OCH_2)_3CCH_3]$ [60].

The trimethyl phosphite ligands in $Ru[P(OCH_3)_3]_4P(OCH_2)_3CCH_3$ all display an asymmetry common to many metal-$P(OCH_3)_3$ complexes [58a]. A fuller discussion of this subject may be found in chapter 5.

The most noteworthy aspect of the X-ray data for $Ru[P(OCH_3)_3]_4P(OCH_2)_3CCH_3$ is the P-Ru-P bond angles. An examination of table 2.3 reveals considerable distortion from an idealized, pseudo-D_{3h} symmetry of the RuP_5 skeleton, as evidenced by the equatorial bond angles: the $(CH_3O)_3P$-Ru-$P(OCH_3)_3$ angle (126.2(3)°) has opened up at the expense of the two angles containing the caged phosphite ligand (115.6(2) and 118.2(2)°). This result suggests that the steric difference between the two types of phosphite ligands ($P(OCH_3)_3$: θ= 107°; $P(OCH_2)_3CCH_3$: θ= 101° [11]) causes measurable distortions in the solid state structure of $Ru[P(OCH_3)_3]_4P(OCH_2)_3CCH_3$. That this relatively small difference (6°) appears capable of causing a noticeable effect indicates that steric considerations in $Ru[P(OCH_3)_3]_4L$ derivatives are important.

A discussion of site preference for the $Ru[P(OCH_3)_3]_4L$ complexes will now be presented. The subject is introduced via the obvious incongruency in the solution and solid state data

for $Ru[P(OCH_3)_3]_4P(OCH_2)_3CCH_3$: the X-ray structure of this complex showed the caged phosphite ligand in an equatorial site while the NMR evidence indicated that the major isomer had a static solution structure with an axial $P(OCH_2)_3CCH_3$ ligand. Recall also that the slow exchange limit $^{31}P\{^1H\}$ NMR data for $Ru[P(OCH_3)_3]_4P(OCH_2)_3CCH_3$ suggested the presence of the equatorially substituted species as a minor isomer (~10%).

A number of theoretical studies concerning the site preference of ligands in trigonal bipyramidal complexes (i.e. D_{3h}) have been published. The work of Hoffmann and Rossi utilized extended Huckel calculations on model compounds; arguments based on symmetry and overlap were used [61]. Their results indicated that good σ-donor ligands prefer axial sites and good π-acceptor ligands favour equatorial sites in a d^8, D_{3h} complex. The prediction that good σ-donor ligands prefer the axial sites in a trigonal bipyramidal, d^8 molecule was also advanced by Burdett, based on an angular overlap model [62]. Similar results were derived from another LCAO molecular orbital treatment [63].

The potential role of steric factors in site preference for trigonal bipyramidal complexes does not appear to have been theoretically investigated. Based on the number of 90° interactions, one might expect that the axial sites are the most sterically crowded. This approach, however, is clearly too simplistic: the mutual interaction of all the ligand atoms in a specific complex must be taken account of before a meaningful

pronouncement of steric site preference can be made. In a more general sense, one might expect the size of L to play some role in a sterically congested species such as $Ru[P(OCH_3)_3]_4L$ (L= phosphine and phosphite). The X-ray crystal structure results for $Ru[P(OCH_3)_3]_4P(OCH_2)_3CCH_3$ provide experimental evidence for this view as does the fact that $Ru[P(OCH_3)_3]_4L$ derivatives could not be prepared for ligands L with large cone angles (vide infra).

The site preference disparity between the solid state and static solution structures of $Ru[P(OCH_3)_3]_4P(OCH_2)_3CCH_3$ may be analyzed with respect to the theoretical predictions. Photoelectron spectroscopy studies have indicated that $P(OCH_3)_3$ is more basic than $P(OCH_2)_3CCH_3$ [64]. This view is consistent with equilibrium studies between various phosphite ligands and BH_3 [65]. These results strongly suggest that $P(OCH_3)_3$ is a better σ-donor ligand than $P(OCH_2)_3CCH_3$. Based on this consideration, the site preference of the caged phosphite group in the solid state structure of $Ru[P(OCH_3)_3]_4P(OCH_2)_3CCH_3$ is in accord with theoretical predictions. One might have expected the opposite result, where electronic effects determined the solution structure; crystal packing forces could then be invoked to explain why the minor (i.e. equatorial) isomer crystallized from solution preferentially. It is tempting to attribute the axial site preference of the $P(OCH_2)_3CCH_3$ ligand in the static solution structure of $Ru[P(OCH_3)_3]_4P(OCH_2)_3CCH_3$ to steric forces. In light of the previous discussion concerning the

difficulty in taking account of all non-bonded interactions, there appears no firm foundation on which to launch a steric argument. The X-ray results for $Ru[P(OCH_3)_3]_4P(OCH_2)_3CCH_3$, however, suggested that steric considerations were valid. Considerably more crystal structure data on related complexes are required before the reasons for the discrepancy between the static solution and solid state geometries of $Ru[P(OCH_3)_3]_4P(OCH_2)_3CCH_3$ may be elucidated.

The results of the variable temperature $^{31}P\{^1H\}$ NMR studies for the $Ru[P(OCH_3)_3]_4L$ derivatives are given in table 2.4. The site preference of L (based on the $^{31}P\{^1H\}$ NMR data) is tabulated along with the corresponding electronic and steric parameters for the ligand [10,11,51]. Analogous data for $Ru[P(OCH_3)_3]_5$ and $Ru[P(OCH_3)_3]_4CO$ are included in table 2.4 [4,6,50].

The $^{31}P\{^1H\}$ NMR studies of the reaction between $Ru[P(OCH_3)_3]_4(\eta^2\text{-}C_2H_4)$ and L (L= various phosphines and phosphites) deserve some discussion. Recall that for L= PPh_3 and $P(i\text{-}Pr)_3$, there was no NMR evidence for the formation of the $Ru[P(OCH_3)_3]_4L$ complex. In addition, the reaction of $Ru[P(OCH_3)_3]_4(\eta^2\text{-}C_2H_4)$ with L= $P(n\text{-}Bu)_3$, P(O-o-tolyl)$_3$, and $PCH_3(C_6H_5)_2$ gave $Ru[P(OCH_3)_3]_4L$ derivatives which rapidly underwent further reaction in solution. The ligand cone angles for $P(i\text{-}Pr)_3$, PPh_3, P(O-o-tolyl)$_3$, $PCH_3(C_6H_5)_2$, and $P(n\text{-}Bu)_3$ are 160°, 145°, 141°, 136°, and 132°, respectively [11]. The corresponding electronic parameters are 2059.2, 2068.9, 2084.1,

Compound	Isomer[a]	θ (deg)[b]	Electronic[c] Parameter (cm^{-1})
$Ru[P(OCH_3)_3]_4P(OCH_2)_3CCH_3$	mostly axial	101	2087.3
$Ru[P(OCH_3)_3]_4PF_3$	equatorial	104	2110.8
$Ru[P(OCH_3)_3]_4P(OC_2H_5)_3$	axial	109	2076.3
$Ru[P(OCH_3)_3]_4Sb(CH_3)_3$	axial	~110[d]	unknown[e]
$Ru[P(OCH_3)_3]_4P(CH_3)_3$	axial	118	2064.1
$Ru[P(OCH_3)_3]_4P(CH_3)_2C_6H_5$	axial	122	2065.3
$Ru[P(OCH_3)_3]_4P(OC_6H_5)_3$	equatorial	128	2085.3
$Ru[P(OCH_3)_3]_4P(OCH(CH_3)_2)_3$	probably axial	130	2075.9
$Ru[P(OCH_3)_3]_4P(C_2H_4CN)_3$	unknown	132	2077.9
$Ru[P(OCH_3)_3]_4PCH_3(C_6H_5)_2$	unknown	136	2067.0
$Ru[P(OCH_3)_3]_4$[f]	—	107	2079.5
$Ru[P(OCH_3)_3]_4CO$[g]	unknown	90-95[h]	see text

Table 2.4 Structural data for $Ru[P(OCH_3)_3]_4L$ and empirical parameters for the free ligands L.
[a]axial or equatorial substitution for the static solution structure [b]cone angle of L (ref 11) [c]electronic parameter of L (ref 11) [d]estimated from ref 11 [e]ref 11 [f]data taken from ref 6 [g]ref 52 [h]see ref 11.

2067.0, and 2060.3, respectively [10,11]. Comparing these values to those for the ligands which formed stable $Ru[P(OCH_3)_3]_4L$ derivatives, the conclusion is obvious: there is a steric threshold for coordination of L to the $Ru[P(OCH_3)_3]_4$ moiety. A qualitative consideration of the molecular structure of $Ru[P(OCH_3)_3]_4P(OCH_2)_3CCH_3$ (figure 2.25) reveals the steric congestion around the central metal in this system. This steric threshold appears to occur for incoming ligands with cone angles of ~132-136°. Recall that $Ru[P(OCH_3)_3]_4PCH_3(C_6H_5)_2$ (θ= 136°) and $Ru[P(OCH_3)_3]_4P(C_2H_4CN)_3$ (θ= 132°) were unstable in solution, in accord with these findings.

The site preferences of L in the $Ru[P(OCH_3)_3]_4L$ derivatives are shown in table 2.4. It is clear that steric considerations are not generally important in determining whether L prefers an axial or an equatorial site. The two complexes with equatorial substitution (i.e. $Ru[P(OCH_3)_3]_4PF_3$ and $Ru[P(OCH_3)_3]_4P(OC_6H_5)_3$) contain ligands L with widely differing cone angles. Conversely, ligands with cone angles similar to those for these two complexes (104° and 128°, respectively) give $Ru[P(OCH_3)_3]_4L$ derivatives which exist as axial isomers in solution at low temperatures. There does appear to be a correlation between the electronic properties of L and the site preference: both PF_3 and $P(OC_6H_5)_3$ have a high value of the electronic parameter. In light of the discussion in chapter 1, this indicates that both ligands have poor σ-donor and/or good π-acceptor characteristics. Arguments based on either of these two

properties predict that the two ligands in question would favour equatorial coordination; Rossi and Hoffmann have predicted that poorer σ-donor and better π-acceptor ligands will prefer the equatorial positions in a d^8, D_{3h} molecule [61]. The inconsistency of this argument relative to $Ru[P(OCH_3)_3]_4P(OCH_2)_3CCH_3$ has already been examined. It is observed that the electronic parameter of the $P(OCH_2)_3CCH_3$ ligand is higher than that of $P(OC_6H_5)_3$ yet $Ru[P(OCH_3)_3]_4P(OCH_2)_3CCH_3$ exists primarily as the axial isomer in solution at low temperature. This could be a case where steric considerations outweigh the general electronic control on the system; the $P(OCH_2)_3CCH_3$ ligand has the smallest cone angle (101°) listed in table 2.4. In addition, there was evidence for a small amount of the equatorial isomer (predicted from electronic considerations) in the slow exchange limit $^{31}P\{^1H\}$ NMR spectrum of $Ru[P(OCH_3)_3]_4P(OCH_2)_3CCH_3$. The remainder of the $Ru[P(OCH_3)_3]_4L$ derivatives (i.e. L= $P(OC_2H_5)_3$, $P(OCH(CH_3)_2)_3$, $P(CH_3)_2C_6H_5$, $P(CH_3)_3$) conform to predictions based on electronic effects: the ligands L in these complexes have electronic parameters smaller than that for $P(OCH_3)_3$ (i.e. are better σ-donors and/or poorer π-acceptors) and occupy axial sites in the corresponding $Ru[P(OCH_3)_3]_4L$ complexes.

For the $Ru[P(OCH_3)_3]_4L$ derivatives, the only strong evidence supporting the presence of both axial and equatorial isomers in solution was for $Ru[P(OCH_3)_3]_4P(OCH_2)_3CCH_3$. This result was somewhat suprising. The site preference for ligands such as

$P(OC_2H_5)_3$, with steric and electronic properties very similar to those of $P(OCH_3)_3$, was expected to be weak. If the $P(OCH_2)_3CCH_3$ ligand has the requisite combination of steric and electronic properties to cause only a weak site preference in $Ru[P(OCH_3)_3]_4L$, it is likely not unique in this regard. The preparation of $Ru[P(OCH_3)_3]_4L$ derivatives with a large number of phosphorus donor ligands L could allow a deeper insight into the factors controlling site preference in this system.

The variable temperature $^{31}P\{^1H\}$ NMR data for the $Ru[P(OCH_3)_3]_4L$ derivatives indicated that intramolecular phosphorus ligand exchange was occurring. The introduction to this chapter presented literature results concerning the stereochemical nonrigidity of the d^8 complexes ML_5^{n+} (n= 0: M= Fe, Ru, Os; n= 1: M= Co, Rh, Ir; n= 2: M= Ni, Pd, Pt; L= phosphite) [6,33,34,35,36]. It was concluded that the Berry pseudo-rotation process was the most likely mechanism to explain axial-equatorial phosphite exchange in these systems (see figure 2.1). There are, however, some fundamental differences between the ML_5 system and the $Ru[P(OCH_3)_3]_4L$ derivatives in this thesis: the unique ligand L of the latter complexes dictates two possible isomers for these trigonal bipyramidal molecules (slow exchange limit). It is possible that the complexes which exhibit ^{31}P resonances due only to an equatorially substituted isomer undergo axial-equatorial ligand exchange by a different mechanism than those which exist as predominantly axial isomers.

The equatorially substituted case will be examined first. The $Ru[P(OCH_3)_3]_4L$ derivatives which exhibited ^{31}P resonances due only to the equatorial isomer were $Ru[P(OCH_3)_3]_4PF_3$ and $Ru[P(OCH_3)_3]_4P(OC_6H_5)_3$. The triphenyl phosphite complex was chosen as the subject for a more detailed mechanistic examination. A consideration of figures 2.1 and 2.8 reveals that axial-equatorial ligand exchange for this complex via a general Berry pseudo-rotation could lead to the axially substituted isomer in some of the permutational conformations. A variation on this general mechanism is shown in figure 2.26; this process may be called a restricted Berry pseudo-rotation in that it involves pairwise exchange of the two axial and two equatorial $P(OCH_3)_3$ ligands but allows the $P(OC_6H_5)_3$ ligand to always remain in an equatorial position. This mechanism is attractive for two reasons. It allows axial-equatorial exchange of the $P(OCH_3)_3$ ligands in a single step. In addition, it does not require the unique ligand to occupy an axial site during the exchange; the reason the axial isomer of $Ru[P(OCH_3)_3]_4P(OC_6H_5)_3$ is not observed in the slow exchange limit $^{31}P\{^1H\}$ NMR spectrum (if indeed it is present) is presumably due to it being thermodynamically less stable than the equatorial counterpart.

The variable $^{31}P\{^1H\}$ NMR spectra of $Ru[P(OCH_3)_3]_4P(OC_6H_5)_3$ (40.54 MHz) were computer-simulated by a line shape calculation program (see experimental section of this chapter for details) based on the mechanism in figure 2.26. The calculated and observed spectra are shown in figure 2.27. Although the poor

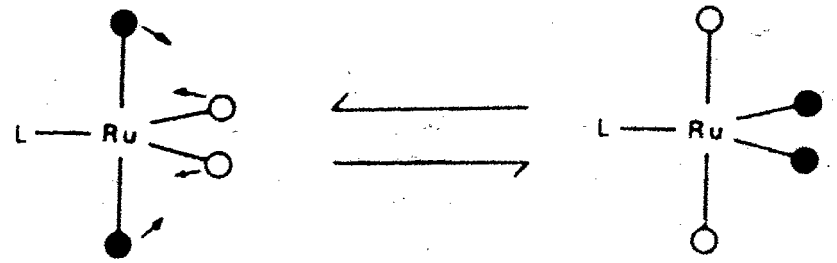

Figure 2.26 A schematic representation of a restricted Berry pseudo-rotation mechanism for an equatorially substituted $Ru[P(OCH_3)_3]_4L$ molecule (○, ● = $P(OCH_3)_3$).

---

signal to noise ratio of the experimental spectra caused some problems in matching the simulated and observed data, the agreement at each temperature appeared good. One notable feature of the simulated data was the presence of three exchange invariant lines in the C part of the A_2B_2C pattern. These three resonances (at the correct frequencies) were clearly present in the experimental spectra as well, although this was more easily seen in the frequency and intensity expanded spectra. These lines eventually became part of the central and outer two resonances of the X quintet in the fast exchange limit A_4X spectrum. The good agreement of the observed and calculated $^{31}P\{^1H\}$ NMR spectra of $Ru[P(OCH_3)_3]_4P(OC_6H_5)_3$ represents mechanistic evidence in favour of the restricted Berry pseudo-rotation process (figure 2.26) as the cause of axial-equatorial $P(OCH_3)_3$ exchange. The Eyring activation parameters as calculated from the rate versus temperature data are as follows: $\Delta H^{\ddagger} = 8.8 \pm 0.3$ kcal mol^{-1}, $\Delta S^{\ddagger} = 3.9 \pm 1.5$

cal/mol-°K, $\Delta G^{\ddagger}$(298 °K)= 7.6±0.4 kcal mol^{-1}. The activation entropy is small, consistent with the intramolecular nature of the exchange.

Intramolecular ligand exchange for the axially substituted $Ru[P(OCH_3)_3]_4L$ derivatives will now be considered. The two axial isomers which will be examined in detail are $Ru[P(OCH_3)_3]_4P(CH_3)_3$ (A_3BX spin system) and $Ru[P(OCH_3)_3]_4Sb(CH_3)_3$ (A_3B spin system). An examination of figures 2.1 and 2.8A reveals that a restricted Berry pseudo-rotation of the type proposed for $Ru[P(OCH_3)_3]_4P(OC_6H_5)_3$ (see figure 2.26) is not possible for an axial isomer: any pairwise exchange of the two axial and two of the equatorial ligands will necessarily form the equatorial isomer. One process which is capable of causing axial-equatorial $P(OCH_3)_3$ exchange while leaving L axial is shown in figure 2.28A. This process is termed a turnstile exchange in that it involves an effective rotation of the axial and two of the equatorial $P(OCH_3)_3$ ligands about a threefold axis. This process is attractive for reasons similar to that discussed for the case of $Ru[P(OCH_3)_3]_4P(OC_6H_5)_3$: the turnstile exchange will lead to scrambling of the axial and three equatorial $P(OCH_3)_3$ ligands (as observed in the fast exchange limit for the axial isomers) without the involvement of the unobserved equatorial isomer.

Even though neither $Ru[P(OCH_3)_3]_4Sb(CH_3)_3$ nor $Ru[P(OCH_3)_3]_4P(CH_3)_3$ exhibited $^{31}P\{^1H\}$ NMR resonances due to the equatorial isomer, the potential participation of this isomer in

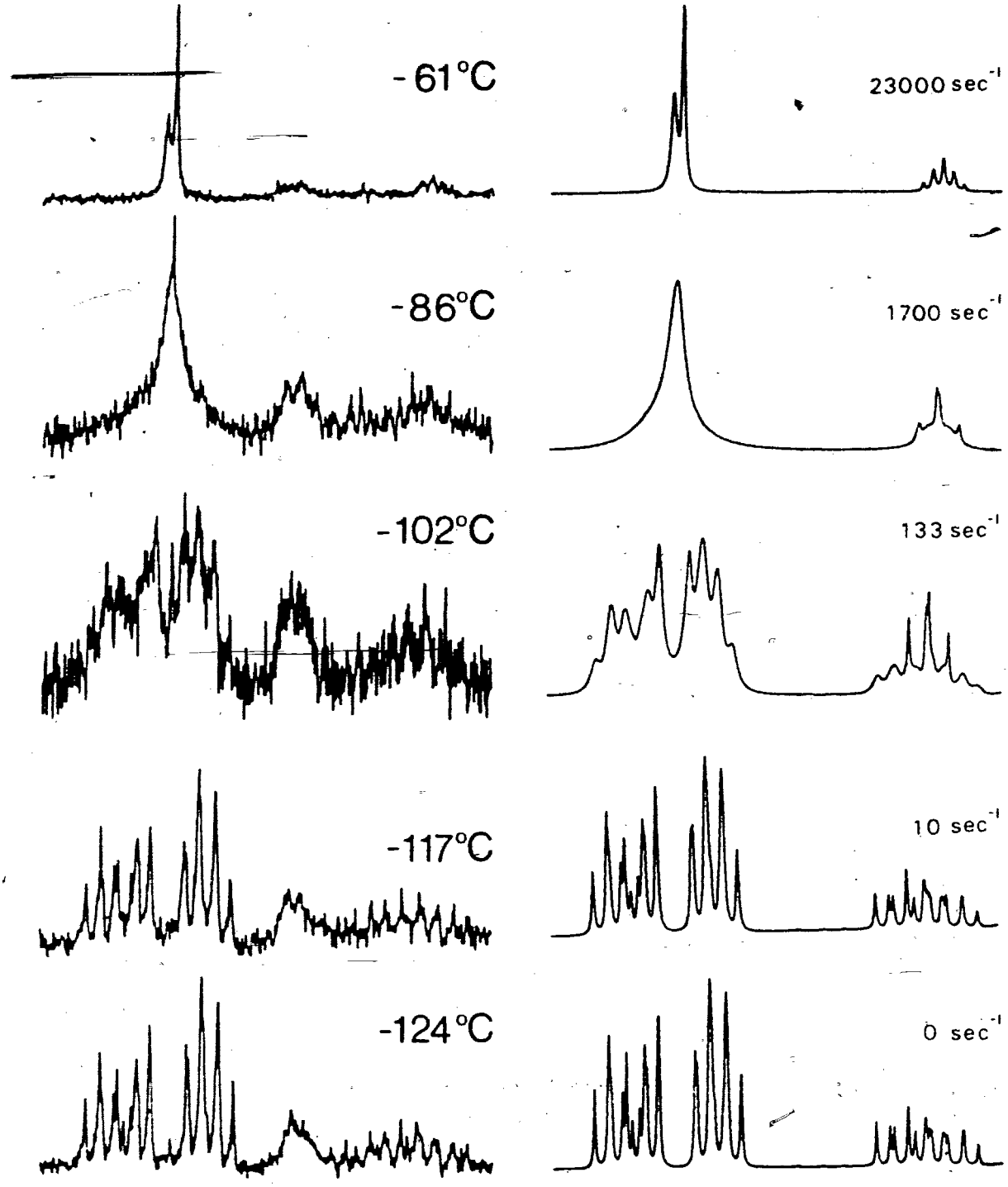

Figure 2.27 Variable temperature $^{31}P\{^{1}H\}$ NMR spectra of $Ru[P(OCH_3)_3]_4P(OC_6H_5)_3$ and calculated spectra based on a restricted Berry pseudo-rotation mechanism (figure 2.26). Observed and calculated spectra are labeled with temperatures and rate constants, respectively.

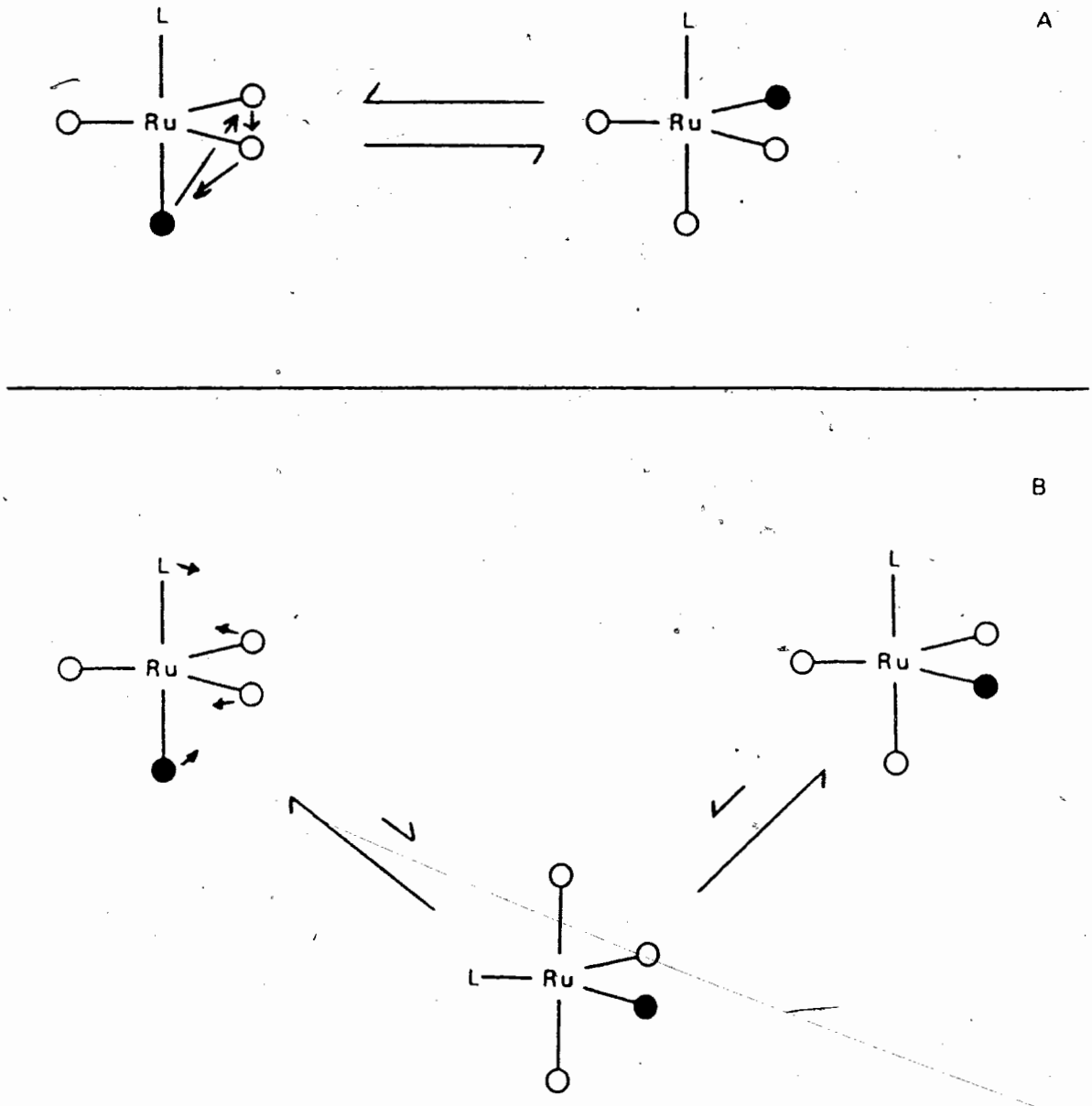

Figure 2.28 Two mechanisms for axial-equatorial ligand exchange in axial $Ru[P(OCH_3)_3]_4L$ derivatives. A: Turnstile mechanism; B: Berry pseudo-rotation process.

a ligand exchange process cannot be ignored. The lack of knowledge concerning the spectral parameters associated with the equatorial isomers for the trimethyl phosphine and trimethyl stibine complexes does, however, place some limitations on determining the permutational nature of an exchange process involving this isomer. The equatorial isomer (once formed in an exchange process) must be treated as a transition state which relatively quickly reconverts to the major (i.e. axial) isomer. One may then examine the permutational consequences of the axial—>equatorial—>axial process.

Based on these assumptions, the effects of the Berry pseudo-rotation process on an axially substituted $Ru[P(OCH_3)_3]_4L$ derivative may be examined. There are two general possibilities to consider. The formation of the axial isomer by this process could be immediately followed by reconversion to the axial counterpart; this situation is shown schematically in figure 2.28B. The equatorial transition state may be formed via any of the three equatorial $P(OCH_3)_3$ ligands fulfilling the "pivotal" role (see figure 2.1). The resultant three species are chemically identical but permutationally distinct and each may reconvert to the axial isomer with either of the two equatorial $P(OCH_3)_3$ ligands in the pivotal position. Thus six permutational "products" are generated during the axial—>equatorial—>axial process via the Berry pseudo-rotation mechanism. A detailed consideration of this exchange reveals that the permutational nature is identical to that found for the turnstile process (see

figure 2.28A). These two mechanisms are thus indistinguishable by dynamic nuclear magnetic resonance techniques.

There is another variation on the general Berry pseudo-rotation process which may be considered. It is possible that the formation of an equatorial "transition state" from an axial isomer (via a Berry process) might not be immediately followed by reconversion to the axial isomer; one could imagine the equatorial species undergoing one or more equatorial<—>equatorial interconversions via the process shown in figure 2.26 before reforming the axial isomer. This could occur if the activation barrier for the process in figure 2.26 was of the same order as that associated with reconversion to the axial form. A detailed examination of the permutational effects due to this axial—>equatorial<—>equatorial—>axial process leads to two equally possible results. One is identical to that found previously for the turnstile exchange. The other corresponds to a pairwise exchange of the axial and one of the equatorial $P(OCH_3)_3$ ligands of the axial isomer. This overall process is theoretically distinguishable (by dynamic nuclear magnetic resonance techniques) from one based solely on the turnstile exchange mechanism.

The pairwise exchange of the axial and one of the equatorial $P(OCH_3)_3$ groups of an axial $Ru[P(OCH_3)_3]_4L$ isomer represents another possible mechanism for axial-equatorial ligand scrambling. Again, this process would cause averaging of the axial and equatorial $P(OCH_3)_3$ groups while allowing the unique

ligand L to remain in an axial site. This process will hereafter be termed the pairwise axial-equatorial mechanism.

Four mechanisms have been considered for an axial $Ru[P(OCH_3)_3]_4L$ isomer in the previous discussion. The permutational nature of the turnstile process (figure 2.28A) and the Berry pseudo-rotation of the type axial—>equatorial—>axial (figure 2.28B) are identical. The permutational details of the Berry pseudo-rotation of the type axial—>equatorial<—>equatorial—>axial and the pairwise axial-equatorial mechanism are distinct from each other and from those associated with the previously mentioned two processes. Thus, there are three permutationally distinct mechanisms under consideration.

The variable temperature $^{31}P\{^1H\}$ NMR spectra of $Ru[P(OCH_3)_3]_4Sb(CH_3)_3$ (40.54 MHz) were computer-simulated by a line shape calculation program based on each of these three mechanisms. There was very little qualitative difference between these three sets of line shapes over the complete range of exchange rates. This is illustrated in figure 2.29 which shows the line shapes for each of these processes (all at k= 50 sec^{-1}).

The calculated line shapes based on the turnstile process were used to simulate the experimental $^{31}P\{^1H\}$ NMR spectra of $Ru[P(OCH_3)_3]_4Sb(CH_3)_3$. The calculated and observed spectra are shown in figure 2.30. The calculated line shapes appeared in

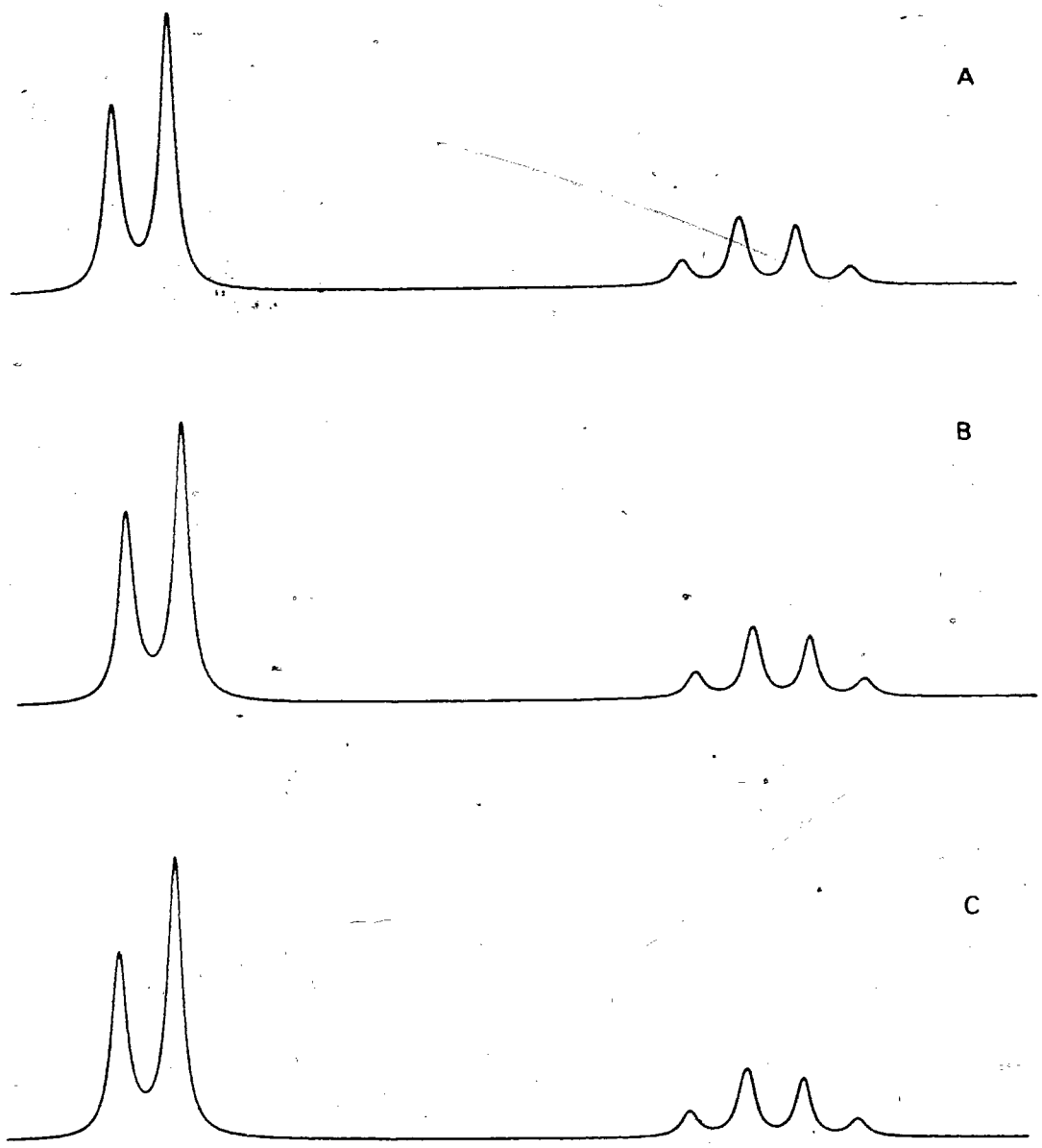

Figure 2.29 Calculated line shapes for the $^{31}P\{^{1}H\}$ NMR spectrum of $Ru[P(OCH_3)_3]_4Sb(CH_3)_3$ (all at k= 50 sec^{-1}) based on three exchange processes. A: Turnstile process; B: Berry pseudo-rotation; C: Pairwise axial-equatorial exchange.

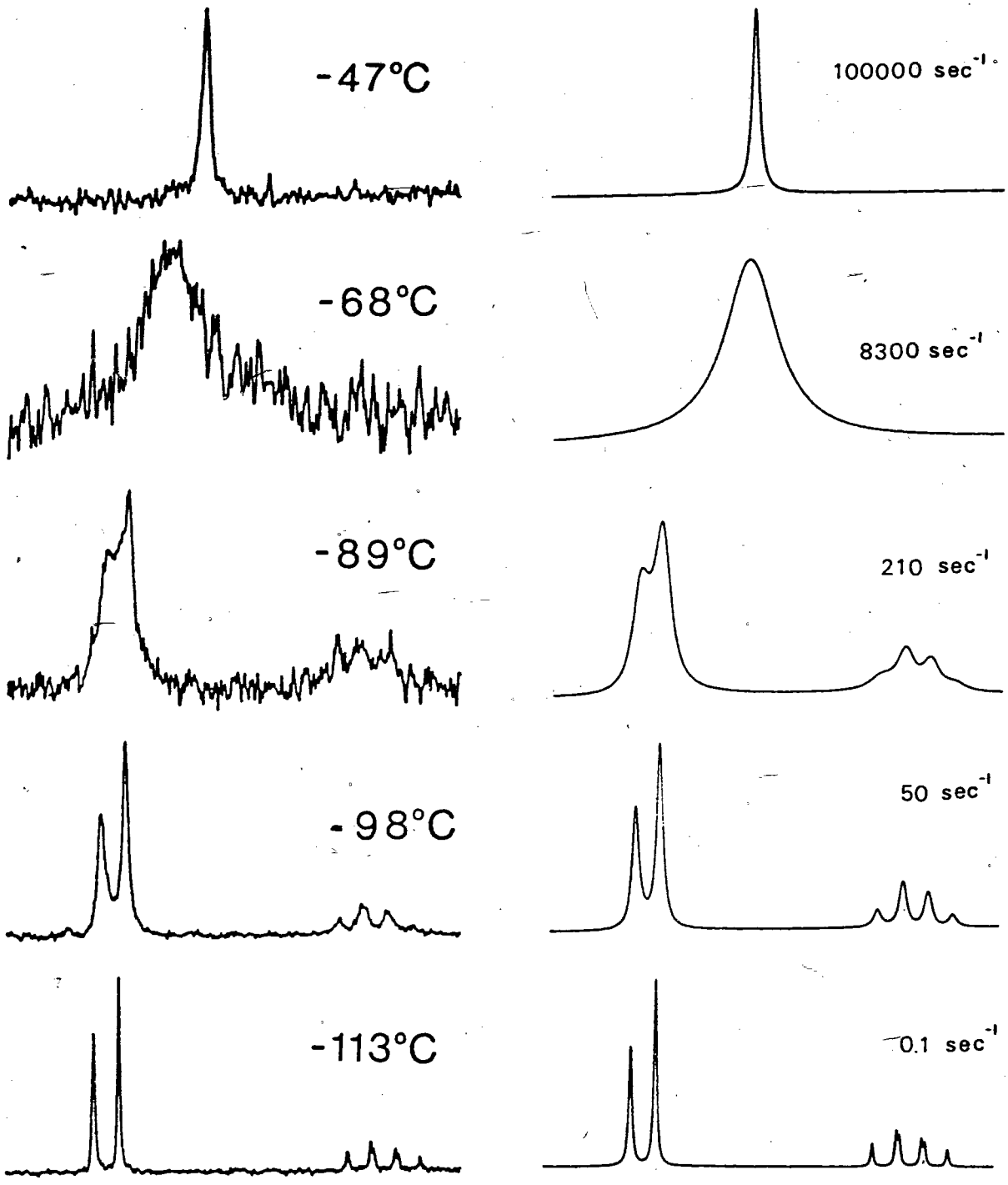

Figure 2.30 Variable temperature $^{31}P\{^{1}H\}$ NMR spectra of $Ru[P(OCH_3)_3]_4Sb(CH_3)_3$ and calculated spectra based on the turnstile mechanism. The observed and calculated spectra are labeled with the temperatures and rates, respectively.

good agreement with the observed spectra. The Eyring activation parameters calculated from the rate versus temperature data are as follows: $\Delta H^{\ddagger}$= 11.6±0.4 kcal mol^{-1}, $\Delta S^{\ddagger}$= 16.3±2.1 cal/mol-°K, $\Delta G^{\ddagger}$ (298 °K)= 6.7±1.1 kcal mol^{-1}. The activation entropy is large and positive; this is not the result expected for an intramolecular ligand exchange. Such $\Delta S^{\ddagger}$ values are often associated with intermolecular processes. This possibility is not considered likely in the present case: the available evidence for the $Ru[P(OCH_3)_3]_4L$ derivatives suggested the operation of an intramolecular exchange mechanism. The Eyring activation parameters for $Ru[P(OCH_3)_3]_4Sb(CH_3)_3$ must be treated with caution.

The variable temperature $^{31}P\{^1H\}$ NMR spectra of $Ru[P(OCH_3)_3]_4P(CH_3)_3$ were computer-simulated based on the three permutational exchanges under consideration. Again, there was little qualitative difference between the three sets of line shapes over the complete range of exchange rates. Calculated spectra based on the turnstile (A) and pairwise axial-equatorial (C) processes (both at k= 250 sec^{-1}) and the matching observed spectrum (B) are shown in figure 2.31. A careful examination of figure 2.31 reveals small differences in the two calculated spectra with respect to the ratio of the widths at half height for the resonances marked 1 and 2. These minor differences, however, are not sufficient to meaningfully favour one of the proposed exchange processes over the others.

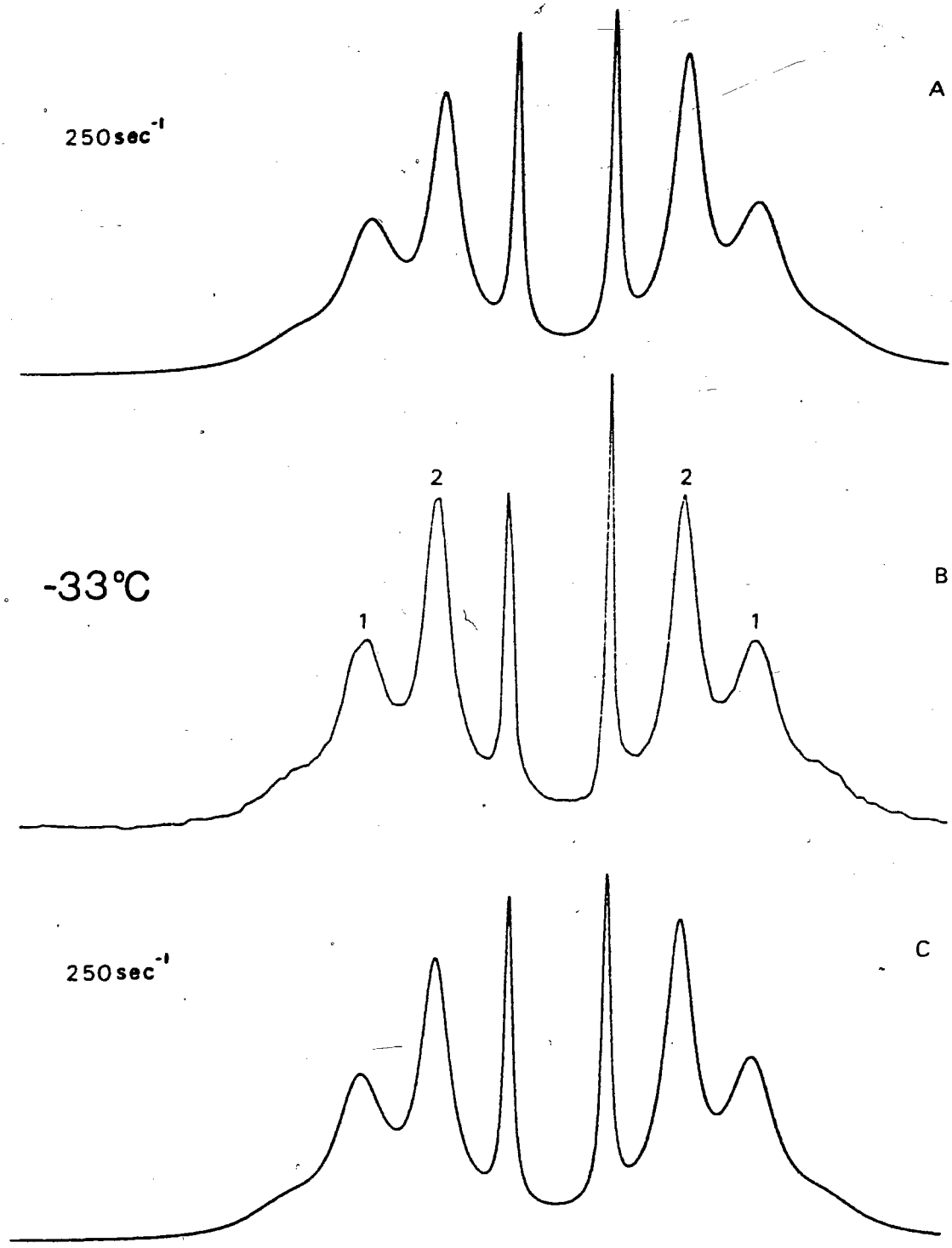

Figure 2.31 Calculated spectra based on the turnstile (A) and pairwise axial-equatorial (C) exchanges and the matching observed $^{31}P\{^{1}H\}$ NMR spectrum of $Ru[P(OCH_3)_3]_4P(CH_3)_3$ (B). The observed and calculated spectra are labeled with the temperature and rates, respectively.

The calculated line shapes based on the turnstile process were used to simulate the variable temperature $^{31}P\{^{1}H\}$ NMR spectra of $Ru[P(OCH_3)_3]_4P(CH_3)_3$. The calculated and observed spectra arising from the A_3B and X parts of the A_3BX spin system are shown in figures 2.32 and 2.33, respectively. The calculated line shapes in figure 2.33 are in excellent agreement with the experimental data. The agreement between the simulated line shapes and the observed data for the A_3B portion of the spectrum (figure 2.32) is poorer than that found for the X region. This is attributed to the complex nature of the apparent A triplet: the central line arises from eight individual transitions while the two outer lines are due to four transitions each. The Eyring activation parameters calculated from the rate versus temperature data are as follows: $\Delta H^{\ddagger}$= 10.9±0.3 kcal mol^{-1}, $\Delta S^{\ddagger}$= -1.9±1.1 cal/mol-°K, $\Delta G^{\ddagger}$ (298 °K)= 11.5±0.4 kcal mol^{-1}. The activation entropy is small, consistent with an intramolecular exchange process.

The results of the line shape calculations for $Ru[P(OCH_3)_3]_4L$ (L= $P(OC_6H_5)_3$, $SbMe_3$, PMe_3) may be interpreted as follows. Firstly, line shapes based on the restricted Berry process shown in in figure 2.26 were in good agreement with the variable temperature $^{31}P\{^{1}H\}$ NMR spectra of $Ru[P(OCH_3)_3]_4P(OC_6H_5)_3$ (an equatorial isomer in the slow exchange limit). The process pictured in figure 2.26 is not available to an axial $Ru[P(OCH_3)_3]_4L$ isomer: any pairwise exchange of the two axial and two equatorial ligands necessarily

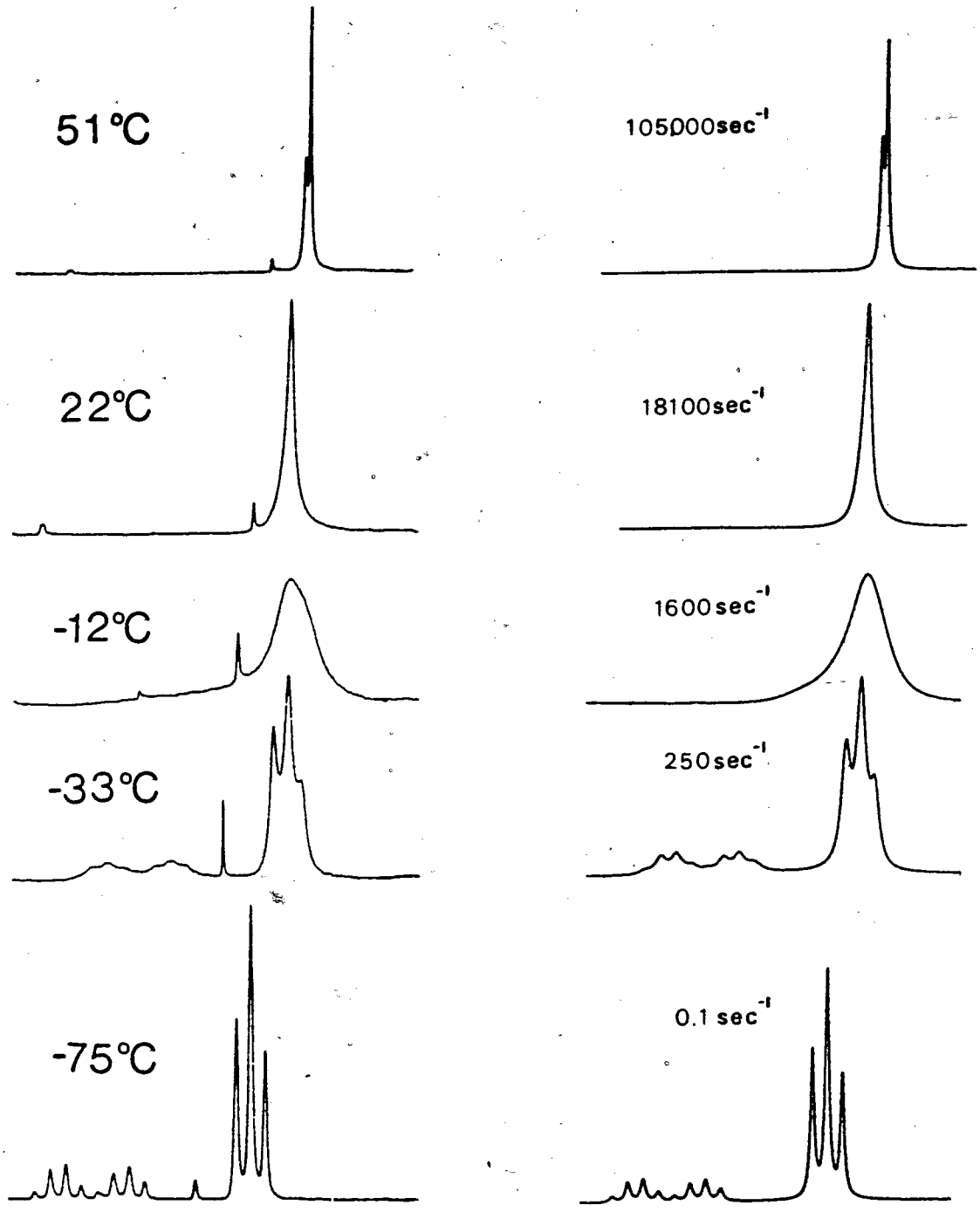

Figure 2.32 The low field portions of the variable temperature $^{31}P\{^{1}H\}$ NMR spectra of $Ru[P(OCH_3)_3]_4P(CH_3)_3$ and matching calculated line shapes based on the turnstile mechanism. The observed and calculated spectra are labeled with the temperatures and rates, respectively.

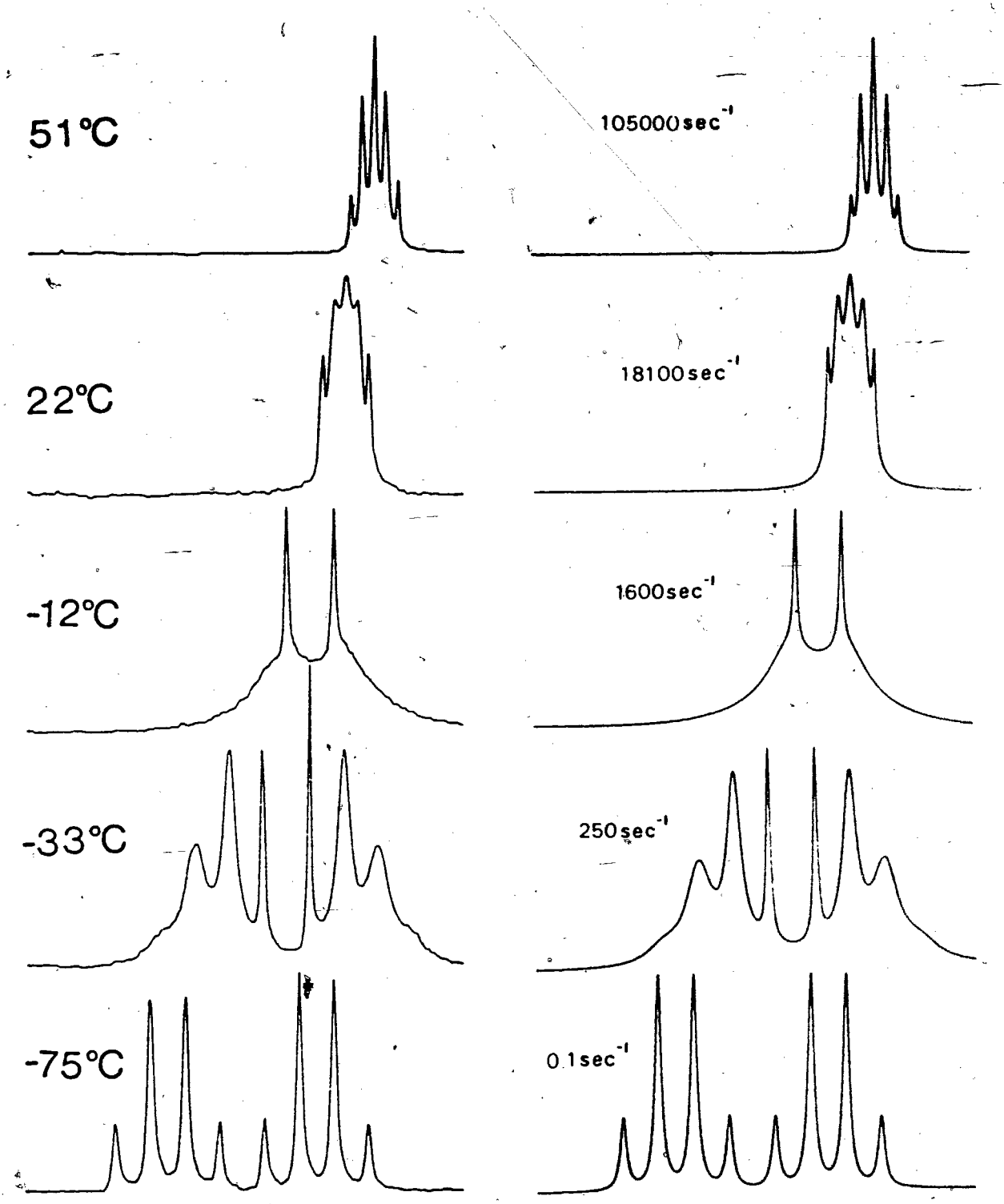

Figure 2.33 The high field portions of the variable temperature $^{31}P\{^{1}H\}$ NMR spectra of $Ru[P(OCH_3)_3]_4P(CH_3)_3$ and matching calculated line shapes based on the turnstile mechanism. The observed and calculated spectra are labeled with the temperatures and rates, respectively.

forms the equatorial isomer (i.e. L does not remain in an axial site). Four different physical mechanisms (three permutationally distinct processes) were considered for the axially substituted species $Ru[P(OCH_3)_3]_4L$ (L= $SbMe_3$, PMe_3). For both complexes, these three permutational sets generated calculated line shapes with differences too minor to meaningfully favour one of the proposed exchange processes over the others. These results suggest that different intramolecular exchange processes may operating for the axial versus the equatorial $Ru[P(OCH_3)_3]_4L$ isomers.

The $\Delta G^{\ddagger}$ (298 °K) values from the Eyring activation parameters for $Ru[P(OCH_3)_3]_4P(OC_6H_5)_3$ and $Ru[P(OCH_3)_3]_4P(CH_3)_3$ are 7.6±0.4 kcal mol^{-1} and 11.5±0.4 kcal mol^{-1}, respectively. The large $\Delta S^{\ddagger}$ value found for $Ru[P(OCH_3)_3]_4Sb(CH_3)_3$ makes the Eyring parameters calculated for this complex suspect. The large difference in $\Delta G^{\ddagger}$ (298 °K) between $Ru[P(OCH_3)_3]_4P(OC_6H_5)_3$ and $Ru[P(OCH_3)_3]_4P(CH_3)_3$ may be interpreted in terms of a lower activation barrier for intramolecular exchange in an equatorial isomer with respect to an axial isomer. However, the effects of the different steric and electronic properties of the PMe_3 and $P(OC_6H_5)_3$ ligands cannot be discounted. If it is assumed that the activation barrier for the intramolecular exchange process operating for an equatorial isomer of $Ru[P(OCH_3)_3]_4L$ is lower than that associated with the (presumably different) exchange process for an axial isomer, some alternate interpretations of earlier results may be advanced. Recall that the low temperature

$^{31}P\{^{1}H\}$ NMR spectrum of $Ru[P(OCH_3)_3]_4P(OCH_2)_3CCH_3$ (162.0 MHz) revealed that resonances due to the minor (i.e. equatorial) isomer were broader than those due to the axial counterpart. In light of the previous discussion, this may be explained in terms of the equatorial isomer possessing a lower energy pathway for ligand exchange with respect to the axial isomer. Recall that the previously proposed rationale for the differences in line widths for the resonances due to the two isomers was based on isomer interconversion.

The assumption of different ligand exchange mechanisms for the axial and equatorial $Ru[P(OCH_3)_3]_4L$ isomers also allows an explanation for the apparent high site preference of a given ligand L: only for $Ru[P(OCH_3)_3]_4P(OCH_2)_3CCH_3$ was there low temperature $^{31}P\{^{1}H\}$ NMR evidence for a minor isomer. For an $Ru[P(OCH_3)_3]_4L$ derivative where the site preference of L was axial, a minor amount of the equatorial isomer might easily go unnoticed by variable temperature $^{31}P\{^{1}H\}$ NMR techniques; a low energy intramolecular exchange process for this minor isomer could leave the associated ^{31}P resonances broadened and unresolved in the baseline.

An approximate method based on differences in NMR line widths near the slow exchange limit was used to calculate free energies of activation associated with the fluxional processes for the $Ru[P(OCH_3)_3]_4L$ derivatives. These $\Delta G^{\ddagger}$ values (at a single temperature) are shown in table 7.1 of appendix 2 (page 350), where a brief presentation of the method is also given.

Our original intention was to examine possible correlations of these values with the steric and electronic properties of the ligand L. However, subsequent results argued against the validity of this approach.

The results of the line shape analyses for $Ru[P(OCH_3)_3]_4L$ (L= $P(OC_6H_5)_3$, PMe_3, $SbMe_3$) suggested that different nonrigid processes may be operating for the axial and equatorial isomers. Any attempt to correlate the activation barrier with the properties of L must reasonably assume a common fluxional mechanism.

The applicability of the approximate method used to calculate the $\Delta G^{\ddagger}$ values for the $Ru[P(OCH_3)_3]_4L$ derivatives is also in question. The line shape analyses for $Ru[P(OCH_3)_3]_4P(OC_6H_5)_3$ and $Ru[P(OCH_3)_3]_4P(CH_3)_3$ allowed determination of the Eyring activation parameters for these two molecules. A free energy of activation calculated from these values is presumably more accurate than one calculated from an approximate method. The agreement between $\Delta G^{\ddagger}$ (at a single temperature) based on the approximate method and the analogous free energy of activation (at that same temperature) based on the Eyring parameters was not good for these two species. The value of $\Delta G^{\ddagger}$ (156 °K) for $Ru[P(OCH_3)_3]_4P(OC_6H_5)_3$ calculated by the approximate method was 9.0 kcal mol^{-1} while the Eyring $\Delta H^{\ddagger}$ and $\Delta S^{\ddagger}$ values gave a corresponding $\Delta G^{\ddagger}$ of 8.2±0.4 kcal mol^{-1} at the same temperature. The free energies of activation for $Ru[P(OCH_3)_3]_4P(CH_3)_3$ based on the approximate method and the

Eyring parameters (both at T= 229 °K) were 12.1 and 11.3±0.4 kcal mol^{-1}, respectively.

The results discussed in the previous two paragraphs cast serious doubt on the validity of using the $\Delta G^{\ddagger}$ values calculated by approximate methods to search for correlations of the activation barriers of the $Ru[P(OCH_3)_3]_4L$ derivatives with the steric and electronic properties of L.

2.3.4 Attempted Preparation of $Ru[P(OCH_3)_3]_4(\eta^2\text{-alkene})$ Derivatives.

The ease with which $Ru[P(OCH_3)_3]_4(\eta^2\text{-}C_2H_4)$ was prepared from $Ru[P(OCH_3)_3]_5$ and excess C_2H_4 under photolytic conditions suggested that other $Ru[P(OCH_3)_3]_4(\eta^2\text{-alkene})$ complexes might be readily synthesized. This was not the case.

The ultraviolet irradiation of $Ru[P(OCH_3)_3]_5$ and excess dimethyl fumurate in hexane for 4 h led to the isolation of a pale yellow, waxy solid. A $^{31}P\{^1H\}$ NMR spectrum of this solid revealed a number of multiplets and a singlet due to unreacted $Ru[P(OCH_3)_3]_5$. None of these resonances could be assigned to the expected $Ru[P(OCH_3)_3]_4(\eta^2\text{-alkene})$ derivative.

The photolysis of $Ru[P(OCH_3)_3]_5$ and excess cyclooctene in hexane for 4 h left a pale yellow solution. From this was isolated a waxy, yellow solid which was analyzed by $^{31}P\{^1H\}$ NMR

spectroscopy. The resulting spectrum again revealed a number of resonances. In this case, these included two broad signals at δ ~15 and 30 (vide infra).

Reasoning that the steric bulk of dimethyl fumurate and cyclooctene were inhibiting coordination to the $Ru[P(OCH_3)_3]_4$ moiety, several smaller alkenes were employed. A solution of $Ru[P(OCH_3)_3]_5$ and excess propene in hexane was photolyzed for 4 h. The resultant colourless, waxy solid was analyzed by variable temperature $^{31}P\{^1H\}$ NMR spectroscopy. The low temperature spectrum (-43 °C, toluene-d_8) revealed resonances due to several species; part of the spectrum underwent collapse as the temperature was raised. The ^1H NMR spectrum of the reaction product (toluene-d_8, 25 °C) also indicated the presence of several species. There was no basis for even a tentative assignment of the resonances in the ^1H and $^{31}P\{^1H\}$ NMR spectra.

The ultraviolet irradiation of $Ru[P(OCH_3)_3]_5$ and excess 1-butene in hexane for 4 h resulted in a pale yellow solution. From this was isolated a pale yellow, waxy solid which was examined by variable temperature $^{31}P\{^1H\}$ NMR spectroscopy. The spectrum at -57 °C (toluene-d_8) again revealed a number of resonances. These included a doublet (δ 20.9, J= 29.5 Hz) and a triplet (δ 40.8, J= 29.7 Hz) of relative intensity 2:1, respectively. As the temperature was increased, these two resonances broadened and were near coalescence at 25 °C. The spectral parameters and variable temperature behaviour of this species were very similar to those of $Ru[P(OCH_3)_3]_3(\eta^4\text{-}C_8H_6)$

(see chapter 2 experimental section). The presence of 1,3-butadiene in the reaction mixture may be reasonably explained; even a small percentage impurity of this diene in 1-butene would result in measurable amounts being present when an excess of the alkene is used in the reaction.

The failure to isolate $Ru[P(OCH_3)_3]_4(\eta^2\text{-alkene})$ derivatives from the UV irradiation of $Ru[P(OCH_3)_3]_5$ and the previously mentioned olefins may be rationalized in terms of both electronic and steric arguments. The ease with which ethylene is thermally lost from $Ru[P(OCH_3)_3]_4(\eta^2\text{-}C_2H_4)$ suggests that the $Ru\text{-}C_2H_4$ bond is considerably weaker than the $Ru\text{-}P(OCH_3)_3$ bonds in this complex. The Ru-alkene bonds for the other olefins used in this study are expected to display similar characteristics. Even if the $Ru[P(OCH_3)_3]_4(\eta^2\text{-alkene})$ complexes were formed in solution, the relatively harsh reaction conditions (i.e. UV irradiation) would reasonably cause olefin dissociation; the availability of alternative reaction modes for the coordinatively unsaturated $Ru[P(OCH_3)_3]_4$ species has been discussed (see earlier in this chapter).

A qualitative consideration of steric effects for olefin ligands in trigonal bipyramidal complexes is informative. Recall that the static solution structure of $Ru[P(OCH_3)_3]_4(\eta^2\text{-}C_2H_4)$ was based on a trigonal bipyramid with the ethylene occupying an equatorial coordination site. This is in accord with theoretical predictions that single-faced π-acceptor ligands prefer equatorial sites in a D_{3h} molecule [61,67]. These studies also

predict the preference for olefin coordination parallel to the equatorial plane. Consider the molecular structure of $Ru[P(OCH_3)_3]_4P(OCH_2)_3CCH_3$ (figure 2.25). If one imagines replacing the $P(OCH_2)_3CCH_3$ ligand with an olefin coordinated in the manner just described, the consequent steric implications may be qualitatively considered. As substituents are added to the olefin, the non-bonded interactions between it and the equatorial $P(OCH_3)_3$ ligands should increase. Assuming that considerable spatial crowding already occurs in an $Ru[P(OCH_3)_3]_4L$ molecule (L= two electron donor ligand), it is reasonable that a steric threshold to coordination of substituted olefins should exist.

When these steric and electronic arguments are used in tandem, the instability of $Ru[P(OCH_3)_3]_4(\eta^2$-alkene) complexes with substituted alkenes is not unexpected: the inherently weak Ru-olefin bond and the steric congestion around the metal centre combine to produce an extremely labile molecule.

An alternative approach was used in an attempt to prepare alkene analogues of $Ru[P(OCH_3)_3]_4(\eta^2-C_2H_4)$. A solution of $Ru[P(OCH_3)_3]_4(\eta^2-C_2H_4)$ and excess propene in hexane was heated at 40 °C for 2 h. The oily, yellow solid isolated from this reaction was analyzed by ^1H NMR spectroscopy, which revealed that ~80% of the starting material remained. When the reaction was allowed to proceed for 7 h at 60 °C, a brown semi-solid was isolated. The ^1H NMR spectrum of this product revealed a number of unidentified resonances in the region δ 0-5.

The thermal reaction of $Ru[P(OCH_3)_3]_4(\eta^2\text{-}C_2H_4)$ and excess cyclooctene in toluene (40 °C) was monitored by $^{31}P\{^1H\}$ NMR spectroscopy. The exchange broadened resonances of the starting material were slowly replaced by two broad signals (δ 32 and 14) over the course of 12 h. Cooling the solution to -37 °C caused these to sharpen into a spectrum due to an A_2B_2 spin system. This spectrum was successfully simulated based on this assumption; the spectral parameters were δ_A 15.6, δ_B 32.4, and J_{AB}= 63.7 Hz. This is exactly the behaviour expected for $Ru[P(OCH_3)_3]_4(\eta^2$-cyclooctene), to which these resonances are assigned. This complex was not stable under the reaction conditions, however. A weak multiplet (δ 5) and a singlet due to $Ru[P(OCH_3)_3]_5$ were also present in the $^{31}P\{^1H\}$ NMR spectrum after 12 h at 45 °C; continued heating increased the intensity of these resonances at the expense of the signals due to $Ru[P(OCH_3)_3]_4(\eta^2$-cyclooctene).

The results of this chapter may be summarized as follows. The complexes $Ru[P(OR)_3]_3(\eta^4\text{-}C_4H_6)$ (R= Me, Et, *i*-Pr) and $Ru[P(OR)_3]_3(\eta^4\text{-}C_5H_8)$ (R= Me, Et) were prepared by the photolysis of $Ru[P(OCH_3)_3]_5$ or $Ru[P(OR)_3]_3(CO)_2$ and excess diene in hexane. These complexes were found to be stereochemically nonrigid in solution by $^{31}P\{^1H\}$ NMR spectroscopy; the slow exchange limit spectra were consistent with a square pyramidal structure with the diene occupying two basal sites. The fluxional barriers for these diene complexes appeared to be mainly dependent upon the steric properties of the phosphite ligands. The complex

$Ru[P(OCH_3)_3]_4(\eta^2\text{-}C_2H_4)$ was prepared by the photolysis of $Ru[P(OCH_3)_3]_5$ and excess C_2H_4 in hexane. The ethylene complex readily lost C_2H_4 under thermal conditions and was used to prepare a series of $Ru[P(OCH_3)_3]_4L$ derivatives (L= $P(OCH_2)_3CCH_3$, PF_3, $P(OC_2H_5)_3$, $P(OCH(CH_3)_2)_3$, $P(OC_6H_5)_3$, $P(CH_3)_3$, $P(CH_3)_2C_6H_5$, $PCH_3(C_6H_5)_2$, $P(C_2H_4CN)_3$, $SbMe_3$). These derivatives were studied by variable temperature $^{31}P\{^1H\}$ NMR spectroscopy which revealed that rapid ligand exchange was occurring in solution at 25 °C. The slow exchange limit $^{31}P\{^1H\}$ NMR spectra of these $Ru[P(OCH_3)_3]_4L$ derivatives were all consistent with trigonal bipyramidal coordination around the metal. Both equatorial (L= PF_3, $P(OC_6H_5)_3$) and axial (L= $P(OC_2H_5)_3$, $P(OCH(CH_3)_2)_3$, $P(CH_3)_3$, $P(CH_3)_2C_6H_5$, $SbMe_3$) isomers were observed; $Ru[P(OCH_3)_3]_4P(OCH_2)_3CCH_3$ existed as a mixture of both isomers (predominantly axial) in solution. The site preference for the $Ru[P(OCH_3)_3]_4L$ derivatives appeared to be correlated mainly with the electronic properties of the ligands, although steric considerations possibly played a role in certain cases. The X-ray crystal structure of $Ru[P(OCH_3)_3]_4P(OCH_2)_3CCH_3$ revealed a trigonal bipyramidal molecule with the caged phosphite in an equatorial position. This result was not in accord with the static solution structure of the molecule. The results of line shape analyses for the $^{31}P\{^1H\}$ NMR spectra of $Ru[P(OCH_3)_3]_4L$ (L= $P(OC_6H_5)_3$, PMe_3, $SbMe_3$) suggested that different fluxional mechanisms might be operating for the axial and equatorial isomers. Efforts to prepare analogues of $Ru[P(OCH_3)_3]_4(\eta^2\text{-}C_2H_4)$ with other alkenes were largely unsuccessful.

2.4 Experimental Section

Materials. Dodecacarbonyltriosmium and dodecacarbonyltriruthenium were prepared by literature methods [68,69] as were $M(CO)_5$ (M= Ru, Os) [70]. The ligands $P(OR)_3$ (R= Me, Et, *i*-Pr, *n*-Bu, Ph, *o*-tolyl) and PR_3 (R= Me, *i*-Pr, *n*-Bu) were obtained commercially (Strem) and stored under nitrogen prior to use. Also purchased (Strem) were PF_3, $P(CH_2CH_2CN)_3$, PPh_3, $PMePh_2$, and PMe_2Ph; the latter two were held under nitrogen prior to use. The caged phosphite $P(OCH_2)_3CCH_3$ was prepared by a literature method [71] and purified twice by sublimation at room temperature. In addition, $P(OCH_3)_3$ was stored in the dark. Florisil (100-200 mesh) for column chromatography and alumina (grade I) were purchased from Fisher Scientific Company. Cyclooctene, 1,5-cyclooctadiene, norbornadiene, methyl iodide, benzyl bromide, ethyl iodide, and allyl bromide were all purchased commercially (Aldrich Chemical Comp.) and used as received. Ethylene (Liquid Air Ltd.), propene, and 1-butene (Matheson) were purchased in lecture bottles. Ammonium hexafluorophosphate (Alfa Products) and $NOPF_6$ (ICN Pharmaceuticals) were used as received.

General Procedures. All manipulations were performed under a nitrogen atmosphere, utilizing either standard Schlenk techniques or a dry box. Hexane, heptane, and toluene were refluxed over potassium, distilled, and stored over 4A-type molecular sieves (all under nitrogen) prior to use. Methylene

chloride was refluxed over P_2O_5 and treated similarly. Tetrahydrofuran was refluxed in the presence of potassium and benzophenone before distillation and CH_3CN was distilled from CaH_2. All dried solvents were stored in vessels fitted with Teflon valves. Ultraviolet irradiations were performed using a Hanovia 200-W lamp inside a water-cooled quartz jacket. The glass Carius tubes (Pyrex) employed for these UV reactions measured 25x2.5 cm and were fitted with Teflon valves. The distance between the UV source and the reaction solution was typically 3 cm. Stirring was accomplished with a magnetic stirring bar and stirrer. Solutions contained in these Carius tubes were degassed as follows. The tube was cooled to -196 °C until the contents were frozen. Residual volatiles were then removed by vacuum pump ($\approx 10^{-3}$ torr). The tube was subsequently warmed to room temperature. This procedure was repeated until the solution melted with minimal gas evolution. Column chromatography was performed using $P(OCH_3)_3$-deactivated Florisil as the adsorbent. This was prepared by slowly running hexane:$P(OCH_3)_3$ (4:1, v/v) down a Florisil column and washing the excess trimethyl phosphite free with pure hexane. Alumina filtrations were performed in a narrow chromatography column (diameter 1.2 cm) under a nitrogen atmosphere. The filtrate was generally washed through the column with several mL of pure solvent.

Analytical Procedures. Elemental analyses were performed by Mr. M. K. Yang of the microanalytical laboratory of Simon Fraser

University or by Canadian Microanalytical Services Ltd., Vancouver, B.C. Melting points were measured in capillary tubes (sealed under nitrogen) on a Gallenkamp apparatus and are uncorrected.

Mass spectrometric data was obtained on a Hewlett-Packard 5985 GC-MS system or a Kratos MS-50 spectrometer. The Hewlett-Packard instrument operated in EI (70 eV), CI (various gases), or FAB (xenon, sulpholane) mode, as indicated, while the Kratos spectrometer operated in EI mode (70 eV) only and was used primarily for compounds with parent ions > *m/e* 1000. Computer simulations of parent ion patterns were obtained from software associated with the Kratos spectrometer or the computer program ISOC, obtained from Professor W. A. G. Graham of the University of Alberta.

All infrared spectra were recorded with a Perkin-Elmer 983G spectrophotometer. The instrument calibration was checked periodically with carbon monoxide gas. The ν(CO) values are thought to be accurate to ±1 cm^{-1}.

Nuclear magnetic resonance data were obtained with a Varian XL-100 spectrometer (fitted with a Nicolet 1080 computer and pulse-FT accessory) for ^{1}H (100.1 MHz), $^{31}P\{^{1}H\}$ (40.5 MHz), and ^{13}C (25.2 MHz), a Bruker SY-100 pulse-FT spectrometer for ^{1}H (100.0 MHz), ^{13}C (25.18 MHz), and ^{31}P (40.54 MHz), and a Bruker WM-400 spectrometer for ^{1}H (400.13 MHz), ^{13}C (100.6 MHz), and ^{31}P (162.0 MHz). Proton decoupling, where indicated, was

accomplished by broad band irradiation using the minimum power required for complete decoupling (i.e. to reduce dielectric heating of the sample). All three spectrometers were fitted with variable temperature units. All chemical shifts are reported as positive when downfield from the reference. Unless otherwise stated, δ values quoted for multiplets refer to the value at the multiplet centre. The ^{1}H NMR chemical shifts are reported relative to TMS at δ 0 at 25 °C (via accepted chemical shifts for residual protons of the deuterated solvent). The ^{13}C NMR chemical shifts are quoted relative to TMS at δ 0 at 25 °C (via accepted ^{13}C shifts for the deuterated solvent). The ^{31}P NMR chemical shifts are given relative to internal $P(OCH_3)_3$ at δ 0 at 25 °C. A solution of 1% $P(OCH_3)_3$ in toluene-d_8/toluene (1:5) at 31 °C was found to exhibit a ^{31}P chemical shift of 140.2 ppm (downfield) relative to external 85% H_3PO_4. The considerable temperature dependence of ^{13}C and particularly ^{31}P chemical shifts necessitated specifying references at a fixed temperature.

The temperatures quoted for the variable temperature $^{31}P\{^{1}H\}$ NMR investigations in this thesis were obtained by several methods. An internal, coaxial capillary containing a toluene-d_8 solution of $P(C_6H_5)_3$ and $OP(C_6H_5)_3$ (both 0.1M) was used for $^{31}P\{^{1}H\}$ NMR spectra run in toluene or toluene-d_8/toluene at 40.54 or 40.5 MHz. The difference in $^{31}P\{^{1}H\}$ chemical shift between these species (Δδ) varies with temperature, and the following relationship, accurate to ± 0.5 °C, has been derived

[72]:

$$T(°C) = -30.929\Delta\delta(ppm) - 937.244$$

Temperatures measured by this method are thought to be accurate to ±1.0 °C. This technique was not practical for variable temperature $^{31}P\{^{1}H\}$ NMR spectra run in $CD_2Cl_2/CHFCl_2$ (1:4). In this case, a 5 mm NMR tube containing the previously described, temperature reference solution was measured by $^{31}P\{^{1}H\}$ NMR over the useful range of the solvent (-90 to ~100 °C). The temperatures so determined were plotted against the corresponding value displayed on the temperature controller unit of the SY-100 spectrometer. This calibration was extrapolated to obtain temperatures below ~-90 °C; these are thought to be accurate to ±2.0 °C. Temperatures for ^{1}H, ^{13}C, and ^{31}P NMR spectra measured on the WM-400 spectrometer were determined from the temperature controller unit. These values are thought to be accurate to ±2-4 °C.

The $^{31}P\{^{1}H\}$ NMR investigations of the complexes $M[P(OR)_3]_x(CO)_{5-x}$ (M= Ru, Os; R= Me, Et, *i*-Pr, *n*-Bu) were performed using NMR tubes fitted with Teflon valves. These tubes were not spun during the acquisition of the spectra. All other NMR investigations were performed in NMR tubes fitted with screw caps containing Teflon liners.

Computer calculated and simulated NMR spectra (static) were obtained from NMRCAL, a program associated with the Nicolet 1080 computer, PANIC, a program written for the Bruker Aspect 2000

computer, or UEA/NMRII, a program written by Dr. R. K. Harris and modified by Dr. A. S. Tracey. The calculation of NMR line shapes for chemically exchanging systems were performed using the programs DNMR3 (from QCPE), EXCHANGE (written by Dr. R. E. D. McClung), and EXSHORT/3 (written by Dr. Whitesides and modified by Dr. R. G. Cavell). The exchange rates were determined by varying the rates used in the calculations until a best visual fit was obtained between the simulated and observed spectra. This process was repeated for five to seven observed spectra in the exchange region for each complex. The k versus T data thus determined were used to calculate activation parameters via a least squares fit to the Eyring equation.

The variable temperature ^{13}C NMR spectra of $Os_3[P(OCH_3)_3]_x(CO)_{12-x}$ (x= 1,2,4) were measured on samples which had been ~50% enriched with ^{13}CO. These samples were synthesized as described for the unenriched compounds, using $Os_3(^{13}CO)_{12}$ as a starting material. The enriched triosmium carbonyl was prepared by stirring $Os_3(CO)_{12}$ in toluene under 2 atm of ^{13}CO (99% ^{13}CO, Cambridge Isotope Laboratories) for 3 days at 100 °C.

Preparation of $Ru[P(OCH_3)_3]_5$. A glass Carius tube was charged with $Ru_3(CO)_{12}$ (0.48 g, 0.75 mmol), $P(OCH_3)_3$ (8 mL, excess), and hexane (20 mL). The solution was degassed with three freeze-pump-thaw cycles as previously described. The stirred solution was irradiated with ultraviolet light for approximately 48 h. The carbon monoxide produced was removed under vacuum (at -196 °C) periodically (e.g. at 4, 8, 20, and 36

h). The very pale yellow solution was transferred to a Schlenk tube and cooled to -78 °C for 6h. The colourless supernatant solution was decanted to another Schlenk tube, leaving an oily yellow residue which was discarded. Vacuum removal of all volatiles left a white, waxy solid. The solid was dissolved in hexane (10 mL) and filtered through alumina (1 cm). The solvent was removed from the filtrate on the vacuum line to yield $Ru[P(OCH_3)_3]_5$ (0.94 g, 66 %) as a waxy, crystalline solid: mp 188-190 °C (dec), ^1H NMR ($CDCl_3$, 25 °C, 100.1 MHz) δ 3.50 (multiplet), $^{31}P\{^1H\}$ NMR (toluene-d_8, 25 °C, 40.54 MHz) δ 26.7 (singlet); mass spectrum (EI, 70 eV), calc. for $^{102}RuC_{15}H_{45}O_{15}P_5$, *m/e* 722, found, *m/e* 722. Anal. calc. for $C_{15}H_{45}O_{15}P_5Ru$: C, 25.01; H, 6.29; P, 21.47. Found: C, 25.06; H, 6.66; P, 22.21.

The penta(phosphite) complex is extremely air-sensitive, decomposing to a brown oil during 10 minutes exposure to air. The extreme solubility of $Ru[P(OCH_3)_3]_5$ in common organic solvents makes recrystallization impractical.

The time required for optimum yields of $Ru[P(OCH_3)_3]_5$ is dependent upon the particular glass tube and UV source used. The reaction is best monitored by $^{31}P\{^1H\}$ NMR spectroscopy. Prolonged irradiation of the reaction solution causes further reaction of $Ru[P(OCH_3)_3]_5$, as evidenced by a number of multiplets in the $^{31}P\{^1H\}$ NMR spectrum [5].

Preparation of $Ru[P(OCH_3)_3]_3(\eta^4\text{-}C_4H_6)$. A hexane solution (20 mL) of $Ru[P(OCH_3)_3]_5$ (0.54 g, 0.75 mmol) was placed in a glass Carius tube and degassed with two freeze-pump-thaw cycles. A 5 mL sample of 1,3-butadiene was condensed into the cold evacuated tube, which was then warmed to 25 °C. The stirred solution was irradiated with ultraviolet light for 8 h and remained colourless during this period. Removal of the volatiles under vacuum yielded an oily solid which became a waxy solid upon stirring. The extreme solubility of the product in all common solvents made recrystallization impractical. The compound was purified by sublimation at 65-70°C onto a 9°C probe ($<10^{-3}$ torr) for 18 h. This resulted in an off-white crystalline solid on the probe and a small amount of yellow oil as residue. The sublimate was washed into another Schlenk tube with hexane and stripped under vacuum to yield $Ru[P(OCH_3)_3]_3(\eta^4\text{-}C_4H_6)$ as a waxy white solid (estimated yield: 0.3 g, 75%): mp 204-208 °C (dec.); ^1H NMR ($CDCl_3$, 25°C, 100.1 MHz) δ 4.90 (triplet, J= 6 Hz, rel. int.= 2), δ 1.38 (broad doublet, $J\simeq$ 6 Hz, rel. int.= 2), δ -0.42 (multiplet, rel. int.= 2), δ 3.52 (doublet, J_{PH}= 11 Hz, rel. int.= 27); $^{31}P\{^1H\}$ NMR ($CDCl_3$, -50 °C, 40.5 MHz) δ 19.8 (doublet, J_{PP}= 26 Hz, rel. int.= 2), δ 41.3 (triplet, J_{PP}= 26 Hz, rel. int.= 1); $^{31}P\{^1H\}$ NMR ($CDCl_3$, 50°C, 40.5 MHz) δ 24.8 (broad singlet).

The $^{31}P\{^1H\}$ NMR spectrum typically showed a small impurity (two multiplets at δ -0.7 and 11.8) of unknown origin; mass spectrum (EI, 70 eV) calc. for $^{102}RuC_{13}H_{33}O_9P_3$ (P), *m/e* 528,

found, *m/e* 528, also *m/e* 474 ($[P-C_8H_6]^+$) and *m/e* 404 ($[P-P(OCH_3)_3]^+$). Anal. calc. for $Ru[P(OCH_3)_3]_3(\eta^4-C_8H_6)$: C, 29.61; H, 6.31. Found: C, 30.05; H, 6.53.

The complex decomposed to a black oil during 30 minutes exposure to air.

Preparation of $Ru[P(OC_2H_5)_3]_3(CO)_2$. A glass Carius tube was charged with $Ru_3(CO)_{12}$ (0.10 g, 0.16 mmol), $P(OC_2H_5)_3$ (2 mL, excess), and hexane 15 mL. The solution was degassed three times as previously described. The tube was heated at 120 °C for 30 h. The progress of the reaction was periodically monitored by IR spectroscopy, which revealed the stepwise formation of $Ru[P(OC_2H_5)_3](CO)_4$ (ν(CO) (hexane) 2068 (s), 1998 (s), 1967 (s), 1951 (s) cm^{-1}) and $Ru[P(OC_2H_5)_3]_2(CO)_3$ (ν(CO) (hexane) 1927 (s), 1915 (s) cm^{-1}) as intermediate products [73]. The bright yellow solution was transferred to a Schlenk tube and the volatiles were removed under vacuum to afford a yellow oil. This was taken up in hexane (5 mL) and cooled to -78 °C. The yellow mother liquor was decanted off the resultant, pale yellow solid, which was washed with hexane (5 mL) at -78 °C. The yield of $Ru[P(OC_2H_5)_3]_3(CO)_2$ was 0.075 g (74 %): mp 48.5-49.0 °C (dec); IR ν(CO) (hexane) 1940 (m), 1888 (s) cm^{-1}; ^1H NMR (hexane, 25 °C, 100.0 MHz) δ 4.12 (multiplet, rel. int.= 2), δ 1.22 (triplet, J_{HH}= 7.0 Hz, rel. int.= 3); $^{31}P\{^1H\}$ NMR (hexane, 25 °C, 40.54 MHz) δ 25.0 (singlet); mass spectrum (EI, 70 eV) calc. for $^{102}RuC_{20}H_{45}O_{11}P_3$ (P), *m/e* 656, found, *m/e* 656, also *m/e* 628 ($[P-CO]^+$) and *m/e* 598 ($[P-2C_2H_5]^+$). Anal. calc. for

$C_{20}H_{45}O_{11}P_3Ru$: C, 36.64; H, 6.92. Found: C, 36.79; H, 7.10.

The tris(phosphite) complex was moderately soluble in hexane and soluble in other common organic solvents. A sample of $Ru[P(OC_2H_5)_3]_3(CO)_2$ turned brown during 20 minutes exposure to air.

The yellow mother liquor just described was reduced in volume (5 mL) and chromatographed on a $P(OCH_3)_3$-deactivated Florisil column. Hexane elution caused development of a yellow band which was collected. Vacuum removal of the solvent gave a yellow solid (~15 mg) which was tentatively identified as $Ru_3[P(OEt)_3]_3(CO)_9$ (see text): mp 166.5-171.5 °C (dec); ν(CO) (hexane) 2022 (s), 1983 (m), 1966 (s) cm^{-1}; ^1H NMR (acetone-d_6, 25 °C, 100.13 MHz) δ 4.08 (multiplet, rel. int.= 2), δ 1.29 (triplet, J_{HH}= 7.1 Hz, rel. int.= 3); $^{31}P\{^1H\}$ NMR (toluene-d_8, -40 °C, 40.54 MHz) δ 6.8 (singlet); $^{31}P\{^1H\}$ NMR (toluene-d_8, 36 °C, 40.54 MHz) δ 4.0 (singlet).

This complex was very soluble in both hexane and CH_2Cl_2.

Preparation of $Ru[P(OCH(CH_3)_2)_3]_3(CO)_2$. A glass Carius tube was charged with $Ru_3(CO)_{12}$ (0.320 g, 0.500 mmol), $P(OCH(CH_3)_2)_3$ (4 mL, excess), and hexane (20 mL). The reaction mixture was degassed three times. The tube was heated at 110 °C for 23 h. A periodical monitoring of the reaction by IR spectroscopy revealed the stepwise formation of $Ru[P(OCH(CH_3)_2)_3](CO)_4$ (ν(CO) (hexane) 2067 (s), 1994 (m), 1953 (s), 1946 (s) cm^{-1}) and $Ru[P(OCH(CH_3)_2)_3]_2(CO)_3$ (ν(CO) (hexane) 1921 (s), 1908 (s) cm^{-1})

as intermediate products [73]. The yellow-orange solution was transferred to a Schlenk tube. The volatiles were removed under vacuum to leave an oily, yellow solid. This was sublimed at 80 °C onto a -78 °C probe ($<10^{-3}$ torr) for several days. The resultant sublimate was a pale yellow solid; an oily, yellow residue remained. The probe material was transferred to a Schlenk tube, affording 0.50 g (43 %) of $Ru[P(OCH(CH_3)_2)_3]_3(CO)_2$: mp 112-117 °C (dec); IR ν(CO) (hexane) 1931 (m), 1877 (s) cm^{-1}; ^1H NMR (acetone-d_6, 25 °C, 100.0 MHz) δ 4.84 (multiplet, rel. int.= 1), δ 1.27 (doublet, J_{HH}= 6.2 Hz, rel. int.= 6); $^{31}P\{^1H\}$ NMR (acetone-d_6, 25 °C, 40.54 MHz) δ 20.2 (singlet); mass spectrum (EI, 70 eV) calc. for $^{102}RuC_{29}H_{63}O_{11}P_3$ (P), *m/e* 782, found, *m/e* 782, also *m/e* 754 ([P-CO]$^+$), *m/e* 723 ([P-(O-*i*-Pr)]$^+$), *m/e* 574 ([P-$P(OCH(CH_3)_2)_3$]$^+$), and *m/e* 546 ([P-$P(OCH(CH_3)_2)_3$-CO]$^+$). Anal. calc. for $C_{29}H_{63}O_{11}P_3Ru$: C, 44.55; H, 8.00. Found: C, 44.35; H, 7.97.

The tris(phosphite) complex was very soluble in common organic solvents. A sample of $Ru[P(OCH(CH_3)_2)_3]_3(CO)_2$ turned brown during a one day exposure to air.

The previously described oily, yellow residue was dissolved in hexane (5 mL) and chromatographed on a $P(OCH_3)_3$-deactivated Florisil column. Hexane elution caused development of a yellow band which was collected. Subsequent filtration of this solution and vacuum removal of the solvent left a waxy, orange-yellow solid (~15 mg). An IR spectrum in hexane revealed a mixture of $Ru[P(OCH(CH_3)_2)_3]_3(CO)_2$ and another species. The latter was

tentatively identified as $Ru_3[P(OCH(CH_3)_2)_3]_3(CO)_9$ (see text): ν(CO) (hexane) 2021 (s), 1980 (m), 1963 (s) cm^{-1}.

Attempted Preparation of $Ru[P(O-n-C_4H_9)_3]_3(CO)_2$. A glass Carius tube containing $Ru_3(CO)_{12}$ (0.10 g, 0.16 mmol), $P(O-n-C_4H_9)_3$ (2 mL, excess), and hexane (15 mL) was cooled to -196 °C. The solution was degassed three times. The tube was heated to 110 °C and the reaction periodically monitored by IR spectroscopy (carbonyl region). Behaviour analogous to that described in the preparations of $Ru[P(OR)_3]_3(CO)_2$ (R= Et, *i*-Pr) was observed: absorptions due to $Ru[P(O-n-C_4H_9)_3](CO)_4$ (ν(CO) (hexane) 2068 (s), 1997 (m), 1966 (s), 1951 (s) cm^{-1}) and $Ru[P(O-n-C_4H_9)_3]_2(CO)_3$ (ν(CO) (hexane) 1928 (s), 1915 (s) cm^{-1}) were present [73]. The reaction solution was pale yellow after 25 h. At this time, IR spectroscopy revealed strong carbonyl absorptions due to $Ru[P(O-n-C_4H_9)_3]_3(CO)_2$ (ν(CO) (hexane) 1938 (m), 1886 (s) cm^{-1}) in addition to several weaker signals. Despite repeated attempts, the tris(phosphite) complex could not be properly purified and isolated.

An attempt was made to separate the previously described mixture by chromatography on a $P(OCH_3)_3$-deactivated Florisil column. Hexane elution caused the development of a yellow band which was collected. This fraction was filtered and evaporated to dryness on the vacuum line, yielding a yellow-orange solid (~30 mg) tentatively identified as $Ru_3[P(O-n-C_4H_9)_3]_3(CO)_5$ (see text): mp 69.5-71.5 °C (dec); IR ν(CO) (hexane) 2021 (vs), 1981 (m), 1964 (s) cm^{-1}; $^{31}P\{^1H\}$ NMR (hexane, 25 °C, 40.54 MHz) δ 4.4

(singlet); mass spectrum (EI, 70 eV) showed *m/e* values >1000, calculated for $C_{45}H_{81}O_{18}P_3Ru_3$, *m/e* 1305. Anal. calc. for $C_{45}H_{81}O_{18}P_3Ru_3$: C, 41.37; H, 6.25. Found: C, 42.25; H, 7.24.

Preparation of $Ru[P(OC_2H_5)_3]_3(\eta^4\text{-}C_4H_6)$. A glass Carius tube was charged with $Ru[P(OC_2H_5)_3]_3(CO)_2$ (0.31 g, 0.47 mmol) and hexane (20 mL). The solution was degassed three times. Into the cold (-196 °C) tube was condensed 1,3-butadiene (3 mL, excess). After warming to room temperature, the stirred solution was irradiated with ultraviolet light for 2.5 h. An IR spectrum of the reaction solution showed complete disappearance of the ν(CO) absorptions due to the starting material. The reaction solution was transferred to a Schlenk tube. The volatiles were removed under vacuum. The resultant yellow oil was sublimed at 55 °C onto a -78 °C probe ($<10^{-3}$ torr) for 48 h. The probe contained a small amount of a white solid which was discarded. The residue was sublimed at 80 °C onto a -78 °C probe ($<10^{-3}$ torr) for 24 h. The colourless sublimate was washed into a separate Schlenk tube with hexane. Vacuum removal of the solvent left $Ru[P(OC_2H_5)_3]_3(\eta^4\text{-}C_4H_6)$ as a waxy, colourless solid (0.16 g, 52%): mp 128-133 °C (dec); ^{1}H NMR (toluene-d_8, -40 °C, 100.0 MHz) δ 5.05 (broad triplet, J= 6 Hz, rel. int.= 1), δ 3.93 (apparent quintet, $J\simeq$ 7 Hz, rel. int.= 9), δ 1.56 (AB doublets, $J\simeq$ 6 Hz, rel. int.= 1), δ 1.14 (triplet, J_{HH}= 7.1 Hz, rel. int.= 14), δ -0.04 (broad, rel. int.= 1); ^{31}P{^{1}H} NMR (toluene-d_8, -60 °C, 40.54 MHz) δ 30.7 (triplet, J_{PP}= 31 Hz, rel. int.= 1), δ 10.8 (doublet, J_{PP}= 31 Hz, rel. int.= 2); ^{31}P{^{1}H} NMR

(toluene-d_8, 51 °C, 40.54 MHz) δ 16.5 (broad singlet); mass spectrum (EI, 70 eV) calc. for $^{102}RuC_{22}H_{51}O_9P_3$ (P), *m/e* 654, found, *m/e* 654, also *m/e* 598 ($[P-C_4H_8]^+$), *m/e* 488 ($[P-P(OC_2H_5)_3]^+$), and *m/e* 432 ($[P-P(OC_2H_5)_3-C_4H_8]^+$). Anal. calc. for $C_{22}H_{51}O_9P_3Ru$: C, 40.43; H, 7.86. Found: C, 40.58; H, 7.91.

The butadiene complex was very soluble in commom organic solvents. A sample became discoloured during 12 h exposure to air.

Preparation of $Ru[P(OCH(CH_3)_2)_3]_3(\eta^4-C_4H_6)$. A solution of $Ru[P(OCH(CH_3)_2)_3]_3(CO)_2$ (0.37 g, 0.47 mmol) in hexane (20 mL) was placed in a glass Carius tube. The solution was degassed three times. Into the cold (-196 °C) tube was condensed 1,3-butadiene (3 mL, excess). After warming to room temperature, the stirred solution was irradiated with UV light for 3.5 h. An IR spectrum of the reaction solution revealed no ν(CO) absorptions due to the starting material. The pale yellow solution was transferred to a Schlenk tube. The volatiles were removed on the vacuum line to give a viscous, yellow oil (crude yield: 0.355 g, 97%).

Purification was accomplished by fractional sublimation. Several impurities were removed by sublimation at 55 °C onto a -78 °C probe ($<10^{-3}$ torr) for 72 h. The probe material was discarded and the oily residue sublimed at 90 °C onto a -78 °C probe ($<10^{-3}$ torr) for 28 h. The colourless sublimate was washed into another Schlenk tube with hexane. Vacuum removal of the

solvent left a waxy, colourless solid. Sublimation of this product for a further 48 h at 70 °C onto a -78 °C probe ($<10^{-3}$ torr) allowed removal of some trace impurities as the sublimate. The residue, a waxy, colourless solid, (0.080g, 20 %) was shown to be $Ru[P(OCH(CH_3)_2)_3]_3(\eta^4\text{-}C_4H_6)$: mp >120 °C (dec); ^1H NMR (acetone-d_6, 25 °C, 100.0 MHz) δ 4.8 (multiplet, rel. int.= 1), δ 1.24 (doublet, J_{HH}= 6.1 Hz, rel. int.= 6), δ -0.4 (multiplet). Expected resonances at δ 1.5 and 5 were obscured by $P(OCH(CH_3)_2)_3$ signals; $^{31}P\{^1H\}$ NMR (toluene-d_8/toluene (1:3), -34 °C, 40.54 MHz) δ 31.9 (triplet, J_{PP}= 33.7 Hz, rel. int.= 1), δ 14.6 (doublet, J_{PP}= 33.7 Hz, rel. int.= 2); $^{31}P\{^1H\}$ NMR (toluene-d_8/toluene (1:3), 93 °C, 40.54 MHz) δ 18.2 (singlet); mass spectrum (EI, 70 eV) calc. for $^{102}RuC_{31}H_{69}O_9P_3$ (P), *m/e* 780, found, *m/e* 780, also *m/e* 724 ($[P\text{-}C_4H_8]^+$), *m/e* 572 ($[P\text{-}P(OCH(CH_3)_2)_3]^+$), and *m/e* 516 ($[P\text{-}P(OCH(CH_3)_2)_3\text{-}C_4H_8]^+$).

The small isolated yield of $Ru[P(OCH(CH_3)_2)_3]_3(\eta^4\text{-}C_4H_6)$ was used to prepare an NMR sample for the variable temperature $^{31}P\{^1H\}$ NMR study. Further characterization was performed on a sample recovered from the NMR solution, which had suffered some decomposition at higher temperatures. Thus, an acceptable elemental analysis was not obtained.

The complex was very soluble in common organic solvents. A sample turned brown over the course of 12 h exposure to air.

Preparation of $Ru[P(OCH_3)_3]_3(\eta^4\text{-}C_5H_8)$. A glass Carius tube was charged with $Ru[P(OCH_3)_3]_5$ (0.200 g, 0.280 mmol), isoprene

(3 mL, excess), and hexane (20 mL). The solution was degassed three times. After warming to room temperature, the stirred solution was irradiated with ultraviolet light for 8 h. The pale yellow solution was transferred to a Schlenk tube and stripped on the vacuum line. The resultant yellow oil (crude yield: 0.152 g, ~100 %) was dissolved in hexane (5 mL) and filtered through alumina (0.5 cm). The solvent was removed from the pale yellow filtrate under vacuum. The resultant, oily solid was sublimed at 40 °C onto a -78 °C probe ($<10^{-3}$ torr) for 4 h. A small amount of colourless, liquid sublimate was discarded. The residue was sublimed at 75 °C onto a -78 °C probe ($<10^{-3}$ torr) for 12 h. The sublimate, a colourless, waxy solid, was washed into another Schlenk tube with hexane. Vacuum removal of the solvent left $Ru[P(OCH_3)_3]_3(\eta^4\text{-}C_5H_8)$ (0.095 g, 63 %) as a waxy, white solid: mp 205-209 °C (dec); ^{1}H NMR (acetone-d_6, 25 °C, 100.0 MHz) δ 4.72 (broad triplet, $J\simeq$ 7 Hz, rel. int.= 1), δ 3.50 (doublet with fine structure, $J\simeq$ 11 Hz, rel. int.= 27), δ ~2.0 (obscured by residual protons of $(CD_3)_2CO$), δ 1.30 (broad singlet, rel. int.= 1), δ 1.14 (doublet of doublets, J_{HH}= 6.4 Hz, J_{HH}= 1.7 Hz, rel. int.= 1), δ -0.37 (broad, rel. int.= 1), δ -0.79 (broad, rel. int.= 1); ^{31}P{^{1}H} NMR (toluene-d_8/toluene (1:4), 79 °C, 40.54 MHz) δ 24.5 (v broad singlet); ^{31}P{^{1}H} NMR (toluene-d_8/toluene (1:4), -37 °C, 40.54 MHz) ABC spin system, δ_A 39.9, δ_B 21.0, δ_C 15.9, J_{AB}= ±30.1 Hz, J_{BC}= ±47.5 Hz, J_{AC}= ±26.5 Hz; mass spectrum (EI, 70 eV) calc. for $^{102}RuC_{14}H_{35}O_9P_3$ (P), *m/e* 542, found, *m/e* 542, also *m/e* 511 ($[P\text{-}OCH_3]^+$, *m/e* 474 ($[P\text{-}C_5H_8]^+$), *m/e* 418 ($[P\text{-}P(OCH_3)_3]^+$), and *m/e* 350

([P-P(OCH_3)$_3$-C_5H_8]$^+$). Anal. calc. for $C_{14}H_{35}O_9P_3Ru$: C, 31.06; H, 6.52. Found: C, 30.79; H, 6.80.

The product was very soluble in organic solvents. A sample turned brown after 24 h exposure to the air.

Preparation of Ru[P(OC_2H_5)$_3$]$_3$(η^4-C_5H_8). A glass Carius tube was charged with Ru[P(OC_2H_5)$_3$]$_3$(CO)$_2$ (0.395 g, 0.600 mmol), isoprene (3 mL, excess), and hexane (20 mL). The solution was degassed three times. The stirred solution was irradiated with UV light for 10 h. An IR spectrum of the reaction solution showed no ν(CO) absorptions due to the starting material. The pale yellow solution was transferred to a Schlenk tube and stripped on the the vacuum line to yield an oily, yellow solid (crude yield: 0.385 g, 96 %).

Purification was accomplished by fractional sublimation. Several impurities were removed by sublimation at 50 °C onto a -78 °C probe ($<10^{-3}$ torr) for 8 h. The probe material (a mixture of colourless oil and white solids) was discarded. Sublimation of the residue at 75 °C onto a -78 °C probe ($<10^{-3}$ torr) resulted in a colourless solid as sublimate. The probe material was washed into another Schlenk tube with hexane. Vacuum removal of the solvent left a waxy, white solid. The previously described fractional sublimination was repeated a second time to yield Ru[P(OC_2H_5)$_3$]$_3$(η^4-C_5H_8) (0.245 g, 61 %): mp 130-135 °C (dec); ^{1}H NMR (acetone-d_6, 25 °C, 100.0 MHz) δ 4.61 (broad triplet, $J\simeq$ 6.5 Hz, rel. int.= 1), δ 3.93 (quintet with fine

structure, J= 6.7 Hz, rel. int.= 18), δ ~2.0 (obscured by residual protons of $(CD_3)_2CO$), δ 1.30 (broad doublet, J= 6 Hz, rel. int.= 1), δ ~1.1 (obscured by the following resonance), δ 1.17 (triplet, J= 7.0 Hz, rel. int.= 27), δ -0.39 (broad, rel. int.= 1), δ -0.78 (broad, rel. int.= 1); $^{31}P\{^1H\}$ NMR (toluene-d_8/toluene (1:3), 83 °C, 40.54 MHz) δ 20.0 (broad singlet); $^{31}P\{^1H\}$ NMR (toluene-d_8/toluene (1:3), -34 °C, 40.54 MHz) ABC spin system, δ_A 34.3, δ_B 16.3, δ_C 11.8, J_{AB}= ±31.4 Hz, J_{AC}= ±28.2 Hz, J_{BC}= ±45.9 Hz; mass spectrum (EI, 70 eV) calc. for $^{102}RuC_{23}H_{53}O_9P_3$ (P), *m/e* 668, found, *m/e* 668, also *m/e* 623 ($[P-OC_2H_5]^+$), *m/e* 598 ($[P-C_5H_{10}]^+$), and *m/e* 502 ($[P-P(OC_2H_5)_3]^+$). Anal. calc. for $C_{23}H_{53}O_9P_3Ru$: C, 41.38; H, 8.00. Found: C, 41.80; H, 8.34.

The product was very soluble in common organic solvents. A sample discoloured after 24 h exposure to the air.

Attempted Preparation of $Ru[P(OCH_3)_3]_3(\eta^4-C_7H_8)$. A solution of $Ru[P(OCH_3)_3]_5$ (0.280 g, 0.388 mmol) in hexane (20 mL) was placed in a glass Carius tube. To this solution was added 2,5-norbornadiene (4 mL, excess). After being degassed three times, the reaction solution was irradiated with UV light for 9 h. At this point, the reaction mixture consisted of a small amount of yellow precipitate under a pale yellow solution. A $^{31}P\{^1H\}$ NMR spectrum of the neat solution revealed no remaining starting material. The mixture was transferred to a Schlenk tube and stripped on the vacuum line. The residue was dissolved in hexane (10 mL) and filtered through alumina (0.5 cm). Removal of

the solvent on the vacuum line left a white solid contaminated with a yellow liquid. A repeat of the alumina filtration gave the same result. The $^{31}P\{^{1}H\}$ NMR spectrum of this product (toluene) was identical to that found for $CH_3Ru[P(O)(OCH_3)_2](P(OCH_3)_3)_4$ [5,4].

Attempted Preparation of $Ru[P(OCH_3)_3]_3(\eta^4\text{-}C_8H_{12})$. A glass Carius tube was charged with $Ru[P(OCH_3)_3]_5$ (0.280 g, 0.388 mmol), 1,5-cyclooctadiene (4 mL, excess), and hexane (20 mL). The solution was degassed three times. The stirred solution was irradiated with ultraviolet light for 9 h. A sample of the almost colourless solution was examined by $^{31}P\{^{1}H\}$ NMR spectroscopy, which showed complete disappearance of $Ru[P(OCH_3)_3]_5$. The solution was transferred to a Schlenk tube and stripped on the vacuum line. Attempted purification of the resultant yellow oil by the methods described in the previous paragraph gave similar results. A $^{31}P\{^{1}H\}$ NMR spectrum of the product (in toluene) was identical to that found for $CH_3Ru[P(O)(OCH_3)_2](P(OCH_3)_3)_4$ [5,4].

Preparation of $Ru[P(OCH_3)_3]_4(\eta^2\text{-}C_2H_4)$. A glass Carius tube containing $Ru[P(OCH_3)_3]_5$ (0.69 g, 0.96 mmol) in hexane (20 mL) was cooled to -196 °C. The solution was degassed three times. Ethylene (2 mL, excess) was condensed into the cold (-196 °C) reaction tube. After warming to 25 °C, the stirred solution was irradiated with ultraviolet light for 4 h. At this time, the tube contained a small amount of fine, white precipitate in a colourless solution. The excess ethylene was vented and the

volatiles were removed under vacuum to give a white, waxy solid (crude yield: 0.60 g, 99 %). This product was extracted with hexane (15 mL). The extracts were filtered through alumina (0.5 cm) and stripped on the vacuum line to yield $Ru[P(OCH_3)_3]_4(\eta^2\text{-}C_2H_4)$ (0.50 g, 83 %) as a white, crystalline solid: mp 100.5-103 °C (dec); ^1H NMR (acetone-d_6, 25 °C, 100.0 MHz) δ 3.50 (multiplet, rel. int.= 9), δ 1.25 (quintet, J_{PH}= 2.7 Hz, rel. int.= 1); $^{31}P\{^1H\}$ NMR (hexane, 50 °C, 40.5 MHz) δ 21.8 (broad singlet); $^{31}P\{^1H\}$ NMR (hexane, -56 °C, 40.5 MHz) δ 30.8 (triplet, J_{PP}= 64.7 Hz, rel. int.= 1), δ 15.8 (triplet, J_{PP}= 64.7 Hz, rel. int.= 1); mass spectrum (EI, 70 eV) calc. for $^{102}RuC_{16}H_{40}O_{12}P_4$ (P), *m/e* 626, found, *m/e* 626, also *m/e* 598 ($[P\text{-}C_2H_4]^+$), and *m/e* 474 ($[P\text{-}C_2H_4\text{-}P(OCH_3)_3]^+$). One higher fragment at *m/e* 677 was also observed; mass spectrum (CI, isobutane) calc. for $^{102}RuC_{16}H_{40}O_{12}P_4$ (P), *m/e* 627, found, *m/e* 627, also *m/e* 599 ($[P\text{-}C_2H_4]^+$). One higher fragment at *m/e* 678 was also observed. Anal. calc. for $C_{16}H_{40}O_{12}P_4Ru$: C, 26.89; H, 6.45. Found: C, 26.80; H, 6.70.

The ethylene complex was very soluble in common organic solvents. A sample turned brown during 2 min exposure to air. The mass spectrum of $Ru[P(OCH_3)_3]_4(\eta^2\text{-}C_2H_4)$ deserves some comment. The mass spectral ions at *m/e* 677 (EI) and 678 (CI) were intially thought to be due to a small amount of starting material (i.e. $Ru[P(OCH_3)_3]_5$) in the sample. However, a careful examination of the total ion current and the ion currents associated with the parent ion (*m/e* 626 (EI), 627 (CI)) and the

m/e 677, 678 ion suggested that this was not the case. These two mass spectral fragments gave no measureable ion current until the ion-source was well over 100 °C. It was expected that a sample of $Ru[P(OCH_3)_3]_4(\eta^2\text{-}C_2H_4)$ would suffer extensive decomposition at this temperature. Removal of the sample from the ion source at this time confirmed that this was the case. The ion at *m/e* 677 (EI) and 678 (CI) are thus assigned to thermal decomposition products of $Ru[P(OCH_3)_3]_4(\eta^2\text{-}C_2H_4)$.

Attempted Preparation of $Ru[P(OCH_3)_3]_4(\eta^2$-cyclooctene). A solution of $Ru[P(OCH_3)_3]_5$ (0.195 g, 0.270 mmol) and cyclooctene (1.5 mL, excess) in hexane (15 mL) was placed in a glass Carius tube. The solution was degassed three times and subjected to UV irradiation for 3.5 h. The solution was a pale yellow colour. After transfer to a Schlenk tube, the solution was stripped on the vacuum line to give a pale yellow oil. This was sublimed at -20 °C onto a -78 °C probe ($<10^{-3}$ torr) for 1 h to remove excess cyclooctene. At this point, the residue was a waxy, yellow solid. A $^{31}P\{^1H\}$ NMR spectrum of the residue (acetone-d_6) revealed a number of resonances. These included two broad signals at approximately 15 and 30 ppm.

Attempted Preparation of $Ru[P(OCH_3)_3]_4(\eta^2$-dimethyl fumurate). A glass Carius tube was charged with $Ru[P(OCH_3)_3]_5$ (0.145 g, 0.201 mmol), dimethyl fumurate (0.29 g, 2.0 mmol), and hexane (20 mL). The reaction mixture was degassed three times and irradiated with UV light for 4 h. The solution was a pale brown colour and contained solid dimethyl fumurate. The solution

was transferred to a Schlenk tube and stripped under vacuum to yield a mixture of white and yellow solids. These were sublimed at -20 °C onto a -78 °C probe ($<10^{-3}$ torr) for 2 h to remove excess dimethyl fumurate. The residue was a pale yellow, waxy solid at this point. A $^{31}P\{^1H\}$ NMR spectrum of the residue showed the major component to be $Ru[P(OCH_3)_3]_5$. There were also several weak multiplets present.

$^{31}P\{^1H\}$ NMR Study: Reaction of $Ru[P(OCH_3)_3]_4(\eta^2\text{-}C_2H_4)$ and $P(OCH_2)_3CCH_3$. Two 5 mm NMR tubes were filled with an ~0.05 M solution of $Ru[P(OCH_3)_3]_4(\eta^2\text{-}C_2H_4)$ in toluene-d_8/toluene (1:4). To each tube was added a tenfold excess of $P(OCH_2)_3CCH_3$. The tubes were sealed with Teflon-lined screw caps. One tube was left to sit at room temperature overnight then sequentially heated from 50 to 90 °C for 48 h. The other tube was irradiated with UV light for a total of 1 h. The progress of the reactions was periodically monitored by $^{31}P\{^1H\}$ NMR spectroscopy; the results are given in the text.

$^{31}P\{^1H\}$ NMR Study: Reaction of $Ru[P(OCH_3)_3]_4(\eta^2\text{-}C_2H_4)$ and L (L= various phosphines and phosphites). NMR tubes (5 mm) were filled with solutions of $Ru[P(OCH_3)_3]_4(\eta^2\text{-}C_2H_4)$ (~0.05 M). To each of these was added one of the ligands L in an approximate tenfold excess. The tubes were sealed with Teflon-lined screw caps and left to sit overnight. The $^{31}P\{^1H\}$ NMR spectra were measured at this point. The tubes were then heated to 55-60 °C and the progress of the reactions periodically monitored by $^{31}P\{^1H\}$ NMR spectroscopy; the results are given in the text.

Preparation of $Ru[P(OCH_3)_3]_4P(OCH_2)_3CCH_3$. A glass Carius tube was charged with $Ru[P(OCH_3)_3]_4(\eta^2\text{-}C_2H_4)$ (0.39 g, 0.62 mmol), $P(OCH_2)_3CCH_3$ (0.30 g, 2.0 mmol), and hexane (25 mL). The solution was degassed three times and heated, with stirring, at 65 °C for 2 h. At this point, the reaction consisted of a small amount of white precipitate under a colourless solution. The mixture was transferred to a Schlenk tube. Vacuum removal of the volatiles gave a white solid. This was sublimed at 25 °C onto a -78 °C probe ($<10^{-3}$ torr) for 1 h to remove excess $P(OCH_2)_3CCH_3$. The brilliant white residue (0.42 g, 91 %) was dissolved in hexane (10 mL) and filtered through alumina (0.5 cm). Vacuum removal of the solvent left $Ru[P(OCH_3)_3]_4P(OCH_2)_3CCH_3$ (0.345 g, 75 %) as a white solid. This was recrystallized from hexane at -15 °C to yield colourless crystals: mp 170-172 °C (dec); ^1H NMR (acetone-d_6, 25 °C, 100.0 MHz) δ 3.98 (doublet, J_{PH}= 4.7 Hz, rel. int.=.2), δ 3.45 (multiplet, rel. int.= 12), δ 0.66 (broad singlet, rel. int.= 1); $^{31}P\{^1H\}$ NMR (toluene-d_8/toluene (1:3), 27 °C, 40.54 MHz) δ 29.8 (doublet, J_{PP}= 41.3 Hz, rel. int.= 4), δ -2.7 (quintet, J_{PP}= 41.2 Hz, rel. int.= 1); $^{31}P\{^1H\}$ NMR ($CD_2Cl_2/CHFCl_2$ (1:4), -21 °C, 40.54 MHz) δ 29.8 (doublet, J_{PP}= 39.5 Hz, rel. int.= 4), δ -1.6 (quintet, J_{PP}= 39.5 Hz, rel. int.= 1); $^{31}P\{^1H\}$ NMR ($CD_2Cl_2/CHFCl_2$ (1:4), -126 °C, 40.54 MHz) Two simulations based on an A_3BC spin system were in reasonable agreement with the experimental spectrum. A_3BC spin system (see figure 2.7A): δ_A 42.0, δ_B 14.6, δ_C 12.0, J_{AB}= ±75.7 Hz, J_{AC}= ±78.6 Hz, J_{BC}= ∓108.3 Hz; A_3BC spin system (see figure 2.7C): δ_A 42.0, δ_B 15.8, δ_C 10.8, J_{AB}= ±77.0 Hz, J_{AC}= ±76.6 Hz, J_{BC}=

∓472.3 Hz; $^{31}P\{^{1}H\}$ NMR ($CD_2Cl_2/CHFCl_2$ (1:4), ~-115 °C, 162.0 MHz) A_3BC spin system: δ_A 42.1, δ_B 16.5, δ_C 11.2, J_{AB}= ±73.4 Hz, J_{AC}= ±76.2 Hz, J_{BC}= ∓522.6 Hz. Several weaker signals (broad) were also evident (see text for further details); mass spectrum (CI, isobutane) calc. for $^{102}RuC_{17}H_{45}O_{15}P_5$, *m/e* 746, found, *m/e* 746. Anal. calc. for $C_{17}H_{45}O_{15}P_5Ru$: C, 27.39; H, 6.08. Found: C, 27.58; H, 6.13.

The complex was moderately soluble in hexane and very soluble in both toluene and CH_2Cl_2. Crystals of $Ru[P(OCH_3)_3]_4P(OCH_2)_3CCH_3$ turned brown over the course of 30 min exposure to air.

Preparation of $Ru[P(OCH_3)_3]_4P(OC_2H_5)_3$. A glass Carius tube was charged with $Ru[P(OCH_3)_3]_4(\eta^2\text{-}C_2H_4)$ (0.245 g, 0.390 mmol), $P(OC_2H_5)_3$ (0.20 mL, 1.2 mmol), and toluene (15 mL). The solution was degassed three times and heated, with stirring, at 65 °C for 2 h. The colourless solution was transferred to a Schlenk tube. Vacuum removal of the volatiles left an oily, white solid. This was sublimed at 25 °C onto a -78 °C probe ($<10^{-3}$ torr) for 2 h to remove excess $P(OC_2H_5)_3$. The waxy, white residue (0.290 g, 97 %) was dissolved in hexane (10 mL) and filtered through alumina (0.5 cm). The solvent was removed under vacuum to give $Ru[P(OCH_3)_3]_4P(OC_2H_5)_3$ (0.220 g, 74 %) as a waxy, crystalline solid: mp 197.5-200 °C (dec); ^{1}H NMR (acetone-d_6, 25 °C, 100.0 MHz) δ 3.69 (quintet with fine structure, $J\simeq$ 6 Hz, rel. int.= 2), δ 3.55 (complex multiplet, rel. int.= 12), δ 1.14 (triplet, J_{HH}= 7.1 Hz, rel. int.= 3); $^{31}P\{^{1}H\}$ NMR (toluene-d_8/toluene

(1:4), 24 °C, 40.54 MHz) A_4B spin system: δ_B= 20.7, δ_A= 26.5, J_{AB}= 52.4 Hz; $^{31}P\{^1H\}$ NMR ($CD_2Cl_2/CHFCl_2$ (1:4), -121 °C, 40.54 MHz) Simulations based on an A_3BC and an A_2B_2C spin system were in reasonable agreement with the slow exhange limit $^{31}P\{^1H\}$ NMR spectrum measured at 40.54 MHz. Neither of these sets of parameters, however, were capable of simulating the slow exchange limit $^{31}P\{^1H\}$ NMR spectrum of $Ru[P(OCH_3)_3]_4P(OC_2H_5)_3$ measured at 162.0 MHz (see below); $^{31}P\{^1H\}$ NMR ($CD_2Cl_2/CHFCl_2$ (1:4), ~-115 °C, 162.0 MHz) A_3BC spin system: δ_A 44.3, δ_B 18.9, δ_C 11.2, J_{AB}= ±72.5 Hz, J_{AC}= ±76.9 Hz, J_{BC}= ∓514.4 Hz; mass spectrum (EI, 70 eV) calc. for $^{102}RuC_{18}H_{51}O_{15}P_5$ (P), *m/e* 764, found, *m/e* 764, also *m/e* 733 ([P-OMe]$^+$). Anal. calc. for $C_{18}H_{51}O_{15}P_5Ru$: C, 28.32; H, 6.73. Found: C, 28.23; H, 6.55.

A sample of $Ru[P(OCH_3)_3]_4P(OC_2H_5)_3$ turned brown during a 1 h exposure to air. The complex was very soluble in hexane, toluene, and CH_2Cl_2.

Preparation of $Ru[P(OCH_3)_3]_4P(OCH(CH_3)_2)_3$. A solution of $Ru[P(OCH_3)_3]_4(\eta^2\text{-}C_2H_4)$ (0.245 g, 0.390 mmol) and $P(OCH(CH_3)_2)_3$ (0.20 mL, 0.93 mmol) in toluene (20 mL) was placed in a glass Carius tube. The solution was degassed three times and heated, with stirring, at 65 °C for 2 h. The colourless solution was transferred to a Schlenk tube and stripped on the vacuum line to yield a colourless oil containing some solid. This was sublimed at 60 °C onto a -78 °C probe ($<10^{-3}$ torr) for 2 h to remove excess $P(OCH(CH_3)_2)_3$. The residue was dissolved in hexane (10 mL) and filtered through alumina (0.5 cm). Vacuum removal of the

solvent left $Ru[P(OCH_3)_3]_4P(OCH(CH_3)_2)_3$ (0.250 g, 80 %) as a waxy, white solid: mp 102-110 °C (dec); ^1H NMR (acetone-d_6, 25 °C 100.0 MHz) δ 4.67 (broad multiplet, rel. int.= 1), δ 3.57 (complex multiplet, rel. int.= 36), δ 1.17 (doublet, J_{HH}= 6.1 Hz, rel. int.= 6); $^{31}P\{^1H\}$ NMR (toluene-d_8, 25 °C, 40.54 MHz) A_4B spin system, δ_B 20.0, δ_A 25.3, J_{AB}= 52.1 Hz; $^{31}P\{^1H\}$ NMR ($CD_2Cl_2/CHFCl_2$ (1:4), -130 °C, 40.54 MHz) δ 37.1 (broad triplet, apparent $J\simeq$ 75 Hz), δ 15 (broad quartet with fine structure, apparent $J\simeq$ 75 Hz). The high field signal was coincident with several impurities, precluding an accurate spectral simulation. The spectrum, however, was qualitatively very similar to that observed for $Ru[P(OCH_3)_3]_4P(OC_2H_5)_3$ at low temperatures; $^{31}P\{^1H\}$ NMR ($CD_2Cl_2/CHFCl_2$ (1:4), ~-115 °C, 162.0 MHz) δ 37 (broad triplet), δ 15 (quartet of broad multiplets). See text for further details; mass spectrum (CI, isobutane) calc. for $^{102}RuC_{21}H_{57}O_{15}P_5$, *m/e* 806, found, *m/e* 803. Anal. calc. for $C_{21}H_{57}O_{15}P_5Ru$: C, 31.31; H, 7.13. Found: C, 31.29; H, 7.33.

A sample of $Ru[P(OCH_3)_3]_4P(OCH(CH_3)_2)_3$ turned brown over the course of 1 h exposure to air. The complex was very soluble in hexane, toluene, and CH_2Cl_2.

Preparation of $Ru[P(OCH_3)_3]_4PF_3$. A glass Carius tube was charged with $Ru[P(OCH_3)_3]_4(\eta^2\text{-}C_2H_4)$ (0.27 g, 0.43 mmol) and toluene (20 mL). The solution was degassed three times. The tube was pressurized with PF_3 (~2 atm). The stirred solution was heated at 60 °C for 2 h. The colourless solution was transferred to a Schlenk tube and stripped on the vacuum line to yield a

white, waxy solid. This was extracted with hexane (25 mL). Vacuum removal of the solvent from the filtered extracts left a white solid (0.26 g, 88 %). This was recystallized from hexane at -78 °C to yield $Ru[P(OCH_3)_3]_4PF_3$: mp 193-194 °C (dec); ^1H NMR (acetone-d_6, 25 °C, 100.0 MHz) δ 3.62 (complex multiplet); $^{31}P\{^1H\}$ NMR ($CD_2Cl_2/CHFCl_2$ (1:4), -23 °C, 40.54 MHz) A_4MX_3 spin system, δ_M -1.4 (quartet of quintets, J_{MX}= 1365 Hz, J_{AM}≃ 49 Hz, rel. int.= 1), δ_A 26.3 (overlapping doublet of quartets, J_{AM}= 48.4 Hz, J_{AX}≃ 25 Hz, rel. int.= 4); $^{31}P\{^1H\}$ NMR ($CD_2Cl_2/CHFCl_2$ (1:4), -129 °C, 40.54 MHz) $A_2B_2CX_3$ spin system δ_A 40.0, δ_B 24.8, δ_C 0, J_{AB}= ±75.5 Hz, J_{AC}= ∓182.4 Hz, J_{BC}= ±90.1 Hz, J_{AX}= ∓44.0 Hz, J_{BX}= ±10 Hz, J_{CX}= ±1000 Hz. These are approximate values (see chapter 2 text and figure 2.14 for details); mass spectrum (EI, 70 eV) calc. for $^{102}RuC_{12}H_{36}F_3O_{12}P_5$ (P), *m/e* 686, found, *m/e* 686, also *m/e* 667 ($[P-F]^+$), *m/e* 655 ($[P-OMe]^+$), *m/e* 598 ($[P-PF_3]^+$), *m/e* 474 ($[P-PF_3-P(OCH_3)_3]^+$), and *m/e* 350 ($[P-PF_3-2P(OCH_3)_3]^+$). Anal. calc. for $C_{12}H_{36}F_3O_{12}P_5Ru$: C, 21.03; H, 5.29. Found: C, 21.08; H, 5.30.

Crystals of $Ru[P(OCH_3)_3]_4PF_3$ turned brown during a 1 h exposure to air. The complex was moderately soluble in hexane and very soluble in both toluene and CH_2Cl_2.

Preparation of $Ru[P(OCH_3)_3]_4P(CH_3)_3$. A solution of $Ru[P(OCH_3)_3]_4(\eta^2-C_2H_4)$ (0.315 g, 0.500 mmol) and $P(CH_3)_3$ (0.11 mL, 1.5 mmol) in toluene (25 mL) was placed in a glass Carius tube. After three degassing cycles, the stirred solution was heated at 60 °C for 2 h. The pale yellow solution was

transferred to a Schlenk tube. The volatiles were removed on the vacuum line to give an oily solid. This was sublimed at 25 °C onto a -78 °C probe ($<10^{-3}$ torr) for 30 min to remove any excess $P(CH_3)_3$. The residue (0.310 g, 92 %) was extracted with hexane (10 mL) and filtered through alumina (0.5 cm). Vacuum removal of the solvent left $Ru[P(OCH_3)_3]_4P(CH_3)_3$ (0.265 g, 79 %) as a colourless, crystalline solid: mp 191-193 °C (dec); ^1H NMR (toluene-d_8, 25 °C, 400.13 MHz) δ 3.58 (broad with fine structure, rel. int.= 4), δ 1.49 (doublet, J_{PH}= 8.7 Hz, rel. int.= 1); $^{13}C\{^1H\}$ NMR (toluene-d_8, -35 °C, 100.6 MHz) δ 23.0 (doublet, J_{PC}= 28.8 Hz, rel. int.= 1), δ 51.0 (singlet, rel. int.= 4); $^{31}P\{^1H\}$ NMR (toluene-d_8, 68 °C, 40.54 MHz) δ 24.8 (doublet, J_{PP}= 23.3 Hz, rel. int.= 4), δ -134.4 (quintet, J_{PP}= 23.3 Hz, rel. int.= 1); $^{31}P\{^1H\}$ NMR (toluene-d_8, 76 °C, 162.0 MHz) δ 24.8 (doublet, J_{PP}= 23 Hz, rel. int.= 4), δ -134.5 (quintet, J_{PP}= 23 Hz, rel. int.= 1); $^{31}P\{^1H\}$ NMR (toluene-d_8, -75°C, 162.0 MHz) A_3BX spin system: δ_A 26.5, δ_B 31.0, δ_X -132.7, J_{AB}= ±71.5 Hz, J_{AC}= ±67.9 Hz, J_{BC}= ∓290.1; mass spectrum (EI, 70 eV) calc. for $^{102}RuC_{15}H_{45}O_{12}P_5$ (P), *m/e* 674, found, *m/e* 674, also *m/e* 643 ($[P-OMe]^+$), *m/e* 598 ($[P-PMe_3]^+$), *m/e* 550 ($[P-P(OCH_3)_3]^+$), and *m/e* 426 ($[P-2P(OCH_3)_3]^+$). Anal. calc. for $C_{15}H_{45}O_{12}P_5Ru$: C, 26.75; H, 6.73. Found: C, 26.77; H, 7.00.

Crystals of $Ru[P(OCH_3)_3]_4P(CH_3)_3$ were extremely air-sensitive, decomposing to a colourless oil during 5 min exposure to air. The complex was very soluble in hexane, toluene, and CH_2Cl_2.

Preparation of $Ru[P(OCH_3)_3]_4P(CH_3)_2C_6H_5$. A glass Carius tube was charged with $Ru[P(OCH_3)_3]_4(\eta^2\text{-}C_2H_4)$ (0.390 g, 0.624 mmol), $P(CH_3)_2C_6H_5$ (0.10 mL, 0.70 mmol), and toluene (25 mL). The solution was degassed three times. The stirred solution was heated for 1 h at 55 °C and became bright yellow after 10 min. This was transferred to a Schlenk tube and stripped on the vacuum line to give an oily, yellow solid. Sublimation at 45 °C onto a -78 °C probe ($<10^{-3}$ torr) for 2 h allowed removal of excess $P(CH_3)_2C_6H_5$. The yellow residue (0.445 g, 97 %) was extracted with toluene (15 mL) and filtered through alumina (0.5 cm). The solvent was removed under vacuum and the resultant yellow solid extracted again with toluene (10 mL). The extracts were filtered through alumina (1.0 cm) and evaporated to dryness under vacuum to yield $Ru[P(OCH_3)_3]_4P(CH_3)_2C_6H_5$ (0.245 g, 53 %) as a yellow, crystalline solid: mp 199-202 °C (dec); ^1H NMR (acetone-d_6, 25 °C, 100.0 MHz) δ 7.77 (multiplet, rel. int.= 2), δ 7.16 (multiplet, rel. int.= 3), δ 3.43 (multiplet, rel. int.= 36), δ 1.62 (doublet of doublets, J_{PH}= 7.5 Hz, J'= 0.9 Hz, rel. int.= 6); $^{31}P\{^1H\}$ NMR ($CD_2Cl_2/CHFCl_2$ (1:4), 6 °C, 40.54 MHz) δ 25.4 (doublet, J_{PP}= 24.3 Hz, rel. int.= 4), δ -127.9 (quintet, J_{PP}= 24.5 Hz, rel. int.= 1); $^{31}P\{^1H\}$ NMR ($CD_2Cl_2/CHFCl_2$ (1:4), -104 °C, 40.54 MHz) A_3BX spin system, δ_A 32.9, δ_B 17.0, δ_X -130.5, J_{AB}= ±74.7 Hz, J_{AX}= ±64.7 Hz, J_{BX}= ∓292.4 Hz; mass spectrum (EI, 70 eV) calc. for $^{102}RuC_{20}H_{47}O_{12}P_5$ (P), *m/e* 736, found, *m/e* 736, also *m/e* 705 ([P-OMe]$^+$), and *m/e* 598 ([P-$P(CH_3)_2C_6H_5$]$^+$). Anal. calc. for $C_{20}H_{47}O_{12}P_5Ru$: C, 32.66; H, 6.44. Found: C, 32.22; H, 6.81.

Crystals of $Ru[P(OCH_3)_3]_4P(CH_3)_2C_6H_5$ were air-sensitive, turning brown during 10 min exposure to air. The complex was soluble in hexane and very soluble in both toluene and CH_2Cl_2.

Preparation of $Ru[P(OCH_3)_3]_4PCH_3(C_6H_5)_2$. A solution of $Ru[P(OCH_3)_3]_4(\eta^2\text{-}C_2H_4)$ (0.310 g, 0.496 mmol) and $PCH_3(C_6H_5)_2$ (0.092 mL, 0.496 mmol) in toluene (20 mL) was placed in a glass Carius tube. After three degassing cycles, the stirred solution was heated for 50 min at 50 °C. The resultant bright yellow solution was transferred to a cold (-15 °C) Schlenk tube and stripped under vacuum to yield an oily, yellow slid. This was extracted with cold (-15 °C) hexane (10 mL) and filtered quickly through alumina (0.5 cm) into a cold (-78 °C) Schlenk tube. Vacuum removal of the solvent left an oily, yellow solid (0.320 g, 81 %). A solution of the solid in hexane was filtered twice more through alumina (0.5 cm). Vacuum removal of the solvent gave a waxy, yellow solid which was sublimed at 25 °C onto a -78 °C probe ($<10^{-3}$ torr) for 16 h. Over this period, a mixture of a colourless liquid and a white solid sublimed, leaving a waxy, yellow solid (0.185 g, 47 %). The $^{31}P\{^1H\}$ NMR spectrum of this solid ($CD_2Cl_2/CHFCl_2$ (1:4), 25 °C) indicated that the major product was $Ru[P(OCH_3)_3]_4PCH_3(C_6H_5)_2$ although several impurities were also present.

Solutions of $Ru[P(OCH_3)_3]_4PCH_3(C_6H_5)_2$ in hexane, toluene, $CD_2Cl_2/CHFCl_2$, and acetone-d_6 (all under N_2) slowly decomposed at room temperature, taking on the characteristic odours of $PCH_3(C_6H_5)_2$ and $P(OCH_3)_3$. The solid complex turned brown during

5 min exposure to air. The following data were obtained for the solid: mp 114-118 °C (dec); ^{1}H NMR (acetone-d_6, 25 °C, 100.0 MHz) The sample decomposed during acquisition of the spectrum. Resonances in the regions expected for the methyl and phenyl substituents of $PCH_3(C_6H_5)_2$ and the methoxy protons of $P(OCH_3)_3$ were observed; $^{31}P\{^1H\}$ NMR ($CD_2Cl_2/CHFCl_2$ (1:4), 3 °C, 40.54 MHz) δ 21.3 (doublet, J_{PP}= 28.7 Hz, rel. int.= 4), δ -108.7 (quintet, J_{PP}= 28.7 Hz, rel. int.= 1); mass spectrum (EI, 70 eV) calc. for $^{102}RuC_{25}H_{49}O_{12}P_5$ (P), *m/e* 799, found *m/e* 794 (unidentified) also *m/e* 598 ($[P-PCH_3(C_6H_5)_2]^+$) and *m/e* 474 ($[P-PCH_3(C_6H_5)_2-P(OCH_3)_3]^+$); mass spectrum (CI, isobutane) calc., *m/e* 800, found, *m/e* 724 (unidentified), also *m/e* 599 ($[P-PCH_3(C_6H_5)_2]^+$); mass spectrum (FAB, sulfolane) calc., *m/e* 799, found *m/e* 685 (unidentified). Anal. calc. for $C_{25}H_{49}O_{12}P_5Ru$: C, 37.65; H, 6.19. Found: C, 36.60; H, 7.03.

Preparation of $Ru[P(OCH_3)_3]_4P(C_2H_4CN)_3$. A glass Carius tube was charged with $Ru[P(OCH_3)_3]_4(\eta^2-C_2H_4)$ (0.385 g, 0.616 mmol), $P(C_2H_4CN)_3$ (0.119 g, 0.616 mmol), and toluene (35 mL). The reaction mixture was degassed three times and heated, with stirring, for 1 h at 55 °C. The colourless solution was transferred to a Schlenk tube and stripped under vacuum to leave an oily solid. This was extracted with toluene (15 mL). The extracts were filtered through alumina (1 cm). Vacuum removal of the solvent left a pale yellow solid which was slightly oily. Hexane washing (2x20 mL) afforded $Ru[P(OCH_3)_3]_4P(C_2H_4CN)_3$ (0.350 g, 72 %) as an off-white powder: mp 163-168 °C (dec); ^{1}H NMR

(toluene-d_8, 25 °C, 100.0 MHz) δ 3.37 (multiplet, rel. int.= 36), δ 2.30 (multiplet, rel. int.= 6), δ 1.65 (multiplet, rel. int.= 6); $^{31}P\{^1H\}$ NMR (toluene-d_8, 27 °C, 40.54 MHz) δ 18.1 (doublet, J_{PP}= 24.7 Hz, rel. int.= 4), δ -96.8 (quintet, J_{PP}= 24.7 Hz, rel. int.= 1); $^{31}P\{^1H\}$ NMR ($CD_2Cl_2/CHFCl_2$ (1:4), -1 °C, 40.54 MHz) δ 18.9 (doublet, J_{PP}= 26.2 Hz, rel. int.= 4), δ -95.3 (quintet, J_{PP}= 26 Hz, rel. int.= 1). The compound slowly decomposed in $CD_2Cl_2/CHFCl_2$ (1:4) and a low temperature, limiting spectrum was not obtained; mass spectrum (EI, 70 eV) calc. for $^{102}RuC_{21}H_{48}N_3O_{12}P_5$ (P), *m/e* 792, found, *m/e* 707 (unidentified), also *m/e* 598 ($[P-P(C_2H_4CN)_3]^+$) and *m/e* 474 ($[P-P(C_2H_4CN)_3-P(OCH_3)_3]^+$); mass spectrum (CI, isobutane) calc., *m/e* 793, found, *m/e* 710 (unidentified), also *m/e* 599 ($[P-P(C_2H_4CN)_3]^+$); mass spectrum (FAB, sulfolane) calc., *m/e* 792, found, *m/e* 597 (unidentified). Anal. calc. for $C_{21}H_{48}N_3O_{12}P_5Ru$: C, 31.90; H, 6.12; N, 5.32. Found: C, 32.02; H, 6.09; N, 5.17.

A sample of $Ru[P(OCH_3)_3]_4P(C_2H_4CN)_3$ turned brown during 5 min exposure to air. The complex was moderately soluble in hexane, soluble in toluene, and very soluble in CH_2Cl_2.

Preparation of $Ru[P(OCH_3)_3]_4P(OC_6H_5)_3$. A solution of $Ru[P(OCH_3)_3]_4(\eta^2-C_2H_4)$ (0.390 g, 0.624 mmol) and $P(OC_6H_5)_3$ (0.164 mL, 0.624 mmol) in toluene (25 mL) was placed in a glass Carius tube. The solution was degassed three times and heated, with stirring, for 75 min at 55 °C. The colourless solution was transferred to a Schlenk tube and stripped on the vacuum line to

give a pale yellow oil. This was sublimed at 25 °C onto a -78 °C probe ($<10^{-3}$ torr) for 1 h, although very little sublimate was observed. The oil was dissolved in hexane (25 mL). The solution was filtered through alumina (0.5 cm) and the solvent was removed under vacuum to yield a colourless oil. The alumina filtration process was repeated twice more to afford $Ru[P(OCH_3)_3]_4P(OC_6H_5)_3$ (0.280 g, 49 %) as a colourless, viscous oil: ^1H NMR (acetone-d_6, 25 °C, 100.0 MHz) δ 7.06 (multiplet, rel. int.= 15), δ 3.43 (multiplet, rel. int.= 36); $^{31}P\{^1H\}$ NMR ($CD_2Cl_2/CHFCl_2$ (1:4), -12 °C, 40.54 MHz) δ 24.6 (doublet, J_{PP}= 48.9 Hz, rel. int.= 4), δ -6.1 (quintet, J_{PP}= 49.0 Hz, rel. int.= 1); $^{31}P\{^1H\}$ NMR ($CD_2Cl_2/CHFCl_2$ (1:4), -124 °C, 40.54 MHz) A_2B_2C spin system δ_A 31.5, δ_B 20.8, δ_C -4.2, J_{AB}= ±74.7 Hz, J_{AC}= ∓179.1 Hz, J_{BC}= ±81.4 Hz. A small (<1 %) singlet due to free $P(OC_6H_5)_3$ was also observed; mass spectrum (EI, 70 eV) calc. for $^{102}RuC_{30}H_{51}O_{15}P_5$ (P), *m/e* 909, found, *m/e* 784 ($[P-P(OCH_3)_3-H]^+$); mass spectrum (CI, isobutane) calc., *m/e* 910, found, *m/e* 786 ($[P-P(OCH_3)_3]^+$); mass spectrum (FAB, sulfolane) calc., *m/e* 909, found, *m/e* 784. Anal. calc. for $C_{30}H_{51}O_{15}P_5Ru$: C, 39.70; H, 5.66. Found: C, 40.02; H, 5.38.

The complex turned brown during several hours exposure to air. The oil dissolved in hexane, toluene, and CH_2Cl_2.

Preparation of $Ru[P(OCH_3)_3]_4Sb(CH_3)_3$. A glass Carius tube was charged with $Ru[P(OCH_3)_3]_4(\eta^2-C_2H_4)$ (0.420 g, 0.67 mmol), and toluene (25 mL). To this solution was added $SbMe_3$ (0.20 mL, 1.8 mmol). After degassing three times, the stirred solution was

heated at 55 °C for 2 h. The solution (bright yellow) was transferred to a Schlenk tube and evaporated to dryness on the vacuum line. The resultant yellow solid (0.505 g, 99 %) was extracted with hexane (15 mL). The extracts were filtered through alumina (0.5 cm). Vacuum removal of the solvent left a yellow solid. The alumina filtration process was repeated, affording $Ru[P(OCH_3)_3]_4Sb(CH_3)_3$ (0.265 g, 52 %) as a yellow, crystalline solid: 201-205 °C (dec); ^1H NMR (toluene-d_8, 25 °C, 100.0 MHz) δ 3.53 (multiplet, rel. int.= 4), δ 0.98 (singlet, rel. int.= 1); $^{31}P\{^1H\}$ NMR ($CD_2Cl_2/CHFCl_2$ (1:4), -12 °C, 40.54 MHz) δ 30.6 (singlet); $^{31}P\{^1H\}$ NMR ($CD_2Cl_2/CHFCl_2$ (1:4), -113 °C, 40.5; MHz) AB_3 spin system, δ_A 36.2, δ_B 20.3, J_{AB}= 66.5 Hz; mass spectrum (EI, 70 eV) calc. for $^{102}Ru^{123}SbC_{15}H_{45}O_{12}P_4$ (P), *m/e* 766, found, *m/e* 766, also *m/e* 642 ($[P-P(OCH_3)_3]^+$), *m/e* 598 ($[P-SbMe_3]^+$), and *m/e* 474 ($[P-SbMe_3-P(OCH_3)_3]^+$). Anal calc. for $C_{15}H_{45}O_{12}P_4RuSb$: C, 23.57; H, 5.93. Found: C, 23.78; H, 5.85.

The product was very air-sensitive, turning brown during 30 sec exposure to air. Samples of $Ru[P(OCH_3)_3]_4Sb(CH_3)_3$ were very soluble in hexane, toluene, and CH_2Cl_2. Solid samples of $Ru[P(OCH_3)_3]_4Sb(CH_3)_3$ under N_2 suffered partial decomposition after 3 weeks at 25 °C.

Thermal Reaction of $Ru[P(OCH_3)_3]_4(\eta^2-C_2H_4)$ and Propene. A solution of $Ru[P(OCH_3)_3]_4(\eta^2-C_2H_4)$ (~0.1 g) in hexane (20 mL) was placed in a glass Carius tube. The tube was degassed three times. Propene (~ 2 mL, excess) was condensed into the tube at -196 °C. After slowly warming to 25 °C, the stirred solution was

heated at 40 °C for 2 h. The excess propene was vented and the colourless solution was transferred to a Schlenk tube. Vacuum removal of the volatiles left a oily, yellow solid. A ^{1}H NMR spectrum (acetone-d_6) of this product indicated that ~80 % of the starting material remained.

The reaction was attempted again: a glass Carius tube was charged with $Ru[P(OCH_3)_3]_4(\eta^2\text{-}C_2H_4)$ (0.260 g, 0.416 mmol) and hexane (20 mL). The solution was degassed three times and propene (~2 mL, excess) was condensed into the tube at -196 °C. After warming, the tube was heated at 60 °C for 7 h. The solution slowly turned yellow-brown over this period. After venting the excess propene, the solution was transferred to a Schlenk tube. Vacuum removal of the volatiles left a waxy solid with some brown impurities. Despite several attempts at purification, the final result was a brown, oily solid. The ^{1}H NMR spectrum of this product revealed, in addition to remaining starting material, a number of unidentified resonances in the region 0-5 ppm.

Photolysis of $Ru[P(OCH_3)_3]_5$ and Propene. A glass Carius tube was charged with $Ru[P(OCH_3)_3]_5$ (0.280 g, 0.388 mmol) and hexane (15 mL). The solution was degassed three times. Propene (~2 mL, excess) was condensed into the tube at -196 °C. After slowly warming to room temperature, the stirred solution was irradiated with UV light for 4 h. At this point, the reaction mixture consisted of a small amount of white precipitate under a colourless solution. After venting the excess propene, the

mixture was transferred to a Schlenk tube. Vacuum removal of the volatiles left an oily solid. This was dissolved in hexane (10 mL) and the solution was filtered through alumina (0.5 cm). The solvent was stripped on the vacuum line to leave a colourless, waxy solid. The alumina filtration process was repeated, affording a similar product (0.115 g).

Although the elemental analysis of this solid was consistent with $Ru[P(OCH_3)_3]_4(\eta^2\text{-}C_3H_6)$, the low temperature $^{31}P\{^1H\}$ NMR spectrum (toluene-d_8, -43 °C, 40.54 MHz) revealed a number of resonances. A doublet (δ 35.2, J= 40.0 Hz, rel. int.≃ 3) and a broad multiplet (δ 21.7, rel. int.≃ 1) accounted for ~80 % of the total intensity. A pair of multiplets (δ 5 and 15) and a weak singlet (~4 %) due to $Ru[P(OCH_3)_3]_5$ made up the balance. As the temperature was increased, a weaker doublet slowly separated from the original doublet and underwent broadening. At the same time, the broad multiplet at δ 21.7 experienced partial collapse although several component signals remained sharp. The weaker multiplets at δ 5 and 15 were temperature invariant.

The ^1H NMR spectrum of this solid (toluene-d_8, 25 °C, 100.0 MHz) featured a major and minor methoxy multiplet (δ 3.51 and 3.7, respectively). In addition, a number of low, broad resonances at δ 5.4, 1.8, 1.2, and 0.9 were observed as was a broad triplet at δ 2.55.

Photolysis of $Ru[P(OCH_3)_3]_5$ and 1-Butene. A solution of $Ru[P(OCH_3)_3]_5$ (0.355 g, 0.465 g) in hexane (20 mL) was placed in

a glass Carius tube. The solution was degassed three times. Into the cold (-196 °C) tube was condensed 1-butene (~2 mL, excess). After slowly warming to room temperature, the stirred solution was irradiated with UV light for 4 h. After venting the excess 1-butene, the pale yellow solution (with a small amount of white precipitate) was transferred to a Schlenk tube. Vacuum removal of the volatiles left an oily, yellow solid. This was extracted with hexane (20 mL) and the extracts were filtered through alumina (0.5 cm). The solvent was removed under vacuum. The previous procedure was repeated, affording a pale yellow solid (0.115 g) which was waxy.

Although the elemental analysis for this solid was consistent with $Ru[P(OCH_3)_3]_4(\eta^2\text{-}C_4H_8)$, the low temperature $^{31}P\{^1H\}$ NMR spectrum (toluene-d_8, -57 °C, 40.54 MHz) revealed a number of resonances. Among these were a doublet (δ 20.9, J= 29.5 Hz, rel.int.= 2) and a triplet (δ 40.8, J= 29.7 Hz, rel. int.= 1). A singlet due to the starting material (δ 27.8) was also present. As the temperature was increased, the doublet and triplet broadened and were near coalescence at 25 °C. The other signals suffered no broadening up to 53 °C.

The ^1H NMR spectrum of this solid (toluene-d_8, 25 °C, 100.0 MHz) revealed a complex methoxy multiplet centred at δ 3.5. Additionally, a number of resonances (mostly broad and featureless) were observed between δ 0 and 5.5.

$^{31}P\{^1H\}$ NMR Study: Reaction of $Ru[P(OCH_3)_3]_4(\eta^2-C_2H_4)$ and Cyclooctene. A 5 mm NMR tube with a Teflon-lined screw cap was filled with a solution of $Ru[P(OCH_3)_3]_4(\eta^2-C_2H_4)$ (0.1 g) and cyclooctene (0.1 mL) in toluene (1 mL). After sealing, the tube was heated at 45 °C. The progress of the reaction was monitored by $^{31}P\{^1H\}$ NMR spectroscopy. The exchange broadened resonances (25 °C) of the starting material were slowly replaced by two broad signals (δ 32 and 14) over the course of 12 h. Cooling the solution to -37 °C caused these to sharpen into an A_2B_2 spin system which was successfully simulated: δ_A 15.6, δ_B 32.4, J_{AB}= 63.7 Hz. In addition, a weak multiplet (δ 5) and a singlet due to $Ru[P(OCH_3)_3]_5$ (δ 28.7) grew in intensity over the 12 h period.

CHAPTER 3

Phosphite Derivatives of Ruthenium. Reaction of $Ru[P(OCH_3)_3]_5$ as a Nucleophile.

3.1 Introduction

In chapter 1 it was predicted that $Ru[P(OCH_3)_3]_5$ would contain a metal centre with high electron density. The products of the reaction between $Ru[P(OCH_3)_3]_5$ and CH_3I, NH_4^+, and X_2 (X= Cl, Br, I) are consistent with this hypothesis. This chapter presents some chemistry resulting from the reaction of pentakis(trimethyl phosphite)ruthenium(0) as a nucleophile. Several of these products have been previously prepared by alternate routes and a number of the analogous iron complexes are known. Consequently, a brief literature survey will be presented.

A number of cationic trimethyl and triethyl phosphite derivatives of gold, silver, and the platinum metals have been prepared by ligand exchange reactions in polar solvents [74]. These complexes include $\{XRu[P(OR)_3]_5\}BPh_4$ (X= H, Cl, Br; R=Me, Et). The precursors to these species were $[RuX_2(C_7H_8)]_n$ (X= Cl, Br), $Ru(H)Cl[PPh_3]_3$, and $RuCl_2[PPh_3]_3$. The cationic ruthenium complexes were characterized by elemental analysis, conductivity, and ^1H NMR spectroscopy; no $^{31}P\{^1H\}$ NMR or mass spectral data were measured.

The cationic iron(II) complexes $\{XFe[P(OR)_3]_5\}^+$ (X= H, Me, Cl, Br, I; R= Me, Et) have been reported [75]. The reaction of $Fe[P(OCH_3)_3]_5$ and CH_3I in THF gave $\{CH_3Fe[P(OCH_3)_3]_5\}^+$, which was isolated as the BPh_4 salt. The treatment of $Fe[P(OR)_3]_3X_2$ (R= Me, Et; X= Br, Cl) with excess phosphite in methanol (followed by addition of $NaBPh_4$) gave $\{XFe[P(OR)_3]_5\}BPh_4$ (X= Br, Cl; R= Me, Et). The hydride complex $\{HFe[P(OCH_3)_3]_5\}PF_6$ was obtained by protonation of $Fe[P(OCH_3)_3]_5$ with NH_4PF_6 in methanol. The reaction of $Fe[P(OCH_3)_3]_5$ with CF_3I (in ether) gave $\{IFe[P(OCH_3)_3]_5\}^+$ as the major product. These cationic Fe(II) complexes were characterized mainly by $^{31}P\{^1H\}$ NMR spectroscopy. This technique revealed spectra arising from an AB_4 spin system in all cases. No conclusions were drawn regarding the ^{31}P spectral parameters of this series of complexes.

Another group simultaneously found results similar to those just presented: the reaction of $Fe[P(OCH_3)_3]_5$ with NH_4PF_6 and CH_3I gave $\{HFe[P(OCH_3)_3]_5\}PF_6$ and $\{CH_3Fe[P(OCH_3)_3]_5\}^+$, respectively [26]; the latter species was isolated as the PF_6 salt. The product from $FeCl_2$ and excess $P(OCH_3)_3$ in methanol (after treatment with $NaBPh_4$) was $\{ClFe[P(OCH_3)_3]_5\}BPh_4$. The reaction of FeI_2 and excess $P(OC_2H_5)_3$ in ethanol gave $\{IFe[P(OC_2H_5)_3]_5\}^+$, isolated as the BPh_4 salt. All of these complexes (hydride, methyl, halide) exhibited temperature invariant $^{31}P\{^1H\}$ NMR spectra consistent with an AB_4 spin system. Nuclear magnetic resonance evidence (^1H) for the

unstable $\{C_2H_5Fe[P(OCH_3)_3]_5\}^+$ cation was obtained from a study of the reaction between equimolar amounts of C_2H_5I and $Fe[P(OCH_3)_3]_5$ in CD_3CN.

The results from these studies will be discussed in greater detail, where appropriate, throughout this chapter.

3.2 Results

The addition of X_2 (X= Br, I) to a hexane solution of $Ru[P(OCH_3)_3]_5$ resulted in an immediate precipitate of $\{XRu[P(OCH_3)_3]_5\}^+X^-$. Although these complexes were isolated and characterized, the PF_6 salts were more convenient to purify. Metathesis of $\{XRu[P(OCH_3)_3]_5\}^+X^-$ (X= Br, I) with NH_4PF_6 in THF gave $\{XRu[P(OCH_3)_3]_5\}PF_6$ (and presumably NH_4X).

The reaction of Cl_2 with $Ru[P(OCH_3)_3]_5$ in hexane also gave an immediate precipitate. This product was extremely air-sensitive and decomposed within seconds in air. Addition of NH_4PF_6 to a THF solution of the complex afforded the more stable $\{ClRu[P(OCH_3)_3]_5\}PF_6$.

The halide complexes $\{XRu[P(OCH_3)_3]_5\}PF_6$ (X= Cl, Br, I) were all recrystallized from THF to give colourless microcrystals which decomposed slowly in air (over a two week period). They dissolved readily in CH_2Cl_2 but were virtually insoluble in hexane.

The reaction of NH_4PF_6 and $Ru[P(OCH_3)_3]_5$ in THF led directly to the formation of $\{HRu[P(OCH_3)_3]_5\}PF_6$. This hydride complex was recrystallized from THF/hexane, yielding colourless crystals which were very soluble in both THF and CH_2Cl_2 but nearly insoluble in hexane. Crystals of $\{HRu[P(OCH_3)_3]_5\}PF_6$ appeared air-stable over a two week period.

The addition of excess CH_3I to a hexane solution of $Ru[P(OCH_3)_3]_5$ gave a white precipitate; the reaction appeared complete within one hour. The product, $\{CH_3Ru[P(OCH_3)_3]_5\}I$, was isolated and characterized. Again, metathesis with NH_4PF_6 allowed isolation of the cation as the PF_6 salt. Recrystallization from THF gave white crystals of $\{CH_3Ru[P(OCH_3)_3]_5\}PF_6$ which suffered no apparent decomposition after two weeks in air. The methyl complex was very soluble in CH_2Cl_2 but virtually insoluble in hexane.

The reaction of $Ru[P(OCH_3)_3]_5$ with a number of other potential electrophiles did not lead to isolation of the desired products. For example, the reaction of pentakis(trimethyl phosphite)ruthenium(0) with excess C_2H_5I in hexane slowly produced a white solid (3 days at 55 °C). Metathesis with NH_4PF_6 and subsequent recrystallization from THF gave a colourless, microcrystalline product. This was shown to be an approximately equimolar mixture of $\{IRu[P(OCH_3)_3]_5\}PF_6$ and $\{C_2H_5Ru[P(OCH_3)_3]_5\}PF_6$ by ^1H and $^{31}P\{^1H\}$ NMR spectroscopy.

When $Ru[P(OCH_3)_3]_5$ and allyl bromide were reacted in hexane at room temperature, a white precipitate resulted. The nature of this product appeared dependent upon the C_3H_5Br:$Ru[P(OCH_3)_3]_5$ ratio and the reaction time. With a twelvefold excess of C_3H_5Br and a three day reaction period, the isolated solid was identified as a mixture of $\{HRu[P(OCH_3)_3]_5\}X$ and $\{BrRu[P(OCH_3)_3]_5\}X$ (~1:5 respectively) by $^{31}P\{^1H\}$ NMR spectroscopy. At an allyl bromide:$Ru[P(OCH_3)_3]_5$ ratio of 100:1 and a six day reaction period, the isolated product (after NH_4PF_6 metathesis) was shown to be exclusively $\{BrRu[P(OCH_3)_3]_5\}PF_6$ by ^1H and $^{31}P\{^1H\}$ NMR spectroscopy.

Similar results were found for the treatment of $Ru[P(OCH_3)_3]_5$ with $C_6H_5CH_2Br$ in hexane. A white precipitate formed over the course of 24 h. Metathesis with NH_4PF_6 and subsequent THF recrystallization afforded colourless microcrystals. These were shown to be $\{BrRu[P(OCH_3)_3]_5\}PF_6$ by ^1H and $^{31}P\{^1H\}$ NMR spectroscopy.

The reactions of $Ru[P(OCH_3)_3]_5$ with $NOPF_6$ and $AgBF_4$ were attempted. These did not give the desired products (i.e. $\{ONRu[P(OCH_3)_3]_5\}PF_6$ and $\{AgRu[P(OCH_3)_3]_5\}BF_4$, respectively). The details of these two reactions are given in the discussion section of this chapter.

The protonation of $Ru[P(OCH_3)_3]_4P(OCH_2)_3CCH_3$ was accomplished by treatment with NH_4PF_6 in THF. The resultant white solid, $\{HRu[P(OCH_3)_3]_4P(OCH_2)_3CCH_3\}PF_6$, appeared

air-stable for two weeks and was soluble in CH_2Cl_2 but insoluble in hexane.

The reader is reminded that some of the results presented in this chapter were part of an undergraduate research project; see chapter 1 for further details.

3.3 Characterization and Discussion

The complexes $\{XRu[P(OCH_3)_3]_5\}PF_6$ (X= H, CH_3, Cl, Br, I) and $\{HRu[P(OCH_3)_3]_4P(OCH_2)_3CCH_3\}PF_6$ were all characterized by elemental analysis and $^{31}P\{^1H\}$ NMR spectroscopy. In addition, the mass spectral and ^1H NMR data were obtained for most of these cationic species.

The $^{31}P\{^1H\}$ NMR spectra of $\{XRu[P(OCH_3)_3]_5\}PF_6$ (X= H, Cl, Br, I) all result from an AB_4 spin system. The qualitative pattern for a given spectrum is dependent upon a single parameter, $J_{AB}/\Delta\delta_{AB}$. This fact was used to successfully simulate the spectra (see the experimental section of chapter 2 for details). The calculated and experimental $^{31}P\{^1H\}$ NMR spectra for $\{HRu[P(OCH_3)_3]_5\}^+$ and $\{BrRu[P(OCH_3)_3]_5\}^+$ are shown in figure 3.1. The spectral parameters for $\{XRu[P(OCH_3)_3]_5\}^+$ (X= H, Cl, Br, I) are given in table 3.1.

The observation of $^{31}P\{^1H\}$ NMR data due to an AB_4 spin system for $\{XRu[P(OCH_3)_3]_5\}^+$ (X= H, Cl, Br, I) is consistent with a nominally octahedral structure for these cations. The variable temperature $^{31}P\{^1H\}$ NMR spectra of these complexes

exhibited no line broadening due to chemical exchange. However, more subtle effects due to different temperature dependencies of the ^{31}P chemical shifts were observed (a more detailed discussion of this phenomenon may be found in chapter 6). The $^{31}P\{^{1}H\}$ NMR spectrum of $\{CH_3Ru[P(OCH_3)_3]_5\}^+$ in CD_2Cl_2 is a singlet at 25 °C. This behaviour is ascribed to an accidental degeneracy of δ_A and δ_B at this temperature; the effects of J_{AB} are not observed in an AB_4 spectrum under this constraint. Different variations in δ with temperature for the two resonances results in a lifting of this degeneracy. The $^{31}P\{^{1}H\}$ NMR spectrum of $\{CH_3Ru[P(OCH_3)_3]_5\}^+$ in CD_2Cl_2 at -73 °C (at 162.0 MHz) is a tightly coupled AB_4 pattern. The calculated and experimental $^{31}P\{^{1}H\}$ NMR spectra of $\{CH_3Ru[P(OCH_3)_3]_5\}^+$ at -73 °C are shown in figure 3.2. The associated spectral parameters are given in table 3.1.

The $^{31}P\{^{1}H\}$ NMR spectra for $\{XRu[P(OCH_3)_3]_5\}PF_6$ (X= H, Me, Cl, Br, I) and $\{HRu[P(OCH_3)_3]_4P(OCH_2)_3CCH_3\}PF_6$ all exhibited a

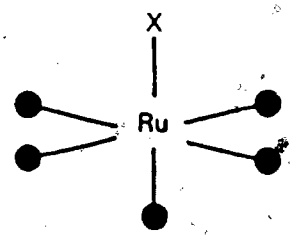

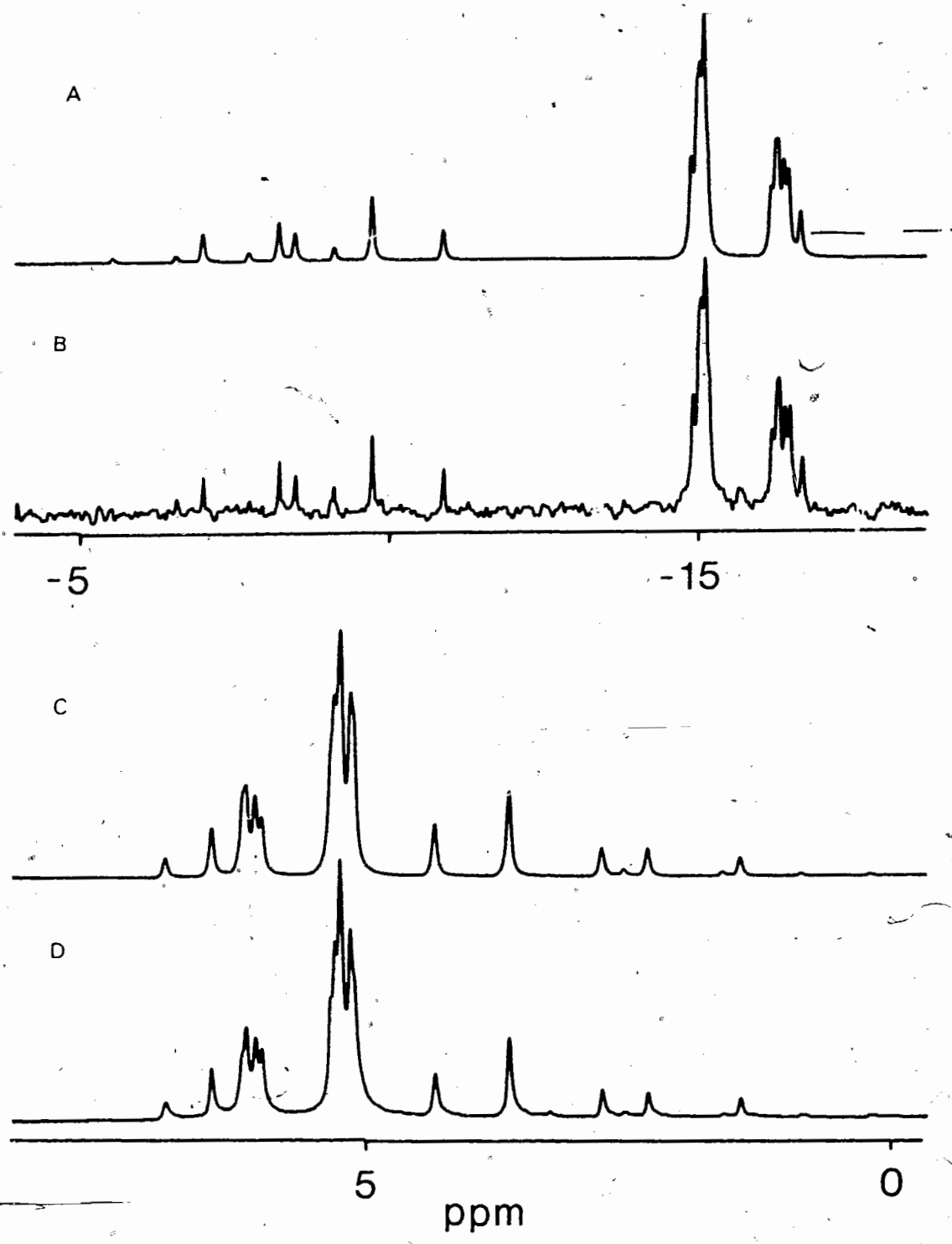

Figure 3.1 The calculated (A) and experimental (B) $^{31}P\{^{1}H\}$ NMR spectra of $\{BrRu[P(OCH_3)_3]_5\}PF_6$. The calculated (C) and experimental (D) $^{31}P\{^{1}H\}$ NMR spectra of $\{HRu[P(OCH_3)_3]_5\}PF_6$. Both experimental spectra in $CDCl_3$. Spectral parameters given in table 3.1 (PF_6^- region not included).

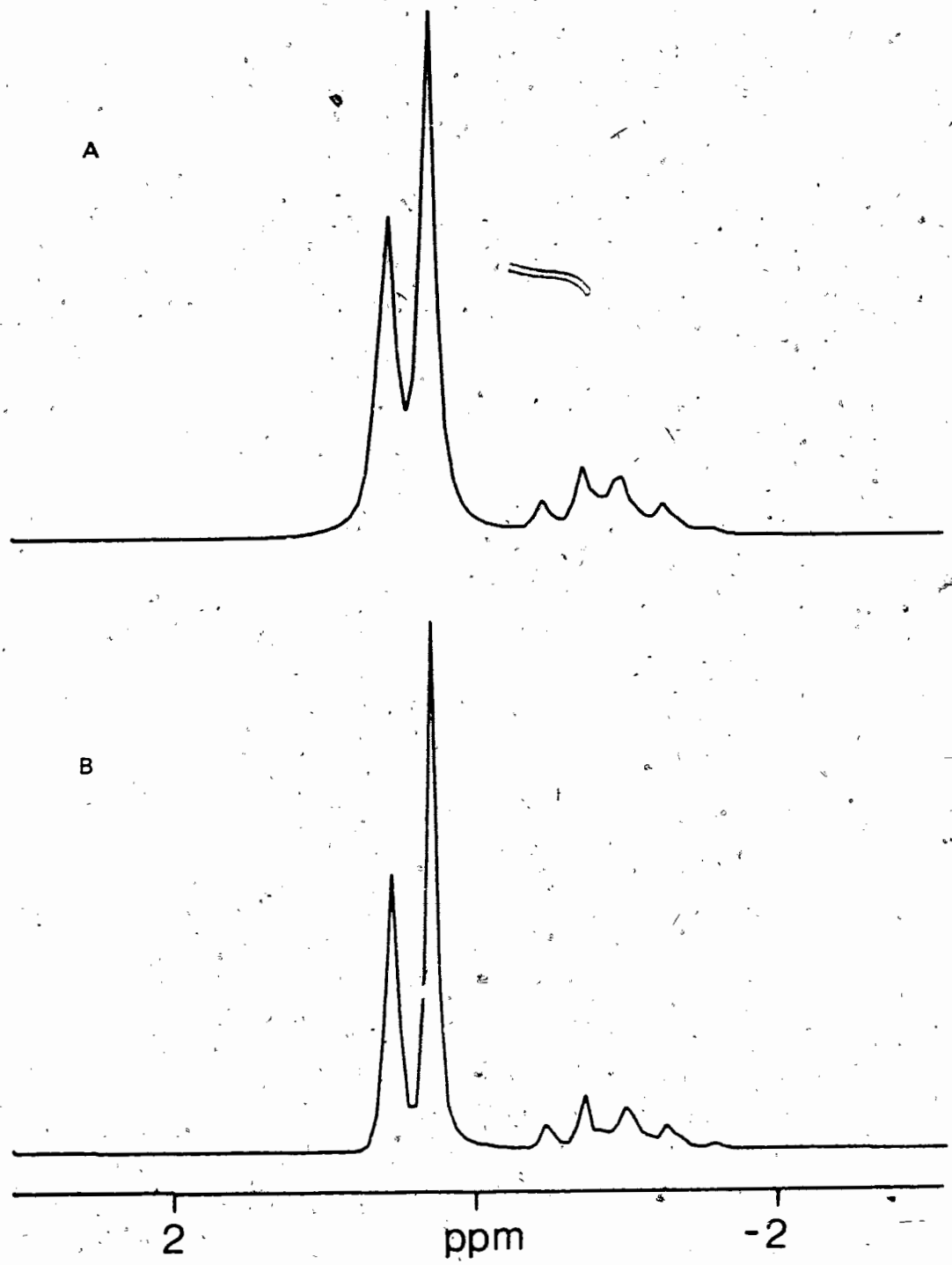

Figure 3.2 The calculated (A) and experimental (B) $^{31}P\{^{1}H\}$ NMR spectra (162.0 MHz) of $\{CH_3Ru[P(OCH_3)_3]_5\}PF_6$ in CD_2Cl_2 at -73°C. Spectral parameters given in table 3.1 (PF_6^- region not included).

Cation	δ_A (ppm)	δ_B (ppm)	J_{AB} (Hz)
$[HRu[P(OCH_3)_3]_5]^{+a}$	2.8	5.7	46.3
$[CH_3Ru[P(OCH_3)_3]_5]^{+a}$ (-73°C)	-0.9	0.5	45.8
$[ClRu[P(OCH_3)_3]_5]^{+b}$	-8.0	-15.0	56.8
$[BrRu[P(OCH_3)_3]_5]^{+b}$	-8.5	-15.7	55.9
$[IRu[P(OCH_3)_3]_5]^{+b}$	-13.2	-16.1	53.6

Table 3.1 The $^{31}P\{^1H\}$ NMR spectral parameters for $[XRu[P(OCH_3)_3]_5]^+$. [a]Recorded in CH_2Cl_2. [b]Recorded in $CDCl_3$.

septet due to the PF_6^- ion. The chemical shift and phosphorus-fluorine coupling constant were relatively insensitive to the counterion: δ -284.1 to -285.3, J_{PF} 710-712 Hz.

The ^1H NMR spectrum of $[HRu[P(OCH_3)_3]_5]PF_6$ (in acetone-d_6) exhibited a methoxy multiplet (δ 3.68) and a weak multiplet at δ -9.49. The chemical shift of the latter resonance occurs in the region expected for a hydrogen attached to ruthenium [5] and is consistent with the literature value for the complex [74].

In addition to a methoxy multiplet (δ 3.65), the ^1H NMR spectrum of $[CH_3Ru[P(OCH_3)_3]_5]PF_6$ in $CDCl_3$ featured a weak multiplet at δ -0.13. Other complexes containing methyl groups

attached to ruthenium also exhibit resonances in this region of the ^1H NMR spectrum [76,77,78].

Included in the $^{13}C\{^1H\}$ NMR spectrum of $\{CH_3Ru[P(OCH_3)_3]_5\}PF_6$ (acetone-d_6) was a weak multiplet at δ -22.6. This resonance was assigned to the CH_3 group attached to ruthenium; high field ^{13}C shifts for such a methyl group have previously been observed [77].

The $^{31}P\{^1H\}$ NMR data for $\{HRu[P(OCH_3)_3]_4P(OCH_2)_3CCH_3\}PF_6$ is more complex than that for $\{XRu[P(OCH_3)_3]_5\}PF_6$ (X= H, Me, Cl, Br, I). This is due to the possibility of two isomers for the $P(OCH_2)_3CCH_3$ derivative; the hydride and $P(OCH_2)_3CCH_3$ ligands may be either *cis* (3a) or *trans* (3b) to one another. The $^{31}P\{^1H\}$ NMR spectrum of $\{HRu[P(OCH_3)_3]_4P(OCH_2)_3CCH_3\}PF_6$ in CD_2Cl_2 is shown in figure 3.3A. The A part of a spectrum due to an AB_4 spin system is evident at higher field and a simulated spectrum based on this assumption is shown in figure 3.3B (δ_A -8.8, δ_B 5.6, J_{AB}= 46.0 Hz). This subspectrum constitutes approximately 25% of the total intensity of the experimental spectrum and arises from isomer 3b. The *cis* isomer 3a is expected to exhibit a $^{31}P\{^1H\}$ NMR spectrum due to an A_2BCD spin system; a simulation of this complex spectrum was not attempted.

The ^1H NMR data for $\{HRu[P(OCH_3)_3]_4P(OCH_2)_3CCH_3\}PF_6$ is consistent with the $^{31}P\{^1H\}$ NMR results. The proton spectrum features a methoxy multiplet (δ 3.62), a broad triplet with poorly resolved shoulders (δ 4.14, J_{PH}= 4 Hz), and a pair of

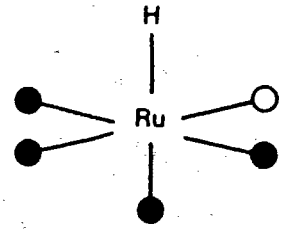

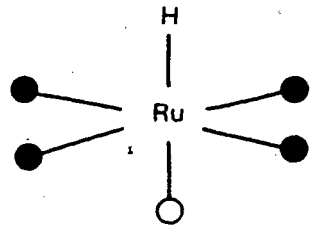

3a **3b**

---

overlapping singlets (δ 0.78, 0.76); the latter signals have a relative intensity of 1:3, respectively. The triplet and singlets may be assigned to the methylene and methyl protons, respectively, of coordinated $P(OCH_2)_3CCH_3$. The observation of two CH_3 signals for the caged phosphite ligand suggests the presence of two isomers with magnetically inequivalent sites for the methyl group.

In addition to the previously described resonances, the ^1H NMR spectrum of $\{HRu[P(OCH_3)_3]_4P(OCH_2)_3CCH_3\}PF_6$ exhibits a complex multiplet centred at δ -9.2. This multiplet is in the region expected for a ruthenium hydride [5] and is shown in figure 3.4B. The structure of this high field multiplet confirms the presence of two isomers. A spectrum due to an AX_4Y spin system is contained within this group of resonances; a simulation of the A part is shown in figure 3.4A (δ -8.72, J_{AY}=

124.2 Hz, J_{AX}= 20.8 Hz). The A part of another computer simulation, based on an AW_2XYZ spin system (δ -9.57, see experimental section for the balance of the spectral parameters) is shown in figure 3.4C. These two subspectra account for all the major lines in the experimental spectrum (figure 3.4B). The resonances of the A part of the AX_4Y pattern comprise approximately 25% of the total intensity for the experimental spectrum. This result is consistent with the observation of two Me signals for the $P(OCH_2)_3CCH_3$ ligand (vide supra).

The ^1H and $^{31}P\{^1H\}$ NMR data for $\{HRu[P(OCH_3)_3]_4P(OCH_2)_3CCH_3\}PF_6$ are thus in accord with the presence of two isomers. The major isomer **3a** is favoured 3:1 over the minor isomer **3b**.

Based on a purely statistical argument, a 4:1 ratio of **3a**:**3b** is expected. The *trans* isomer thus appears weakly favoured. This could be due to steric effects. The addition of a sixth ligand (albeit a proton) to the already crowded $Ru[P(OCH_3)_3]_4P(OCH_2)_3CCH_3$ molecule is expected to be sensitive to steric constraints. If the transition state is viewed as arising from a nucleophilic attack of $Ru[P(OCH_3)_3]_4P(OCH_2)_3CCH_3$ (in a C_{4v} conformation) on a proton, a small bias towards *trans* addition would be expected: the potential sixth coordination site would be less crowded with the smaller $P(OCH_2)_3CCH_3$ ligand (cone angle 101° versus 107° for $P(OCH_3)_3$ [10,51]) in the apical position. This suggestion might be tested experimentally. The availability of $Ru[P(OCH_3)_3]_4L$ (L= various phosphines and

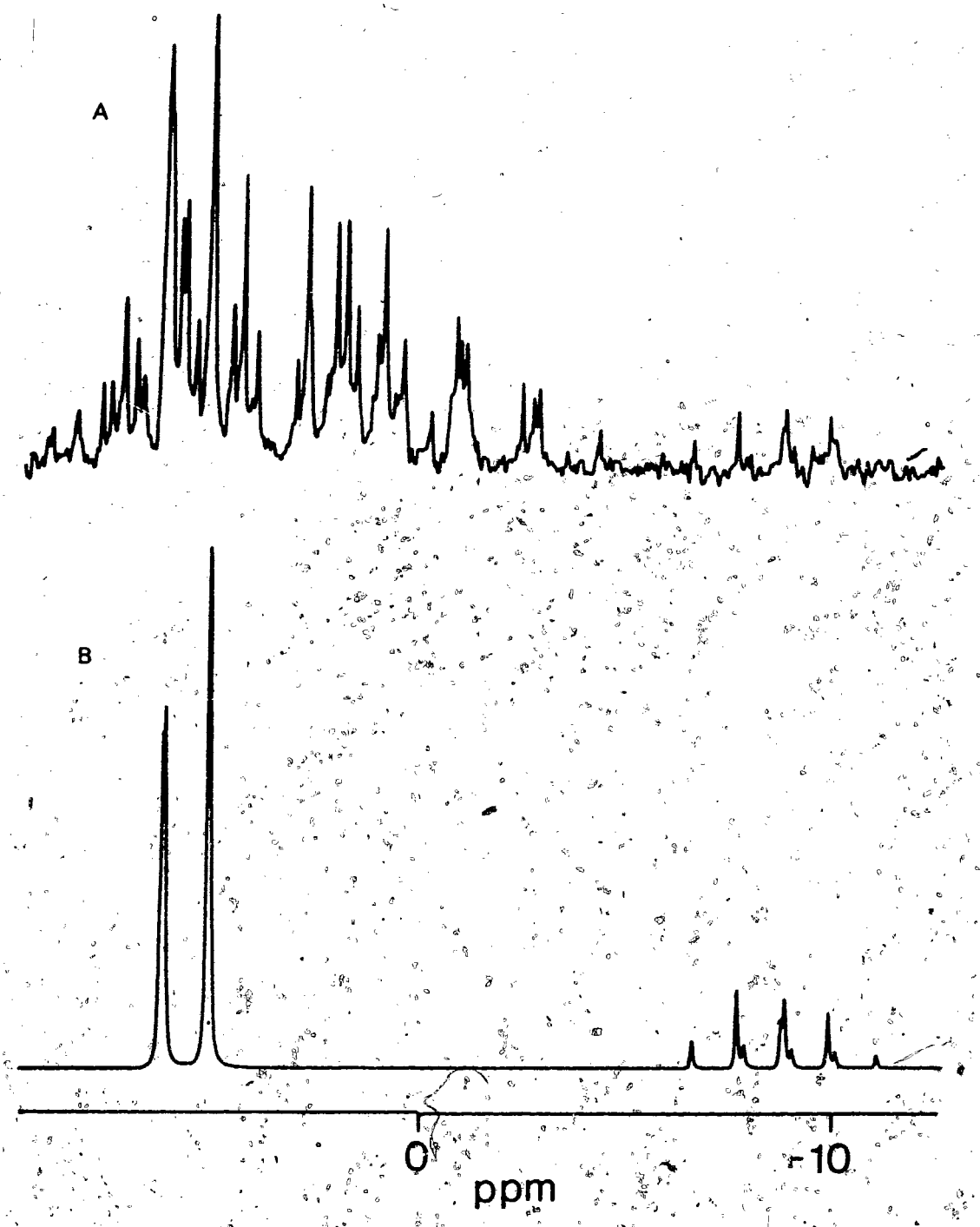

Figure 3.3 $^{31}P\{^{1}H\}$ NMR spectrum (in CD_2Cl_2) of $\{HRu[P(OCH_3)_3]_4P(OCH_2)_3CCH_3\}PF_6$ (A) and a partial spectral simulation based on an AB_4 spin system (B). Spectral parameters given in text (PF_6^- region not included).

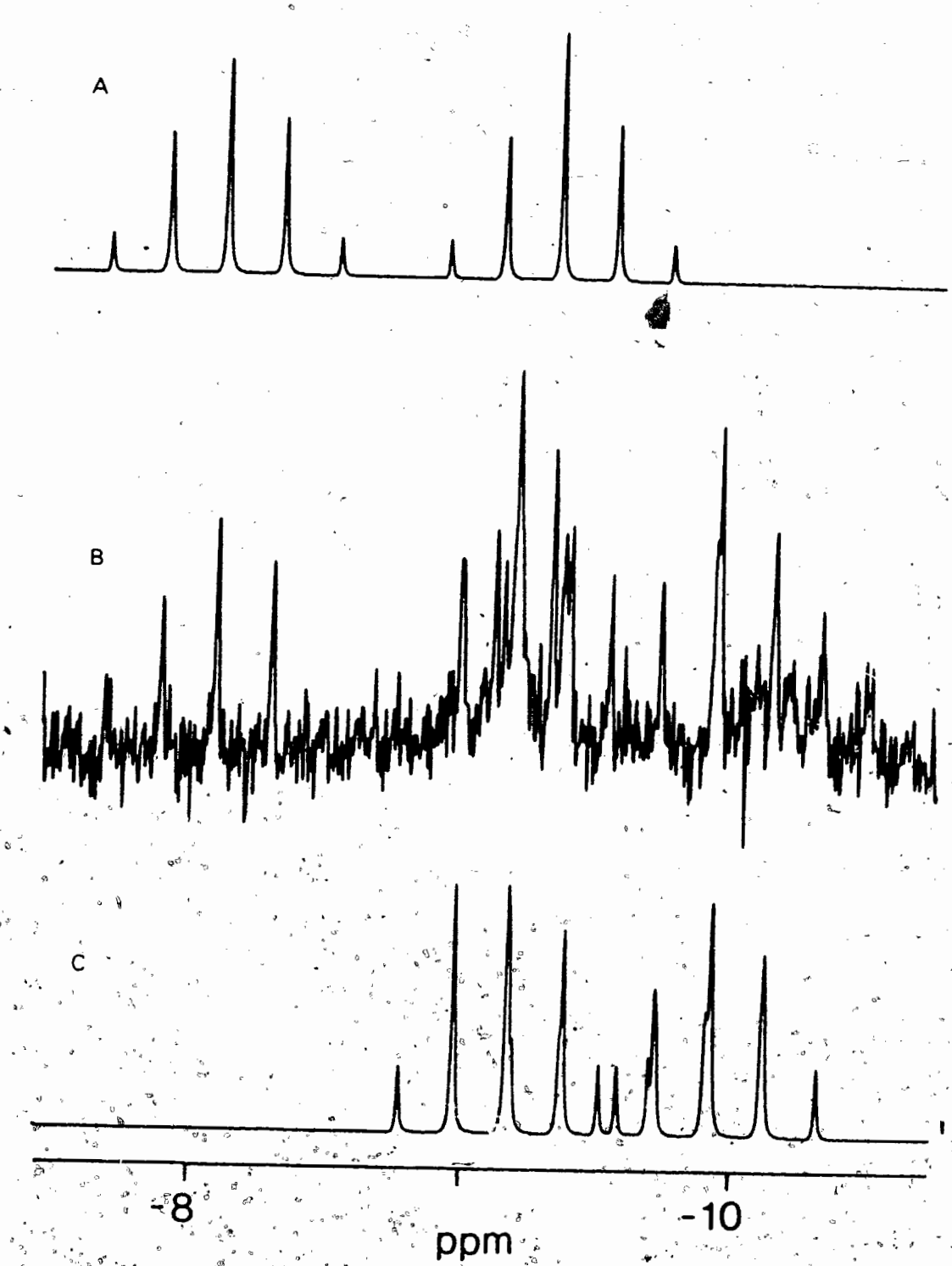

Figure 3.4 The high field ^1H NMR spectrum (CD_2Cl_2) of $\{HRu[P(OCH_3)_3]_4P(OCH_2)_3CCH_3\}PF_6$ (B). The A_4 parts of spectral simulations based on an AX_4Y and an AW_2XYZ spin system (A and C, respectively). Spectral parameters given in text.

phosphites) would likely allow preparation of $\{HRu[P(OCH_3)_3]_4L\}^+$. An analysis of the *cis:trans* isomeric ratios for these cations could permit a more quantitative estimation of the factors involved.

The mass spectra of the complexes $\{XRu[P(OCH_3)_3]_5\}PF_6$ (X= H, CH_3, Br, I) and $\{HRu[P(OCH_3)_3]_4P(OCH_2)_3CCH_3\}PF_6$ were measured by the fast atom bombardment technique. Parent ions for $\{HRu[P(OCH_3)_3]_4(P(OCH_2)_3CCH_3)\}^+$ and the hydride, methyl, and iodide cations were observed. Fragments due to $[BrRu(P(OCH_3)_3)_x]^+$ (x= 4,3,2) were found for $\{BrRu[P(OCH_3)_3]_5\}^+$; the characteristic mass spectral patterns due to ^{79}Br and ^{81}Br were also present.

The reaction of $Ru[P(OCH_3)_3]_5$ with excess C_2H_5I in hexane did not lead to isolation of the $\{C_2H_5Ru[P(OCH_3)_3]_5\}$ cation. After three days at 55 °C, the resultant white solid was reacted with NH_4PF_6, allowing isolation of colourless crystals. The $^{31}P\{^1H\}$ NMR spectrum of this solid revealed two sets of resonances. One, due to an AB_4 spin system, was identified as $\{IRu[P(OCH_3)_3]_5\}PF_6$. The other set of resonances appeared as a very narrow multiplet, similar to that found in the $^{31}P\{^1H\}$ NMR spectrum of $\{CH_3Ru[P(OCH_3)_3]_5\}PF_6$ at low temperatures (figure 3.2). The two multiplets were of approximately equal intensity. The ^1H NMR spectrum of this product revealed a complex methoxy multiplet (δ 3.7). A triplet (δ 1.33) and a multiplet (δ -0.15) of relative intensity 3:2 were also observed. These proton resonances occurred in the regions expected for the methyl and

methylene moieties of a C_2H_5 group attached to ruthenium. The position of the methylene resonance was consistent with that of the methyl signal in $\{CH_3Ru[P(OCH_3)_3]_5\}^+$ (δ -0.13). All of the spectroscopic evidence was consistent with the presence of approximately equimolar amounts of $\{IRu[P(OCH_3)_3]_5\}PF_6$ and $\{C_2H_5Ru[P(OCH_3)_3]_5\}PF_6$; the elemental analysis was in accord with this result. The ^1H and $^{31}P\{^1H\}$ NMR spectra were identical before and after metathesis with NH_4PF_6. Despite several attempts, the two species could not be separated.

The presence of $\{IRu[P(OCH_3)_3]_5\}PF_6$ as a product in the reaction of $Ru[P(OCH_3)_3]_5$ and excess C_2H_5I in hexane was unexpected. The presence of $\{HRu[P(OCH_3)_3]_5\}^+$, resulting from β-elimination of C_2H_4 from $\{C_2H_5Ru[P(OCH_3)_3]_5\}^+$, would have been easily explained. A $^{31}P\{^1H\}$ NMR study of the reaction between $Fe[P(OCH_3)_3]_5$ and excess C_2H_5I (at 25 °C in CD_3CN) showed such behaviour [26]. Although resonances due to $\{C_2H_5Fe[P(OCH_3)_3]_5\}^+$ were observed early in the reaction, the final products were C_2H_4 and $\{HFe[P(OCH_3)_3]_5\}^+$.

A mechanism which can explain the presence of both the iodide and ethyl cations in the reaction of $Ru[P(OCH_3)_3]_5$ and excess C_2H_5I is shown below.

$$Ru[P(OCH_3)_3]_5 + C_2H_5I \longrightarrow \{C_2H_5Ru[P(OCH_3)_3]_5\}I$$

$$\{C_2H_5Ru[P(OCH_3)_3]_5\}I \longrightarrow \{\cdot Ru[P(OCH_3)_3]_5\}I + \cdot C_2H_5$$

$$\{\cdot Ru[P(OCH_3)_3]_5\}I + C_2H_5I \longrightarrow \{IRu[P(OCH_3)_3]_5\}I + \cdot C_2H_5$$

It has been shown that C_2H_5I and other alkyl halides react with Pt^0-phosphine complexes via a radical pathway [79]. No effort was made to exclude light from the reaction of $Ru[P(OCH_3)_3]_5$ and C_2H_5I or to test for a radical mechanism.

The reactions of ethyl iodide with $Ru[P(OCH_3)_3]_5$ and the iron analogue appear to proceed by different pathways. Solvent and solubility effects cannot be ignored. The ruthenium reaction was carried out in hexane, in which the cationic species are virtually insoluble, while $Fe[P(OCH_3)_3]_5$ was treated with C_2H_5I in CD_3CN, in which the cations readily dissolve. A different result might have occurred if $\{C_2H_5Ru[P(OCH_3)_3]_5\}I$ had remained in solution.

Another cause of the differing response of $Ru[P(OCH_3)_3]_5$ and $Fe[P(OCH_3)_3]_5$ to treatment with C_2H_5I could lie in the requirements of the β-elimination mechanism. As $\{C_2H_5M[P(OCH_3)_3]_5\}^+$ (M= Fe, Ru) are coordinatively saturated, a vacant site must be generated before hydrogen transfer can occur in the subsequent step. If the equilibrium constant for the ligand dissociation

$$\{C_2H_5M[P(OCH_3)_3]_5\}^+ \rightleftharpoons \{C_2H_5M[P(OCH_3)_3]_4\}^+ + P(OCH_3)_3$$

was considerably smaller for Ru than for Fe, one would expect β-elimination to be inhibited in the former, potentially allowing another process to occur preferentially.

The reaction of $Ru[P(OCH_3)_3]_5$ and excess allyl bromide in hexane (25 °C) slowly gave a white precipitate over the course of several days. The product distribution appeared dependent upon the C_3H_5Br:$Ru[P(OCH_3)_3]_5$ ratio and the reaction time. With a twelvefold excess of C_3H_5Br and a reaction time of 3 days, the isolated product was identified as a mixture of $\{HRu[P(OCH_3)_3]_5\}X$ and $\{BrRu[P(OCH_3)_3]_5\}X$ (~1:5, respectively) by ^1H and $^{31}P\{^1H\}$ NMR spectroscopy (X was presumably Br). At an allyl bromide:$Ru[P(OCH_3)_3]_5$ ratio of 100:1 and a reaction time of six days, the isolated product (after NH_4PF_6 metathesis) was exclusively $\{BrRu[P(OCH_3)_3]_5\}PF_6$. Again, no effort was made to exclude light from the reaction.

There was no evidence for the expected nucleophilic attack of $Ru[P(OCH_3)_3]_5$ on allyl bromide, yielding either $\{C_3H_5Ru[P(OCH_3)_3]_5\}Br$ or $\{(\eta^3\text{-}C_3H_5)Ru[P(OCH_3)_3]_4\}Br$. Either an allyl cation was not formed or upon formation underwent immediate reaction. The presence of the hydride cation is not easily explained. It is possible that fast β-elimination from an allyl cation could yield $\{HRu[P(OCH_3)_3]_5\}^+$ and propadiene (allene). However, we could find no precedent in the literature for allene elimination from an allyl complex. A gas chromatographic analysis of the reaction mixture would have aided the identification of the organic products.

Several mechanisms may be proposed to rationalize the presence of $\{BrRu[P(OCH_3)_3]_5\}^+$, the only product isolated at high allyl bromide concentrations and long reaction times. A

mechanism involving free radical attack of the allyl radical on the hydride cation is plausible.

$$C_3H_5Br \longrightarrow Br\cdot + C_3H_5\cdot$$

$$C_3H_5\cdot + \{HRu[P(OCH_3)_3]_5\}^+ \longrightarrow C_3H_6 + \{\cdot Ru[P(OCH_3)_3]_5\}^+$$

$$\{\cdot Ru[P(OCH_3)_3]_5\}^+ + C_3H_5Br \longrightarrow \{BrRu[P(OCH_3)_3]_5\}^+ + \cdot C_3H_5$$

This pathway is consistent with the exclusive isolation of the bromide cation at high allyl bromide concentrations. One might also postulate an ionic mechanism in which $Ru[P(OCH_3)_3]_5$ slowly reacts with C_3H_5Br in the opposite sense to that expected.

$$Ru[P(OCH_3)_3]_5 + C_3H_5Br \xrightarrow{slow} \{BrRu[P(OCH_3)_3]_5\}^+ + C_3H_5^-$$

$$C_3H_5^- + C_3H_5Br \xrightarrow{fast} C_6H_{10} + Br^-$$

The latter mechanism is consistent with results found for the analogous iron reaction: the reaction of $Fe[P(OCH_3)_3]_5$ and allyl bromide gave 1,5-hexadiene but no propene [26]. The transition metal product of this reaction, however, was not reported and the relationship of this result to the present discussion is not clear. A more detailed study of the reaction between $Ru[P(OCH_3)_3]_5$ and C_3H_5Br could answer a key question: is $\{HRu[P(OCH_3)_3]_5\}^+$ the sole primary product and precursor to $\{BrRu[P(OCH_3)_3]_5\}^+$ or are both the hydride and bromide cations formed simultaneously? The operation of a radical pathway could also be tested by appropriate experiments. It is of interest that the reaction between some Pt^0-phosphine complexes and

C_3H_5Br did not appear to proceed via a free radical mechanism [79]. The reaction of $Ir(CO)Cl(PMe_3)_2$ with allyl halides RX to form $Ir(CO)Cl(P(CH_3)_3)_2R(X)$ was also found to occur by a non-radical mechanism [80].

The reaction of $Ru[P(OCH_3)_3]_5$ and excess $C_6H_5CH_2Br$ in hexane (25 °C) gave a white precipitate over the course of 24 h. After isolation and metathesis with NH_4PF_6, the resultant solid was shown to be $\{BrRu[P(OCH_3)_3]_5\}PF_6$ by ^1H and $^{31}P\{^1H\}$ NMR spectroscopy.

Several mechanisms analogous to those just described for the reaction of $Ru[P(OCH_3)_3]_5$ with allyl bromide may be advanced in the present case. The reaction of benzyl bromide and several Pt^0-phosphine complexes was found not to be free radical in nature [79]. The reaction of $Ir(CO)Cl(P(CH_3)_3)_2$ with benzyl halides RX to form $Ir(CO)Cl(P(CH_3)_3)_2R(X)$ was also found to occur via a non-radical process [80]. The reaction of $Fe[P(OCH_3)_3]_5$ with $C_6H_5CH_2I$ gave bibenzyl and $Fe[P(OCH_3)_3]_3I_2$ quantitatively [26]. The available evidence is insufficient to favour a particular mechanism.

A solution of $Ru[P(OCH_3)_3]_5$ in CH_3CN immediately turned pale brown upon addition of a stoichiometric amount of $NOPF_6$. The resultant mixture of white and brown solids were extracted with CH_2Cl_2; the filtered extracts gave a pale brown product. The $^{31}P\{^1H\}$ NMR spectrum of this solid (CD_2Cl_2) revealed resonances due to two species. The major product (~80%) was

$\{HRu[P(OCH_3)_3]_5\}PF_6$. The other set of resonances appeared to be an AB_4 pattern. Despite several attempts, separation of the two complexes was not achieved. When the reaction was performed in THF, only the hydride cation was isolated. This is likely due to the instability of $NOPF_6$ in THF: nitrosyl hexafluorophosphate reacted vigorously with pure THF but appeared stable in CH_3CN.

The reaction of $Ru[P(OCH_3)_3]_5$ with $NOPF_6$ was originally viewed as a simple nucleophilic attack, hopefully resulting in $\{ONRu[P(OCH_3)_3]_5\}PF_6$. When examined in light of the 18 electron rule, this complex would contain NO acting as a one electron donor ligand. This situation is less common than the alternative bonding mode for a terminal NO, where it acts as a three electron donor. The preparation of $\{FeNO[P(OR)_3]_4\}BPh_4$ (R= Me, Et) by treatment of FeX_2 (X= Cl, Br) and excess phosphite in methanol with NO has recently been reported [81]. These complexes contain NO in its more common role as a three electron donor ligand. There was no reaction between $\{FeNO[P(OR)_3]_4\}BPh_4$ (R= Me, Et) and phosphite in refluxing methanol or ethanol. This result is evidence that the proposed $\{ONRu[P(OCH_3)_3]_5\}^+$ species is not the stable form of an $M[P(OR)_3]_nNO$ (M= Fe, Ru; R= alkyl) type complex.

The addition of $Ru[P(OCH_3)_3]_5$ in toluene to an equimolar solution of $AgBF_4$ caused an immediate green-brown precipitate. This solid was extracted with CH_2Cl_2 and the resultant heterogeneous mixture filtered; the filter paper was coated with a metallic sludge. Subsequent filtration left a yellow-brown

solid which was further purified by slow addition of hexane to a CH_2Cl_2 solution of the product. A $^{31}P\{^1H\}$ NMR spectrum of the resultant yellow-brown solid (CD_2Cl_2) revealed a spectrum due to an AB_4 spin system (figure 3.5B). A computer simulation of this spectrum (δ_A -4.8, δ_B -16.9, J_{AB}= 60.5 Hz) is shown in figure 3.5A. The ^1H NMR spectrum (CD_2Cl_2) showed only a methoxy multiplet at δ 3.95. The ^{19}F NMR spectrum of the product (CD_2Cl_2) featured two singlets. While these were in the proper region for the BF_4 anion, none of the expected effects due to coupling with the ^{11}B nucleus were observed [82]. The ^{31}P spectral parameters may be compared to those in table 3.1; the product did not contain the $\{HRu[P(OCH_3)_3]_5\}$ cation. The well-defined AB_4 pattern argues against a formulation of $\{FRu[P(OCH_3)_3]_5\}^+$: the ^{19}F nucleus would certainly lead to an AB_4X spin system. The expected product, $\{AgRu[P(OCH_3)_3]_5\}^+$, may be ruled out on similar grounds. Both ^{107}Ag and ^{109}Ag have I=1/2. The values of $^2J(^{107}\ ^{109}Ag\text{-}P)$ for $\{Ag_2Ru_4(\mu_3\text{-}H)[\mu\text{-}Ph_2P(CH_2)_nPPh_2](CO)_{12}\}$ (n= 1,2,4) are 5-13 Hz [83].

The fast atom bombardment mass spectrum of the solid revealed fragments due to $\{Ru[P(OCH_3)_3]_x\}^+$ (x= 4,3) and one unidentified fragment at a higher (*m/e* 617) mass number. Both the elemental analysis and x-ray fluorescence revealed the presence of Ag in samples of the product. The percentage of Ag (4.26%), however, did not agree with any chemically reasonable formulation. The product remains unidentified.

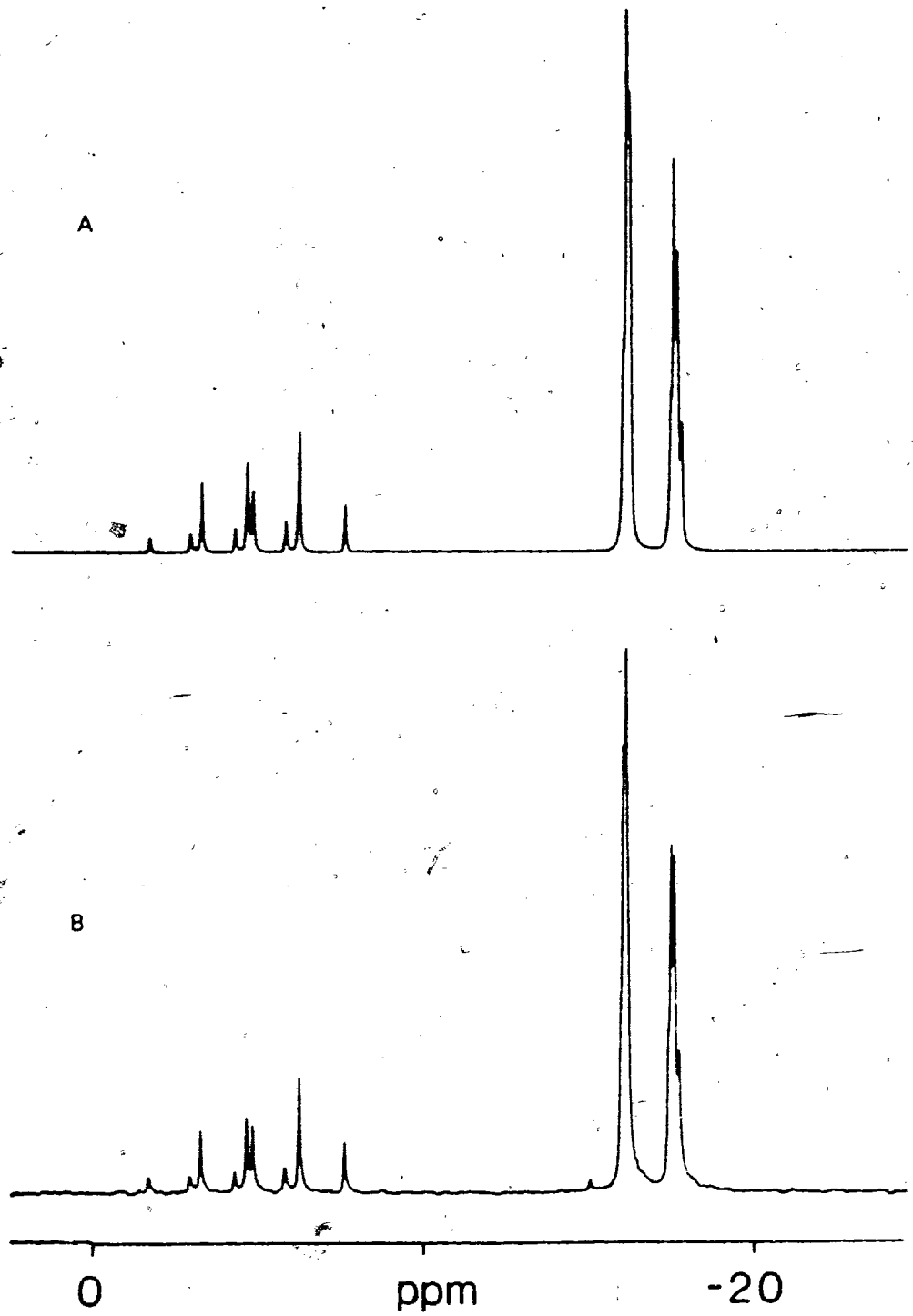

Figure 3.5 The experimental (B) and simulated (A) $^{31}P\{^{1}H\}$ NMR spectra of the product from reaction of $Ru[P(OCH_3)_3]_5$ with $AgBF_4$. Spectrum recorded in CD_2Cl_2. Spectral parameters given in text.

The yield of this product (0.100 g) relative to the amount of starting material (i.e. $Ru[P(OCH_3)_3]_5$: 0.450 g) indicated a considerable decomposition of $Ru[P(OCH_3)_3]_5$ during the course of the reaction. Recall the metallic sludge filtered out of the reaction mixture. This sludge likely contained silver metal arising from the oxidation of $Ru[P(OCH_3)_3]_5$ by Ag^+; the silver(I) ion is an oxidizing agent and $Ru[P(OCH_3)_3]_5$ contains a metal centre with high electron density. The reaction of *trans*-$OsCl_2(P(CH_3)_3)_4$ with $AgPF_6$ in methanol gave metallic silver and $\{OsCl_2(P(CH_3)_3)_4\}PF_6$ [84].

The $^{31}P\{^1H\}$ NMR spectral parameters for $\{XRu[P(OCH_3)_3]_5\}^+$ (X= H, CH_3, Cl, Br, I) are given in table 3.1. These may be compared to the analogous values (see table 3.2) for two related systems: $\{XFe[P(OCH_3)_3]_5\}^+$ (X= H, CH_3, Cl, Br, I) and $\{XFe[P(OC_2H_5)_3]_5\}^+$ (X= H, Cl, Br, I) [75]. The most prominent feature of the data in tables 3.1 and 3.2 is the larger magnitude of J_{AB} for X= halogen relative to X= H and CH_3. This disparity is more pronounced for the iron complexes. This result is consistent with Bent's rule, which states that more electronegative substituents "prefer" hybrid orbitals having less *s* character and more electropositive substituents "prefer" hybrid orbitals having more *s* character [85]. For complexes of the type $\{XM[P(OR)_3]_5\}^+$, this rule suggests that the metal-phosphorus bonding orbitals have enhanced *s* character. The Fermi contact term, generally accepted to be the major contributor to spin-spin coupling for ^{31}P nuclei, is directly

proportional to the *s* electron densities at the two coupled nuclei [86]. Thus, the larger values of J_{AB} for X= halogen relative to X= H or CH_3 are expected.

The only obvious trend in the ^{31}P chemical shifts of tables 3.1 and 3.2 is the upfield shift of δ_A and δ_B when Fe is replaced by Ru. An upfield shift for a ligand nucleus, as the central metal is replaced by the one below it in the periodic table, has been observed for several nuclei; these include ^{31}P, ^{13}C, and ^{29}Si [87,88]. For the three series of cations featured in tables 3.1 and 3.2, it is noted that δ_A is downfield from δ_B for X= halogen; this is reversed for X= H, CH_3. The theory of ^{31}P chemical shifts, especially for coordinated phosphorus donor ligands, is not well understood [89,90]. There is undoubtedly a subtle interplay between a number of causative factors.

The results presented in this chapter may be summarized as follows. The reaction of $Ru[P(OCH_3)_3]_5$ with X_2 (X= Cl, Br, I) gave $\{XRu[P(OCH_3)_3]_5\}^+$, which were isolated as the PF_6 salts. The sequential treatment of $Ru[P(OCH_3)_3]_5$ with CH_3I and NH_4PF_6 produced $\{CH_3Ru[P(OCH_3)_3]_5\}PF_6$. The reaction of $Ru[P(OCH_3)_3]_5$ with NH_4PF_6 led directly to the isolation of $\{HRu[P(OCH_3)_3]_5\}PF_6$. The cations $\{XRu[P(OCH_3)_3]_5\}^+$ (X= H, CH_3, Cl, Br, I) all exhibited $^{31}P\{^1H\}$ NMR spectra due to an AB_4 spin system, consistent with a nominally octahedral geometry about the Ru atom. The mixed phosphite complex $Ru[P(OCH_3)_3]_4P(OCH_2)_3CCH_3$ reacted with NH_4PF_6 to produce $\{HRu[P(OCH_3)_3]_4P(OCH_2)_3CCH_3\}PF_6$ which existed as a mixture of

Complex	δ_A (ppm)	δ_B (ppm)	J_{AB} (Hz)
$\{HFe[P(OCH_3)_3]_5\}^+$	25.9	29.2	82.5
$\{CH_3Fe[P(OCH_3)_3]_5\}^+$	27.4	28.4	79.5
$\{ClFe[P(OCH_3)_3]_5\}^+$	22.9	8.8	126
$\{BrFe[P(OCH_3)_3]_5\}^+$	24.7	10.7	124
$\{IFe[P(OCH_3)_3]_5\}^+$	33.5	14.0	124
$\{HFe[P(OC_2H_5)_3]_5\}^+$	21.3	23.9	93
$\{ClFe[P(OC_2H_5)_3]_5\}^+$	19.1	4.5	125
$\{BrFe[P(OC_2H_5)_3]_5\}^+$	20.5	5.5	124
$\{IFe[P(OC_2H_5)_3]_5\}^+$	29.5	10.5	123

Table 3.2 The $^{31}P\{^1H\}$ NMR spectral parameters for the complexes $\{XFe[P(OCH_3)_3]_5\}^+$ (X= H, CH_3, Cl, Br, I) and $\{XFe[P(OC_2H_5)_3]_5\}^+$ (X= H, Cl, Br, I) [3c]. All spectra recorded in CH_2Cl_2.

cis (3a) and *trans* (3b) isomers in an approximate 3:1 ratio, respectively. The reaction of $Ru[P(OCH_3)_3]_5$ and C_2H_5I led to an inseparable mixture of $\{HRu[P(OCH_3)_3]_5\}^+$ and $\{IRu[P(OCH_3)_3]_5\}^+$ while $Ru[P(OCH_3)_3]_5$ and C_3H_5Br gave $\{BrRu[P(OCH_3)_3]_5\}^+$ as the final product; these cations were all isolated as the PF_6^- salts by reaction with NH_4PF_6. Treatment of $Ru[P(OCH_3)_3]_5$ with $C_6H_5CH_2Br$ also produced $\{BrRu[P(OCH_3)_3]_5\}^+$. The reaction of $AgBF_4$ and $Ru[P(OCH_3)_3]_5$ gave a phosphite-containing product which remains unidentified. When $Ru[P(OCH_3)_3]_5$ and $NOPF_6$ were reacted, the major product was $\{HRu[P(OCH_3)_3]_5\}PF_6$.

In general, the thesis that the high electron density on the Ru centre would lead to the reaction of $Ru[P(OCH_3)_3]_5$ as a nucleophile was validated. The reaction of NH_4^+ with $Ru[P(OCH_3)_3]_5$ to yield $\{HRu[P(OCH_3)_3]_5\}^+$ implies that $Ru[P(OCH_3)_3]_5$ is a stronger base than NH_3. The results of the reactions between $Ru[P(OCH_3)_3]_5$ and RBr (R= C_3H_5, $C_6H_5CH_2$), however, suggest that other reaction pathways are possible. The treatment of $Ru[P(OCH_3)_3]_5$ with Ag^+ showed that reaction modes other than nucleophilic attack are available to pentakis(trimethyl phosphite)ruthenium(0).

3.4 Experimental Section

Preparation of $\{CH_3Ru[P(OCH_3)_3]_5\}PF_6$ and $\{CH_3Ru[P(OCH_3)_3]_5\}I$. In a 100 mL Schlenk tube, $Ru[P(OCH_3)_3]_5$ (0.71 g, 0.98 mmol) and hexane (20 mL) were stirred. To this

clear, colourless solution was added CH_3I (1.0 mL, 16 mmol) dropwise. The resultant reaction mixture was stirred for 24 h at 20 °C. During this period a white precipitate formed. The solvent and excess CH_3I were decanted away for the white solid, which was washed with hexane (2x5 mL) and dried on the vacuum line. The product, $\{CH_3Ru[P(OCH_3)_3]_5\}I$ (0.83 g, 98%), was obtained as an analytically pure, white powder: mp 185-187 °C (dec.); ^1H NMR ($CDCl_3$, 25 °C, 100.1 MHz) δ= -0.13 (multiplet), δ= 3.65 (multiplet); $^{31}P\{^1H\}$ NMR (CH_2Cl_2, 25 °C, 40.5 MHz) δ= -3.3 (singlet). Anal. calc. for $C_{16}H_{48}IO_{15}P_5Ru$: C, 22.26; H, 5.60; P, 17.94; I, 14.70. Found: C, 22.05; H, 5.48; P, 18.36; I, 15.20.

In a 100 mL Schlenk tube, $\{CH_3Ru[P(OCH_3)_3]_5\}I$ (0.63 g, 0.73 mmol) was added to 20 mL of THF. To this stirred mixture was added NH_4PF_6 (0.16 g, 1.0 mmol). The reaction was stirred for 12 h at room temperature. The pale yellow suspension was stripped to dryness on the vacuum line and the resultant off-white solid was extracted with CH_2Cl_2 (2 x 10 mL). Vacuum removal of CH_2Cl_2 from the filtered extracts left the desired product, $\{CH_3Ru[P(OCH_3)_3]_5\}PF_6$ (0.55 g, 86%), as a pale yellow solid. Recrystallization from THF produced a white, crystalline solid which suffered no apparent decomposition after several weeks exposure to air. The product was very soluble in CH_2Cl_2, soluble in THF, but insoluble in hexane.

$\{CH_3Ru[P(OCH_3)_3]_5\}PF_6$: mp 222-223.5 °C (dec.); $^{13}C\{^1H\}$ NMR (acetone-d_6, 25 °C, 100.6 MHz) δ -22.6 (multiplet), δ 49.1

(doublet, J_{PC}= 10.0 Hz), δ 52-55 (multiplet); $^{31}P\{^{1}H\}$ NMR (acetone-d_6, 25 °C, 162.0 MHz) δ -1.8 (singlet); $^{31}P\{^{1}H\}$ NMR (CD_2Cl_2, -73 °C, 162.0 MHz) AB_4 spin system, δ_A= -0.9, δ_B= 0.5, J_{AB}= 45.8 Hz, also δ -284.1 (septet, J_{PF}= 712 Hz); mass spectrum (FAB, sulfolane) calculated for $^{102}RuC_{16}H_{48}O_{15}P_5$ (P), *m/e* 737, found, *m/e* 737 (very weak), also *m/e* 723 ($[P-CH_2]^+$), *m/e* 597 ($[P-Me-P(OCH_3)_3]^+$), and *m/e* 613, 489, 365 ($[P-nP(OCH_3)_3]^+$ n=1,2,3). Anal. calc. for $C_{16}H_{48}F_6O_{15}P_6Ru$: C, 21.80; H, 5.49; P, 21.08. Found: C, 22.13; H, 5.27; P, 20.59.

Preparation of $\{HRu[P(OCH_3)_3]_5\}PF_6$. To a stirred solution of $Ru[P(OCH_3)_3]_5$ (0.34 g, 0.47 mmol) in 20 mL THF in a 100 mL Schlenk tube was added NH_4PF_6 (0.24 g, 1.5 mmol). The resultant suspension was stirred for 24 h. The solution was evaporated to dryness on the vacuum line and the white residue extracted with CH_2Cl_2 (3 x 5 mL). The extracts were filtered and stripped to dryness to yield a white solid. Recrystallization of this solid from THF:hexane (50:50, v/v) afforded colourless, microcrystalline plates of $\{HRu[P(OCH_3)_3]_5\}PF_6$: yield 0.36 g (88%); mp 247-249 °C (dec.); ^{1}H NMR (acetone-d_6, 25 °C, 100.1 MHz) δ= 3.68 (multiplet), δ= -9.49 (multiplet); $^{31}P\{^{1}H\}$ NMR ($CDCl_3$, 25°C, 40.5 MHz) AB_4 spin system, δ_A= 2.8, δ_B= 5.7, J_{AB}= 46.3 Hz, also δ -284.3 (septet, J_{PF}= 712 Hz); mass spectrum (FAB, sulfolane) calculated for $^{102}RuC_{15}H_{46}O_{15}P_5$ (P), *m/e* 723, found, *m/e* 723 (strong), also *m/e* 597, 473, 349 ($[P-H_2-nP(OCH_3)_3]^+$ n=1,2,3). Anal. calc. for $C_{15}H_{46}F_6O_{15}P_6Ru$: C, 20.77; H, 5.34; P, 21.43. Found: C, 20.68; H, 5.38; P, 21.09.

Preparation of $\{IRu[P(OCH_3)_3]_5\}I$ and $\{IRu[P(OCH_3)_3]_5\}PF_6$. To a 20 mL hexane solution of $Ru[P(OCH_3)_3]_5$ (0.175 g, 0.243 mmol) in a 100 mL Schlenk tube was added I_2 (0.062 g, 0.243 mmol). The reaction was stirred for 2 h, during which time the iodine dissolved to leave a colourless solution. Removal of solvent under vacuum yielded a pale yellow powder. The solid was washed with hexane (3 x 5 mL) to remove any unreacted $Ru[P(OCH_3)_3]_5$ and recrystallized from toluene:CH_2Cl_2 to give $\{IRu[P(OCH_3)_3]_5\}I$ as a white, microcrystalline solid which decomposed very slowly in air: yield 0.16 g (68%); mp 192.5-193.5 °C; $^{31}P\{^1H\}$ NMR (see below). Anal. calc. for $C_{15}H_{45}I_2O_{15}P_5Ru$: C, 18.47; H, 4.65; P, 15.88. Found: C, 18.98; H, 4.67; P, 16.47.

To 20 mL of THF in a 100 mL Schlenk tube was added $\{IRu[P(OCH_3)_3]_5\}I$ (0.165 g, 0.184 mmol). To the resultant mixture was added NH_4PF_6 (0.030 g, 0.184 mmol). The reaction mixture was stirred for 14 h. Removal of solvent under vacuum yielded a white residue which was extracted with CH_2Cl_2 (3x5 mL). Insoluble NH_4I and NH_4PF_6 were removed by filtration. Removal of the solvent under vacuum gave a white solid which was recrystallized from THF to yield colourless, microcrystalline plates of $\{IRu[P(OCH_3)_3]_5\}PF_6$. The yield was not measured but appeared >50%.

$\{IRu[P(OCH_3)_3]_5\}PF_6$: mp 212-214 °C (dec.); $^{31}P\{^1H\}$ NMR ($CDCl_3$, 25 °C, 40.5 MHz) AB_4 spin system, δ_A= -13.2, δ_B= -16.1, J_{AB}= 53.6 Hz, also δ -284.3 (septet, J_{PF}= 712 Hz); mass spectrum (FAB, sulfolane) calc. for $^{102}RuC_{15}H_{45}O_{15}P_5$ (P), *m/e* 849, found,

m/e 849 (very weak) also *m/e* 725, 601 ($[P-nP(OCH_3)_3]^+$ n=1,2). Anal. calc. for $C_{15}H_{45}F_6IO_{15}P_6Ru$: C, 18.14; H, 4.57; P, 18.71; I, 12.78. Found: C, 17.50; H, 4.45; P, 18.14; I, 10.99.

Preparation of $\{BrRu[P(OCH_3)_3]_5\}Br$ and $\{BrRu[P(OCH_3)_3]_5\}PF_6$. In a 100 mL Schlenk tube were mixed $Ru[P(OCH_3)_3]_5$ (0.260 g, 0.360 mmol) and hexane (20 mL). To the resultant, colourless solution was added Br_2 (0.015 mL, 0.362 mmol), which caused the immediate formation of a yellow precipitate. The solution was stirred for 20 min and the solvent decanted away from the fine, yellow powder. The solid was washed with hexane (3x5 mL) (to remove any unreacted $Ru[P(OCH_3)_3]_5$) and dried on the vacuum line; recrystallization was impractical. The product, $\{BrRu[P(OCH_3)_3]_5\}Br$, decomposed very slowly in air: yield 0.255 g (96%); mp 175.5-177 °C (dec.); $^{31}P\{^1H\}$ NMR (see below). Anal. calc. for $C_{15}H_{45}Br_2O_{15}P_5Ru$: C, 20.44; H, 5.15; P, 17.57, Br, 18.13. Found: C, 19.58; H, 4.67; P, 17.57; Br, 18.95.

A suspension of $\{BrRu[P(OCH_3)_3]_5\}Br$ (0.240 g, 0.272 mmol) in 20 mL THF was placed in a 100 mL Schlenk tube. To this mixture was added NH_4PF_6 (0.050 g, 0.307 mmol). The reaction was stirred for 15 h. Removal of the solvent under vacuum left a white residue which was extracted with CH_2Cl_2 (3x5 mL). The filtered extracts were stripped on the vacuum line and the resultant white solid was recrystallized from THF to yield colourless, microcrystalline plates. The yield of $\{BrRu[P(OCH_3)_3]_5\}PF_6$ was not measured but appeared >50%.

{$BrRu[P(OCH_3)_3]_5$}PF_6: mp 214-217 °C (dec.); ^1H NMR ($CDCl_3$, 25 °C, 100.0 MHz) δ 3.77 (multiplet); $^{31}P\{^1H\}$ NMR ($CDCl_3$, 25 °C, 40.5 MHz) AB_4 spin system, δ_A -8.5, δ_B -15.7, J_{AB}= 56.0 Hz, also δ -284.3 (septet, J_{PF}= 712 Hz); mass spectrum (FAB, sulfolane) calc. for $^{102}Ru^{81}BrC_{15}H_{45}O_{15}P_5$ (P), *m/e* 803, no parent ion observed but *m/e* 679, 555, 350 ($[P-nP(OCH_3)_3]^+$ n=1,2,3) and *m/e* 598 ($[P-Br-P(OCH_3)_3]^+$). Characteristic mass spectral patterns due to ^{79}Br and ^{81}Br were observed. Anal. calc. for $C_{15}H_{45}BrF_6O_{15}P_6Ru$: C, 19.04; H, 4.79; P, 19.64; Br, 8.44. Found: C, 18.64; H, 4.77; P, 19.28; Br, 7.40.

Preparation of {$ClRu[P(OCH_3)_3]_5$}PF_6. A solution of $Ru[P(OCH_3)_3]_5$ (0.75 g, 1.04 mmol) in 15 mL hexane was prepared in a 100 mL Schlenk tube. With vigorous stirring, a thin stream of Cl_2 gas was passed over (not in) the solution quickly. A pale yellow precipitate formed immediately. This process was repeated until no more precipitate formation was observed. After 15 min stirring, the solution was decanted away from the solid, which was washed with hexane (5x5 mL) and dried on the vacuum line. The resultant, pale pink powder was extremely sensitive to the air, decomposing to a colourless liquid on a few seconds exposure. The yield (which assumed the product to be {$ClRu[P(OCH_3)_3]_5$}Cl) was 0.79 g (96%).

A 100 mL Schlenk tube was charged with {$ClRu[P(OCH_3)_3]_5$}Cl (0.76 g, 0.90 mmol), NH_4PF_6 (0.20 g, 1.20 mmol), and THF (15 mL). The reaction mixture was stirred for 15 h. Vacuum removal of the volatiles left a white solid which was extracted with

CH_2Cl_2 (3x5 mL). The filtered extracts were stripped on the vacuum line to yield a white solid, which was recrystallized from THF to afford colourless, microcrystalline plates of $\{ClRu[P(OCH_3)_3]_5\}PF_6$. The yield was not measured but appeared >50%. The product slowly decomposed in air over the course of two weeks.

$\{ClRu[P(OCH_3)_3]_5\}PF_6$: mp 204-208 °C (dec.); $^{31}P\{^1H\}$ NMR ($CDCl_3$, 25 °C, 40.5 MHz) AB_4 spin system, δ_A -8.0, δ_B -15.0, J_{AB}= 56.8 Hz, also δ -284.3 (septet, J_{PF}= 712 Hz). Anal. calc. for $C_{15}H_{45}ClF_6O_{15}P_6Ru$: C, 19.98; H, 5.03. Found: C, 20.04; H, 5.04.

Attempted Preparation of $\{C_2H_5Ru[P(OCH_3)_3]_5\}PF_6$. A glass Carius tube was charged with $Ru[P(OCH_3)_3]_5$ (0.47 g, 0.65 mmol), C_2H_5I (1.5 mL, excess), and hexane (20 mL). The solution was degassed three times and stirred for 3 days at 50 °C. A white precipitate slowly formed during this period. The reaction mixture was transferred to a Schlenk tube and the supernatant solution removed. Hexane washing (3x5 mL) left a pale yellow powder which was extremely air sensitive. The ^1H and $^{31}P\{^1H\}$ NMR spectra of this solid were measured. The balance of the product was isolated as the PF_6 salt by metathesis with NH_4PF_6 as described previously. Final purification was by recrystallization from THF at -15 °C, yielding a colourless, microcrystalline solid.

The $^{31}P\{^1H\}$ NMR spectrum ($CDCl_3$, 25 °C, 40.5 MHz) of this product revealed 2 sets of resonances. One, due to an AB_4 spin system, was identified as $\{IRu[P(OCH_3)_3]_5\}PF_6$. The other set of resonances appeared as a very narrow multiplet, similar to that observed for $\{CH_3Ru[P(OCH_3)_3]_5\}I$ at low temperatures [5]. This was consistent with a tightly coupled AB_4 multiplet with δ_A and δ_B both within the range of -2.6 to -3.2 ppm and J_{AB} ~45-60 Hz. The two sets of resonances were of approximately the same intensity.

The ^1H NMR spectrum ($CDCl_3$, 25 °C, 100.0 MHz) of the final product revealed a complex methoxy multiplet with two major peaks (δ 3.77 and 3.68), a broad triplet (δ 1.33, J= 7 Hz), and a multiplet (δ -0.15). The triplet and multiplet had relative integrations of ca. 3:2, respectively.

All the spectroscopic evidence was consistent with the presence of approximately equal amounts of $\{IRu[P(OCH_3)_3]_5\}PF_6$ and $\{C_2H_5Ru[P(OCH_3)_3]_5\}PF_6$. The elemental analysis was in accord with this result: Calc: C, 20.47; H, 5.09. Found: C, 20.55; H, 4.97. The ^1H and $^{31}P\{^1H\}$ NMR spectra were identical before and after NH_4PF_6 metathesis.

The Reaction of $Ru[P(OCH_3)_3]_5$ and C_3H_5Br. Stirred hexane solutions of $Ru[P(OCH_3)_3]_5$ and allyl bromide slowly yielded brilliant white precipitates over the course of several days at room temperature. The distribution of products appeared dependent upon the allyl bromide:$Ru[P(OCH_3)_3]_5$ ratio and the

reaction time. With a twelvefold excess of C_3H_5Br and a three day reaction period, the isolated solid was identified as a mixture of $\{HRu[P(OCH_3)_3]_5\}X$ and $\{BrRu[P(OCH_3)_3]_5\}X$ (~1:5 respectively) by $^{31}P\{^1H\}$ NMR spectroscopy (X assumed to be Br). At an allyl bromide:$Ru[P(OCH_3)_3]_5$ ratio of 100:1 and reaction time of 6 days, the isolated product (after NH_4PF_6 metathesis) was shown to be exclusively $\{BrRu[P(OCH_3)_3]_5\}PF_6$ by ^1H and $^{31}P\{^1H\}$ NMR techniques.

Attempted Preparation of $\{C_6H_5CH_2Ru[P(OCH_3)_3]_5\}PF_6$. A hexane (10 mL) solution of $C_6H_5CH_2Br$ (1 mL, excess) was added dropwise to a stirred solution of $Ru[P(OCH_3)_3]_5$ (0.20 g, 0.28 mmol) in hexane (25 mL). Over the course of 24 h, a white precipitate formed. The colourless supernatant solution was removed and the solid dissolved in THF (15 mL). To this stirred solution was added NH_4PF_6 (0.11 g, 0.7 mmol). After 5 h, the reaction mixture was stripped on the vacuum line. The resultant white solid was extracted with CH_2Cl_2 (3x10 mL). The filtered extracts were again evaporated on the vacuum line to yield a white solid which was recrystallized from THF at -15 °C. The resultant colourless, microcrystalline solid (0.07 g) was identified as $\{BrRu[P(OCH_3)_3]_5\}PF_6$ by ^1H and $^{31}P\{^1H\}$ NMR spectroscopy.

Attempted Preparation of $\{ONRu[P(OCH_3)_3]_5\}PF_6$. A solution of $Ru[P(OCH_3)_3]_5$ (0.200 g, 0.277 mmol) in CH_3CN (20 mL) was prepared. To this stirred solution was added $NOPF_6$ (0.048 g, 0.277 mmol). The reaction solution immediately turned pale brown. After 1 h, the solvent was removed under vacuum to yield

a mixture of white and brown solids. This product was extracted with CH_2Cl_2 (15 mL). The filtered extracts were stripped on the vacuum line to afford a pale brown powder (0.22 g). The $^{31}P\{^1H\}$ NMR spectrum of this solid in CD_2Cl_2 revealed two species. The major product (~80 %) was $\{HRu[P(OCH_3)_3]_5\}PF_6$. In addition, another AB_4 multiplet was present ($\delta_B \approx -15$). Despite several attempts, separation of the two complexes was not achieved.

When the reaction was performed in THF, only $\{HRu[P(OCH_3)_3]_5\}PF_6$ was isolated. Nitrosyl hexafluorophosphate reacted vigorously with pure THF but appeared stable in CH_3CN.

Preparation of $\{HRu[P(OCH_3)_3]_4P(OCH_2)_3CCH_3\}PF_6$. To a stirred solution of $Ru[P(OCH_3)_3]_4P(OCH_2)_3CCH_3$ (0.020 g, 0.027 mmol) in THF (20 mL) was added NH_4PF_6 (0.005 g, 0.03 mmol). After 1 h, the solvent was removed under vacuum to yield a white solid. This was extracted with CH_2Cl_2 (2x10 mL). The filtered extracts were stripped on the vacuum line to give a white solid. This was washed with hexane (2x10 mL) and dried on the vacuum line. The yield of $\{HRu[P(OCH_3)_3]_4P(OCH_2)_3CCH_3\}PF_6$ was 0.021 g (88 %): mp 194-200 °C (dec), ^1H NMR (CD_2Cl_2, 25 °C, 100.0 MHz) δ 4.14 (broad triplet with poorly resolved shoulders, $J \approx 4$ Hz, rel. int.= 6), δ 3.62 (multiplet, rel. int.= 36), δ 0.78, 0.76 (broad overlapping singlets, total rel. int.=3, high field signal ~3 times integral of low field signal), δ centred at -9.2 (complex multiplet, rel. int.= 1). The high field multiplet contained a doublet of quintets at δ -8.72 which was successfully simulated: $J_{trans\,PH} \approx 124.2$ Hz, $J_{cis\,PH} \approx 20.8$ Hz). All of the major remaining

resonances in this multiplet were simulated reasonably accurately based on an AW_2XYZ spin system with δ_A= -9.57 and J_{AW}= 20.2 Hz, J_{AX}= 75.8 Hz, J_{AY}= 19.9 Hz, J_{AZ}= 19.4 Hz J_{WX}= 20 Hz, J_{WY}= 20 Hz, J_{WZ}= 70 Hz, J_{XY}= 20 Hz, J_{XZ}= 70 Hz, J_{YZ}= 200 Hz. The doublet of quintets subspectrum comprised approximately 1/4 of the total integration of the high field multiplet, consistent with the intensity of the two Me signals; $^{31}P\{^1H\}$ NMR (CD_2Cl_2, 25 °C, 40.54 MHz) A complex spectrum between δ 10 and -10 was observed. This multiplet contained resonances due to an AB_4 spin system and these were successfully simulated: δ_A= -8.8, δ_B= 5.6, J_{AB}= 46.0 Hz. This subspectrum comprised ca. 25% of the total intensity of the complete multiplet. The ^{31}P spectrum measured with only the methoxy protons decoupled (i.e. $^{31}P\{OCH_3-^1H\}$) was noticeably broader than when the methoxy and hydride protons were decoupled. Also δ -285.3 (septet, J_{PF}= 710 Hz); mass spectrum (FAB, sulfolane) calculated for $^{102}RuC_{17}H_{46}O_{15}P_5$, *m/e* 747, found *m/e* 747. Anal. calc. for $C_{17}H_{46}F_6O_{15}P_6Ru$: C, 22.91; H, 5.20. Found: C, 23.01; H, 5.16.

The ionic complex was soluble in CH_2Cl_2 but insoluble in hexane and toluene. There was no apparent decomposition of $\{HRu[P(OCH_3)_3]_4P(OCH_2)_3CCH_3\}PF_6$ after two weeks exposure to air.

The Reaction of $Ru[P(OCH_3)_3]_5$ and $AgBF_4$. A solution of $AgBF_4$ (0.120 g, 0.61 mmol) in toluene (15 mL) was prepared. To this was slowly added $Ru[P(OCH_3)_3]_5$ (0.450 g, 0.624 mmol) in toluene (15 mL). An immediate green-brown precipitate was formed. The colourless supernatant was decanted away and the solid washed

with toluene (3x10 mL). The product was extracted with CH_2Cl_2 (3x10 mL) and the extracts filtered. The filter paper was coated with a dull, metallic sludge. Removal of the solvent from the filtrate under vacuum left a yellow-brown solid with some dark impurities. This was again extracted with CH_2Cl_2 (2x10 mL), followed by filtration through Celite. After vacuum removal of the solvent, a yellow-brown solid remained. Further purification was done by slow addition of hexane to CH_2Cl_2 solutions of the solid (performed twice) to give the final product (0.100 g). The following data were obtained from this sample: mp 183-185 °C (dec); ^1H NMR (acetone-d_6, 25 °C, 100.0 MHz) δ 3.95 (multiplet); $^{31}P\{^1H\}$ NMR (CD_2Cl_2, 25 °C, 40.54 MHz) AB_4 spin system, δ_A -4.8, δ_B -16.9, J_{AB}= 60.5 Hz; ^{19}F NMR (CD_2Cl_2, 25 °C, 94.2 MHz, δ relative to external CF_3COOH) δ -75.19 (singlet, rel. int.= 11), δ -75.24 (singlet with fine structure, rel. int.= 4); mass spectrum (FAB, sulfolane) *m/e* 617 (unidentified), *m/e* 598 ($\{Ru[P(OCH_3)_3]_4\}^+$), *m/e* 474 ($\{Ru[P(OCH_3)_3]_3\}^+$). Anal. : C, 19.59; H, 5.07; P, 14.9; Ag, 4.26.

In addition, an X-ray fluorescence analysis indicated that [Ag]/[Ru]~0.2.

CHAPTER 4

Attempted Preparation of $Ru[P(OR)_3]_5$ (R= Et, i-Pr, n-Bu), $Os[P(OCH_3)_3]_5$, and $Ru[P(OCH_2)_3CCH_3]_5$.

4.1 Introduction

The problem introduced in this thesis was twofold. Selected studies concerning the chemistry of $Ru[P(OCH_3)_3]_5$ have been presented in chapters 2 and 3. The second aspect of the problem was the generality of the synthesis of pentakis(trimethyl phosphite)ruthenium(0). This will be the topic of chapter 4.

We have previously reported evidence (IR and $^{31}P\{^1H\}$ NMR spectroscopy) for the step-wise formation of $Ru[P(OCH_3)_3]_x(CO)_{5-x}$ (x= 1-5) during the synthesis of $Ru[P(OCH_3)_3]_5$ [5]. Alternative syntheses for the complexes with x= 1-4 were reported along with the associated IR ν(CO) and $^{31}P\{^1H\}$ NMR data. The $^{31}P\{^1H\}$ NMR spectra of $Ru[P(OCH_3)_3]_x(CO)_{5-x}$ (x=1-5) all exhibited single resonances. We believe that these five complexes are fluxional in solution on the NMR time scale. With this IR and NMR evidence available, the ultraviolet irradiation of $Ru_3(CO)_{12}$ and excess $P(OR)_3$ (R= Et, *i*-Pr, *n*-Bu) in hexane was studied.

4.2 Results and Discussion

For these three reactions, IR (ν(CO)) and $^{31}P\{^{1}H\}$ NMR spectroscopy revealed the step-wise formation of $Ru[P(OR)_3]_x(CO)_{5-x}$ (x= 1-4). However, no ^{31}P signals due to the pentasubstituted products were observed. Instead, four complex multiplets (three weak and one strong) grew in intensity as the UV irradiation continued. These multiplets were qualitatively similar to the $^{31}P\{^{1}H\}$ NMR NMR spectra of $CH_3Ru[P(O)(OCH_3)_2](P(OCH_3)_3)_4$ (formed by thermolysis of $Ru[P(OCH_3)_3]_5$ at 100 °C in hexane) and the products from exhaustive UV irradiation of $Ru_3(CO)_{12}$ and excess $P(OCH_3)_3$ in hexane [5]. It appears likely that $Ru[P(OR)_3]_5$ (R= Et, *i*Pr, *n*-Bu), if formed at all, rapidly undergo an isomerization similar to that observed for $Ru[P(OCH_3)_3]_5$.

The reason for this apparent enhanced stability (under the reaction conditions) of the pentakis(trimethyl phosphite) complex versus those with the other alkyl phosphites is unclear. An explanation based on steric arguments may be advanced. The larger cone angles of $P(OR)_3$ (R= Et, *i*-Pr, *n*-Bu) versus $P(OCH_3)_3$ [10,51] would lead to an increased steric pressure for ligand dissociation from $Ru[P(OR)_3]_5$. We have shown [5] that the isomerization (with methyl migration) of $Ru[P(OCH_3)_3]_5$ to $CH_3Ru[P(O)(OCH_3)_2](P(OCH_3)_3)_4$ likely occurs via the 16 electron species $Ru[P(OCH_3)_3]_4$, arising from the equilibrium

$$Ru[P(OCH_3)_3]_5 \rightleftharpoons Ru[P(OCH_3)_3]_4 + P(OCH_3)_3$$

The shift of this equilibrium to the right for phosphites of larger cone angle than $P(OCH_3)_3$ could explain the apparent ease with which the complexes $Ru[P(OR)_3]_5$ (R= Et, *i*-Pr, *n*-Bu) undergo rearrangement, relative to $Ru[P(OCH_3)_3]_5$. For the case of $P(OCH(CH_3)_2)_3$ (cone angle $\simeq$ 130° [11,51]), one might postulate that the pentasubstituted product is not formed to any appreciable extent in solution. Loss of CO from $Ru[P(OCH(CH_3)_2)_3]_4CO$ would give $Ru[P(OCH(CH_3)_2)_3]_4$, which would be sterically inhibited from coordinating the fifth bulky $P(OCH(CH_3)_2)_3$ ligand.

The available data for stability of the free ligands is not consistent with the trend found here for the coordinated ligands: it has been shown that $P(OC_2H_5)_3$ is thermally more stable than $P(OR)_3$ (R=Me, *i*-Pr) [91].

The ultraviolet irradiation of $Os(CO)_5$ and excess $P(OCH_3)_3$ in hexane was studied. The IR (ν(CO)) and $^{31}P\{^1H\}$ NMR evidence were very similar to that observed for the corresponding reactions of $Ru_3(CO)_{12}$ with $P(OR)_3$ (R= Et, *i*-Pr, *n*-Bu): the step-wise formation of $Os[P(OCH_3)_3]_x(CO)_{5-x}$ (x= 1-4) was indicated. However, the $^{31}P\{^1H\}$ NMR spectrum revealed a weak singlet in the region expected for $Os[P(OCH_3)_3]_5$. The intensity of this resonance did not increase as the irradiation continued. Instead, a set of four complex multiplets grew in intensity.

Similar behaviour was observed for the photolysis of $Os[P(OCH_3)_3]_x(CO)_{5-x}$ (x= 1 or 2) with excess $P(OCH_3)_3$ in hexane.

The weak singlet just described is assigned to $Os[P(OCH_3)_3]_5$ on the basis of the literature data for this complex. Given the temperature dependence of ^{31}P chemical shifts and the different solvents used, the literature value of the chemical shift for $Os[P(OCH_3)_3]_5$ ($\delta \simeq -11$ in toluene-d_8/$CClF_2H$) [6] agrees well with the value found here: δ -12.4 (hexane, 25 °C).

The difference between the reactions of $Ru_3(CO)_{12}$ and $Os(CO)_5$ with excess $P(OCH_3)_3$ is noted. When $Ru_3(CO)_{12}$ and $P(OCH_3)_3$ are photolyzed in hexane, $Ru[P(OCH_3)_3]_5$ is the major product after 48h; continued photolysis causes slow conversion of the penta(phosphite) species to other products. The corresponding reaction between $Os(CO)_5$ and $P(OCH_3)_3$ has a different outcome: the concentration of $Os[P(OCH_3)_3]_5$ never becomes appreciable. The $^{31}P\{^1H\}$ NMR evidence suggests that $Os[P(OCH_3)_3]_5$ undergoes an isomerization similar to that observed for $Ru[P(OCH_3)_3]_5$ [5]. A steric argument based on the formation of the coordinatively unsaturated $M[P(OCH_3)_3]_4$ species (M= Ru, Os) cannot rationalize the different characteristics of the two reactions. For d^8 complexes within group VIII, it is known that the tendency to undergo oxidative-addition reactions increases both down the periodic table and to the left [91a]. Complexes containing Os(0) are thus relatively activated towards oxidative-addition; the CH_3 migration in $Ru[P(OCH_3)_3]_5$ (giving $CH_3Ru[P(O)(OCH_3)_2](P(OCH_3)_3)_4$) is an example of such a reaction

[5]. This argument is thus in accord with the experimental results.

The reaction of $Ru(CO)_5$ with the caged phosphite $P(OCH_2)_3CCH_3$ was also examined. It was hoped that the penta(phosphite) derivative, if isolable, would have favourable recrystallization characteristics and allow growth of a crystal suitable for analysis by x-ray diffraction. The room temperature reaction of $Ru(CO)_5$ and excess $P(OCH_2)_3CCH_3$ in hexane gave a near quantitative yield (by IR spectroscopy) of $Ru[P(OCH_2)_3CCH_3](CO)_4$ in solution (ν(CO) (hexane) 2092 (vw), 2076 (m), 2015 (sh), 2007 (m), 1976 (s) cm^{-1} [58,92]). Heating this complex in the presence of excess $P(OCH_2)_3CCH_3$ (in hexane) for 3 h at 100 °C gave a pale yellow solid which was identified as $Ru[P(OCH_2)_3CCH_3]_2(CO)_3$ (ν(CO) (CH_2Cl_2) 1938 cm^{-1}). This assignment was based upon the single ν(CO) band expected for a diaxially substituted derivative of $Ru(CO)_5$ (i.e. with D_{3h} symmetry) [93]. The IR spectrum (carbonyl region) of $Ru[P(OCH_3)_3]_2(CO)_3$ in hexane revealed two bands (1933 (s), 1923 (s) cm^{-1}); the caged phosphite ligand is incapable of exhibiting the asymmetry observed for $Ru[P(OCH_3)_3](CO)_4$ [58] (and presumably $Ru[P(OCH_3)_3]_2(CO)_3$ [5]). This yellow solid and excess $P(OCH_2)_3CCH_3$ were heated in toluene to 100 °C for 16 h. The resultant tan solid featured two IR ν(CO) absorptions in CH_2Cl_2 (1961 (m), 1907 (s) cm^{-1}) and was identified as $Ru[P(OCH_2)_3CCH_3]_3(CO)_2$. This was based on the similarity to the IR ν(CO) data to that of $Ru[P(OCH_3)_3]_3(CO)_2$ (hexane: 1948 (m),

1894 (s) cm^{-1}) [5]. This complex was only sparingly soluble in methylene chloride. Further exhaustive heating of $Ru[P(OCH_2)_3CCH_3]_3(CO)_2$ and excess $P(OCH_2)_3CCH_3$, in either toluene or CH_2Cl_2, was unproductive.

The photolysis of $Ru[P(OCH_2)_3CCH_3](CO)_4$ and excess $P(OCH_2)_3CCH_3$ was also examined. The UV irradiation of these two reagents in hexane for 24 h gave off-white crystals of $Ru[P(OCH_2)_3CCH_3]_2(CO)_3$. These crystals and excess $P(OCH_2)_3CCH_3$ were subsequently photolyzed in toluene. A slow conversion to the tris(phosphite) species was observed over the course of 72 h. The irradiation of $Ru[P(OCH_2)_3CCH_3]_3(CO)_2$ and excess $P(OCH_2)_3CCH_3$ in CH_2Cl_2 for 6h resulted in a colourless solution. Infrared and $^{31}P\{^1H\}$ NMR spectroscopy indicated the presence of several products, none of which appeared to be $Ru[P(OCH_2)_3CCH_3]_4CO$ or $Ru[P(OCH_2)_3CCH_3]_5$.

The failure to isolate the penta(phosphite) product appeared partially due to the extreme insolubility of the mixed $P(OCH_2)_3CCH_3$-CO derivatives. Further reaction of $Ru[P(OCH_2)_3CCH_3]_3(CO)_2$ was likely inhibited by its near insolubility in toluene. The mixture of products derived from the photolysis of $Ru[P(OCH_2)_3CCH_3]_3(CO)_2$ and $P(OCH_2)_3CCH_3$ in CH_2Cl_2 was not suprising: this result has been observed in the UV irradiation of other Ru-phosphite complexes in CH_2Cl_2 [94] and is thought to be due to free radical chlorination.

The $^{31}P\{^{1}H\}$ chemical shifts of the various species observed in the UV irradiations of $Ru_3(CO)_{12}$ with $P(OR)_3$ (R= Me, Et, *i*-Pr, *n*-Bu) and $Os(CO)_5$ with $P(OCH_3)_3$ (in hexane) are shown in table 4.1. The chemical shifts of the free ligands $P(OR)_3$ (R= Me, Et, *i*-Pr, *n*-Bu) are δ 0, -2.6, -2.8, -2.2, respectively [94]. For the Ru complexes, the chemical shift of the phosphite moves downfield upon coordination; this is reversed for the case of osmium. This result is virtually general for the Ru and Os complexes studied in this thesis (some exceptions are several cationic Ru species discussed in chapter 3). Results consistent with this observation have been found for similar systems: an upfield shift of the ^{31}P resonances for $M(CO)_5L$ (M= Cr, Mo, W; L= various phosphines) and several related series was observed upon descending the periodic table [88,95].

Some general trends are evident from the data in table 4.1. For all the series of complexes, the ^{31}P chemical shifts move downfield as the degree of phosphite substitution increases from x= 1 to x= 3. With the substitution of the fourth CO group for a $P(OR)_3$ ligand, the chemical shift is either upfield or unchanged. For the two series of complexes where the penta(phosphite) member was observed, the ^{31}P chemical shift continues to move upfield upon coordination of the fifth $P(OCH_3)_3$ ligand.

These changes in the ^{31}P chemical shifts with increased phosphite substitution for the five series of complexes in table 4.1 are clearly not random; a rationale for this behaviour,

Compound (M/ligand)	Chemical Shift (ppm)[a] x= 1	x= 2	x= 3	x= 4	x= 5
$Ru/P(OCH_3)_3$	21.5	29.6	31.4	29.2	26.0
$Ru/P(OC_2H_5)_3$	13.7	23.1	25.0	23.3	
$Ru/P(OCH(CH_3)_2)_3$	9.7	20.1	21.2	21.2	
$Ru/P(O\text{-}n\text{-}C_4H_9)_3$	13.5	23.0	25.0	23.4	
$Os/P(OCH_3)_3$	-23.3	-16.5	-9.9	-9.8	-12.4

Table 4.1 $^{31}P\{^1H\}$ chemical shifts for some of the complexes $M[P(OR)_3]_x(CO)_{5-x}$ (M= Ru Os; R= Me, Et *i*-Pr, *n*-Bu). [a]δ values are for the complex in hexane plus an ~tenfold excess of ligand.

however, is not apparent. The theory of ^{31}P chemical shifts is poorly understood [89,90]. Several theoretical studies based on the free phosphine and phosphite ligands have been undertaken. These implicated intraligand bond angles, ionic and double bond character, and hybridization as important determinants for ^{31}P chemical shifts. Up to 1978, there had been no reported calculations of ^{31}P shifts for coordinated trivalent phosphorus [89].

We have previously shown that an explanation for the behaviour shown in table 4.1, based on the fourth and fifth phosphite ligands occupying equatorial sites of a trigonal bipyramid, was inconsistent with other ^{31}P NMR data [5]. X-ray and low temperature $^{31}P\{^{1}H\}$ NMR data indicate that $Ru[P(OCH_3)_3]_x(CO)_{5-x}$ (x= 1,2,5) exhibit trigonal bipyramidal geometry about the central metal [5,6,58,96]. However, the assumption that the tris- and tetrakis(trimethyl phosphite) members (and the corresponding complexes from table 4.1) also have this structure is not totally justified. In fact, the large steric requirements of a $P(OR)_3$ ligand (relative to CO) suggests that deviation from trigonal bipyramidal geometry for $Ru[P(OR)_3]_x(CO)_{5-x}$ (x= 3,4) would be a reasonable expectation. The X-ray crystal structure results for $Ru[P(OCH_3)_3]_4P(OCH_2)_3CCH_3$ support this view (see chapter 2). The consequent changes in bond angles and molecular orbital overlap, relative to the trigonal bipyramidal case, could be the cause of the trends in ^{31}P chemical shifts shown in table 4.1. A more satisfying explanation awaits advances in the theory of ^{31}P shielding constants for coordinated phosphorus ligands.

The results of this chapter may be summarized as follows. The ultraviolet irradiation of $Ru_3(CO)_{12}$ and excess $P(OR)_3$ (R= Et, *i*-Pr, *n*-Bu) in hexane did not produce $Ru[P(OR)_3]_5$. There was evidence (IR (ν(CO)) and $^{31}P\{^{1}H\}$ NMR), however, for the step-wise formation of $Ru[P(OR)_3]_x(CO)_{5-x}$ (x= 1-4). Similar results were observed for the UV irradiation of $Os(CO)_5$ and

excess $P(OCH_3)_3$ in hexane; in this case, however, there was some evidence ($^{31}P\{^1H\}$ NMR) for the formation of $Os[P(OCH_3)_3]_5$ in small amounts. In both the Ru and Os cases, the $^{31}P\{^1H\}$ NMR results suggested that the ultimate products were rigid, six-coordinate species arising via alkyl migration from ligand to metal. Both the thermal and photolytic activation of $Ru(CO)_5$ in the presence of excess $P(OCH_2)_3CCH_3$ were examined. The anticipated penta(phosphite) product was not formed although there was strong evidence (IR ν(CO) spectroscopy) for the formation of $Ru[P(OCH_2)_3CCH_3]_x(CO)_{5-x}$ (x= 1,2,3). The preparation of $Ru[P(OCH_3)_3]_5$ from the UV irradiation of $Ru_3(CO)_{12}$ and excess $P(OCH_3)_3$ in hexane did not appear to be a general route to $M[P(OR)_3]_5$ (M= Ru, Os; R= alkyl) complexes.

4.3 Experimental

Attempted Preparation of $Ru[P(OCH_2)_3CCH_3]_5$. To a stirred solution of $Ru(CO)_5$ (0.57 mmol) in hexane (20 mL) was added $P(OCH_2)_3CCH_3$ (4.8 g, excess). The mixture was stirred at room temperature for 22 h. An IR spectrum (carbonyl region) of the very pale yellow solution showed complete conversion of the starting material to $Ru[P(OCH_2)_3CCH_3](CO)_4$ (2092 (vw), 2076 (m), 2015 (sh), 2007 (m), 1976 (s) cm^{-1}) [58,92].

The reaction mixture was split into two equal portions, each transferred to a glass Carius tube. Both solutions were degassed three times.

One tube was heated at 100 °C for 3 h. The tube contained a pale yellow solid under a colourless solution. The latter exhibited virtually no ν(CO) absorptions in the IR spectrum while the solid (in CH_2Cl_2) featured a single infrared band in the carbonyl region (1938 cm^{-1}). The solid was identified as $Ru[P(OCH_2)_3CCH_3]_2(CO)_3$ by analogy to the IR results for $Ru[P(OCH_3)_3]_2(CO)_3$ [5].

The bis(phosphite) complex and excess $P(OCH_2)_3CCH_3$ were subsequently heated for 16 h at 100 °C in a separate Carius tube, using toluene as a solvent. The tube contained a pale brown, supernatant solution over a tan solid. An IR spectrum (CH_2Cl_2) of the solid showed two ν(CO) absorptions (1961 (m), 1907 (s) cm^{-1}) which indicated the product was probably $Ru[P(OCH_2)_3CCH_3]_3(CO)_2$ [5].

Further heating of the tris(phosphite) complex and excess $P(OCH_2)_3CCH_3$ in either CH_2Cl_2 or toluene was unproductive.

The second portion of the original $Ru[P(OCH_2)_3CCH_3](CO)_4$ solution was irradiated with ultraviolet light for 24 h. The resultant white crystals were shown to be the bis(phosphite) complex by IR spectroscopy (CH_2Cl_2). This precipitate was subsequently irradiated in the presence of excess $P(OCH_2)_3CCH_3$, in a separate Carius tube, using toluene as a solvent. A slow conversion to the tris(phosphite) species, over the course of 72 h, was observed. Further UV irradiation was unproductive. Photolysis of $Ru[P(OCH_2)_3CCH_3]_3(CO)_2$ and excess $P(OCH_2)_3CCH_3$ in

CH_2Cl_2 for 6 h resulted ir a colourless solution. Infrared and $^{31}P\{^1H\}$ NMR spectroscopy indicated the presence of several products, none of which appeared to be $Ru[P(OCH_2)_3CCH_3]_4CO$ or $Ru[P(OCH_2)_3CCH_3]_5$.

$^{31}P\{^1H\}$ NMR Studies: Reaction of $Ru_3(CO)_{12}$ with $P(OR)_3$ (R= Et, i-Pr, n-Bu). The previously described NMR tubes were charged with $Ru_3(CO)_{12}$ and the ligand (~1:10) in hexane. After degassing, the tubes were irradiated with UV light. The reactions were monitored by IR (ν(CO)) and $^{31}P\{^1H\}$ NMR spectroscopy; the results are given in the text.

$^{31}P\{^1H\}$ NMR Studies: Reaction of $Os(CO)_5$ and $Os[P(OCH_3)_3]_x(CO)_{5-x}$ (x= 1,2) with $P(OCH_3)_3$. These were performed in a manner analogous to that just described and the results are given in the text.

CHAPTER 5

Phosphite Derivatives of Osmium. Synthesis and Characterization. X-Ray Structure of $Os_3[P(OCH_3)_3]_6(CO)_6$.

5.1 Introduction

As discussed in Chapter 1, this thesis was partly concerned with the generality of the method used for the synthesis of $Ru[P(OCH_3)_3]_5$. An examination of the reaction of $Fe(CO)_5$ and $Os_3(CO)_{12}$ with $P(OCH_3)_3$ was proposed. The UV irradiation of $Fe(CO)_5$ and $P(OCH_3)_3$ in hexane gave a brown oil. The $^{31}P\{^1H\}$ NMR spectrum of this oil revealed several broad resonances, likely due to paramagnetic impurities. This was unfortunate, as $^{31}P\{^1H\}$ NMR spectroscopy was the main structural tool used in this study. In addition, $Fe[P(OCH_3)_3]_5$ has been previously prepared (by an alternate route) and studied [26]. It was therefore decided not to pursue this avenue of research.

The results regarding the reaction of $Os_3(CO)_{12}$ and $P(OCH_3)_3$, while not paralleling those for the Ru case, were interesting in their own right. These results are the topics of Chapters 5 and 6. It would seem appropriate, then, to briefly survey the literature concerning selected complexes of osmium with group V donor ligands, in particular those also containing carbonyl ligands.

The complex $Os[P(OCH_3)_3](CO)_4$ has been mentioned briefly [97], although no characterization data was presented. A

literature search revealed no further mention of this complex. The disubstituted $Os[P(OCH_3)_3]_2(CO)_3$ has been reported [98] and the IR $\nu(CO)$ data presented, but again no further reference to this complex has appeared in the literature. The two previously mentioned complexes were isolated as side products of synthetic routes focused in other directions. The binary, osmium-phosphite complex $Os[P(OCH_3)_3]_5$ [6] has been discussed in chapter 2. The tri- and tetrasubstituted phosphite complexes of the parent $Os(CO)_5$ have not been reported.

A considerable number of phosphite, phosphine, and arsine derivatives of $Os_3(CO)_{12}$ have been described in the literature. The monosubstituted triosmium complexes $Os_3L(CO)_{11}$ (L= PPh_3, $AsPh_3$, $PMePh_2$, PMe_2Ph, PEt_2Ph, PEt_3, $P(OCH_3)_3$) have been reported [99-105]. Triosmium derivatives of the type $Os_3L_2(CO)_{10}$ (L= PPh_3, PPh_2Me, PMe_2Ph, PEt_3, PEt_2Ph, PMe_3, $P(OCH_3)_3$) [99,100,102-104,106] have been described in the literature, as have trisubstituted species such as $Os_3L_3(CO)_9$ (L= PPh_3, $PMePh_2$, PEt_3, $PPhEt_2$, $P(p\text{-}MeC_6H_4)_3$, PMe_3) [99,100,102-104]. The bis(phosphite) complex, $Os_3[P(OCH_3)_3]_2(CO)_{10}$, has been briefly mentioned in a communication [106] but the promised characterization and structural data have not subsequently appeared in the literature. We have prepared this complex and the previously unknown $Os_3[P(OCH_3)_3]_3(CO)_9$; these results form part of this thesis.

Several major routes have been utilized in the preparation of the three series of complexes $Os_3L_x(CO)_{12-x}$ (x= 1,2,3). These

include reflux of $Os_3(CO)_{12}$ and the appropriate ligand in aromatic solvents [99,100,102,104], displacement of NCMe by L from $Os_3(NCMe)_x(CO)_{12-x}$ (x=1,2) [101,105,106], and radical ion-initiated cleavage of an osmium-osmium bond in $Os_3(CO)_{12}$ followed by substitution and bond reformation [103].

The spectroscopic evidence was consistent with the phosphorus ligands being attached to different Os atoms for all the previously discussed di- and trisubstituted triosmium complexes. There has also been a report concerning mixed derivatives of the type 1,2-$[Os_3LL'(CO)_{10}]$, although only the example where L,L'= $P(OCH_3)_3$, P(p-tolyl) was discussed in detail [106]. For this complex, L and L' were also on different Os atoms. A very recent publication gave details of 1,2,3-$[Os_3L_2[P(OCH_3)_3](CO)_9]$ (L= PPh_3, PMe_2Ph), where the three phosphorus ligands were bound to unique osmium atoms [107]. Another recent report featured new isomers of $Os_3[PMe_2Ph]_x(CO)_{12-x}$ (x= 2,3) [108]; both 1,1-$\{Os_3[PMe_2Ph]_2(CO)_{10}\}$ and 1,1,2-$\{Os_3[PMe_2Ph]_3(CO)_9\}$ were prepared.

All of the spectroscopic and structural data currently available suggests that phosphorus ligands exclusively adopt equatorial positions in these substituted derivatives of $Os_3(CO)_{12}$. X-ray crystal structures of $Os_3[P(OCH_3)_3](CO)_{11}$ [109] and the related ruthenium complexes $Ru_3[P(C_6H_{11})_3](CO)_{11}$, $Ru_3[P(OCH_3)_3]_2(CO)_{10}$, and $Ru_3[PMe_3]_3(CO)_9$ [110] all show that the group 5 ligands occupy equatorial sites in the solid state.

The low temperature ^{13}C and ^{31}P NMR spectra for $Os_3[PEt_3]_x(CO)_{12-x}$ [111], $Os_3[PMe_2Ph]_x(CO)_{12-x}$ (x= 2,3) [107,108], and 1,2,3-$[Os_3[P(OCH_3)_3]L_2(CO)_9]$ (L= PPh_3, PMe_2Ph) [107] are all consistent with the phosphorus ligands occupying equatorial sites in the slow exchange limit in solution. Our own work is in complete agreement with these results [112].

To our knowledge, there have been no literature reports of substituted $Os_3(CO)_{12}$ derivatives containing more than three group 5 ligands, except for our very recent report [112]. Several complexes of the type $Os_3[L\text{-}L]_3(CO)_6$, where L-L is a bidentate, group 5 donor ligand such as $Ph_2PCH_2CH_2PPh_2$, have been prepared [113]. There has also been a report of $Os_3[L\text{-}L]_2(CO)_8$ and $Os_3[L\text{-}L](CO)_{10}$, where L-L are fluorinated, bidentate, group 5 ligands [114]. Again, the available evidence suggested the donor atoms were in the equatorial plane. A very small number of tetrasubstituted derivatives of $Ru_3(CO)_{12}$ such as $Ru_3L_4(CO)_8$ (L= PMe_3; $PPh(OMe)_2$) have been prepared [115,116,117].

In this chapter, the synthesis and characterization of the complexes $Os_3[P(OCH_3)_3]_x(CO)_{12-x}$ (x= 1-6) and related compounds are discussed. The structure and stereochemical nonrigidity of these compounds in solution, as deduced from their multinuclear variable temperature NMR behaviour, are presented in the following chapter.

5.2 Synthesis

The ultraviolet irradiation of $Os_3(CO)_{12}$ and $P(OCH_3)_3$ in hexane did not yield the anticipated $Os[P(OCH_3)_3]_5$. Prolonged photolysis had very little effect, and the bulk of the dodecacarbonyltriosmium was recovered unchanged [118].

In an effort to cause osmium-osmium bond scission and subsequent phosphite substitution, $Os_3(CO)_{12}$ and excess $P(OCH_3)_3$ in hexane were reacted thermally. The nature and distribution of products from this reaction was critically dependent upon the temperature. Heating at 115 °C for one week produced a golden yellow solution, which was shown by IR spectroscopy to contain $Os[P(OCH_3)_3](CO)_4$, $Os[P(OCH_3)_3]_2(CO)_3$, and smaller amounts of the complexes $Os_3[P(OCH_3)_3]_x(CO)_{12-x}$ (x= 2-5). The mono- and disubstituted monomers were separated by fractional sublimation; both the resultant white solids were very soluble in polar and nonpolar solvents.

The ultraviolet irradiation of either the mono- or bis(phosphite) complex in the presence of excess $P(OCH_3)_3$ gave disappointing results. The reaction was monitored by $^{31}P\{^1H\}$ NMR spectroscopy, which clearly indicated the stepwise formation of $Os[P(OCH_3)_3]_x(CO)_{5-x}$ (x= 2,3,4). A very weak signal, tentatively identified as $Os[P(OCH_3)_3]_5$ from $^{31}P\{^1H\}$ NMR literature data [6], was observed but did not grow in intensity. Instead, a set of 4 complex multiplets were noted; these increased in height as the irradiation proceeded. The latter behaviour is similar to

that observed when $Ru[P(OCH_3)_3]_5$ was heated [4,5] or photolyzed [94]. The evidence suggests that, as $Os[P(OCH_3)_3]_5$ is formed, it quickly undergoes an intramolecular rearrangement to a six coordinate, rigid species. The photolysis of $Os(CO)_5$ and excess $P(OCH_3)_3$ in hexane produced results identical to those just described [118]. The experimental data for and a more comprehensive discussion of the series $Os[P(OCH_3)_3]_x(CO)_{5-x}$ were presented in chapter 4.

By far the most extensive chemistry derived from the $Os_3(CO)_{12}/P(OCH_3)_3$ system was that associated with the substitution of the carbonyl ligands from the parent by trimethyl phosphite. When $Os_3(CO)_{12}$ and $P(OCH_3)_3$ (1:2 mole ratio) were heated at 125 °C in hexane for 8 h, a yellow-orange solution resulted. An infrared spectrum (carbonyl region) indicated the presence of $Os_3[P(OCH_3)_3]_2(CO)_{10}$ and $Os_3[P(OCH_3)_3](CO)_{11}$, in an approximately 4:1 molar ratio, in addition to a small amount of $Os_3[P(OCH_3)_3]_3(CO)_9$. The ratio of the mono- and disubstituted products was strongly dependent upon the reaction time; the same reaction after 2 h gave high yields of $Os_3[P(OCH_3)_3](CO)_{11}$. Chromatography allowed separation of the mono- and bis(phosphite) triosmium clusters as yellow and yellow-orange crystals, respectively. Both complexes were soluble in hexane although $Os_3[P(OCH_3)_3]_2(CO)_{10}$ was less so.

Adjustment of the mole ratio of $Os_3(CO)_{12}$ to $P(OCH_3)_3$ and the reaction time caused another product to be favoured. With a threefold excess of the ligand in xylene, a reaction time of 20h

at 125 °C produced an orange-yellow solution. An IR spectrum (carbonyl region) revealed an approximately 2:1 molar ratio of $Os_3[P(OCH_3)_3]_3(CO)_9$ to $Os_3[P(OCH_3)_3]_2(CO)_{10}$, in addition to small amounts of the mono- and tetrasubstituted triosmium complexes. Separation by chromatography resulted in the isolation of $Os_3[P(OCH_3)_3]_3(CO)_9$ as bright yellow-orange crystals; these were only moderately soluble in hexane.

To maximize the yield of triosmium derivatives with higher substitution, excess $P(OCH_3)_3$ and higher temperatures were required. Thus, heating $Os_3(CO)_{12}$ and a large excess of trimethyl phosphite in heptane for 24 h at 145 °C gave an orange solution. Cooling to room temperature overnight resulted in the precipitation of orange crystals. The infrared spectrum (carbonyl region) of these crystals indicated a high percentage of $Os_3[P(OCH_3)_3]_4(CO)_8$ with a minor amount of $Os_3[P(OCH_3)_3]_5(CO)_7$. Separation by chromatography gave $Os_3[P(OCH_3)_3]_4(CO)_8$ as light orange crystals. This tetrakis(phosphite) complex was only sparingly soluble in hexane but extremely soluble in CH_2Cl_2.

To affect penta- and hexasubstitution of $Os_3(CO)_{12}$ by $P(OCH_3)_3$, a combination of thermal and photolytic techniques were required. A heptane solution containing a high percentage of $Os_3[P(OCH_3)_3]_4(CO)_8$ was prepared as described in the previous paragraph. The reaction vessel was heated to dissolve the orange solid. The stirred solution was subsequently irradiated with UV light for 8 h at 25 °C. At this time, the reaction mixture

consisted of an orange solution over an orange solid. Analysis of the solid by IR spectroscopy showed strong carbonyl absorptions corresponding to $Os_3[P(OCH_3)_3]_5(CO)_7$, in addition to weaker signals due to $Os_3[P(OCH_3)_3]_4(CO)_8$ and $Os_3[P(OCH_3)_3]_6(CO)_6$. Chromatographic separation of this mixture allowed isolation of $Os_3[P(OCH_3)_3]_5(CO)_7$ as orange crystals that were virtually insoluble in hexane but quite soluble in CH_2Cl_2.

The hexasubstituted triosmium complex was prepared as described for the pentakis(phosphite) species except with an irradiation period of 48 h. A small $Os_3[P(OCH_3)_3]_5(CO)_7$ impurity was removed by washing the resultant orange solid with hexane/toluene. This produced analytically pure $Os_3[P(OCH_3)_3]_6(CO)_6$ without the use of chromatography. The orange-red crystals were insoluble in hexane, slightly soluble in toluene or acetone, and soluble in CH_2Cl_2.

The ultraviolet irradiation of $Os_3[P(OCH_3)_3]_5(CO)_7$ and excess $P(OC_2H_5)_3$ in hexane produced $Os_3[P(OCH_3)_3]_5\{P(OC_2H_5)_3\}(CO)_6$, although the yield was poor and product isolation was difficult (see chapter 5 experimental section for details). These complications appear to be a function of relative solubilities and the physical process involved in the photolytically induced substitution. The replacement of CO by $P(OCH_3)_3$ in $Os_3[P(OCH_3)_3]_x(CO)_{12-x}$ (x= 4,5) is believed to occur by the sequential dissolving of the reactant, substitution in solution, and precipitation of the substituted product. This assumption is based upon visual

inspection of the reaction mixture with time, IR spectroscopy, and relative solubilities of the series $Os_3[P(OCH_3)_3]_x(CO)_{12-x}$ (x= 4-6) in hexane or heptane. It appears that the decreasing solubility with increasing substitution in these clusters (in heptane) is an important factor in allowing the successful isolation of this series of compounds. The solubility of $Os_3[P(OCH_3)_3]_5\{P(OC_2H_5)_3\}(CO)_6$ in heptane is considerably greater than that of $Os_3[P(OCH_3)_3]_6(CO)_6$. The failure of $Os_3[P(OCH_3)_3]_5\{P(OC_2H_5)_3\}(CO)_6$ to precipitate upon formation is felt to be a key element influencing the low yield of the complex (vide infra).

The marked variability of the product distribution from the thermal reaction of $Os_3(CO)_{12}$ and excess $P(OCH_3)_3$ may be summarized as follows. At 100 °C (in xylene or toluene) the stepwise formation of $Os_3[P(OCH_3)_3]_x(CO)_{12-x}$ (x= 1-3) was observed. The mononuclear products $Os[P(OCH_3)_3]_x(CO)_{5-x}$ (x= 1-2) were favoured when the reaction was carried out at ~125 °C in hexane (small amounts of the substituted trinuclear species were also present). When performed at 140-145 °C (in heptane) the major product was $Os_3[P(OCH_3)_3]_4(CO)_8$, although significant amounts of $Os[P(OCH_3)_3]_2(CO)_3$ were also present. The mechanism(s) by which these thermal substitutions occur remain(s) unclear.

The observation of a mixture of products from the thermal reaction of $M_3(CO)_{12}$ (M= Fe, Ru, Os) with group V donor ligands is not limited to this thesis. The reaction of $Fe_3(CO)_{12}$ with

excess PPh_3 led to $Fe[PPh_3](CO)_4$ and $Fe[PPh_3]_2(CO)_3$ [119] while the same reaction with phosphites $P(OR)_3$ usually gave $Fe_3[P(OR)_3]_3(CO)_9$ [120a]. The reaction of $Ru_3(CO)_{12}$ with $P(OC_6H_5)_3$ or $P(OCH_2)_3CEt$ led to the stepwise formation of $Ru_3L_x(CO)_{12-x}$ (x= 1-3) [121,122]. The same reaction, utilizing $P(OC_2H_5)_3$ or PBu^n_3, gave trisubstituted clusters and $RuL_x(CO)_{12-x}$ (x= 1,2) [122,123]. The distribution of products from the reaction of $Os_3(CO)_{12}$ and $P(n\text{-}C_4H_9)_3$ was found to be dependent upon the temperature and the concentration of $P(n\text{-}C_4H_9)_3$ [124]. High temperatures and low $[P(n\text{-}C_4H_9)_3]$ led exclusively to substitution products (i.e. $Os_3[P(n\text{-}C_4H_9)_3]_x(CO)_{12-x}$; x= 1-3). In contrast, low temperatures and high $[P(n\text{-}C_4H_9)_3]$ gave the mononuclear species $Os[P(n\text{-}C_4H_9)_3](CO)_4$ and $Os[P(n\text{-}C_4H_9)_3]_2(CO)_3$ almost exclusively.

There has been little attempt to rationalize these results in the literature. The thermal reaction of $M_3(CO)_{12}$ (M= Ru, Os) with $P(n\text{-}C_4H_9)_3$ was shown to follow the rate equation

$$k_{obs} = k_1 + k_2[P(n\text{-}C_4H_9)_3]$$

where k_{obs} is the pseudo first order rate constant for loss of the reacting cluster [124]. The k_1 pathway, favoured by high temperatures and low concentration of $P(n\text{-}C_4H_9)_3$, led only to substitution products (i.e. $M_3L_x(CO)_{12-x}$; x= 1-3). Lower temperatures and high $[P(n\text{-}C_4H_9)_3]$ favoured the k_2 route which gave almost exclusively mononuclear products (i.e. $ML(CO)_4$ and $ML_2(CO)_3$). It was originally proposed that the reaction of

$Ru_3(CO)_{12}$ and $P(n\text{-}C_4H_9)_3$ took place by homolytic fission of $Ru_3(CO)_{12}$ to give $Ru(CO)_4$ units [123]. These could then undergo CO exchange with $P(n\text{-}C_4H_9)_3$ and trimerize to generate the required mono- and trinuclear products.

A more satisfying mechanism for the substitution of carbonyls by group V donor ligands in $M_3(CO)_{12}$ (M= Fe, Ru, Os) clusters has recently appeared in the literature. It was proposed that the primary step (although not necessarily rate determining) involved the heterolytic fission of a metal-metal bond; this generates a trimetal unit containing one 18 electron, saturated metal atom and one 16 electron, unsaturated metal atom [120]. The next step involves addition of the incoming ligand, L, to the unsaturated metal centre. All of the required products (both monomeric and trimeric) may be generated by subsequent mono- and bimolecular processes. This mechanism can explain, at least qualitatively, much of the observed diversity in the thermal reaction between $M_3(CO)_{12}$ (M= Fe, Ru, Os) and group V donor ligands.

The reactions of $Os_3(CO)_{12}$ and $P(OCH_3)_3$ carried out in this thesis were all performed with a large excess of the ligand. Although careful control of the temperature allowed mono- or trinuclear species to be favoured, quantitative yields of any one product were not obtained. By analogy to the kinetic study of the reaction between $M_3(CO)_{12}$ (M= Ru, Os) and $P(n\text{-}C_4H_9)_3$ [124], it would appear that both the k_1 and $k_2[P(OCH_3)_3]$ pathways were operating in the present case. The previously

discussed mechanism involving heterolytic cleavage of a metal-metal bond is the most reasonable one yet proposed to rationalize substitution by phosphorus donor ligands in $Os_3(CO)_{12}$. Additional kinetic work is required, however, before the quantitative aspects of this mechanism are more clearly understood.

Attempts to increase the phosphite substitution in $Os_3[P(OCH_3)_3]_6(CO)_6$ were unsuccessful. Neither the photolysis of $Os_3[P(OCH_3)_3]_6(CO)_6$ in toluene/$P(OCH_3)_3$ (5:1, v/v) nor the heating of the same complex in heptane/$P(OCH_3)_3$ (1:1, v/v) at 110 °C produced any observable amounts of $Os_3[P(OCH_3)_3]_x(CO)_{12-x}$ (x>6). In both cases, the solid $Os_3[P(OCH_3)_3]_6(CO)_6$ slowly disappeared as the solutions became pale yellow in colour. Infrared spectra of the solutions exhibited a number of absorptions in the carbonyl region; the only identifiable ones were those due to $Os[P(OCH_3)_3]_2(CO)_3$.

Although the substitutional reversibility of the series $Os_3[P(OCH_3)_3]_x(CO)_{12-x}$ (x= 1-6) was not studied in detail, an examination of $Os_3[P(OCH_3)_3]_4(CO)_8$ was performed spectroscopically. A solution of the tetrasubstituted triosmium complex in toluene was pressurized with 2 atm of carbon monoxide and irradiated with ultraviolet light. The reaction was monitored by $^{31}P\{^1H\}$ NMR techniques, which revealed that no observable change had occurred after 8 h.

5.3 Characterization and Discussion

All the complexes described in the previous section, with the exception of $Os_3[P(OCH_3)_3](CO)_{11}$ and $Os_3[P(OCH_3)_3]_5\{P(OC_2H_5)_3\}(CO)_6$, were fully characterized by elemental analysis, mass spectrometry, IR spectroscopy, and nuclear magnetic resonance methods (^1H, ^{13}C, and $^{31}P\{^1H\}$). The previously described $Os_3[P(OCH_3)_3](CO)_{11}$ [125] was characterized by infrared spectroscopy (carbonyl region) alone, and the mass spectrum of the mixed phosphite complex was not measured.

The $\nu(CO)$ absorptions from the IR spectra of $Os_3[P(OCH_3)_3]_x(CO)_{12-x}$ (x= 1-6), $Os[P(OCH_3)_3]_x(CO)_{5-x}$ (x= 1,2), and $Os_3[P(OCH_3)_3]_5\{P(OC_2H_5)_3\}(CO)_6$ are shown in table 5.1. The IR spectra (carbonyl region) of $Os[P(OCH_3)_3](CO)_4$ and $Os[P(OCH_3)_3]_2(CO)_3$ are shown in figures 5.1 and 5.2, respectively. The spectrum in figure 5.1 very closely resembles that for $Ru[P(OCH_3)_3](CO)_4$ [58]. The X-ray crystal structure of the ruthenium complex was determined, revealing an approximately trigonal bipyramidal geometry about the metal atom with the $P(OCH_3)_3$ ligand occupying an axial position (see figure 5.3). The trimethyl phosphite ligand was found not to possess threefold symmetry. This fact was used to rationalize the presence of an extra IR carbonyl band; an axially substituted, trigonal bipyramidal $M(CO)_4L$ molecule with C_{3v} symmetry would be expected to exhibit only three IR active absorptions in the carbonyl region [93]. It would appear likely, then, that the

Table 5.1 IR ν(CO) data: some phosphite derivatives of osmium.

Compound	Solvent	ν(CO) (cm^{-1})
$Os[P(OCH_3)_3](CO)_4$	hexane	2073s, 1997m, 1963vs, 1950vs
$Os[P(OCH_3)_3]_2(CO)_3$	hexane	1925s, 1915s
$Os_3[P(OCH_3)_3](CO)_{11}$	hexane	2111w, 2056s, 2040m, 2022s, 2003w, 1993m, 1983w, 1970w
$Os_3[P(OCH_3)_3]_2(CO)_{10}$	hexane	2094w, 2037m, 2020m, 2008s, 1987m, 1964wsh
$Os_3[P(OCH_3)_3]_3(CO)_9$	hexane	2072vw, 2010m, 1992s, 1954mbr
	CH_2Cl_2	2068vw, 2002m, 1985s, 1948mbr
$Os_3[P(OCH_3)_3]_4(CO)_8$	CH_2Cl_2	2049vw, 1989m, 1969s, 1941msh, 1909wsh
$Os_3[P(OCH_3)_3]_5(CO)_7$	CH_2Cl_2	2033w, 1952sbr, 1902w, 1889wsh
$Os_3[P(OCH_3)_3]_6(CO)_6$	CH_2Cl_2	2013vw, 1938sbr, 1881w
$Os_3(CO)_6[P(OCH_3)_3]_5$ -$[P(OEt)_3]$	CH_2Cl_2	1935sbr, 1879wbr

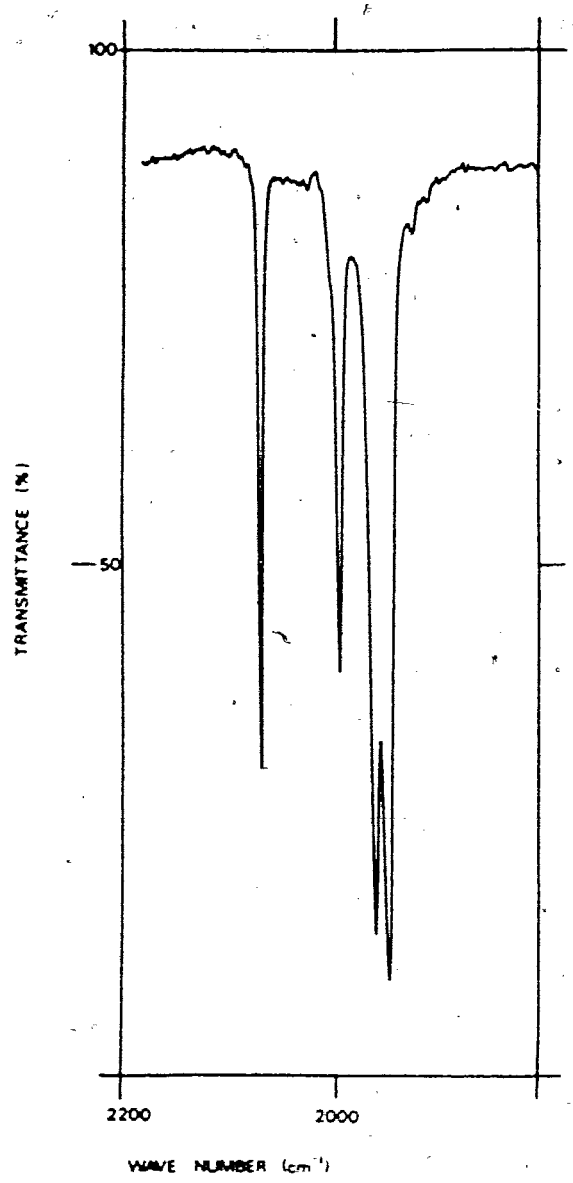

Figure 5.1 The IR spectrum (ν(CO) region) of $Os[P(OCH_3)_3](CO)_4$ in hexane.

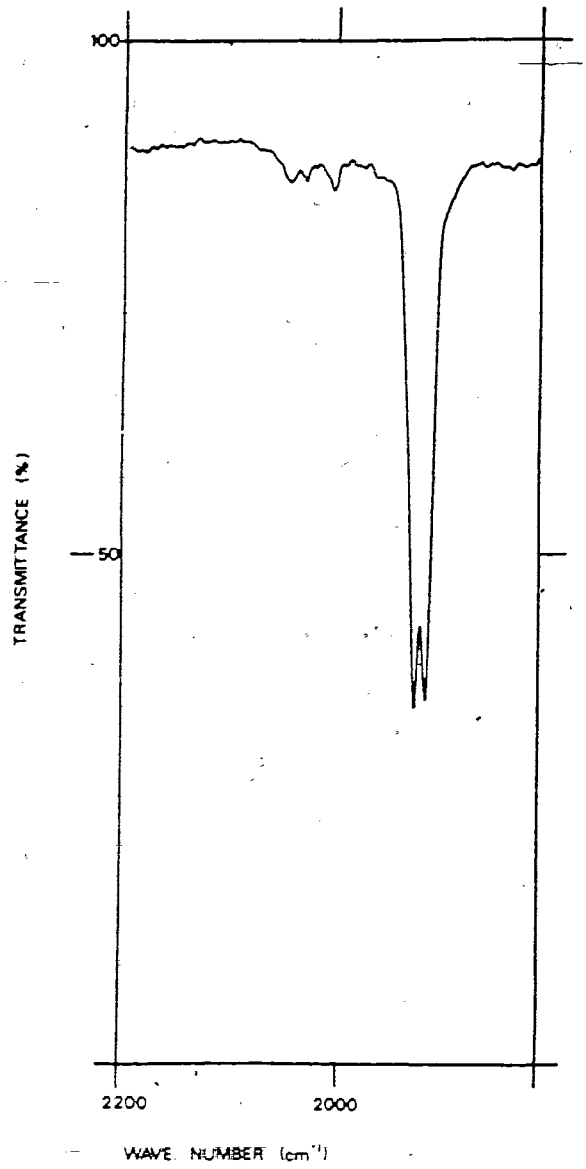

Figure 5.2 The IR spectrum (ν(CO) region) of $Os[P(OCH_3)_3]_2(CO)_3$ in hexane.

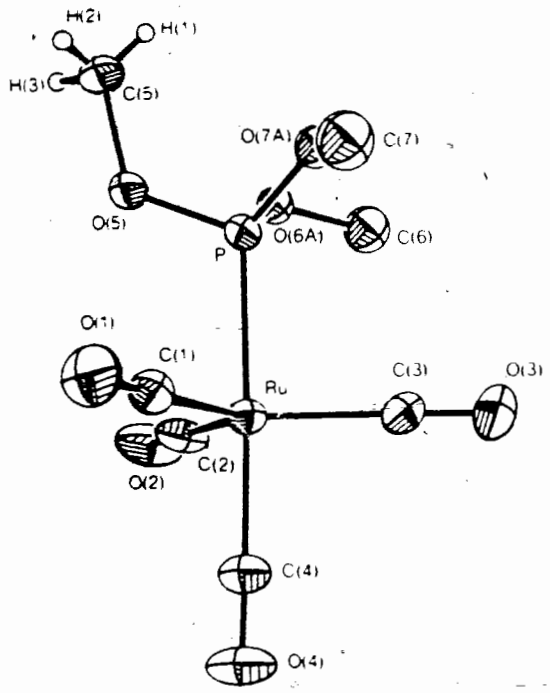

Figure 5.3 The molecular structure of $Ru[P(OCH_3)_3](CO)_4$.

---

instantaneous solution structure of $Os[P(OCH_3)_3](CO)_4$, as inferred from data obtained on the IR time scale, is very similar to the solid state structure of $Ru[P(OCH_3)_3](CO)_4$. This asymmetry of the trimethyl phosphite ligand is a ubiquitous feature of metal-$P(OCH_3)_3$ complexes and has been documented [58a,110].

Similar considerations may be applied to $Os[P(OCH_3)_3]_2(CO)_3$. The carbonyl portion of the infrared spectrum (figure 5.2) shows absorptions at 1925 and 1915 cm^{-1}. These are in excellent agreement with the only previous literature values [98]. The X-ray structure of the analogous $Fe[P(OCH_3)_3]_2(CO)_3$ showed the phosphite ligands occupying axial sites in a trigonal

bipyramidal geometry. In addition, an asymmetry very similar to that just described was noted for both the $P(OCH_3)_3$ ligands of this complex [127]. Two strong IR ν(CO) absorptions were also observed for this iron complex, separated by approximately 10 cm^{-1} [128]. An X-ray crystal structure of $Os(CO)_3[PPh_3]_2$ has also revealed a diaxially substituted, trigonal bipyramidal geometry [129]. An $M(CO)_3L_2$ molecule with D_{3h} symmetry would be expected to exhibit only a single IR active ν(CO) absorption [93]. The alternative structural possibilities for this stoichiometry, such as an axial-equatorial (C_s) or diequatorial (C_{2v}) trigonal bipyramidal structure [126], or a square-based pyramidal $M(CO)_3L_2$ molecule with apical-basal/*cis*-basal (both C_s) or *trans*-basal (C_{2v}) geometry would be expected to exhibit three IR active carbonyl absorptions [93,130]. The available evidence, then, clearly suggests that the instantaneous solution structure of $Os[P(OCH_3)_3]_2(CO)_3$ may be described as a diaxially substituted, trigonal bipyramid. The extra carbonyl absorption may be explained as a result of the asymmetric nature of the $P(OCH_3)_3$ ligands, reducing the idealized D_{3h} symmetry.

The trend in IR ν(CO) values for the series $Os_3[P(OCH_3)_3]_x(CO)_{12-x}$ (x= 1-6) (table 5.1) is worthy of mention. A steady decrease in the energy of these absorptions with increased phosphite substitution is observed. This is an expected result. As the number of phosphite substituents on the triosmium framework increases, the better σ-donor and poorer π-acceptor properties of the $P(OCH_3)_3$ ligand (versus carbon

monoxide) results in more electron density in the π^* orbitals of the remaining CO ligands. This causes a decrease in the values of ν(CO). Detailed analysis of the IR spectra for this series was not attempted. In solution, both $Os_3[P(OCH_3)_3]_2(CO)_{10}$ and $Os_3[P(OCH_3)_3]_4(CO)_8$ were found to exist as interconverting isomers at ambient temperatures by NMR methods (see chapter 6). These isomers would be easily detected by IR spectroscopy. In addition, it is possible that the previously discussed asymmetry of the $P(OCH_3)_3$ ligand could cause spectral complexity. For complexes with several phosphite groups, rotation about the Os-P bonds could lead to a number of inequivalent conformations. This would be expected to broaden the IR spectrum. The IR spectra (carbonyl region) of $Os_3[P(OCH_3)_3]_5(CO)_7$ and $Os_3[P(OCH_3)_3]_6(CO)_6$ are shown in figures 5.4 and 5.5, respectively. Both IR spectra consist of broad ν(CO) absorptions with unresolved shoulders. This is in contrast to the sharp absorptions exhibited by typical metal carbonyl complexes.

The mass spectra of $Os[P(OCH_3)_3](CO)_4$, $Os[P(OCH_3)_3]_2(CO)_3$, and $Os_3[P(OCH_3)_3]_x(CO)_{12-x}$ (x= 2-6) were generally as expected. For all except $Os_3[P(OCH_3)_3]_6(CO)_6$, parent ions in excellent agreement with computer simulated P^+ patterns were observed. Daughter ions due to simple loss of carbon monoxide and/or $P(OCH_3)_3$ from the parent were also present in the mass spectra. Although the spectrum of $Os_3[P(OCH_3)_3]_6(CO)_6$ exhibited a group of peaks in the region expected for P^+, they were not in agreement with the computer simulated parent pattern. The

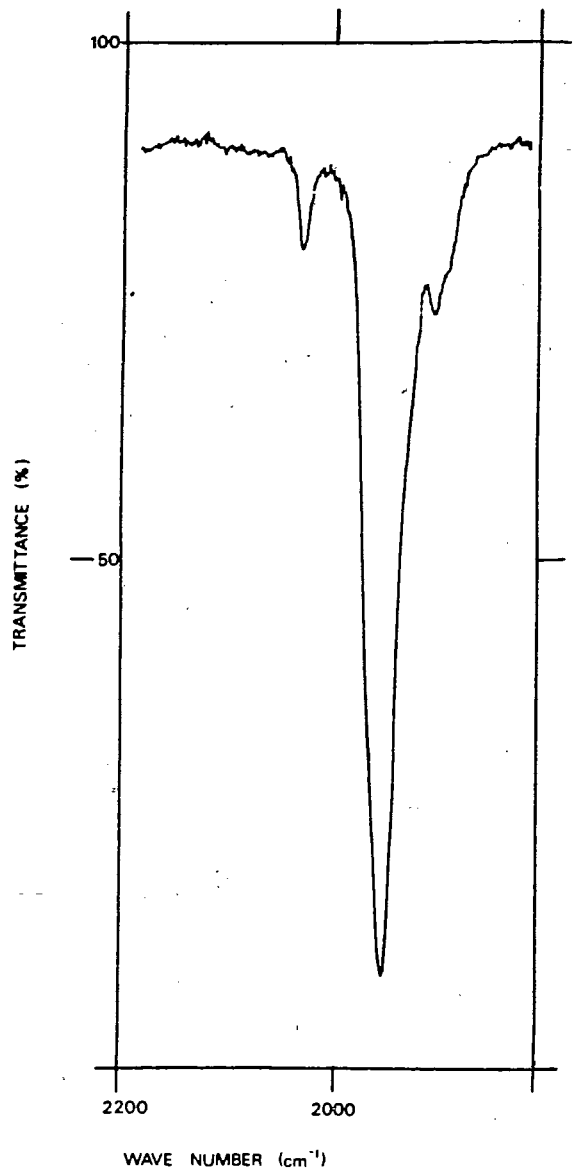

Figure 5.4 The IR spectrum (ν(CO) region) of $Os_3[P(OCH_3)_3]_5(CO)_7$ in CH_2Cl_2.

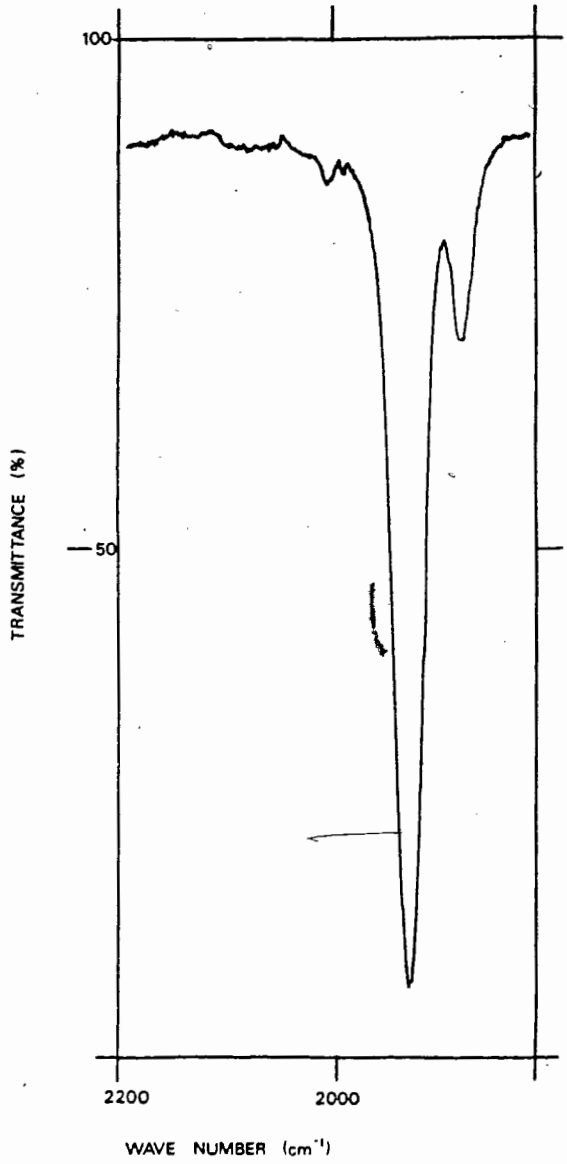

Figure 5.5 The IR spectrum (ν(CO) region) of $Os_3[P(OCH_3)_3]_6(CO)_6$ in CH_2Cl_2.

highest mass group displaying the correct pattern corresponded to the $[P-P(OCH_3)_3-2Me]^+$ ion; the corresponding ion in the mass spectrum of $Os_3[P(OCH_3)_3]_5(CO)_7$ was also intense.

The nuclear magnetic resonance data for $Os[P(OCH_3)_3](CO)_4$ and $Os[P(OCH_3)_3]_2(CO)_3$ are unremarkable. The ^1H NMR chemical shifts for the mono- and disubstituted complexes occur at 3.60 and 3.81 ppm, respectively. These are typical values for the protons of $P(OCH_3)_3$ when bonded to a transition metal [5,25,26]. The ^1H NMR signal for $Os[P(OCH_3)_3](CO)_4$ appears as a doublet (J_{PH}= 12.0 Hz); this coupling constant is characteristic for $P(OCH_3)_3$ in an organometallic complex [5,58]. The analogous resonance for $Os[P(OCH_3)_3]_2(CO)_3$ is an apparent triplet (J= 6 Hz), with the central signal broader than the two outer ones. This type of behaviour has also been noted for $Ru[P(OCH_3)_3]_2(CO)_3$ [5] and other complexes [131] and is attributed to strong spin-spin coupling between magnetically inequivalent phosphorus nuclei *trans* to one another; this effect is often called virtual coupling [132].

The resonances in the $^{31}P\{^1H\}$ NMR spectra of both $Os[P(OCH_3)_3](CO)_4$ and $Os[P(OCH_3)_3]_2(CO)_3$ are singlets. The positions of these resonances with respect to those of the free ligand have been discussed in chapter 4. Although a single signal for both the mono- and disubstituted complexes is expected, no information regarding any dynamic properties of these species in solution is directly derivable. Stereochemical nonrigidity is a common feature of five-coordinate transition

metal complexes [7]. The ^{13}C NMR spectrum of $Ru[P(OCH_3)_3](CO)_4$ exhibited only a single resonance due to the carbonyl groups even at -120 °C [58]. The $^{31}P\{^1H\}$ NMR spectra of both $Ru[P(OCH_3)_3](CO)_4$ and $Ru[P(OCH_3)_3]_2(CO)_3$ consisted of a single line at -120 °C [5]. It is predicted that both $Os[P(OCH_3)_3](CO)_4$ and $Os[P(OCH_3)_3]_2(CO)_3$ are stereochemically nonrigid in solution at ambient temperatures. A variable temperature ^{13}C NMR study of $Os[P(OCH_3)_3](CO)_4$ would provide further evidence.

The ^1H, ^{13}C, and $^{31}P\{^1H\}$ NMR data for $Os_3[P(OCH_3)_3]_x(CO)_{12-x}$ (x= 1-6) are intimately related to the question of stereochemical nonrigidity in the series. As such, the nuclear magnetic resonance parameters for these complexes will be discussed in chapter 6.

The changes in solubility of the series $Os_3[P(OCH_3)_3]_x(CO)_{12-x}$ (x= 1-6) in hexane have been noted in an earlier section of this chapter. It is tempting to put forth a qualitative explanation of the decreasing solubility with increasing phosphite substitution in terms of changes in dipole moment. No clear pattern emerges, however. The factors causing the dramatic increase in hexane solubility on going from $Os_3(CO)_{12}$ to $Os_3[P(OCH_3)_3](CO)_{11}$ and the subsequent steady decrease in solubility with increased phosphite substitution are not obvious.

The complexes $Os_3[P(OCH_3)_3]_x(CO)_{12-x}$ (x= 4-6) represent the most highly phosphite-substituted derivatives of $Os_3(CO)_{12}$

prepared to date. All the previous literature findings are consistent with group V donor ligands adopting exclusively equatorial positions in derivatives of $M_3(CO)_{12}$ (M= Fe, Ru, Os) [99-109]. The present results are in complete agreement with this conclusion (see chapter 6). A considerable amount of steric congestion might be expected in these complexes (particularly for $Os_3[P(OCH_3)_3]_6(CO)_6$) given that the cone angle for $P(OCH_3)_3$ is 107° [11]. Suprisingly, there was no NMR evidence for phosphite dissociation from any of these three complexes in solution even at elevated temperatures.

One might also expect some electronic implications of a highly phosphite-substituted triosmium complex. The better σ-donor and poorer π-acceptor properties of $P(OCH_3)_3$, versus CO, are predicted to confer a high electron density on the complexes $Os_3[P(OCH_3)_3]_x(CO)_{12-x}$ (x= 4-6). Several experiments performed to verify this expectation were unsuccessful. The attempted protonation of $Os_3[P(OCH_3)_3]_4(CO)_8$ by NH_4PF_6 in THF did not proceed and the tetrasubstituted triosmium complex was recovered unchanged. This may be contrasted to the behaviour of $Ru[P(OCH_3)_3]_5$ and NH_4PF_6 in THF, where $\{HRu[P(OCH_3)_3]_5\}PF_6$ (and presumably NH_3) were formed virtually within time of mixing (see chapter 3).

The attempted protonation of $Os_3[P(OCH_3)_3]_6(CO)_6$ with $HBF_4 \cdot Et_2O$ was not straightforward. IR spectroscopy revealed the presence of several products which were not easily separable. A variable temperature $^{31}P\{^1H\}$ and ^1H NMR study of one partially

separated product mixture was conducted. The ^1H NMR spectrum (25 °C) revealed a complex methoxy multiplet in addition to several weak multiplets in the M-H region (-15 to -25 ppm). These resonances were all temperature invariant. The $^{31}P\{^1H\}$ NMR spectrum (25 °C) featured a number of complex multiplets which were also temperature independent. In addition, selective ^1H decoupling of the methoxy protons and broad band decoupling of all protons resulted in identical ^{31}P NMR spectra. These results argue against the presence of $\{HOs_3[P(OCH_3)_3]_6(CO)_6\}BF_4$ as a major component of the product mixture.

Additionally, a $^{31}P\{^1H\}$ NMR investigation of $Os_3[P(OCH_3)_3]_6(CO)_6$ and CH_3I in toluene was performed. No apparent reaction was observed after 24 h at 25 °C.

5.4 X-Ray Crystal Structure of $Os_3[P(OCH_3)_3]_6(CO)_6$.

Crystals of $Os_3[P(OCH_3)_3]_6(CO)_6$ suitable for X-ray diffraction were grown by slow diffusion of hexane into a CH_2Cl_2 solution of the complex. The crystal structure determination was done by Dr. Richard Jones and Prof. F. W. B. Einstein; their work was greatly appreciated. The molecular structure of $Os_3[P(OCH_3)_3]_6(CO)_6$ is shown in figure 5.6.

The crystal structure determination revealed a random disorder between two orientations of the molecule. These two orientations are related by a 60° rotation of the cluster about an axis normal to the Os_3 plane. The high symmetry of

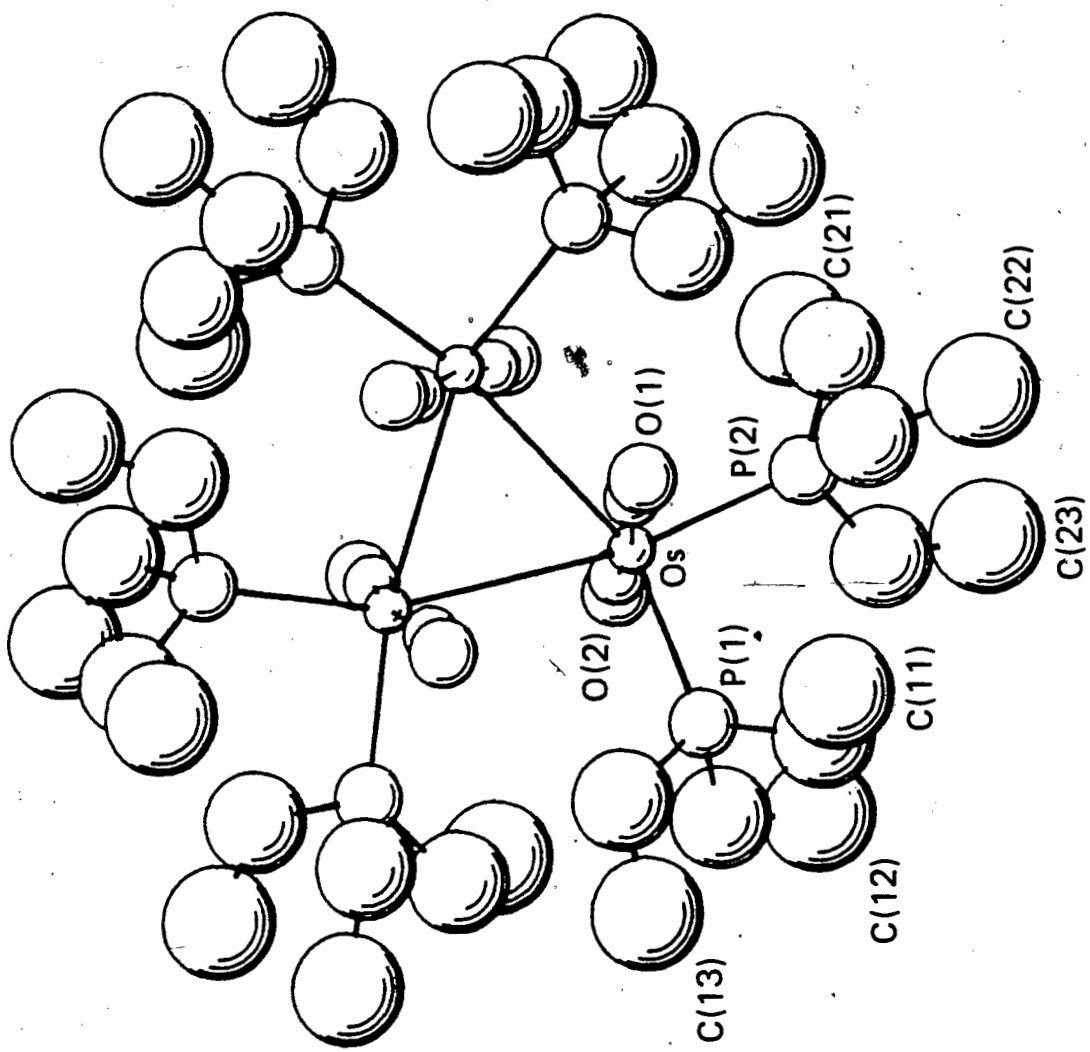

Figure 5.6 The molecular structure of $Os_3[P(OCH_3)_3]_6(CO)_6$.

$Os_3[P(OCH_3)_3]_6(CO)_6$ results in the phosphorus atoms occupying almost identical positions in both arrangements. This 'Star of David' disorder has been previously observed for $Fe_3(CO)_{12}$ and several $Ru_3(CO)_{12}$ derivatives [133]. The crystallographic symmetry of $Os_3[P(OCH_3)_3]_6(CO)_6$ ($\bar{3}$) dictates a single Os-Os bond distance and a pair of Os-P bond lengths.

The molecular structure of $Os_3[P(OCH_3)_3]_6(CO)_6$ (figure 5.6) shows that the $P(OCH_3)_3$ ligands occupy the six equatorial sites of the triosmium cluster. This result is in complete accord with the solution structure of the complex (see chapter 6). Considerable experimental evidence that phosphorus donor ligands exclusively adopt equatorial positions in substituted derivatives of $Os_3(CO)_{12}$ has been presented in the introduction to this chapter; presumably the equatorial sites are the least sterically hindered for this system.

The average Os-P bond length for $Os_3[P(OCH_3)_3]_6(CO)_6$ is 2.237(7) Å. This may be compared to the analogous values for $Os_3[P(OCH_3)_3](CO)_{11}$ [109], $Os_3[P(OCH_3)_3](CO)_8(NO)_2$ [134], $(\mu\text{-H})(\mu\text{-}\eta^2\text{-HCNC}_6H_5)Os_3[P(OCH_3)_3](CO)_9$ [135], and $Os_3[P(OCH_3)_3](CO)_9(\mu_2\text{-NO})_2$ [136]: 2.285(5), 2.327(14), 2.281(2), and 2.281(2) Å, respectively. The Os-P bond distance in $Os_3[P(OCH_3)_3]_6(CO)_6$ is significantly shorter that those observed for the related complexes. Steric considerations might have suggested the opposite behaviour; the non-bonded interaction of *cis* phosphites on the same Os atom should lead to an increased Os-P bond length. Electronic arguments, on the other hand, are

in accord with the short osmium-phosphorus bond distance in $Os_3[P(OCH_3)_3]_6(CO)_6$. The good σ-donor characteristics of the two $P(OCH_3)_3$ ligands on each Os atom is expected to cause increased π back-bonding to the phosphite groups, thus decreasing the Os-P bond length.

The osmium-carbon bond lengths in $Os_3[P(OCH_3)_3]_6(CO)_6$ (1.89(2) and 1.93(2)Å) are not significantly different from the Os-C bonds for the axial carbonyl ligands of $Os_3(CO)_{12}$ (average $Os-C_{ax}$= 1.946(6)Å) [137]. This is not the case for the metal-metal bond lengths. The Os-Os distance in $Os_3[P(OCH_3)_3]_6(CO)_6$ (2.927(1)Å) is considerably longer than that found in $Os_3(CO)_{12}$ (average Os-Os= 2.8771(27)Å) [137]. These values may also be compared to the average osmium-osmium bond length for $Os_3[P(OCH_3)_3](CO)_{11}$ (2.897(10)Å) [109]. There appears to be a trend towards longer Os-Os bonds as the $P(OCH_3)_3$ substitution increases on the triosmium framework. Although electronic effects cannot be ruled out, the steric congestion in the equatorial plane of $Os_3[P(OCH_3)_3]_6(CO)_6$ likely plays a significant role in the long metal-metal bonds for this complex; the $P(OCH_3)_3$ ligands *cis* to each other on adjacent Os atoms are in close proximity (see figure 5.6).

Evidence for this lengthening of the osmium-osmium bond with increasing degree of phosphite substitution may be observed by UV-visible spectroscopy. The UV-visible spectrum of $Os_3(CO)_{12}$ in CCl_4 at 25 °C revealed two absorptions at 330 and 385 nm. These values are consistent with those found in the literature

[138,139]. The two bands in question have been assigned to the $\sigma \longrightarrow \sigma^*$ and the $\sigma^{*'} \longrightarrow \sigma^*$ transitions, respectively [138]. The former involves a transition between bonding and antibonding molecular orbitals with considerable metal-metal σ-bond character. The UV-visible spectrum of $Os_3[P(OCH_3)_3]_3(CO)_9$ in CCl_4 at 25 °C revealed that these two bands had shifted to lower energy (350 and 414 nm, respectively). This shift continued for the case of $Os_3[P(OCH_3)_3]_6(CO)_6$: the absorptions in question appeared at 412 and 475 nm, respectively, in the UV-visible spectrum of this complex at 25 °C in CH_2Cl_2. This decrease in energy of the σ to σ^* transition with increasing phosphite substitution implies a weakening, and thus lengthening, of the osmium-osmium bond. This result is, of course, consistent with the X-ray crystal structures of $Os_3(CO)_{12}$ and $Os_3[P(OCH_3)_3]_6(CO)_6$. This weakening of the metal-metal bonds in $Os_3[P(OCH_3)_3]_6(CO)_6$ is also in accord with the observation of Os-Os bond scission upon attempts to increase the phosphite substitution, although steric effects are likely an important factor here as well.

The effects of this shift in the $\sigma \longrightarrow \sigma^*$ and $\sigma^{*'} \longrightarrow \sigma^*$ transition energies may be observed more qualitatively. A gradual change in colour is observed as x increases from 0 to 6 in $Os_3[P(OCH_3)_3]_x(CO)_{12-x}$; $Os_3(CO)_{12}$ is yellow, $Os_3[P(OCH_3)_3]_2(CO)_{10}$ is orange-yellow, $Os_3[P(OCH_3)_3]_4(CO)_8$ is orange, and crystals of the hexa(phosphite) complex are orange-red. These colour changes are a consequence of the shift

of absorptions in the visible region of the electromagnetic spectrum.

5.5 Experimental Section

Preparation of $Os_3[P(OCH_3)_3](CO)_{11}$. Two methods were used to prepare this compound. A literature preparation [125] involving initial formation of $Os_3[NCMe](CO)_{11}$ and subsequent reaction with $P(OCH_3)_3$ gave reasonable yields of the desired product: IR ν(CO) (hexane) 2111 (w), 2056 (s), 2040 (m), 2022 (s), 2003 (w), 1993 (m), 1983 (w), 1970 (w) cm^{-1}. Lit. [101]: 2111 (m), 2055 (s), 2038 (m), 2021 (s), 2002 (w), 1992 (m), 1981 (w), 1967 (w) cm^{-1}.

A more direct and preferred route is described below.

Preparation of $Os_3[P(OCH_3)_3](CO)_{11}$ and $Os_3[P(OCH_3)_3]_2(CO)_{10}$. A glass Carius tube containing $Os_3(CO)_{12}$ (0.50 g, 0.55 mmol) and $P(OCH_3)_3$ (0.15 mL, 1.3 mmol) in hexane (15 mL) was evacuated at -196 °C and the solution degassed with three freeze-pump-thaw cycles. The tube was heated at 125 °C for 8 h. An infrared spectrum (carbonyl region) at this time indicated the presence of $Os_3[P(OCH_3)_3](CO)_{11}$ and $Os_3[P(OCH_3)_3]_2(CO)_{10}$ in an approximate 1:4 ratio, with a small amount of $Os_3[P(OCH_3)_3]_3(CO)_9$ also present. The homogeneous reaction mixture was yellow-orange.

The ratio of the mono- and disubstituted products was strongly dependent on the reaction time. The same reaction,

after 2 h, gave high yields of $Os_3[P(OCH_3)_3](CO)_{11}$.

The mono- and bis(phosphite) complexes were separated by chromatography on $P(OCH_3)_3$-deactivated Florisil, the preparation of which is described in the experimental section, chapter 2. Vacuum removal of the hexane and excess $P(OCH_3)_3$ from the reaction mixture yielded an orange oil, which was dissolved in toluene (3 mL) and chromatographed on the deactivated Florisil column (3.5x11 cm). Elution with hexane caused separation of a yellow band, which was collected. Removal of solvent under vacuum afforded $Os_3[P(OCH_3)_3](CO)_{11}$ (0.05 g, 9%) as bright yellow crystals. Further elution with hexane:toluene (4:1, v/v) caused development of a second yellow band. Vacuum removal of solvent from the collected fraction yielded orange-yellow crystals of $Os_3[P(OCH_3)_3]_2(CO)_{10}$ (0.24 g, 40%).

Both products may be recrystallized from hexane and are soluble in common organic solvents. Crystals of $Os_3[P(OCH_3)_3]_2(CO)_{10}$ were stable for several weeks in air and melted without decomposition: mp 96.5-97 °C; IR ν(CO) (hexane) 2094 (w), 2037 (m), 2020 (m), 2008 (s), 1987 (m), 1964 (wsh) cm^{-1}; ^1H NMR (toluene-d_8, 25 °C; 100.13 MHz) δ 3.73 (doublet, J_{PH}= 12.2 Hz); ^1H NMR (toluene-d_8, -47 °C, 400.13 MHz) δ 3.72 (doublet, J_{PH}= 12.4 Hz, rel. int.= 3), δ 3.69 (doublet, J_{PH}= 12.4 Hz, rel. int.= 3), δ 3.68 (doublet, J_{PH}= 12.3 Hz, rel. int.= 2); ^{13}C NMR (toluene-d_8, -66 °C, 100.6 MHz) [measured on a sample approximately 50% enriched with ^{13}CO] δ 192.5 (doublet, J_{PC}= 10.8 Hz, rel. int.= 32), δ 191.7 (doublet, J_{PC}= 11.7 Hz,

rel. int.= 55), δ 187.5 (singlet, rel. int.= 11), δ 186.7 (singlet, rel. int.= 32), δ 179.6 (singlet, rel. int.=16), δ 178.7 (singlet, rel. int.= 11), δ 177.1 (singlet, rel. int.= 16), δ 176.2 (singlet, rel. int.=16), δ 175.0 (singlet, rel. int.=11), δ 173.9 (singlet, rel. int.=16); ^{13}C NMR (toluene-d_8, 87 °C, 100.6 MHz) [^{13}CO enrichment as above] δ 184.4 (broad singlet); $^{31}P\{^1H\}$ NMR (toluene-d_8/toluene (1:5), -59 °C, 40.5 MHz) δ -42.7 (doublet, J_{PP}= 1.8 Hz, rel. int.= 7), δ -40.8 (singlet, rel. int.= 5), δ -39.6 (doublet, J_{PP}= 1.9 Hz, rel. int.= 7); $^{31}P\{^1H\}$ NMR (toluene-d_8/toluene (1:5), 79 °C, 40.5 MHz) δ -42.6 (singlet); mass spectrum (EI, 70 eV) calc. for $C_{16}H_{18}O_{16}Os_3P_2$ (P) (computer simulation of P^+ pattern), *m/e* 1100, found, *m/e* 1100, also *m/e* 1072, 1044, 1016, 988, 960 ($[P-nP(OCH_3)_3]^+$ n=1,2,3,4,5). Anal. calc. for $C_{16}H_{18}O_{16}Os_3P_2$: C, 17.48; H, 1.65; P, 5.64. Found: C, 17.19; H, 1.61; P, 5.74.

NMR Data for $Os_3[P(OCH_3)_3](CO)_{11}$. $^{13}C\{^1H\}$ NMR (toluene-d_8, -53 °C, 100.6 MHz) [measured on a sample approximately 50% enriched with ^{13}CO] δ 189.8 (doublet, J_{PC}= 12.3 Hz, rel. int.= 2), δ 185.1 (singlet, rel. int.= 2), δ 184.2 (singlet, rel. int.= 2), δ 176.0 (singlet, rel. int.= 1), δ 174.5 (singlet, rel. int.= 1), δ 172.9 (singlet, rel. int.= 1), δ 171.8 (singlet, rel. int.= 1), δ 170.8 (singlet, rel. int.= 1); $^{31}P\{^1H\}$ NMR (toluene-d_8/toluene (1:5), 25 °C, 162.0 MHz) δ -43.7 (singlet).

Preparation of $Os_3[P(OCH_3)_3]_3(CO)_9$. A glass Carius tube containing $Os_3(CO)_{12}$ (0.250 g, 0.276 mmol) and $P(OCH_3)_3$ (0.10

mL, 0.85 mmol) in xylene (15 mL) was evacuated at -196 °C and the solution degassed three times. The tube was heated to 125 °C for 20 h, at which time the reaction solution was a clear orange-yellow. An IR spectrum (carbonyl region) indicated a mixture of $Os_3[P(OCH_3)_3]_2(CO)_{10}$ and $Os_3[P(OCH_3)_3]_3(CO)_9$ in an approximate 1:2 ratio with small amounts of $Os_3[P(OCH_3)_3]_4(CO)_8$ and $Os_3[P(OCH_3)_3](CO)_{11}$ also present. Solvent and excess $P(OCH_3)_3$ were removed on the vacuum line and the resultant bright orange oil was dissolved in toluene (4 mL). This solution was chromatographed on a Florisil column (11x3.5 cm) prepared as previously described. Elution with hexane:toluene (1:1, v/v) removed $Os_3[P(OCH_3)_3](CO)_{11}$ and $Os_3[P(OCH_3)_3]_2(CO)_{10}$, leaving an orange band near the top of the column. Elution with pure toluene caused development of a yellow-orange band, which was collected, while an orange band remained at the top of the column. Vacuum removal of the toluene afforded a yellow-orange crystalline solid (0.11 g, 33%). The product appeared stable in air for a several week period. Hexane recrystallization at -15 °C produced bright yellow-orange crystals of $Os_3[P(OCH_3)_3]_3(CO)_9$: mp 158-159 °C (dec); IR ν(CO) (hexane) 2072 (vw), 2010 (m), 1992 (s), 1954 (mbr) cm^{-1}; ν(CO) (CH_2Cl_2) 2068 (vw), 2002 (m), 1985 (s), 1948 (mbr) cm^{-1}; ^1H NMR (acetone-d_6, 25 °C, 100.1 MHz) δ 3.67 (doublet, J_{PH}= 12.2 Hz); ^{13}C NMR (toluene-d_8/toluene (1:4), -65 °C, 100.6 MHz) δ 193.3 (doublet, J_{PC}= 10.3 Hz, rel. int.= 2), δ 179.9 (singlet, rel. int.= 1); $^{31}P\{^1H\}$ NMR (toluene-d_8/toluene (1:2), 31 °C, 40.5 MHz) δ -40.7 (singlet); $^{31}P\{^1H\}$ NMR (toluene-d_8/toluene (1:2), -91 °C, 40.5

MHz) δ -39.4 (singlet); mass spectrum (EI, 70 eV) calc. for $C_{18}H_{27}O_{18}Os_3P_3$ (P) (computer simulation of P^+ pattern), *m/e* 1196, found, *m/e* 1196 (good agreement with computer simulated pattern), also *m/e* 1168, 1140, 1112, 1084, 1056 ($[P-nP(OCH_3)_3]^+$ n=1,2,3,4,5). Anal. calc. for $C_{18}H_{27}O_{18}Os_3P_3$: C, 18.09; H, 2.28; P, 7.78. Found: C, 18.18; H, 2.29; P, 7.97.

Preparation of $Os_3[P(OCH_3)_3]_4(CO)_8$. Dodecacarbonyl triosmium (0.50 g, 0.55 mmol), $P(OCH_3)_3$ (4 mL, excess), and heptane (20 mL) were placed in a glass Carius tube. The solution was degassed three times and subsequently heated at 140-145 °C for 24 h. At this point, the solution was medium orange in colour and clear. An infrared spectrum (carbonyl region) of the reaction solution in heptane exhibited a strong absorption at 1971 cm^{-1} due to $Os_3[P(OCH_3)_3]_4(CO)_8$, two strong bands at 1925 and 1915 cm^{-1} caused by $Os[P(OCH_3)_3]_2(CO)_3$, as well as several weaker absorptions at higher energy. Cooling of the reaction solution at room temperature overnight resulted in the precipitation of orange crystals. The yellow-orange supernatant solution was decanted off. The crystals were washed with hexane (4x10 mL), and dried on the vacuum line. The yield of the crude product, which consisted mainly of $Os_3[P(OCH_3)_3]_4(CO)_8$ ($Os_3[P(OCH_3)_3]_5(CO)_7$ impurity), was 0.33 g (46%). The crude product was dissolved in toluene (4 mL) and placed on a $P(OCH_3)_3$-deactivated Florisil column (3.5x14 cm). Elution with toluene or toluene:CH_2Cl_2 mixtures allowed collection of an orange band (the pentasubstituted impurity descended only a few

cm). Vacuum removal of the eluant yielded $Os_3[P(OCH_3)_3]_4(CO)_8$ as an analytically pure, orange solid.

The product distribution of this reaction was crucially dependent on the temperature. At temperatures lower than 140 °C, considerable amounts of $Os[P(OCH_3)_3](CO)_4$ (ν(CO) (hexane) 2073 (s), 1997 (m), 1963 (vs), 1950 (vs) cm^{-1}) remained in solution and yields of $Os_3[P(OCH_3)_3]_4(CO)_8$ were poor. At temperatures above 145 °C, the tetrasubstituted triosmium compound underwent metal-metal bond rupture: the reaction solution became pale yellow.

The desired product was stable in air for a several month period. Although sparingly soluble in hexane, $Os_3[P(OCH_3)_3]_4(CO)_8$ may be recrystallized from hexane:toluene or hexane:CH_2Cl_2 mixtures at -15 °C, yielding light orange plates: mp 163-165 °C (dec.); IR ν(CO) (CH_2Cl_2) 2049 (vw), 1989 (m), 1969 (s), 1941 (msh), 1909 (wsh) cm^{-1}; ^1H NMR ($CDCl_3$, 25 °C, 400.13 MHz) δ 3.62 (doublet, J_{PH}= 12.2 Hz, rel. int.= 1), δ 3.61 (doublet, J_{PH}= 11.8 Hz, rel. int.= 1); ^1H NMR (toluene-d_8, -78 °C, 400.13 MHz) The spectrum was not in the slow exchange limit. At least four sets of broad doublets centred at δ 3.42 (J_{PH}= ~10-12 Hz) were observed; ^{13}C NMR (toluene-d_8, -83 °C, 100.6 MHz) [measured on a sample approximately 50% enriched with ^{13}CO] δ 200.2 (poorly resolved triplet, J_{PC}= 10.8 Hz, rel. int.= 4), δ 198.8 (poorly resolved triplet, J_{PC}≃ 10 Hz, rel. int.= 3), δ 195.1 (broad singlet with poorly resolved satellites, rel. int.= 10), δ 194.1 (doublet, J_{PC}= 6.4 Hz, rel. int.= 4), δ 181.9

(singlet, rel. int.= 2), δ 180.8 (singlet, rel. int.= 3), δ 178.7 (singlet, rel. int.= 2); ^{13}C NMR (toluene-d_8, 80 °C, 100.6 MHz) [^{13}CO enrichment as above] δ 198.4 (triplet, J_{PC}= 11.2 Hz, rel. int.= 1), δ 189.1 (singlet, rel. int.= 3); ^{13}C NMR (toluene-d_8, -70 °C, 25.2 MHz) The two poorly resolved triplets (-83 °C, 100.6 MHz) appeared as well resolved triplets: δ 200.4 (triplet, J_{PC}= 11.0 Hz), δ 198.9 (triplet, J_{PC}= 11.5 Hz); ^{31}P{^{1}H} NMR (toluene-d_8/toluene (1:5), -81 °C, 40.5 MHz) δ -33.4 (doublet, J_{PP}= 4.4 Hz), δ -33.6 (singlet), δ -35.0 (singlet), δ -36.4 (doublet, J_{PP}= 4.2 Hz), δ -36.7 (broad singlet), δ -39.6 (doublet, J_{PP}= 3.9 Hz); ^{31}P{^{1}H} NMR (toluene-d_8/toluene (1:5), 53 °C, 40.5 MHz) δ -38.5 (singlet, rel. int.= 1), δ -40.1 (singlet, rel. int.= 1).

The ^{31}P{^{1}H} variable temperature NMR spectra measured at 162 MHz showed analogous behaviour except for the couplings, which were not resolved. The individual resonances, however, were better resolved and detailed analysis of several low temperature (-91, -84, -76 °C) spectra allowed calculation of accurate integrals for all signals: ^{31}P{^{1}H} NMR (toluene-d_8, -91 °C, 162.0 MHz) δ -33.2, -33.3 (overlapping singlets, total rel. int.= 37, divided as 22 and 15, respectively), δ -34.7 (singlet, rel. int.= 14), δ -36.1 (singlet, rel. int.= 24), δ -36.7 (singlet, rel. int.= 14), δ -39.6 (singlet, rel. int.= 14); ^{31}P{^{1}H} NMR (toluene-d_8/toluene (1:4), 93 °C, 162.0 MHz) δ -39.3 (singlet, rel. int.= 1), δ -40.8 (singlet, rel. int.= 1); Mass spectrum (EI, 70 eV) calc. for $C_{20}H_{36}O_{20}Os_3P_4$ (P) (computer simulation of P$^+$ pattern), *m/e* 1292, found, *m/e* 1292 (excellent agreement with

computer simulated pattern), also *m/e* 1264, 1236, 1208, 1180, 1152 ($[P-nP(OCH_3)_3]^+$ n=1,2,3,4,5). Anal. calc. for $C_{20}H_{36}O_{20}Os_3P_4$: C, 18.61; H, 2.81; P, 9.60. Found: C, 18.46; H, 2.67; P, 10.55.

Preparation of $Os_3[P(OCH_3)_3]_5(CO)_7$. A glass Carius tube was charged with $Os_3(CO)_{12}$ (0.50 g, 0.55 mmol), $P(OCH_3)_3$ (4 mL, excess), and heptane (20 mL). The solution was degassed three times. The tube was heated at 140-145 °C as for the $Os_3[P(OCH_3)_3]_4(CO)_8$ synthesis. The reaction mixture was cooled and degassed with one freeze-pump-thaw cycle and then reheated to dissolve the precipitated orange solid. After partial cooling, the tube was irradiated with ultraviolet light. The reaction appeared to involve successive substitution of carbonyls for phosphites by photolytic activation. The speed at which this occurred was affected by the particular UV source and the glass tube used. Thus, the ~~reaction was~~ best monitored by infrared spectroscopy (carbonyl region) to determine when the product distribution favoured $Os_3[P(OCH_3)_3]_5(CO)_7$. A typical reaction time was 8 h. As the reaction proceeded, an orange solid precipitated from the orange solution. The reaction mixture was transferred to a Schlenk tube and the supernatant solution decanted away. The remaining orange solid was washed with hexane (5x10 mL) and dried on the vacuum line. This crude mixture (0.36 g) contained small amounts of $Os_3[P(OCH_3)_3]_4(CO)_8$ and $Os_3[P(OCH_3)_3]_6(CO)_6$, in addition to the desired product. The crude product was dissolved in toluene (5 mL) and placed on a

$P(OCH_3)_3$-deactivated Florisil column (3.5x14 cm). Elution with toluene:CH_2Cl_2 mixtures or pure CH_2Cl_2 allowed removal of $Os_3[P(OCH_3)_3]_4(CO)_8$. A large orange band remained at the top of the column. A change of eluant to CH_2Cl_2:$P(OCH_3)_3$ (6:1, v/v) caused development of an orange band, which was collected. A deep orange-red band was left on the column; the band had moved only a few centimetres. Removal of solvent from the collected fraction on the vacuum line left $Os_3[P(OCH_3)_3]_5(CO)_7$ as a crystalline, orange solid (0.26 g, 34%). The product was stable in air over a several week period and appeared stable in water for a 48 h time span. Although insoluble in hexane, $Os_3[P(OCH_3)_3]_5(CO)_7$ was recrystallized from toluene or hexane:toluene at -15 °C to yield orange plates: mp 162.5-163 °C (dec.); IR ν(CO) (CH_2Cl_2) 2033 (w), 1952 (sbr), 1902 (w), 1889 (wsh) cm^{-1}; ^1H NMR ($CDCl_3$, 25 °C, 400.13 MHz) δ 3.620 (doublet, J_{PH}= 11.6 Hz, rel. int.= 2), δ 3.615 (doublet, J_{PH}= 11.5 Hz, rel. int.= 2), δ 3.610 (doublet, J_{PH}= 12.3 Hz, rel. int.= 1); ^1H NMR (toluene-d_8, -57 °C, 400.13 MHz) δ 3.57 (doublet, J_{PH}= 11.6 Hz, rel. int.= 1), δ 3.56 (doublet, J_{PH}= 11.5 Hz, rel. int.= 1), δ 3.54 (doublet, J_{PH}= 11.7 Hz, rel. int.= 1), δ 3.49 (doublet, J_{PH}= 11.5 Hz, rel. int.= 1), δ 3.44 (doublet, J_{PH}= 12.5 Hz, rel. int.= 1); $^{13}C\{^1H\}$ NMR (toluene-d_8/toluene (1:5) plus ~5% (mol) $Cr(acac)_3$, 75 °C, 25.2 MHz) δ 198.5 (singlet, rel. int.= 4), δ 188.8 (singlet, rel. int.= 3); $^{13}C\{^1H\}$ NMR (toluene-d_8/toluene (1:5) plus ~5% (mol) $Cr(acac)_3$, 2 °C, 25.2 MHz) δ 198.8 (triplet, J_{PC}= 10.9 Hz); $^{13}C\{^1H\}$ NMR (toluene-d_8/toluene (1:5) plus 5% (mol) $Cr(acac)_3$, -50 °C, 25.2 MHz) δ 199.7,199.2

(overlapping triplets [see data at 100.6 MHz], J_{PC}= 11.5,11.4 Hz, total rel. int.= 4), δ 194.1 (doublet, J_{PC}= 11.4 Hz, rel. int.= 2), δ 179.2 (singlet, rel. int.= 1); ^{13}C NMR (toluene-d_8, -44 °C, 100.6 MHz) δ 200.7 (poorly resolved triplet, rel. int.= 2), δ 200.1 (poorly resolved triplet, rel. int.= 2), δ 195.1 (doublet, J_{PC}= 10.5 Hz, rel. int.= 2), δ 180.2 (singlet, rel. int.= 1). It is noted that these chemical shifts differ by approximately 1 ppm from those at 25.2 MHz. This difference is likely attributable to an improper chemical shift reference in the 100.6 MHz data; ^{31}P{^{1}H} NMR (toluene-d_8/toluene (1:5), 69 °C, 40.5 MHz) δ -38.6 (singlet, rel. int.= 1), δ -39.3 (singlet, rel. int.= 2), δ -42.6 (singlet, rel. int.= 2); ^{31}P{^{1}H} NMR (toluene-d_8/toluene (1:5), -55 °C, 40.5 MHz) δ -34.5 (doublet, J_{PP}= 6.4 Hz, rel. int.= 1), δ -36.2 (doublet, J_{PP}= 6.1 Hz, rel. int.= 1), δ -37.9 (doublet, J_{PP}= 7.6 Hz, rel. int.= 1), δ -38.2 (singlet, rel. int.= 1), δ -43.0 (doublet, J_{PP}= 7.3 Hz, rel. int.= 1). The variable temperature ^{31}P{^{1}H} NMR spectra at 162 MHz were identical except for the $^3J_{PP}$ couplings, which were not as well resolved as those at 40.5 MHz. Mass spectrum (EI, 70 eV) calc. for $C_{22}H_{45}O_{22}Os_3P_5$ (P) (computer simulation of P$^+$ pattern), *m/e* 1388, found, *m/e* 1387 (excellent agreement with computer simulated pattern), also *m/e* 1235 [P-P(OCH$_3$)$_3$-2Me]$^+$ and *m/e* 1207, 1179, 1151 (corresponding to successive loss of three carbonyl ligands from the previous ion). Anal. calc. for $C_{22}H_{45}O_{22}Os_3P_5$: C, 19.05; H, 3.27; P, 11.17. Found: C, 18.94; H, 3.28; P, 11.13.

Preparation of $Os_3[P(OCH_3)_3]_6(CO)_6$. Dodecacarbonyl triosmium (0.50 g, 0.55 mmol), $P(OCH_3)_3$ (4 mL, excess), and heptane (20 mL) were placed in a glass Carius tube. The reaction mixture was degassed three times and subsequently heated, with stirring, at 140-145 °C for 24 h. The tube was cooled and the solution degassed once. The precipitated orange solid was redissolved at 100 °C. The stirred solution was then irradiated with UV light for 48 h. During this period, an orange solid precipitated. The reaction mixture was transferred to a Schlenk tube and the orange solution was decanted off. The remaining orange solid was successively washed with hexane (5x10 mL) and hexane:toluene (1:1, v/v, 3x10 mL), affording analytically pure $Os_3[P(OCH_3)_3]_6(CO)_6$ as an orange solid (0.25 g, 31%).

As described previously, this reaction appeared to proceed by successive substitution of trimethyl phosphite for CO. Sufficient time must be allowed for the tetra- and pentasubstituted species to react. Upon prolonged irradiation, however, $Os_3[P(OCH_3)_3]_6(CO)_6$ slowly underwent metal-metal bond scission, yielding monomeric phosphite-carbonyl products (vide infra).

The hexasubstituted product slowly decomposed in air over a two week period. Recrystallization from toluene or slow diffusion of hexane into concentrated CH_2Cl_2 solutions of $Os_3[P(OCH_3)_3]_6(CO)_6$ yielded nicely formed, red-orange crystals. The hexa(phosphite) product was only moderately soluble in acetone and hot toluene and insoluble in hexane: mp 166.5-168 °C

(dec.); IR ν(CO) (CH_2Cl_2) 2013 (vw), 1938 (sbr), 1881 (w) cm^{-1}; ^1H NMR (CD_2Cl_2, -50 °C, 400.13 MHz) δ 3.53 (doublet, J_{PH}= 11.2 Hz); $^{13}C\{^1H\}$ NMR (CH_2Cl_2/CD_2Cl_2 (4:1), -57 °C, 100.6 MHz) δ 203.4 (triplet, J_{PC}= 12 Hz); $^{31}P\{^1H\}$ NMR (toluene-d_8/toluene (1:5), 30 °C, 40.5 MHz) δ -42.0 (singlet); $^{31}P\{^1H\}$ NMR (toluene-d_8/toluene (1:5), -89 °C, 40.5 MHz) δ -39.8 (singlet); $^{31}P\{^1H\}$ NMR (CD_2Cl_2, -50 °C, 162.0 MHz) δ -41.4 (singlet); $^{31}P\{^1H\}$ NMR (CD_2Cl_2, 25 °C, 162.0 MHz) δ -42.6 (broad singlet). Further details of the temperature dependent ^1H and $^{31}P\{^1H\}$ NMR behaviour of this complex are given in the text of chapter 6; mass spectrum (EI, 70 eV) calc. for $C_{24}H_{54}O_{24}Os_3P_6$ (P) (computer simulation of P^+ pattern), *m/e* 1484, found, *m/e* 1484 (very weak and not of the same shape as computer simulated pattern). The $[P-P(OCH_3)_3-2Me]^+$ ion, *m/e* 1330, was the highest mass with the proper pattern (also very intense for $Os_3[P(OCH_3)_3]_5(CO)_7$). Masses corresponding to the successive loss of two CO ligands from this ion were also observed. Anal. calc. for $C_{24}H_{54}O_{24}Os_3P_6$: C, 19.44; H, 3.67; P, 12.53. Found: C, 19.21; H, 3.75; P, 12.63.

Preparation of $Os_3[P(OCH_3)_3]_5\{P(OC_2H_5)_3\}(CO)_6$. A glass Carius tube was charged with $Os_3[P(OCH_3)_3]_5(CO)_7$ (0.20 g, 0.14 mmol), $P(OC_2H_5)_3$ (3 mL, excess), and hexane (15 mL). The solution was degassed three times. The stirred solution was irradiated by UV light for 24 h. The resultant reaction mixture was composed of a small amount of orange solid under an orange solution. The solid and solution were transferred to separate

Schlenk tubes. The IR spectra (carbonyl region) of the solution and solid in CH_2Cl_2 indicated that the solid was a mixture of $Os_3[P(OCH_3)_3]_5(CO)_7$ and $Os_3[P(OCH_3)_3]_5\{P(OC_2H_5)_3\}(CO)_6$, while the solution contained $Os_3[P(OCH_3)_3]_5\{P(OC_2H_5)_3\}(CO)_6$ and monomeric species but little $Os_3[P(OCH_3)_3]_5(CO)_7$. The solid was washed with hexane:toluene (5:1, v/v, 3x15 mL) and dried on the vacuum line overnight. The supernatant solution was evaporated under vacuum and the resultant orange oil redissolved in hexane (20 mL). This process was repeated three times, yielding an orange oil with some orange solid evident. The oil and solid were dissolved in hexane (5 mL) and cooled to -78 °C for 12 h. The pale yellow mother liquor was decanted away from a tacky orange solid, which was washed with hexane (3x10 mL) and dried on the vacuum line. An infrared spectrum (carbonyl region) in CH_2Cl_2 indicated both $Os_3[P(OCH_3)_3]_5(CO)_7$ and $Os_3[P(OCH_3)_3]_5\{P(OC_2H_5)_3\}(CO)_6$ were present, the latter being the major component. This solid was combined with that from the original reaction mixture.

These combined orange solids were dissolved in toluene (3 mL) and chromatographed on a Florisil column (3.5x7 cm) prepared as before. Elution with toluene:$P(OCH_3)_3$ (10:1, v/v) caused development of an orange band, which was discarded. A red-orange band remained at the top of the column. The adsorbent from the top 2 cm of the column was physically transferred to a 500 mL flask and repeatedly extracted with CH_2Cl_2:$P(OCH_3)_3$ (1:1, v/v). The combined yellow extracts were stripped on the vacuum line to

leave an orange-red oil containing a small amount of orange solid. This material was sublimed at 60 °C onto a -78 °C probe ($<10^{-3}$ torr) for one week. During this period, small amounts of clear liquid impurities sublimed, leaving an orange semi-solid as a residue. This solid was dissolved in CH_2Cl_2, filtered, and evaporated to dryness under vacuum. This product was recrystallized from hot hexane at -15 °C to give orange crystals. The crystals were dried on the vacuum line to yield analytically pure $Os_3[P(OCH_3)_3]_5\{P(OC_2H_5)_3\}(CO)_6$. The yield was approximately 25 mg (~10%): mp 151-152.5 °C (dec.); IR ν(CO) (CH_2Cl_2) 1935 (sbr), 1879 (wbr) cm^{-1}; ^1H NMR (toluene-d_8, 25 °C, 100.1 MHz) δ 4.11 (broad quartet with fine structure, J= ~7 Hz, rel. int.= 2), δ 3.59 (broad multiplet, rel. int.= 16), δ 1.29 (triplet, J_{HH}= 7.0 Hz, rel. int.= 3); $^{31}P\{^1H\}$ NMR (toluene-d_8, 25 °C, 162.0 MHz) δ -41.4 (doublet, J_{PP}= 10.5 Hz, rel. int.= 1), δ -41.8 (doublet, J_{PP}= 9.0 Hz, rel. int.= 1), δ -42.7 (broad singlet with asymmetric shoulders, rel. int.= 3), δ -47.6 (doublet, J_{PP}= 10.4 Hz, rel. int.= 1); $^{31}P\{^1H\}$ NMR (toluene-d_8, 80 °C, 162.0 MHz) δ -41.4 (doublet, J_{PP}= 10.6 Hz, rel. int.= 1), δ -41.9 (ill-resolved doublet, rel. int.= 1), δ -42.7 (singlet with asymmetric shoulders, rel. int.= 3), δ -47.5 (doublet, J_{PP}= 9.6 Hz, rel. int.= 1). Anal. calc. for $C_{27}H_{60}O_{24}Os_3P_6$: C, 21.26; H, 3.96. Found: C, 21.72; H, 3.81.

Preparation of $Os[P(OCH_3)_3](CO)_4$ and $Os[P(OCH_3)_3]_2(CO)_3$. A glass Carius tube was charged with $Os_3(CO)_{12}$ (0.60 g, 0.66 mmol), $P(OCH_3)_3$ (4 mL, excess), and heptane (15 mL). The

solution was degassed three times. The stirred reaction mixture was heated to 115 °C for one week. An IR spectrum (carbonyl region) of the golden yellow solution indicated the presence of $Os[P(OCH_3)_3](CO)_4$ and $Os[P(OCH_3)_3]_2(CO)_3$, in addition to smaller amounts of the complexes $Os_3[P(OCH_3)_3]_x(CO)_{12-x}$ (x= 2-5). The solvent and excess $P(OCH_3)_3$ were removed under vacuum at 0 °C and the resultant orange oil sublimed at 0 °C onto a -78 °C probe ($<10^{-3}$ torr) for 24 h. An IR spectrum (carbonyl region) of the sublimate (white solid) indicated the presence of an $Os[P(OCH_3)_3](CO)_4$:$Os[P(OCH_3)_3]_2(CO)_3$ mixture in an approximate 10:1 molar ratio. An analytically pure sample of $Os[P(OCH_3)_3](CO)_4$ was obtained from a subsequent sublimation of the probe material under the same conditions. Further sublimation of the original residue, at 35 °C onto a -78 °C probe ($<10^{-3}$ torr) for 24 h, afforded a white solid sublimate. The infrared spectrum of this material exhibited carbonyl signals due to $Os[P(OCH_3)_3](CO)_4$ and $Os[P(OCH_3)_3]_2(CO)_3$ in an approximate 1:10 ratio. Recrystallization of the sublimate from hexane at -15 °C yielded analytically pure $Os[P(OCH_3)_3]_2(CO)_3$.

Although both the mono- and disubstituted phosphite derivatives may be recrystallized from hexane, the high solubility of $Os[P(OCH_3)_3](CO)_4$ results in poor yields for this complex. When pure, both $Os[P(OCH_3)_3](CO)_4$ and $Os[P(OCH_3)_3]_2(CO)_3$ are colourless crystals which are very soluble in polar and nonpolar solvents alike. Both yellow upon exposure to air, although the disubstituted complex is

considerably more robust.

$Os[P(OCH_3)_3](CO)_4$: mp 45.5-46.5 °C (dec.); IR ν(CO) (hexane) 2073 (s), 1997 (m), 1963 (vs), 1950 (vs) cm^{-1}; ^1H NMR ($CDCl_3$, 25 °C, 60 MHz) δ 3.60 (doublet, J_{PH}= 12.0 Hz); $^{31}P\{^1H\}$ NMR (hexane, 25 °C, 40.5 MHz) δ -23.3 (singlet); mass spectrum (EI, 70 eV) calc. for $C_7H_9O_7OsP$ (P) (computer simulation of P^+ pattern), *m/e* 428, found, *m/e* 428 (excellent agreement with computer simulated pattern), also *m/e* 400 ($[P-CO]^+$). Anal. calc. for $C_7H_9O_7OsP$: C, 20.69; H, 3.47. Found: C, 20.89; H, 3.53.

$Os[P(OCH_3)_3]_2(CO)_3$: mp 61.5-62.0 °C (dec.); IR ν(CO) (hexane) 1925 (s), 1915 (s) cm^{-1}; ^1H NMR (acetone-d_6, 25 °C, 100.13 MHz) δ 3.70 (singlet, rel. int.= 9), δ 3.64 (broad singlet, rel. int.= 18), δ 3.57 (singlet, rel. int.= 9); $^{31}P\{^1H\}$ NMR (hexane, 25 °C, 40.5 MHz) δ -16.5 (singlet); mass spectrum (EI, 70 eV) calc. for $C_9H_{18}O_9OsP_2$ (P) (computer simulation of P^+ pattern), *m/e* 524, found *m/e* 524 (excellent agreement with computer simulated pattern), also *m/e* 496 ($[P-CO]^+$). Anal. calc. for $C_9H_{18}O_9OsP_2$: C, 19.72; H, 2.13. Found: C, 19.92; H, 1.99.

Preparation of $Os_3[P(OCH_2)_3CCH_3](CO)_{11}$ and $Os_3[P(OCH_2)_3CCH_3]_2(CO)_{10}$. A glass Carius tube was charged with $Os_3(CO)_{12}$ (0.500 g, 0.551 mmol), $P(OCH_2)_3CCH_3$ (0.735 g, 4.96 mmol), and hexane (20 mL). The solution was degassed three times. The stirred solution was heated at 130 °C for 2 h. At this point, the reaction mixture consisted of yellow and orange solids under a yellow solution. The mixture was transferred to a

Schlenk tube and the solution discarded. The solids were sublimed at 25 °C onto a -78 °C probe ($<10^{-3}$ torr) for 2 h to remove excess $P(OCH_2)_3CCH_3$. The residue was dissolved in toluene:CH_2Cl_2 (10:1, 10 mL) and placed on a $P(OCH_3)_3$-deactivated Florisil column packed in hexane. Elution with hexane:toluene (1:1) caused separation of a yellow band which was collected. Subsequent elution with toluene:CH_2Cl_2 (5:1) allowed collection of a second yellow band, leaving a small yellow-orange band near the top of the column.

The first fraction was stripped on the vacuum line to give yellow crystals. These were dissolved in CH_2Cl_2 (15 mL) and the solution filtered. Removal of the solvent under vacuum gave $Os_3[P(OCH_2)_3CCH_3](CO)_{11}$ as yellow crystals (0.180 g, 32 %) which were recrystallized from toluene:hexane at -15 °C: mp 174.5-176 (dec); IR ν(CO) (hexane) 2114 (w), 2058 (s), 2048 (s), 2026 (vs), 2004 (m), 1995 (s), 1977 (w) cm^{-1}; ^1H NMR (acetone-d_6, 25 °C, 400.13 MHz) δ 4.47 (doublet, J_{PH}= 5.3 Hz, rel int.= 2), δ 0.89 (singlet, rel. int.= 1); $^{31}P\{^1H\}$ NMR (toluene-d_8/toluene (1:4), 25 °C, 40.54 MHz) δ -58.3 (singlet), $^{31}P\{^1H\}$ NMR (-60 °C) δ -58.9 (singlet); mass spectrum calc. for $C_{15}H_9O_{13}Os_3P$ (P) (computer simulated parent ion pattern). *m/e* 1028, found, *m/e* 1028 (excellent agreement with simulated pattern), also *m/e* 1000, 972, 944, 916, and 888 ($[P-nCO]^+$ n=1-5). Anal. calc. for $C_{15}H_9O_{13}Os_3P$: C, 18.72; H, 0.88. Found: C, 18.83; H, 0.77.

Crystals of $Os_3[P(OCH_2)_3CCH_3](CO)_{11}$ appeared air stable for several months. The compound was moderately soluble in hexane,

soluble in toluene, and very soluble in CH_2Cl_2.

The second fraction was stripped on the vacuum line to give an oily, yellow-orange solid. This was dissolved in CH_2Cl_2 (15 mL) and the solution was filtered. Vacuum removal of the solvent gave a yellow-orange crystalline solid (0.210 g, 33 %). Recrystallization by slow diffusion of hexane into a toluene solution of the solid gave orange-yellow crystals. These crystals gave an elemental analysis consistent with $Os_3[P(OCH_2)_3CCH_3]_2(CO)_{10}\cdot 1/2C_7H_8$. Heating these at 100 °C for 24 h under vacuum left an orange-yellow powder which gave a satisfactory analysis for $Os_3[P(OCH_2)_3CCH_3]_2(CO)_{10}$: mp 265-268 °C (dec); IR ν(CO) (CH_2Cl_2) 2097 (w), 2040 (s), 2025 (m), 2010 (vs), 1976 (mbr) cm^{-1}; ^1H NMR (acetone-d_6, 25 °C, 100.0 MHz) δ 4.39 (doublet, J_{PH}= 5.1 Hz, rel. int.= 2), δ 0.9 (singlet, rel. int.= 1); $^{31}P\{^1H\}$ NMR (toluene-d_8, 97 °C, 40.54 MHz) δ -58.9 (very broad singlet), $^{31}P\{^1H\}$ NMR (toluene-d_8, -37 °C, 40.54 MHz) δ -57.9 (doublet, J_{PP}= 3.6 Hz, rel. int.= 5), δ -59.5 (doublet, J_{PP}= 3.7 Hz, rel. int.= 5), δ -60.4 (singlet, rel. int.= 2); mass spectrum calculated for $C_{20}H_{18}O_{16}Os_3P_2$ (P) (computer simulated parent ion pattern): *m/e* 1148, found *m/e* 1148 (excellent agreement with simulated pattern), also *m/e* 1120, 1092, 1064, 1036, 1008 ([P-nCO]$^+$ n=1-5). Anal. calc. for $C_{20}H_{18}O_{16}Os_3P_2$: C, 20.95; H, 1.58. Found: C, 21.04; H, 1.51.

After several months exposure to air, $Os_3[P(OCH_2)_3CCH_3]_2(CO)_{10}$ sufferred not apparent decompostion. The complex was sparingly soluble in hexane, moderately soluble

in toluene, and very soluble in CH_2Cl_2.

Attempts to Synthesize $Os_3[P(OCH_3)_3]_x(CO)_{12-x}$ (x>6). A sample of $Os_3[P(OCH_3)_3]_6(CO)_6$ (~0.1 g) was dissolved in toluene/$P(OCH_3)_3$ (15 mL:4 mL) and placed in a glass Carius tube. After three freeze-pump-thaw cycles, the reaction solution was photolyzed for 48 h, the results of which were monitored by IR spectroscopy (carbonyl region). The absorption due to $Os_3[P(OCH_3)_3]_6(CO)_6$ slowly disappeared during this period, as the solution color changed from orange to pale yellow. Although a number of carbonyl bands were present in the infrared spectrum at this time, the only ones assignable were due to $Os[P(OCH_3)_3]_2(CO)_3$.

In a further attempt to increase the phosphite substitution of $Os_3[P(OCH_3)_3]_6(CO)_6$, a glass Carius tube was charged with this reactant (~0.15 g) in heptane/$P(OCH_3)_3$ (15 mL:15 mL) and the mixture degassed as before. The stirred reaction mixture was heated for 1 week at 110 °C. Over this period, the orange solid slowly dissolved, leaving a bright yellow solution with a small amount of white, flocculent precipitate. An IR spectrum of the solution revealed a number of carbonyl absorptions; the only bands assigned were again those due to $Os[P(OCH_3)_3]_2(CO)_3$.

Attempted Reaction of $Os_3[P(OCH_3)_3]_4(CO)_8$ with CO. A solution of $Os_3[P(OCH_3)_3]_4(CO)_8$ (.05 g) in toluene (2 mL) was introduced into a glass NMR tube fitted with a Teflon valve. The solution was degassed three times, pressurized with CO (2 atm),

and irradiated by ultraviolet light. As monitored by $^{31}P\{^{1}H\}$ NMR spectroscopy, there were no spectral changes (e.g. a free $P(OCH_3)_3$ resonance) after 8.5 h photolysis.

Attempted Protonation of $Os_3[P(OCH_3)_3]_4(CO)_8$. A sample of solid NH_4PF_6 (0.015 g, 0.09 mmol) was added to a THF solution (20 mL) of $Os_3[P(OCH_3)_3]_4(CO)_8$ (0.080 g, 0.062 mmol) in a 100 mL Schlenk tube. The reaction mixture was stirred under N_2 for 24 h. The solvent was removed under vacuum and the orange residue extracted with CH_2Cl_2. After filtering, the extracts were stripped to dryness on the vacuum line to yield an orange solid, identified by IR spectroscopy (carbonyl region) as $Os_3[P(OCH_3)_3]_4(CO)_8$.

Attempted Protonation of $Os_3[P(OCH_3)_3]_6(CO)_6$. A solution of $Os_3[P(OCH_3)_3]_6(CO)_6$ (0.235 g, 0.158 mmol) in CH_2Cl_2 (10 mL) and hexane (10 mL) was prepared in a Schlenk tube. To this stirred solution was slowly added $HBF_4 \cdot Et_2O$ (0.0255 mL, 0.158 mmol). The solution immediately turned deep red as some red oil precipitated. After 5 minutes, the volatiles were removed under vacuum to give a mixture of light and dark orange solids. An IR spectrum (carbonyl region) of the product (in CH_2Cl_2) revealed a number of absorptions. The solid was washed with hexane:CH_2Cl_2 (1:1, 2x20 mL) and dried under vacuum. Further purification was attempted by slow addition of hexane to a CH_2Cl_2 solution (15 mL) of the solid. The resultant orange oil was collected in two fractions. The first gave a mixture of light and dark orange solids after evaporation on the vacuum line. An IR spectrum

(carbonyl region) of these solids showed little change from that of the initial product. The second fraction afforded a dark orange solid after vacuum removal of the solvent. An IR spectrum of this solid (in CH_2Cl_2) showed two strong ν(CO) bands (2032 (s), 1993 (s) cm^{-1}) and a number of shoulders. These two absorptions featured prominently in the IR spectrum of the crude product.

An elemental analysis of the product from the second fraction was consistent with the expected product (Calc. for $\{HOs_3[P(OCH_3)_3]_6(CO)_6\}BF_4$: C, 18.35; H, 3.53. Found: C, 17.68; H, 3.26). The variable temperature ^1H and $^{31}P\{^1H\}$ NMR data, however, were inconsistent with this formulation. Neither the ^1H nor the $^{31}P\{^1H\}$ NMR spectrum were temperature dependent. The $^{31}P\{^1H\}$ NMR spectrum (CD_2Cl_2) revealed four multiplets in addition to several impurities. A spectrum obtained by selectively decoupling only the OCH_3 protons was identical to that measured with both the methoxy and hydride regions decoupled. The ^1H NMR spectrum (CD_2Cl_2) showed a complex methoxy multiplet (δ 3.77) and several weak multiplets in the region δ -15 to -25. None of these multiplets were consistent with any rational coupling scheme expected for $\{HOs_3[P(OCH_3)_3]_6(CO)_6\}BF_4$.

$^{31}P\{^1H\}$ NMR Study: Reaction of $Os_3[P(OCH_3)_3]_6(CO)_6$ and CH_3I. A 5 mm NMR tube with a screw cap and Teflon liner was charged with a solution of $Os_3[P(OCH_3)_3]_6(CO)_6$ (0.03 g) and CH_3I (0.1 mL) in CD_2Cl_2 (1 mL). The tube was sealed and the contents were monitored by $^{31}P\{^1H\}$ NMR spectroscopy. No apparent reaction

occurred over the course of 72 h.

CHAPTER 6

Phosphite Derivatives of Osmium. Structure and Stereochemical Nonrigidity in $Os_3[P(OCH_3)_3]_x(CO)_{12-x}$ (x= 1-6)

6.1 Introduction

A number of studies concerning the stereochemical nonrigidity of $Os_3(CO)_{12}$ and its derivatives have been reported (vide infra). These results indicate that several different fluxional processes are possible, dependent upon the identity of the complex in question. In addition, the evidence suggests that two or more distinct exchange processes may occur for the same compound at different temperatures. Much of the experimental support for these conclusions comes from variable temperature NMR data.

What appear to be lacking are systematic studies where a closely related group of compounds are examined. Such experiments can potentially allow important conclusions to be drawn regarding the factors which control the individual fluxional processes; the elucidation of the relative influence that steric, electronic, and geometric elements play may be facilitated.

It was felt that variable temperature ^1H, ^{13}C, and $^{31}P\{^1H\}$ NMR data for the series $Os_3[P(OCH_3)_3]_x(CO)_{12-x}$ (x= 1-6) would satisfy these criteria. Before examining these results, a brief summary of the literature regarding stereochemical nonrigidity

in $Os_3(CO)_{12}$ and related derivatives will be presented.

Of the trinuclear carbonyls of the iron triad, only $Os_3(CO)_{12}$ (**6a**) exhibits a low temperature limiting ^{13}C NMR spectrum at accessible temperatures; both the iron and ruthenium congeners give rise to a single resonance in the carbonyl region at -100 °C [140,141,142]. Indeed, $Fe_3(CO)_{12}$ has been shown to undergo rapid axial-equatorial carbonyl exchange at -150 °C [143,144].

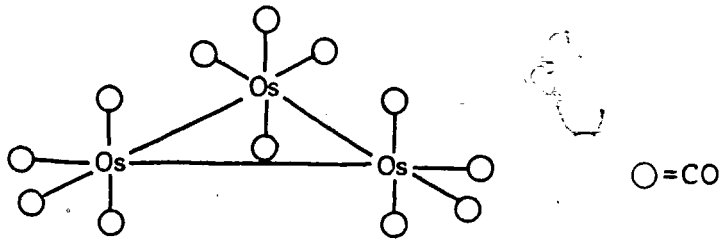

6a

The ^{13}C NMR spectrum of $Os_3(CO)_{12}$ at room temperature features two signals of equal intensity (axial and equatorial carbonyls). As the temperature is increased, these resonances broaden and collapse; the rapid exchange of axial and equatorial ligands causes only a single line to be observed at 150 °C [141,142]. Some recent and very elegant work, involving a variable temperature ^{13}C NMR study of $^{187}Os_3(^{13}CO)_{12}$, has shown that the exchange process occurs via an internuclear mechanism where all CO groups have access to the three osmium atoms [145].

An examination of stereochemical nonrigidity in $Os_3[PEt_3]_x(CO)_{12-x}$ (x= 1-3) by ^{13}C NMR techniques has been

undertaken [111]. For both the mono- and disubstituted derivatives, two distinct fluxional processes were shown to occur at different temperatures. The one with the lowest energy caused temperature dependent NMR spectral changes consistent with a mechanism involving an intermediate with a double carbonyl bridge. This mechanism was first postulated by Cotton [143] (figure 6.1). A higher energy process caused broadening, collapse, and coalescence of all carbonyl signals; this resulted in a single resonance at ~40 °C. No firm conclusions were drawn regarding this behaviour.

The variable temperature ^{13}C and $^{31}P\{^{1}H\}$ NMR data for 1,1- and 1,2-$\{Os_3[P(CH_3)_2C_6H_5]_2(CO)_{10}\}$ have been reported [108]. The ^{13}C NMR results for the 1,1 isomer indicated two successive stages of fluxionality, the lower energy one consistent with the

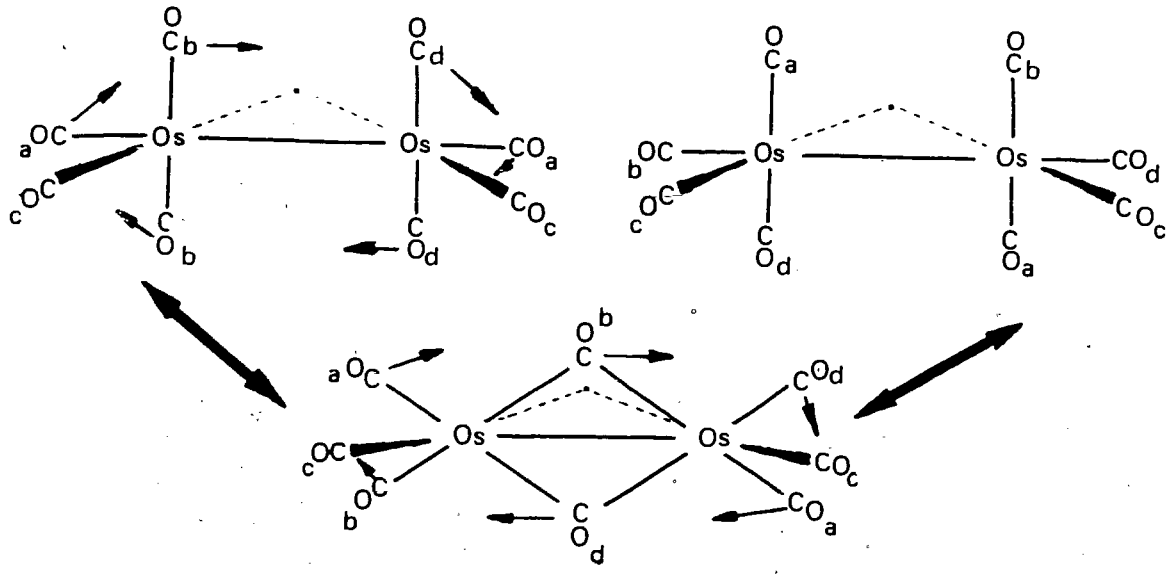

Figure 6.1 A general representation of axial-equatorial carbonyl exchange via a double carbonyl bridge intermediate.

exchange mechanism shown in figure 6.1. The process occurring at higher energy was attributed to a "turnstile" mechanism, although there was no speculation on the permutational details. The $^{31}P\{^{1}H\}$ NMR spectra of 1,2-$\{Os_3[P(CH_3)_2C_6H_5]_2(CO)_{10}\}$ were measured over the temperature range -80 °C to 100 °C [107,108]. The presence of two isomers was indicated. The changes to the spectra with temperature were attributed to the exchange of the inequivalent PMe_2Ph ligands in one isomer, followed by interconversion between the two isomers. The isomers were assigned to the structures shown in figure 6.2. The low temperature ^{13}C NMR spectrum of this complex showed carbonyl signals due only to the major isomer (a), precluding a more detailed investigation of the exchange processes involved. Some of these results concerning the 1,2 isomer are closely related to the findings presented in this thesis and will be discussed further later.

The variable temperature ^{31}P and ^{13}C NMR spectra for 1,2,3-$\{Os_3[P(OCH_3)_3]L_2(CO)_9\}$ (L= PPh_3, PMe_2Ph) were measured and details of the PPh_3 complex described [107]. It was claimed that the changes in these spectra with temperature were in accord with a coupled "turnstile" mechanism, involving all three osmium atoms. Again, these results are related to our work and will be commented upon in more detail later in this chapter.

Another site exchange mechanism has been proposed for substituted derivatives of $Os_3(CO)_{12}$. The norbornadiene complex, $Os_3(CO)_{10}(C_7H_8)$, has been prepared and studied by variable

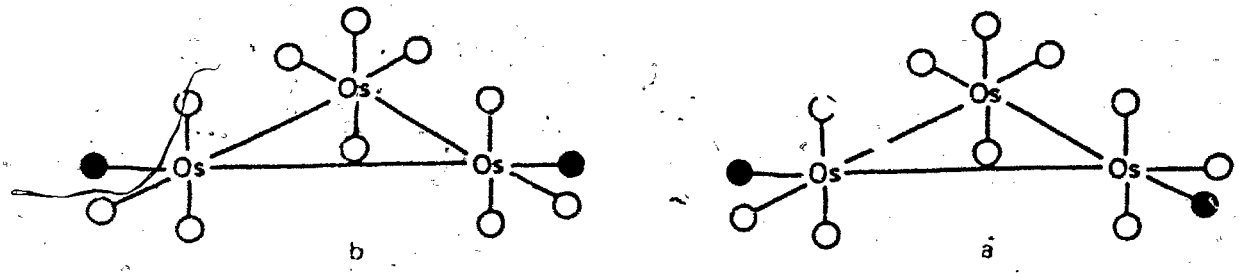

●=PMe_2Ph ○=CO

Figure 6.2 The two proposed isomers for 1,2-{$Os_3[P(CH_3)_2C_6H_5]_2(CO)_{10}$}.

temperature ^{13}C and ^{1}H NMR techniques [146]. Two successive fluxional processes were inferred from the NMR data. The spectral changes due to the one occurring at the lowest temperature were consistent with a mechanism involving three single carbonyl bridges; this is pictured in figure 6.3. This type of exchange has been proposed [147,148] and discussed [140,149] by other workers and is commonly called the "merry-go-round" process. It is of interest to note the difference between this process and that pictured in figure 6.1.

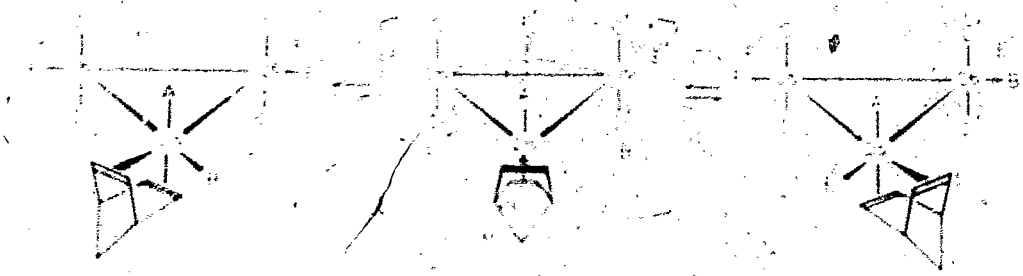

Figure 6.3 The mechanism suggested for the lowest energy carbonyl scrambling process in $Os_3(CO)_{10}(C_7H_8)$. (from reference 146).

Both involve bridging carbonyls but the latter causes axial-equatorial CO exchange while the "merry-go-round" involves only equatorial ligands.

A third type of fluxionality proposed for substituted derivatives of $Os_3(CO)_{12}$ may be generally described as localized exchange at an osmium atom. Various specific examples have been labelled "turnstile" exchanges [107,108], polytopal rearrangements [40,150], and "twist" mechanisms [148]. One early description of this type of exchange was presented as a possible mode for axial-equatorial carbonyl scrambling in $M_3(CO)_{12}$ (M= Ru, Os) [141]. The permutational details are shown in figure 6.5. In essence, this might be labelled a pseudo-fourfold rotation of four carbonyl ligands about a single metal centre. It is relatively simple to picture such a process involving only one axial and two equatorial ligands; this might be described as a pseudo-threefold rotation. The description of these two processes as rotations is illustrated in figure 6.4 [140].

There is considerable precedent in the literature for these localized processes at a single metal centre [140,149].

Figure 6.4 Pseudo-threefold and -fourfold rotations of carbonyl ligands at a single metal centre of a trimetallic cluster.

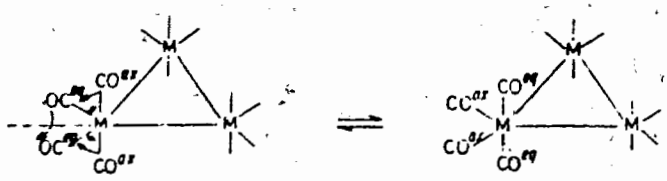

Figure 6.5 A localized process proposed to explain axial-equatorial site exchange in $M_3(CO)_{12}$ [M= Ru, Os].

Temperature dependent changes in the ^{13}C NMR spectra of $Os_3(CO)_{10}HX$ (X= SEt, SPh, N(H)Bu, OH, Cl, Br, I, CO_2Me, CO_2CF_3) [151] were consistent with fourfold, polytopal rearrangements of $M(CO)_4$ units. There have been reports of pseudo-threefold rotations involving $M(CO)_3$ moieties for $(C_8H_8N_2)Os_3(CO)_{10}$ [152], $Fe_3(\mu_3\text{-}PC_6H_5)_2(CO)_9$ [153], $[Os_3(CO)_{10}(\mu\text{-}NO)]^-$ [154], $Os_6(CO)_{18}$ [155], and $Os_3(CO)_{10}(C_6H_8)$ [148], based on variable temperature ^{13}C NMR data. The case for $Os_3(CO)_{10}(C_6H_8)$ was ambiguous, and either a threefold or fourfold process appeared capable of explaining the spectral changes. Polytopal rearrangement of $M(CO)_3$ units has been proposed for $H_2Os_3(CO)_{10}L$ (L= PR_3, $P(OR)_3$, CNR, AsR_3) [156,157], $H_2FeRu_3(CO)_{13}$ [158,159], $H_2FeRu_2Os(CO)_{13}$ [159], and $H_2FeRuOs_2(CO)_{13}$ [159], although bridging carbonyls and bridging hydrides were believed to be involved in these trigonal exchange processes.

The complexity sometimes observed for site exchange in derivatives of $Os_3(CO)_{12}$ is illustrated by the dynamic behaviour of $Os_3(CO)_{10}(C_6H_8)$. The temperature dependent ^{13}C (carbonyl region) and ^1H NMR spectra of the complex were measured and the

slow exchange limiting ^{13}C data suggested that the 1,3-cyclohexadiene ligand occupied an axial and equatorial site on the same osmium atom [148]. The spectral changes with temperature revealed the existence of four independent, dynamic processes for $Os_3(CO)_{10}(C_6H_8)$ involving site exchange of both the organic moiety and the various carbonyl ligands.

Our results concerning the stereochemical nonrigidity of $Os_3[P(OCH_3)_3]_5(CO)_7$ have been published [112]. A restricted threefold twist of an $Os(CO)_2P(OCH_3)_3$ unit was proposed to rationalize the variable temperature ^{13}C and $^{31}P\{^1H\}$ NMR data. Other workers have concurrently arrived at a similar (although less well defined) conclusion for the fluxional behaviour of 1,2-$\{Os_3[P(CH_3)_2C_6H_5]_2(CO)_{10}\}$ and 1,2,3-$\{Os_3[P(OCH_3)_3]L_2(CO)_9\}$ (L= PPh_3, PMe_2Ph) [107,108]. To our knowledge, these were the first reports of a pseudo-threefold exchange involving an $ML(CO)_2$ moiety attached to an $M_3(CO)_{12}$ derivative.

In this chapter, results of the variable temperature ^1H, ^{13}C, and $^{31}P\{^1H\}$ NMR studies for the series of complexes $Os_3[P(OCH_3)_3]_x(CO)_{12-x}$ (x= 1-6) are reported. Two different fluxional processes are proposed. When invoked individually or in combination, these can completely explain the observed temperature dependent NMR data. The factors which appear to affect the activation energies of these two processes are discussed. The overall results are also compared to those from similar, stereochemically nonrigid systems.

6.2 Structure and Stereochemical Nonrigidity

The interpretation of the variable temperature NMR data for each member of the series $Os_3[P(OCH_3)_3]_x(CO)_{12-x}$ (x= 1-6) was aided by information derived from the results for the other members. The analysis of the temperature dependent ^{13}C and $^{31}P\{^1H\}$ NMR data for $Os_3[P(OCH_3)_3]_5(CO)_7$ was reasonably straightforward and led to some firm conclusions regarding the site exchange mechanism involved. Consequently, this complex will be discussed first, followed by the other members of the series in an order which builds on the results obtained from the previous members.

6.2.1 $Os_3[P(OCH_3)_3]_5(CO)_7$

The exclusive adoption of equatorial sites by phosphorus donor ligands in substituted derivatives of $Os_3(CO)_{12}$ has been discussed in chapter 5. Based on this premise, the only possible structure for $Os_3[P(OCH_3)_3]_5(CO)_7$, in the slow exchange limit, is **6b**.

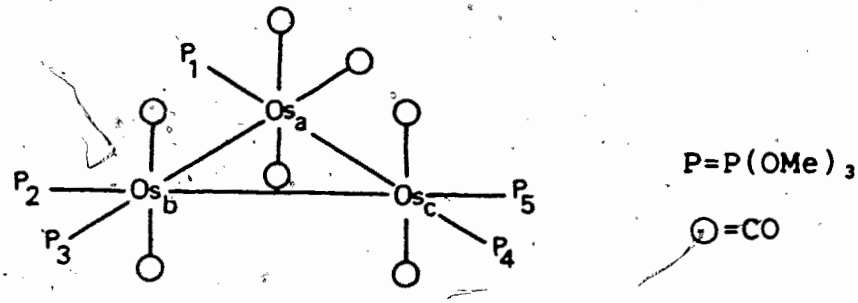

6b

The low temperature $^{13}C\{^1H\}$ NMR spectrum of $Os_3[P(OCH_3)_3]_5(CO)_7$ (25.2 MHz) is consistent with this structure. At -50 °C, four carbonyl resonances of relative intensity 2:2:2:1 are observed at δ 199.7, 199.2, 194.1, and 179.2 ppm; the first two appear as overlapping triplets (J_{PC}= 11.5 and 11.4 Hz, respectively), the third as a doublet (J_{PC}= 11.4 Hz), and the high field resonance as a singlet. The ^{13}C NMR spectrum measured at 100.6 MHz (-44 °C), shows the two triplets completely resolved with respect to chemical shift, although the coupling is poorly resolved (see figure 6.6).

The doublet may be assigned to the axial carbonyl groups of the singly substituted Os_a in **6b**, while the singlet is due to the unique equatorial carbonyl ligand. The coupling of phosphorus ligands to only axial carbonyl groups has been observed in similar systems [107,111]. The two triplets may be assigned to inequivalent axial pairs of carbonyl groups on Os_b and Os_c in **6b**.

It is worthwhile to note two points here. The signals due to axial carbonyl groups occur at lower fields than that due to the equatorial counterpart. This phenomenon appears quite general for derivatives of $M_3(CO)_{12}$ (M= Fe, Ru, Os) and has been mentioned in the literature [111,146,156]. More importantly, the resonances due to the axial CO groups bonded to Os atoms bearing two phosphite ligands occur at lower field than that due to the axial carbonyl groups on the $Os[P(OCH_3)_3](CO)_3$ moiety. This

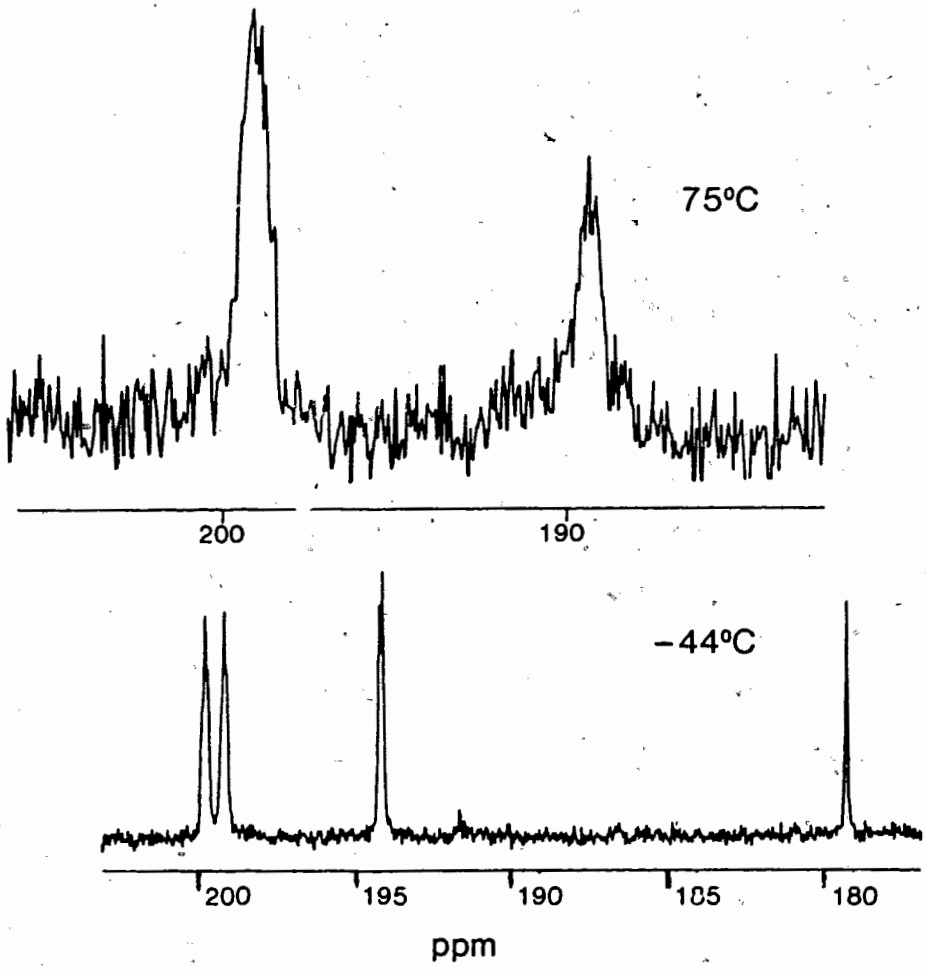

Figure 6.6 Low and high temperature $^{13}C\{^{1}H\}$ NMR spectra of $Os_3[P(OCH_3)_3]_5(CO)_7$ in toluene-d_8 measured at 100.6 and 25.2 MHz respectively.

behaviour was found to be part of a useful empirical relationship for the series $Os_3[P(OCH_3)_3]_x(CO)_{12-x}$ (x= 1-6) and will be discussed later in this chapter.

The $^{31}P\{^1H\}$ NMR spectrum of $Os_3[P(OCH_3)_3]_5(CO)_7$ in toluene-d_8 at -57 °C (see figure 6.7) is also completely in accord with the proposed static solution structure **6b**. Five signals of equal intensity are observed, four of which are doublets. The chemical shifts and coupling constants (in brackets, Hz) are: δ -34.5 (6.4), -36.2 (6.1), -37.9 (7.6), -38.2, and -43.0 (7.3) ppm. These values are taken from the $^{31}P\{^1H\}$ NMR data measured at an operating frequency of 40.5 MHz (as opposed to 162.0 MHz for figure 6.7). The couplings are considerably better resolved at the lower frequency. The broadening at the higher operating frequency is attributed to chemical shift anisotropy [160]. The couplings are not identical but are divided into two pairs of equal magnitude, within experimental error. This result is, of course, very useful in making the spectral assignments.

There are two reasonable assignments for the slow exchange limit $^{31}P\{^1H\}$ NMR spectrum of $Os_3[P(OCH_3)_3]_5(CO)_7$, based on different assumptions concerning the observed couplings. Interpreting the spectral splittings as due to two bond *cis* coupling of magnetically inequivalent phosphorus nuclei on the same osmium atom, the singlet (at δ -38.2) might be assigned to the ligand attached to Os_a of **6b** (i.e. P_1). This assignment, however, is inconsistent with spectral changes as the

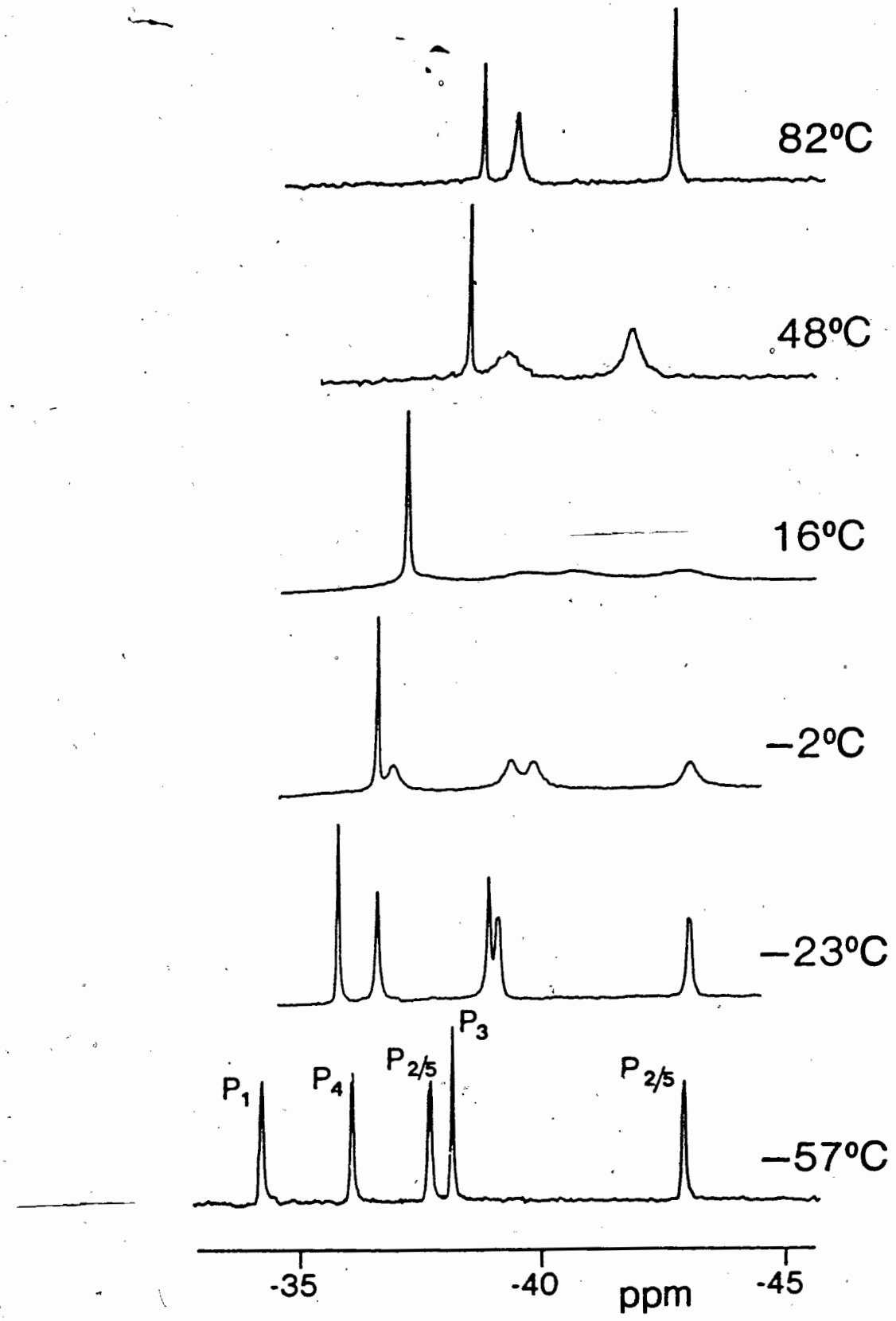

Figure 6.7 The variable temperature $^{31}P\{^{1}H\}$ NMR spectra of $Os_3[P(OCH_3)_3]_5(CO)_7$ in toluene-d_8 measured at 162.0 MHz.

temperature is increased; this resonance broadens, collapses, and ultimately coalesces with another signal (vide infra).

This behaviour was not due to an intermolecular phosphite exchange. The resonance due to added free $P(OCH_3)_3$ did not broaden during the collapse of the $Os_3[P(OCH_3)_3]_5(CO)_7$ $^{31}P\{^1H\}$ NMR spectrum. Intermolecular $P(OCH_3)_3$ exchange is thus eliminated as a possible cause for the collapse of the singlet.

The only process, then, that could cause magnetic equivalency between P_1 and any other phosphorus nucleus of $Os_3[P(OCH_3)_3]_5(CO)_7$ would have to involve phosphite exchange between two osmium atoms. It is difficult to imagine this type of exchange occurring by a mechanism other than one involving a bridging phosphite intermediate. To our knowledge only two reports suggesting such an intermediate have appeared in the literature [161,162], both involving aryl phosphines as opposed to $P(OCH_3)_3$. In neither report was any experimental evidence proposed to support the contention. It is possible that the phenyl substituent on the phosphine could be involved in the exchange of the phosphorus ligand between two metal atoms. We are of the view that phosphite ligands are incapable of bridging two metals and are supported by other researchers in the field [107,108,111]. It is noted that a definitive answer to the question of bridging phosphite intermediates in $Os_3(CO)_{12}$ derivatives might be available, based on an experiment similar to that performed by A. A. Koridze et al on $^{187}Os_3(^{13}CO)_{12}$ [145,163]. In summary, then, an assignment of the $^{31}P\{^1H\}$ NMR

resonances of $Os_3[P(OCH_3)_3]_5(CO)_7$ based on cis-$^2J_{PP}$ couplings is inconsistent with any reasonable exchange process.

The alternate assignment of the five ^{31}P signals due to $Os_3[P(OCH_3)_3]_5(CO)_7$ interprets the spectral splittings as three bond couplings betweeen magnetically inequivalent phosphorus nuclei *trans* to one another (i.e. on different Os atoms). The empirical observation that spin-spin coupling constants between ^{31}P and other spin 1/2 nuclei are often considerably larger for a *trans* orientation, relative to *cis*, has been noted and utilized by many researchers [164]. The present case appears to be a dramatic example of such behaviour, where cis-$^2J_{PP}$ is considerably smaller (i.e. unobservable) than $trans$-$^3J_{PP}$. Similar results have been found for $Os_3[P(OCH_3)_3]_4(CO)_8$ (vide infra).

Based on this premise, the previously discussed pairwise coupling constants, and the changes in the $^{31}P\{^1H\}$ NMR spectrum with temperature, the resonances of $Os_3[P(OCH_3)_3]_5(CO)_7$ may be readily assigned and a fluxional process proposed. The variable temperature $^{31}P\{^1H\}$ NMR spectra of the pentasubstituted triosmium complex are shown in figure 6.7. As a toluene-d_8 solution of this complex was heated from -57 °C, four signals (three doublets and a singlet) broadened, collapsed, and coalesced to two singlets above 80 °C. The remaining doublet sufferred only the loss of its coupling during this process. The resultant three singlets were of relative intensity 2:2:1, respectively. These changes were completely reversible and,

clearly, exchange between ^{31}P nuclei was indicated. It is stressed that the resonance due to added free $P(OCH_3)_3$ did not broaden during the collapse of the $Os_3[P(OCH_3)_3]_5(CO)_7$ spectrum, ruling out an intermolecular $P(OCH_3)_3$ exchange process. The fact that the two coalescing signals were of equal intensity argues for two pairs of resonances each collapsing to a singlet.

The observation that the low field resonance (δ -34.5) lost only its coupling during this process leads to the assignment of P_1 (see **6b**). In light of the previous discussion concerning bridging phosphites, no reasonable exchange mechanism can render P_1 equivalent to any other phosphorus nuclei of $Os_3[P(OCH_3)_3]_5(CO)_7$. The size of *trans*-$^3J_{PP}$ for this low field resonance, in concert with the previous discussion concerning these coupling constants, allows the assignment of the signal at δ -36.2 as P_4. The ligand labelled P_3 in **6b** may be ascribed to the lone singlet in the low temperature $^{31}P\{^1H\}$ NMR spectrum (δ -38.2); it is the only $P(OCH_3)_3$ ligand in $Os_3[P(OCH_3)_3]_5(CO)_7$ with no phosphorus atom in a *trans* three bond position. The two remaining resonances are attributed to P_2 and P_5. The available spectral evidence does not allow differentiation, but this is not essential to the following discussion regarding the site exchange process. In fact, the succeeding calculations allow individual assignments of this pair.

An examination of figure 6.7 indicates the considerable temperature dependence of the ^{31}P chemical shifts for $Os_3[P(OCH_3)_3]_5(CO)_7$. This is a general feature of the variable

temperature $^{31}P\{^1H\}$ NMR data in this thesis and has been observed by others [6]. It was necessary to plot the variation in ^{31}P chemical shift versus temperature, for each resonance, at or near the slow exchange limit where the individual signals were observable. These plots were then extrapolated into the temperature region of interest. A typical plot is shown in appendix 1. Note the nonlinearity of the plot and the consequent potential for large error when extrapolating to high temperatures. None the less, calculations based on this type of data were very useful. Calculating weighted average chemical shifts for all possible pairwise permutations of P_x (x= 2-5), it was found that the calculated and experimental data (fast exchange limit) were in excellent agreement only for the exchanges: $P_2 \longleftrightarrow P_5$, $P_3 \longleftrightarrow P_4$. The simplest process which would result in the observed variable temperature $^{31}P\{^1H\}$ NMR behaviour of $Os_3[P(OCH_3)_3]_5(CO)_7$ is a shift of P_1 between equatorial positions of Os_a, as indicated in figure 6.8.

The $^{13}C\{^1H\}$ NMR data for $Os_3[P(OCH_3)_3]_5(^{13}CO)_7$ (see experimental section, chapter 2, for details of ^{13}CO enrichment) over the temperature range -80 °C to 75 °C is completely consonant with the site exchange shown in figure 6.8. Over this temperature span, the two triplets broadened and coalesced to a broad singlet (figure 6.6). The spectrum measured at 2 °C clearly shows this resonance to be a single triplet (J_{PC}= 10.9 Hz). At the same time, the singlet and doublet collapsed, coalescing into a single signal. That the resultant signals

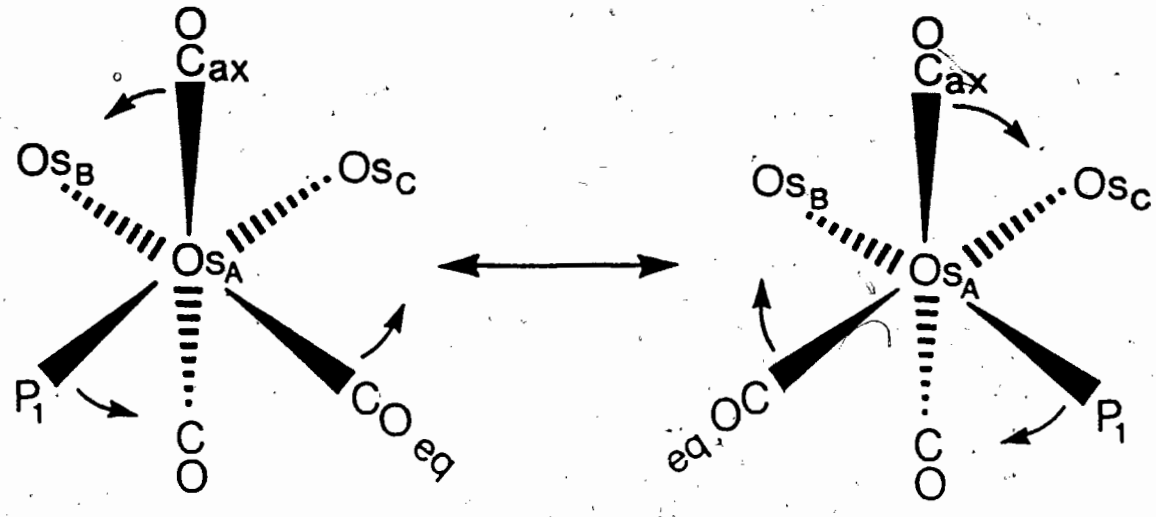

Figure 6.8 Proposed mechanism for site exchange in $Os_3[P(OCH_3)_3]_5(CO)_7$.

appear at the required weighted average position may be qualitatively observed in figure 6.6. It may be ascertained that the process in figure 6.8 would cause averaging of the signals due to the axial carbonyl ligands on osmium atoms b and c. In addition, axial-equatorial carbonyl site exchange would occur on Os_a. Furthermore, these two exchanges were qualitatively shown to occur at the same rate, taking into account chemical shift differences. This suggests that a single rearrangement was responsible. The onset of signal broadening to the resonances of both the $^{13}C\{^1H\}$ and $^{31}P\{^1H\}$ NMR spectra of $Os_3[P(OCH_3)_3]_5(CO)_7$ was observed to occur at qualitatively the same temperature (~-35 °C); this is further evidence that the same process was responsible for changes to the two sets of spectra.

The line shape for the portion of the $^{13}C\{^1H\}$ NMR spectrum of $Os_3[P(OCH_3)_3]_5(CO)_7$ due to the axial and equatorial CO

ligands of Os_a was calculated (based on the mechanism in figure 6.8). This calculated line shape was matched to an experimental spectrum in the intermediate exchange region (-20 °C). The agreement between the simulated and observed data was good. The rate constant for this simulated spectrum (k= 40±2 sec^{-1}) was used to calculate a value for the free energy of activation at the temperature of the experimental spectrum (253±2 °K): $\Delta G^{\ddagger}$= 12.9±0.4 kcal mol^{-1}. The details of this calculation are presented in appendix 2.

Although the ^1H NMR spectrum of $Os_3[P(OCH_3)_3]_5(CO)_7$ was not measured over a full temperature range, the slow and fast exchange limiting spectra were in accord with the proposed static solution structure and fluxional mechanism. At -57 °C, the spectrum (measured in toluene-d_8 at 400.13 MHz) exhibited five doublets (J_{PH}= 11.5 to 12.5 Hz). This type of behaviour was observed for other members of $Os_3[P(OCH_3)_3]_x(CO)_{12-x}$ (x= 1-6) (vide infra); no virtual coupling effects were apparent and each $P(OCH_3)_3$ ligand acted like an isolated AX_9 spin system. The chemical shift of the protons appeared to be related to the magnetic environment of the local ^{31}P nucleus. A magnetically unique phosphorus (i.e. a resolved ^{31}P NMR resonance) led to a resolved doublet in the ^1H NMR spectrum. The ^1H NMR spectrum of $Os_3[P(OCH_3)_3]_5(CO)_7$ (400.13 MHz, toluene-d_8), measured at 25 °C, featured three doublets (J_{PH}= 11.5-12.5 Hz) in a relative intensity ratio of 2:2:1. The averaging of two pairs of ^{31}P NMR resonances by the process shown in figure 6.8 would lead to this

observed simplification of the proton spectrum.

A discussion regarding the uniqueness of the site exchange pictured in figure 6.8 is considered necessary. We have labelled this a "trigonal twist" mechanism, and present it as the **simplest** rearrangement capable of accounting for the observed spectral changes in $Os_3[P(OCH_3)_3]_5(CO)_7$. Note the difference between the specific trigonal twist in figure 6.8 and a **rotation**. For the former, the $P(OCH_3)_3$ ligand never occupies an axial position but simply moves from one equatorial site to the other. All of the nuclear magnetic resonance data presented for $Os_3[P(OCH_3)_3]_5(CO)_7$ may also be rationalized on the basis of a trigonal or tetragonal rotation of the $Os[P(OCH_3)_3](CO)_3$ unit. These two processes (for $M(CO)_4$ moieties) are shown in figures 6.4 and 6.5. Both these require the phosphite ligand to assume an axial position in some of the rotational conformations. We do not favour this situation; simple models have shown that a trimethyl phosphite ligand in an axial position of an $M_3(CO)_{12}$ derivative would suffer severe steric interactions with the axial carbonyl groups on the same side of the triosmium plane. Other workers have found similar results [125] and reached the same conclusion [165,166]. It would appear reasonable that the activation energy required for the formation of an axial-phosphite intermediate or transition state would be prohibitively high.

In summary, then, the nuclear magnetic resonance data is completely consonant with **6b** as the solution structure of

$Os_3[P(OCH_3)_3]_5(CO)_7$ in the slow exchange limit. The changes to the ^1H, ^{13}C, and $^{31}P\{^1H\}$ NMR spectra with temperature may be fully explained by the operation of a single, localized exchange process. The simplest, and favoured, mechanism is the trigonal twist shown in figure 6.8. Although the available evidence cannot unequivocally rule out a trigonal or tetragonal rotation, these are considered unlikely alternatives.

6.2.2 $Os_3[P(OCH_3)_3]_6(CO)_6$ and $Os_3[P(OCH_3)_3]_5\{P(OC_2H_5)_3\}(CO)_6$

In light of the previous discussion concerning site preference for phosphorus ligands in $M_3(CO)_{12}$ derivatives (M= Fe, Ru, Os), the only feasible geometry for $Os_3[P(OCH_3)_3]_6(CO)_6$ is 6c. This is, of course, consistent with the solid state structure.

The nuclear magnetic resonance data obtained in toluene or toluene-d_8/toluene (1:5) was in complete accord with this structure. The $^{31}P\{^1H\}$ NMR spectrum of the hexa(phosphite)

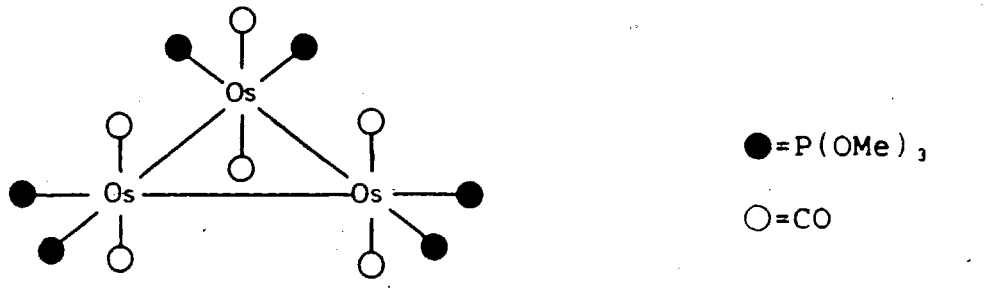

6c

complex in the latter solvent at -89 °C showed a single resonance; the pseudo-D_{3h} symmetry of **6c** makes this the expected result. The signal did not broaden as the temperature was increased to 25 °C. A resonance due to added $P(OCH_3)_3$ remained sharp over this temperature range; this argued against a rapid, intermolecular phosphite exchange in solution. The ^1H NMR spectrum of $Os_3[P(OCH_3)_3]_6(CO)_6$ in toluene-d_8 at 25 °C revealed a doublet (δ 3.61, J_{PH}= 10.9 Hz). Again, this is the expected result based on the high symmetry of the complex. A triplet (δ 203.4 ppm, J_{PC}= 12 Hz) was observed in the $^{13}C\{^1H\}$ NMR spectrum of $Os_3[P(OCH_3)_3]_6(CO)_6$ in CD_2Cl_2 at -57 °C. This result is consistent with the $^{13}C\{^1H\}$ NMR findings for $Os_3[P(OCH_3)_3]_5(CO)_7$ and the chemical equivalency of the three $Os[P(OCH_3)_3]_2(CO)_2$ units in the hexa(phosphite) species. In contrast to the results just discussed, the ^1H and $^{31}P\{^1H\}$ NMR spectra of $Os_3[P(OCH_3)_3]_6(CO)_6$ in CD_2Cl_2 and $CDCl_3$ displayed anomalous behaviour; these will be discussed later in this section.

The detection of stereochemical nonrigidity in $Os_3[P(OCH_3)_3]_6(CO)_6$ would be considerably more difficult than for the pentasubstituted congener. From arguments based on the inability of a phosphite ligand to bridge two metals and the instability of an axial-phosphite intermediate, dynamic behaviour analogous to that observed for $Os_3[P(OCH_3)_3]_5(CO)_7$ in solution is not considered a likely possibility for $Os_3[P(OCH_3)_3]_6(CO)_6$. However, one could envisage a mechanism based on pairwise exchange of *cis* phosphite ligands on the same

osmium atom, via a high energy transition state involving tetragonal rotation of one or all of the $Os[P(OCH_3)_3]_2(CO)_2$ units. Indeed, such a process involving the two corresponding moieties of $Os_3[P(OCH_3)_3]_5(CO)_7$ was considered a possibility early in the investigation of the temperature dependent $^{31}P\{^1H\}$ NMR behaviour of this complex.

Accepting for the moment that such a pairwise exchange of *cis* phosphite ligands in $Os_3[P(OCH_3)_3]_6(CO)_6$ might occur, the nature of the problem becomes apparent. Such a process would be invisible by $^{31}P\{^1H\}$ NMR spectroscopy: the chemical shifts of each member of an exchanging pair would be identical due to the high symmetry of $Os_3[P(OCH_3)_3]_6(CO)_6$. In an attempt to ascertain whether such a process might occur, the complex $Os_3[P(OCH_3)_3]_5\{P(OC_2H_5)_3\}(CO)_6$ was prepared. The presumed structure of this derivative (six equatorial phosphite ligands) has the required asymmetry to allow observation of any fluxional behaviour, of the type previously proposed, by $^{31}P\{^1H\}$ NMR techniques. No such behaviour was observed. Although a definitive assignment of the resonances was precluded by a degeneracy, the presence of six inequivalent ^{31}P nuclei was indicated by the $^{31}P\{^1H\}$ NMR spectrum of $Os_3[P(OCH_3)_3]_5\{P(OC_2H_5)_3\}(CO)_6$ (toluene-d_8) at 25 °C. All resolved resonances appear as doublets. Although spectral changes due to temperature dependencies of the chemical shifts were apparent, there was no indication of broadened signals due to chemical exchange up to 80 °C. This result clearly argues

against the occurrence of any localized rotation of an $Os[P(OCH_3)_3]_2(CO)_2$ moiety, at least at accessible temperatures.

The nuclear magnetic resonance behaviour of $Os_3[P(OCH_3)_3]_6(CO)_6$ in CD_2Cl_2 and $CDCl_3$ was considerably different than that observed in toluene. The ^1H NMR spectrum of this complex in CD_2Cl_2 at -50 °C revealed a doublet (δ 3.53, J_{PH}= 11.2 Hz); as the temperature was increased, this signal underwent collapse to a broad singlet (δ 3.60) at 25 °C. Similar behaviour was observed in the $^{31}P\{^1H\}$ NMR spectrum of $Os_3[P(OCH_3)_3]_6(CO)_6$: the relatively sharp singlet ($\Delta\nu$ ~5 Hz) at -50 °C was broadened sixfold at 25 °C. Recall that this was totally inconsistent with the corresponding temperature dependent results for the complex in toluene.

A number of NMR experiments were performed in an effort to identify the process causing these temperature dependent changes. A hypothesis based on the occurrence of phosphite dissociation in solution was not in accord with the experimental evidence. Such a process should be inhibited by the addition of free $P(OCH_3)_3$; the $^{31}P\{^1H\}$ NMR signal for $Os_3[P(OCH_3)_3]_6(CO)_6$ was found to broaden as the amount of added ligand was increased at 25 °C. In addition, there was no line broadening of the free ligand singlet which suggested that it was not taking part in the process in question. Similar behaviour was observed when this experiment was performed in $CDCl_3$. In another experiment, a solution of $Os_3[P(OCH_3)_3]_6(CO)_6$ and $P(OC_2H_5)_3$ (~1:5) in CD_2Cl_2/CH_2Cl_2 (1:4) was allowed to sit at 25 °C for 24 h. A

$^{31}P\{^{1}H\}$ NMR spectrum subsequently revealed no incorporation of triethyl phosphite into the cluster; this result is also inconsistent with phosphite dissociation from the hexa(phosphite) complex in solution.

An alternative hypothesis, based on the participation of CH_2Cl_2 in the process causing line broadening, was tested. The ^{1}H NMR spectrum of a solution of $Os_3[P(OCH_3)_3]_6(CO)_6$ and CH_2Cl_2 (~1:1) in toluene-d_8 (25 °C) was measured; no line broadening of either signal was observed. This result argues against the CH_2Cl_2/CD_2Cl_2 solvent being an integral part of process in question.

One process which is consistent with the results of the previous experiments involves the formation of an ion pair in solution; it is suggested that the following equilibrium is established.

$$2Os_3[P(OCH_3)_3]_6(CO)_6 \rightleftharpoons \{Os_3[P(OCH_3)_3]_6(CO)_6CH_3\}^{+}\{Os_3[P(OCH_3)_3]_5[P(O)(OCH_3)_2](CO)_6\}^{-}$$

It is known that Me migration in $Ru[P(OCH_3)_3]_5$ and the addition of Me^{+} to $CH_3Ru[P(O)(OCH_3)_2](P(OCH_3)_3)_4$ are relatively facile processes [4,5]. The lack of ^{31}P signal broadening for $Os_3[P(OCH_3)_3]_6(CO)_6$ in toluene may be explained on the basis of solvation effects. The solubility of the ion pair should be considerably greater in CH_2Cl_2 (and $CDCl_3$) than in toluene. The equilibrium would thus lie much farther to the right in CH_2Cl_2 than in toluene which would lead to the observed line broadening

in the former solvent. The effect of added $P(OCH_3)_3$ may also be explained in terms of solvation; it was generally observed that the phosphite derivatives of ruthenium and osmium presented in this thesis were considerably more soluble in a solvent when free $P(OCH_3)_3$ was added. The temperature dependent broadening of the ^1H and $^{31}P\{^1H\}$ NMR signals for $Os_3[P(OCH_3)_3]_6(CO)_6$ in CD_2Cl_2 is in accord with the proposed bimolecular process: the activation barrier for Me transfer inhibits fast ion pair formation at low temperatures. The lack of $P(OC_2H_5)_3$ incorporation into $Os_3[P(OCH_3)_3]_6(CO)_6$ in CD_2Cl_2 is also consonant with the ion pair equilibrium.

The nature of an experiment designed to directly support the proposed process is not obvious. The scrambling of a CH_3 (or CD_3) group would provide some corroboration but this behaviour is not a requirement of the ion pair equilibrium. There is, however, one piece of experimental evidence consistent with the proposed process. The rate of the forward reaction for the equilibrium in question should be directly proportional to the concentration of $Os_3[P(OCH_3)_3]_6(CO)_6$ to the second power. The observed NMR line broadening for the resonance due to $Os_3[P(OCH_3)_3]_6(CO)_6$ should thus increase as the concentration of this complex is increased. The experimental evidence is in accord with this requirement: the widths at half height for the $^{31}P\{^1H\}$ NMR signals of two samples of $Os_3[P(OCH_3)_3]_6(CO)_6$ in CD_2Cl_2/CH_2Cl_2 (1:4) were 28 Hz and 17.5 Hz for $Os_3[P(OCH_3)_3]_6(CO)_6$ concentrations of ~10 mg/mL and ~1 mg/mL,

respectively. However, until further supporting evidence is available the ion pair mechanism must remain a tentative proposal.

In summary, the evidence strongly suggests that neither $Os_3[P(OCH_3)_3]_6(CO)_6$ (which has structure **6c**) nor $Os_3[P(OCH_3)_3]_5\{P(OC_2H_5)_3\}(CO)_6$ undergo inter- or intramolecular phosphite exchange in solution. An ion pair mechanism is tentatively proposed to rationalize the ^1H and $^{31}P\{^1H\}$ NMR behaviour of $Os_3[P(OCH_3)_3]_6(CO)_6$ in CD_2Cl_2.

6.2.3 $Os_3[P(OCH_3)_3](CO)_{11}$

Based on previous arguments, the equatorially substituted structure **6d** is assigned to $Os_3[P(OCH_3)_3](CO)_{11}$. In addition, the axially substituted alternative is not in accord with the limiting low temperature $^{13}C\{^1H\}$ NMR spectrum (vide infra). The $^{31}P\{^1H\}$ NMR spectrum of the monosubstituted triosmium complex exhibits a single signal. This is clearly the result expected from structure **6d**, irrespective of whether the phosphite ligand undergoes chemical exchange in solution or not.

At -53 °C, the $^{13}C\{^1H\}$ NMR spectrum of $Os_3[P(OCH_3)_3](^{13}CO)_{11}$ (see experimental section, chapter 2, for details of ^{13}CO enrichment) displays eight carbonyl resonances (δ 189.8 (doublet, J_{PC}= 12.3 Hz), 185.1, 184.2, 176.0, 174.5, 172.9, 171.8, and 170.8) with an intensity ratio of 2:2:2:1:1:1:1:1, respectively. This spectrum is shown in figure 6.9. The spectrum

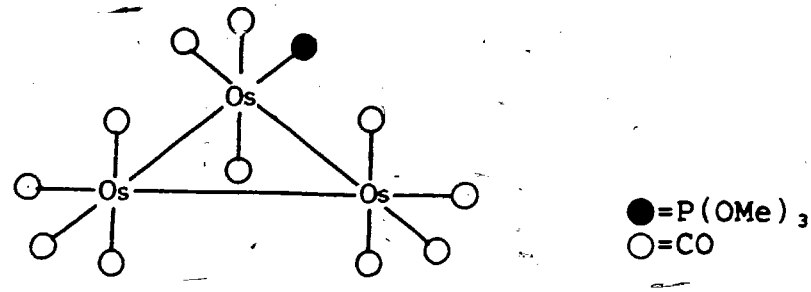

6d

may be partially assigned on the basis of relative intensities, coupling, and chemical shifts. The occurrence of resonances due to equatorial carbonyl groups at higher fields than their axial analogues, in concert with the above intensity data, allows assignment of the five high field resonances (D,E,F,G,H) to the equatorial carbonyl ligands. The doublet is readily designated as arising from the two axial carbonyl groups (A) of the unique $Os(CO)_3P(OCH_3)_3$ unit, while the remaining singlets (B,C) are due to pairs of axial carbonyl ligands on the $Os(CO)_4$ moieties. This low temperature ^{13}C data is qualitatively very similar to that observed for $Os(CO)[PEt_3]_{11}$ [111]. The detailed assignment of the resonances in figure 6.9 is based on the observed exchange processes (vide infra).

There are three reasonably well defined stages of fluxionality which occur for $Os_3[P(OCH_3)_3](CO)_{11}$. The first of these may be observed in the three lowest temperature spectra of figure 6.9. Two axial and two equatorial signals start to broaden at -24 °C and are almost collapsed at 5 °C, while the remainder of the spectrum is just beginning to broaden. This

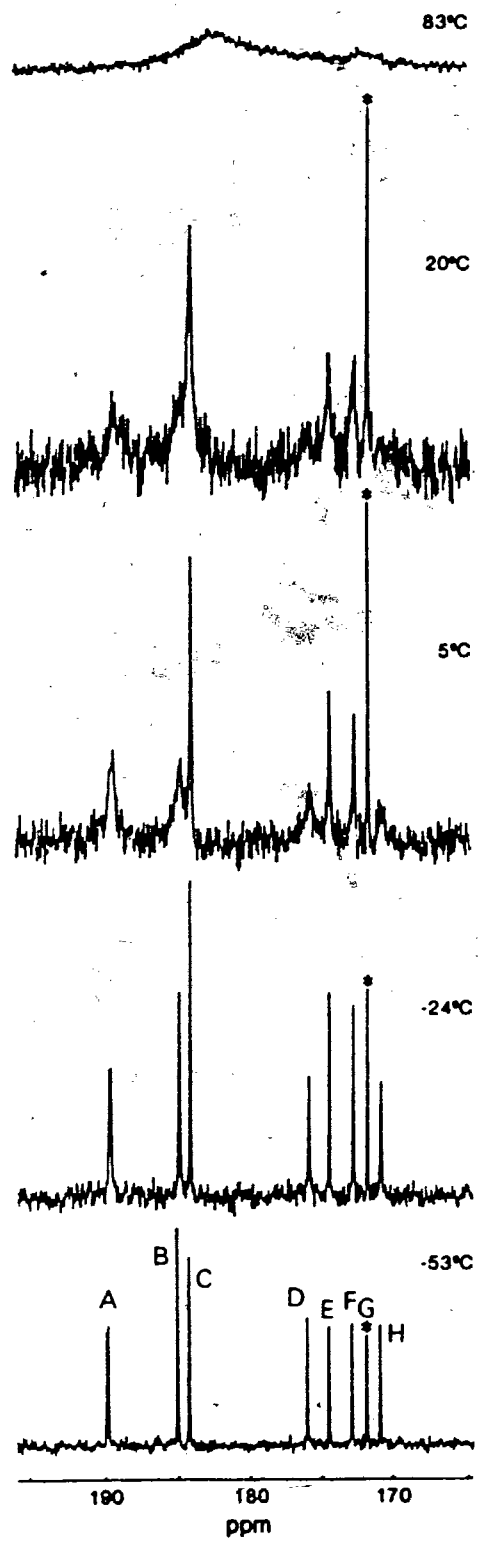

Figure 6.9 The variable temperature $^{13}C\{^{1}H\}$ NMR spectra of $Os_3[P(OCH_3)_3](^{13}CO)_{11}$ in toluene-d_8 (100.6 MHz).

behaviour is very similar to that presented for $Os_3[PEt_3](CO)_{11}$ [111], and the mechanism proposed to account for the spectral changes in this PEt_3 derivative appears the only physically reasonable one in the present case. This process involves an intermediate with two bridging carbonyls, and affects the cyclic permutation of six carbonyl groups which lie approximately in a vertical plane. A general representation of this rearrangement, hereafter called the "axial-equatorial merry-go-round" mechanism, is pictured in figure 6.10. In addition to the approximately planar arrangement of the affected carbonyl ligands, note the non-participation of the two ligands *trans* to the metal-metal bonds not included in the plane. These ligands have been shown to occupy virtually identical positions in both the bridged and unbridged structures, as inferred from the x-ray

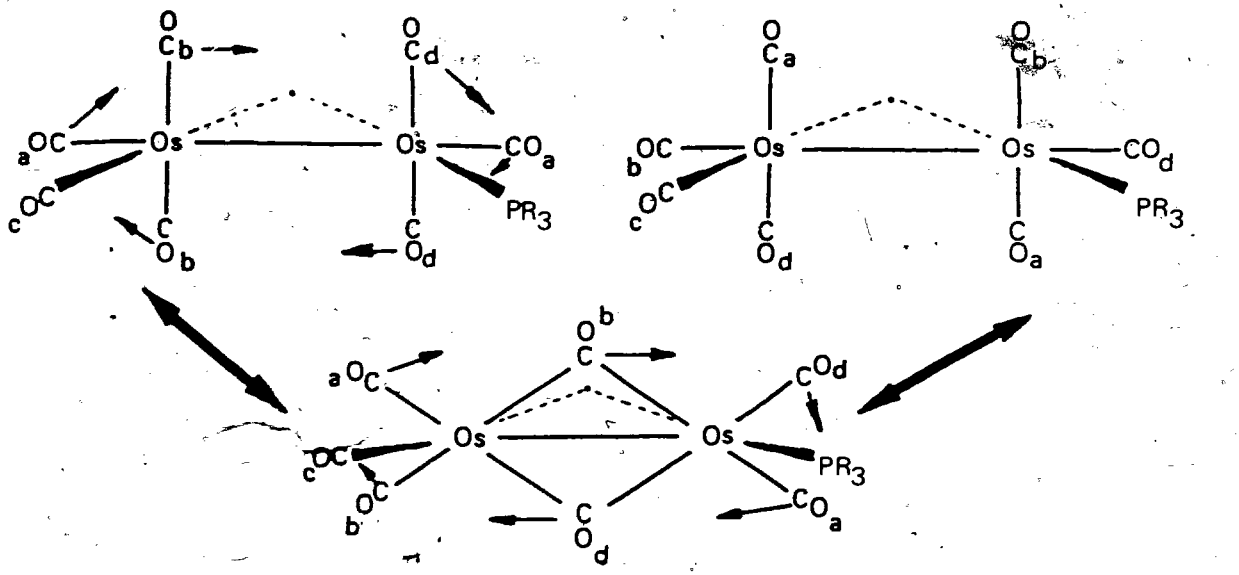

Figure 6.10 The axial-equatorial merry-go-round mechanism for carbonyl site exchange in a general $M_3[PR_3](CO)_{11}$ complex.

structures of $Fe_3(CO)_{12}$ [143,167] and $Fe_3[PPh_3](CO)_{11}$ [168]. Another important feature of the mechanism shown in figure 6.10 is the restriction imposed by a phosphorus donor ligand. The inability of such a ligand to occupy a bridging position effectively limits the extent of the cyclic permutation in any vertical plane containing that ligand. Although it is possible for a $P(OCH_3)_3$ group to adopt an axial position in a high energy intermediate or transition state, this ligand would be unable to move to another metal centre in the succeeding step of the exchange process.

The specific case of this exchange applied to $Os_3[P(OCH_3)_3](CO)_{11}$ is shown in figure 6.11. The two allowed planes for the axial-equatorial merry-go-round mechanism are labelled a and b while the forbidden permutational plane contains the phosphite ligand. The observation that the low field doublet is involved in the site exchange (figure 6.9) uniquely defines the cyclic permutation in plane a as the lowest energy process. This result allows assignment of resonances A,B,C and the pairwise designation of D/H. It is of interest that the plane analogous to a in $Os_3[PEt_3](CO)_{11}$ was also the one involved in the lowest energy site exchange for that complex [111].

The effects of the second stage of fluxionality occurring in $Os_3[P(OCH_3)_3](CO)_{11}$ may be examined in the ^{13}C NMR spectra at 5 and 20 °C (figure 6.9). In the former, the last unbroadened axial resonance (C) and two of the three remaining equatorial

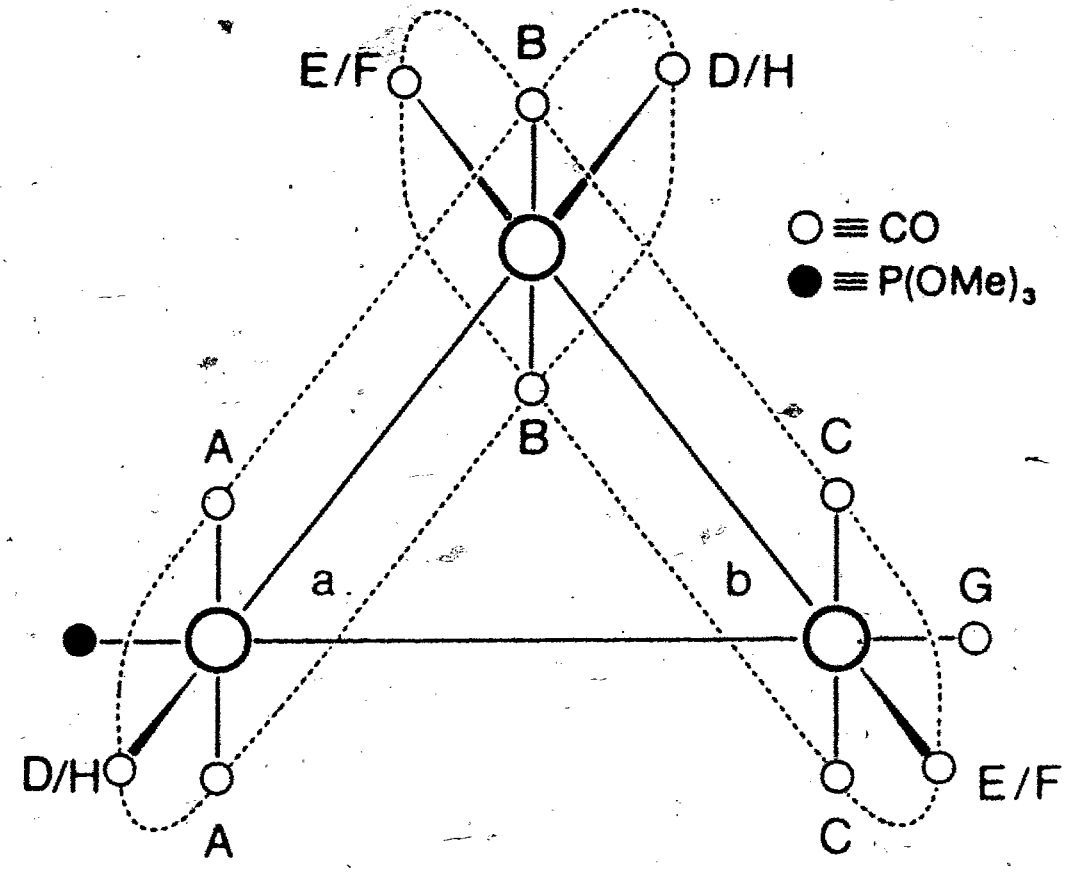

Figure 6.11 The axial-equatorial merry-go-round exchange as as applied to $Os_3[P(OCH_3)_3]_3(CO)_{11}$ (see also fig. 6.9).

---

resonances (E,F) start to broaden. At 20 °C, these three signals have become quite broad, while the remaining ^{13}C carbonyl resonance is just beginning to show signs of chemical exchange. These spectral changes are consistent with the onset of an axial-equatorial merry-go-round process in plane b of figure 6.11. Resonance B, due to the axial carbonyl groups common to the two allowed planes, is involved in both the cyclic permutations. As the rate of exchange is inversely proportional to the lifetime of a nucleus in a specific site, resonance B is expected to show increased broadening relative to the other affected signals. Detailed observation of this phenomenon is

made difficult by overlap of this signal with resonance C. This second axial-equatorial merry-go-round process allows pairwise assignment of resonances E/F and uniquely defines G. This signal (G) is due to the equatorial carbonyl group *trans* to the $P(OCH_3)_3$ ligand; this CO group is geometrically barred from participation in either of the two planar exchanges.

The observation of a second axial-equatorial merry-go-round process for $Os_3[P(OCH_3)_3](CO)_{11}$ is in contrast to the behaviour exhibited by $Os_3[PEt_3](CO)_{11}$ [111]. For this derivative only two stages of fluxionality were observed, the second causing broadening and coalescence of all carbonyl resonances. The high temperature limiting ^{13}C NMR spectrum was not obtained and the nature of the second site exchange mechanism was not addressed. These results will be discussed in more detail later in this chapter.

The ^{13}C spectral data for $Os_3[P(OCH_3)_3](CO)_{11}$ indicates that the two axial-equatorial merry-go-round exchanges have different free energies of activation. The two allowed planes are coupled via the carbonyls corresponding to resonance B (see figures 6.9 and 6.11) which gives rise to a ten site exchange system. The line shape for the resonances affected by this exchange was calculated based on the mechanism in figure 6.11; an experimental spectrum in the intermediate exchange region was chosen as the target spectrum. Spectra using a variety of pairs of rate constants associated with the two permutational planes were calculated to give the best fit to the experimental data.

The calculated spectrum and the observed ^{13}C data (T= 20 °C) are shown in figure 7.1 of appendix 2. It may be observed that these are in good agreement. From the value of the rate constant for the simulated line shape of the lowest energy axial-equatorial exchange (k= 230±5 sec^{-1}) a value of $\Delta G^{\ddagger}$ was calculated at the temperature of the observed spectrum (T= 293±2 °K): $\Delta G^{\ddagger}$= 14.0±0.4 kcal mol^{-1}. The analogous value for the higher energy process (i.e. in plane b of figure 6.11) was calculated in the same manner: for k= 50±2 sec^{-1} at T= 293±2 °K, $\Delta G^{\ddagger}$= 14.9±0.4 kcal mol^{-1}. The details of these calculations may be found in appendix 2.

An indirect result of the previous findings is worthy of note here. This examination of the stereochemical nonrigidity of $Os_3[P(OCH_3)_3](CO)_{11}$ was but a part of a larger study concerned with the nature of any chemical exchange occurring for the complete series $Os_3[P(OCH_3)_3]_x(CO)_{12-x}$ (x= 1-6). Our initial findings regarding $Os_3[P(OCH_3)_3]_5(CO)_7$ suggested that the trigonal twist mechanism (figure 6.8) might be quite general for phosphite derivatives of $Os_3(CO)_{12}$. It is stressed that the changes in the $^{13}C\{^1H\}$ NMR spectra of $Os_3[P(OCH_3)_3](CO)_{11}$ due to the two lowest energy site exchanges are not in accord with a trigonal twist mechanism involving an $Os[P(OCH_3)_3](CO)_3$ moiety. Neither are they consistent with a trigonal or tetragonal rotation, involving one or both of the $Os(CO)_4$ portions of the molecule.

The onset of the final stage of fluxionality is observed in the $^{13}C\{^{1}H\}$ NMR spectrum of $Os_3[P(OCH_3)_3](CO)_{11}$ at 20 °C (figure 6.9). Resonance G starts to broaden and is completely collapsed in the spectrum at 83 °C. Several processes appear capable of causing this behaviour. A trigonal/tetragonal rotation (see figure 6.4) of the $Os(CO)_4$ moiety bearing the carbonyl in question would result in direct line broadening due to site exchange of axial and equatorial groups. A trigonal twist of the $Os[P(OCH_3)_3](CO)_3$ unit would also bring about chemical exchange of carbonyl G, in an indirect manner: when the $P(OCH_3)_3$ ligand moves to its alternate equatorial position as a result of the trigonal twist, this carbonyl ligand is consequently free to participate in an axial-equatorial merry-go-round process in the previously forbidden plane (see figure 6.11). The available evidence is insufficient to favour one of these mechanisms over the other.

The results concerning the stereochemical nonrigidity of $Os_3[P(OCH_3)_3](CO)_{11}$ may be summarized as follows. The nuclear magnetic resonance data, in the slow exchange limit, is completely consonant with **6d** as the static solution structure. Three distinct fluxional processes occur, based on changes in the variable temperature $^{13}C\{^{1}H\}$ NMR spectra. The changes due to the two processes happening at lowest energy are consistent with an approximately planar, cyclic permutation of four axial and two equatorial carbonyl ligands in each of the two vertical planes not containing the trimethyl phosphite group. These two

site exchanges occur with different rates and thus possess different $\Delta G^{\ddagger}$ values. These were calculated. The third (and highest energy) fluxional process appears to involve a localized (i.e. non-bridging) rearrangement of ligands, although the spectroscopic evidence does not allow a unique choice from among the possibilities.

6.2.4 $Os_3[P(OCH_3)_3]_3(CO)_9$

The low temperature NMR data for $Os_3[P(OCH_3)_3]_3(CO)_9$ readily allows the assignment of the static solution structure. The $^{31}P\{^1H\}$ NMR spectrum of this trisubstituted complex (toluene/toluene-d_8, 2:1) at -91 °C exhibits a single resonance. The only structural possibility in accord with this result (and involving only equatorial coordination of the $P(OCH_3)_3$ ligands) is that shown as **6e**. In fact, the only other possible isomer with only equatorial phosphites (and one $P(OCH_3)_3$ group per metal atom) is **6e'**.

The ^{13}C NMR spectrum of $Os_3[P(OCH_3)_3]_3(CO)_9$ (toluene/toluene-d_8, 4:1) in the slow exchange limit (-65 °C) corroborates the structural assignment in **6e**. A doublet (J_{PC}= 10.3 Hz) and a singlet are observed at δ 193.3 and 179.9 ppm with relative intensities 2:1, respectively. The first resonance may be assigned to the axial carbonyl ligands, equivalent by symmetry and each coupled to an equatorial ^{31}P nucleus, while the second is due to the equatorial carbonyl groups.

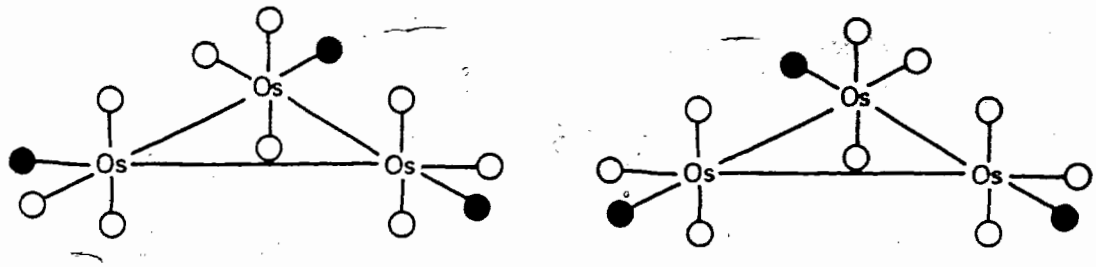

6e **6e'**

●=$P(OCH_3)_3$ ○=CO

The ^1H NMR spectrum of $Os_3[P(OCH_3)_3]_3(CO)_9$ (acetone-d_6, 25 °C) exhibits a doublet ($^3J_{PH}$= 12.2 Hz).

The structural assignment of $Os_3[P(OCH_3)_3]_3(CO)_9$ may be compared to studies of similar complexes. The x-ray structure of $Ru_3[P(CH_3)_3]_3(CO)_9$ revealed a pseudo-D_{3h} symmetry analogous to that shown in **6e** [110]. The low temperature ^{13}C NMR spectrum of $Os_3[PEt_3]_3(CO)_9$ ~~in toluene~~ featured 2 resonances, of relative intensities 2:1, with the more intense (lower field) signal appearing as a doublet [111]. These two experimental findings clearly add weight to the assignment of $Os_3[P(OCH_3)_3]_3(CO)_9$ to structure **6e**.

The fluxional nature of $Os_3[P(OCH_3)_3]_3(CO)_9$ in solution is evinced by the variable temperature ^{13}C NMR data. The two signals begin to increase in width at approximately -20 °C and at -2 °C are severely broadened. The spectrum at 60 °C reveals complete collapse of the signals into the baseline. Site

exchange between axial and equatorial ligands is clearly indicated.

The nature of the dynamic process responsible for these temperature dependent changes to the ^{13}C NMR spectra of $Os_3[P(OCH_3)_3]_3(CO)_9$ may be partially elucidated by an examination of the geometrical constraints imposed by structure **6e**. The axial-equatorial merry-go-round mechanism proposed for $Os_3[P(OCH_3)_3](CO)_{11}$ (see figure 6.11) is forbidden for **6e**; each of the three potential planes contains a $P(OCH_3)_3$ ligand. This result argues strongly against this cyclic permutation as the cause of the observed axial-equatorial carbonyl site exchange, at least initially.

The trigonal twist mechanism, however, is capable of rationalizing the observed spectral behaviour of $Os_3[P(OCH_3)_3]_3(CO)_9$. Such a process, occurring about each of the three equivalent $Os(CO)_3P(OCH_3)_3$ units, would lead to axial-equatorial exchange of all the carbonyl ligands (see figure 6.8). The permutational details deserve some discussion. If the trigonal twist exchanges about the three Os atoms are synchronous (i.e. coupled and occur simultaneously), the overall dynamic process would involve the interconversion shown in figure 6.12A. If the trigonal twist exchanges are asynchronous and occur sequentially, a fluxional process such as that depicted in figure 6.12B would result. It is noted that, although these isomers in (B) are permutationally distinct, they are all equivalent to **6e'**. The implications of the slow exchange

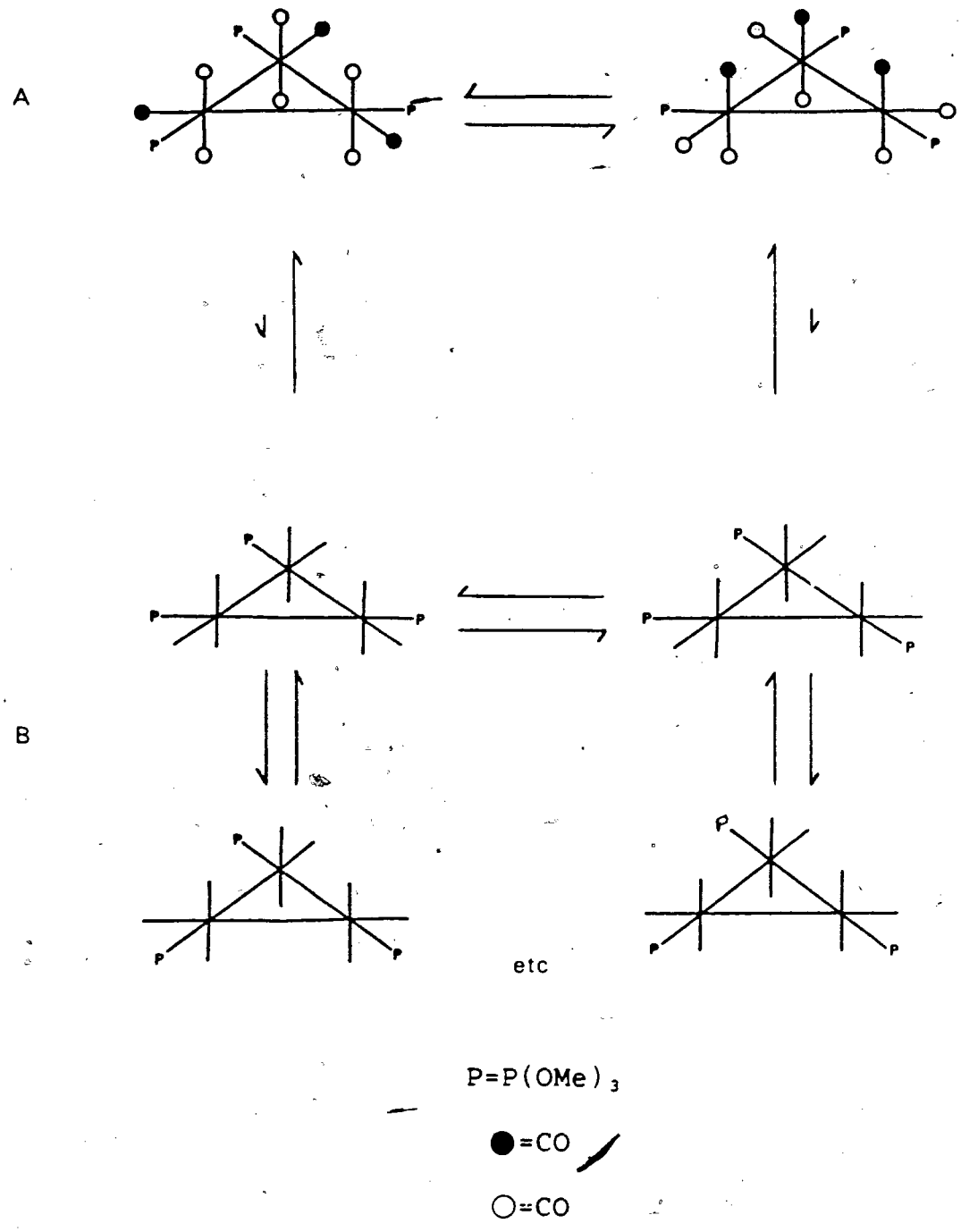

Figure 6.12 Various possibilities for a trigonal twist exchange process in $Os_3[P(OCH_3)_3]_3(CO)_9$.

limiting ^{13}C and $^{31}P\{^1H\}$ NMR spectra of $Os_3[P(OCH_3)_3]_3(CO)_9$ argue against the asynchronous trigonal twist mechanism as the major contributor to the observed spectral changes: only resonances due to isomer **6e** are exhibited in the low temperature ^{13}C and $^{31}P\{^1H\}$ NMR spectra at -65 and -91 °C, respectively. This fact demonstrates that the equilibrium concentration of **6e'** can be, at most, 1% of the symmetric isomer **6e** at these temperatures. This result implies that **6e** is lower in free energy with respect to **6e'**. Consequently, the activation barrier for a synchronous trigonal twist process (figure 6.12A) should be lower than that associated with a **6e**—>**6e'** conversion, a necessary first step in activating the asynchronous trigonal twist mechanism (figure 6.12B).

Although this argument implicates the process in figure 6.12A as the major contributor to the ^{13}C NMR spectral changes with temperature, one cannot rule out the asynchronous mechanism as a minor participant. Indeed, there are some small changes in the variable temperature $^{31}P\{^1H\}$ NMR spectra of $Os_3[P(OCH_3)_3]_3(CO)_9$ which are consistent with this view. The $^{31}P\{^1H\}$ NMR spectrum of $Os_3[P(OCH_3)_3]_3(CO)_9$ (toluene/toluene-d_8, 2:1) exhibits only a single resonance from -91 to +31 °C, although the chemical shift moves upfield 1.3 ppm over this temperature range. The resonance due to added $P(OCH_3)_3$ remains sharp during this process. The only evidence for any chemical exchange appears in the spectrum at 1 °C. The line width at half-height for the signal due to $Os_3[P(OCH_3)_3]_3(CO)_9$ at this

temperature was approximately 1.8 times as large as the analogous values measured at -21 and +22 °C. The resonance due to internal $P(OCH_3)_3$ did not show a similar broadening at +1 °C. This is exactly the behaviour one might expect as a consequence of two simultaneous exchange processes occurring. The dominant process, a synchronous trigonal twist, would cause no ^{31}P NMR line broadening. The minor process, an asynchronous trigonal twist representing a highly population biased (i.e. <1:100) exchange between isomers containing magnetically inequivalent ^{31}P nuclei, would produce a small amount of line broadening overlayed on the major signal.

The line shape for the ^{13}C NMR spectrum of $Os_3[P(OCH_3)_3]_3(CO)_9$ was calculated based on a synchronous trigonal twist process (figure 6.12A). This calculated line shape was matched to an experimental spectrum in the intermediate exchange region (-2 °C). The agreement between the simulated and observed data was good. The rate constant for the simulated spectrum ($k= 40\pm2$ sec^{-1}) was used to calculate a value of the free energy of activation at the temperature of the experimental spectrum ($T= 271\pm2$ °K): $\Delta G^{\ddagger}= 13.8\pm0.4$ kcal mol^{-1}.

In summary, the temperature dependent changes in the ^{13}C NMR spectrum of $Os_3[P(OCH_3)_3]_3(CO)_9$ lead to the following conclusions. In the slow exchange limit, the solution structure of this complex is **6e**. A localized (i.e. non-bridging) site exchange, causing scrambling of axial and equatorial carbonyl ligands, is shown to occur. The experimental evidence suggests

that the major process responsible for this scrambling is a synchronous trigonal twist of the three $Os[P(OCH_3)_3](CO)_3$ moieties of $Os_3[P(OCH_3)_3]_3(CO)_9$ (figure 6.12A). There is also some evidence for a minor contribution to the observed chemical exchange that could be due to a mechanism involving successive trigonal twists about the individual $Os[P(OCH_3)_3](CO)_3$ units (figure 6.12B).

6.2.5 $Os_3[P(OCH_3)_3]_4(CO)_8$

The variable temperature ^{13}C and $^{31}P\{^1H\}$ NMR data for $Os_3[P(OCH_3)_3]_4(CO)_8$ is considerably more complex than that associated with the previously discussed members of the series i.e. $Os_3[P(OCH_3)_3]_x(CO)_{12-x}$ (x= 1,3,5,6). Signal degeneracies, strong temperature dependencies of the chemical shifts (^{31}P in particular), and the existence of two isomers at low temperatures all contribute to this complexity. Consequently, the assignment of signals and elucidation of the dynamic processes involved required additional experimental information. This was provided in the form of $^{31}P\{^1H\}$, and to a lesser extent, ^{13}C NMR data measured at different operating frequencies. For example, a set of variable temperature $^{31}P\{^1H\}$ NMR spectra of $Os_3[P(OCH_3)_3]_4(CO)_8$ were obtained at both 40.5 and 162.0 MHz. While the basic temperature dependent variations were identical at both field strengths (as expected), each set of data provided some unique information which was combined to allow a clear explanation of the nonrigid behaviour of $Os_3[P(OCH_3)_3]_4(CO)_8$. References to the operating frequency will

be noted where appropriate.

Two $^{31}P\{^{1}H\}$ NMR spectra of the tetrasubstituted triosmium complex (toluene-d_8), in the slow exchange limit, are shown in figure 6.13. The top spectrum (A) was measured at 40.5 MHz while (B) was obtained at 162.0 MHz. There are several important features of these spectra to note. Firstly, the couplings observed for the three resonances in spectrum A are not resolved at the higher field. This behaviour was observed for $Os_3[P(OCH_3)_3]_5(CO)_7$ as well, and is again attributed to chemical shift anisotropy [160]. Although the signals are broader in the spectrum measured at 162.0 MHz, the higher field has also caused them to span a wider frequency range; the individual resonances are better resolved with respect to one another. In fact, by carefully analyzing the integrals for several low temperature spectra (all in the slow exchange limit) measured at 162.0 MHz, accurate relative intensities were calculated for all six signals. These relative intensities are marked on figure 6.13B while figure 6.13A features a numbering system for the resonances.

Clearly, the presence of six resonances indicates the existence of more than one isomer of $Os_3[P(OCH_3)_3]_4(CO)_8$ in solution in the slow exchange limit. Within the restriction of equatorial substitution, the four possible isomers are represented by structures **6f** to **6i**. Isomer **6i** is considered an unlikely possibility. The remaining three isomers would collectively exhibit eight resonances (barring degeneracies),

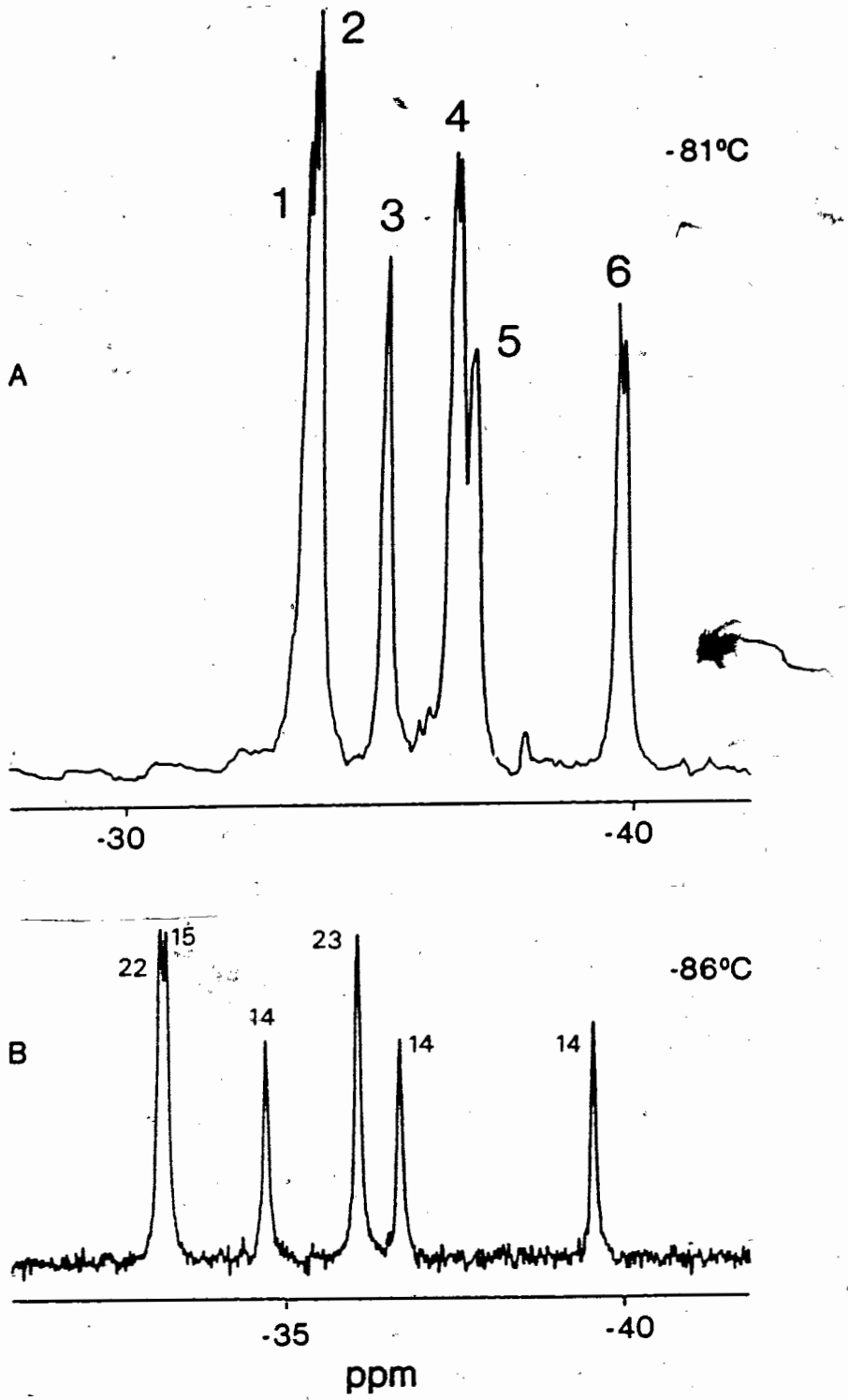

Figure 6.13 Two low temperature $^{31}P\{^{1}H\}$ NMR spectra of $Os_3[P(OCH_3)_3]_4(CO)_8$ (A) in toluene/toluene-d_8 (1:4) at 40.5 MHz (B) in toluene-d_8 at 162.0 MHz. The top spectrum features a numbering scheme while the bottom spectrum gives relative intensities.

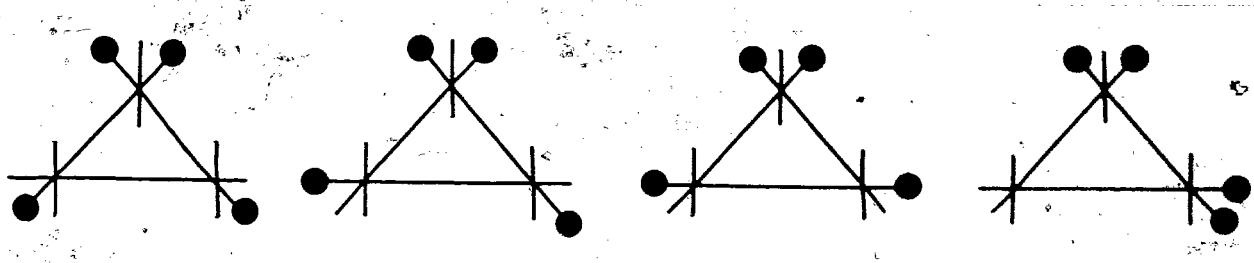

6f **6g** **6h** **6i**

●=$P(OMe)_3$

---

implying that only two are present. One of these must be **6g** (with four magnetically inequivalent ^{31}P nuclei). The second isomer present is thought to be **6f**, which exhibits fewer steric interactions between phosphite groups (relative to **6h**). Some indirect ^{13}C NMR evidence supporting this choice will be presented later.

Assuming, then, that **6f** and **6g** are the two isomers of $Os_3[P(OCH_3)_3]_4(CO)_8$ present in solution in the slow exchange limit, coupling constant data and relative intensities readily allow a consistent assignment. From careful observation of the coupling constants (data at 40.5 MHz) it is found that within experimental error, the splittings of resonances 1 and 4 are the same and different from that of resonance 6 (figure 6.13). If it is assumed that these couplings are due to $trans\text{-}^3J_{PP}$ (as for $Os_3[P(OCH_3)_3]_5(CO)_7$), then along with the intensity data, the assignments shown in figure 6.14 can be made. The assignment of resonance 5 was made on the assumption that it is an unresolved doublet. This is a reasonable assumption when its physical appearance (considerably broader than other singlets in the slow

exchange limit spectra) and the uniqueness of the position in question are examined; it is the only phosphite-substituted site in the two isomers which is involved in a *trans*-$^2J_{PP}$ as well as a *cis*-$^2J_{PP}$ coupling to magnetically inequivalent nuclei. The low temperature $^{31}P\{^1H\}$ NMR data alone does not allow a unique assignment of the remaining resonances and, therefore, they are pairwise designated.

The full set of variable temperature $^{31}P\{^1H\}$ NMR spectra for $Os_3[P(OCH_3)_3]_4(CO)_8$ (in toluene-d_8, at 162.0 MHz) are shown in figure 6.15. All the signals begin to broaden, at qualitatively the same rate, around -57 °C. The six resonances collapse and subsequently coalesce to two signals at 61 °C. Although it is not obvious from the high temperature data in figure 6.15, when the $^{31}P\{^1H\}$ NMR spectrum of $Os_3[P(OCH_3)_3]_4(CO)_8$ in toluene-d_8 was measured with a long (~5 sec) delay time between scans, the two signals were of equal intensity. Again, the resonance due to

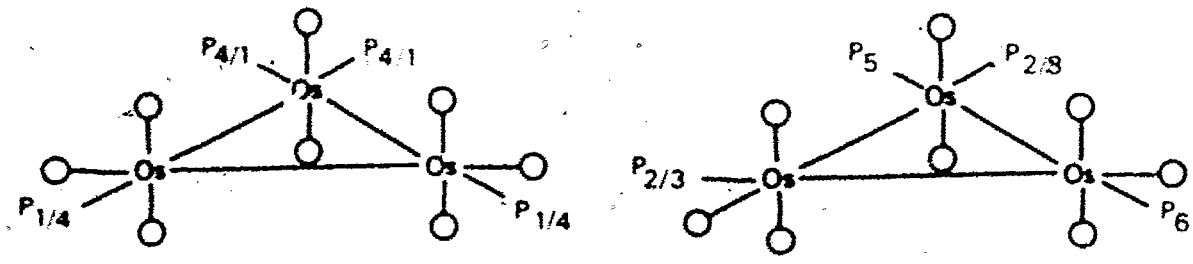

6f 6g

Figure 6.14 Schematic representation showing partial assignment of the phosphite ligands in the two isomers of $Os_3[P(OCH_3)_3]_4(CO)_8$.

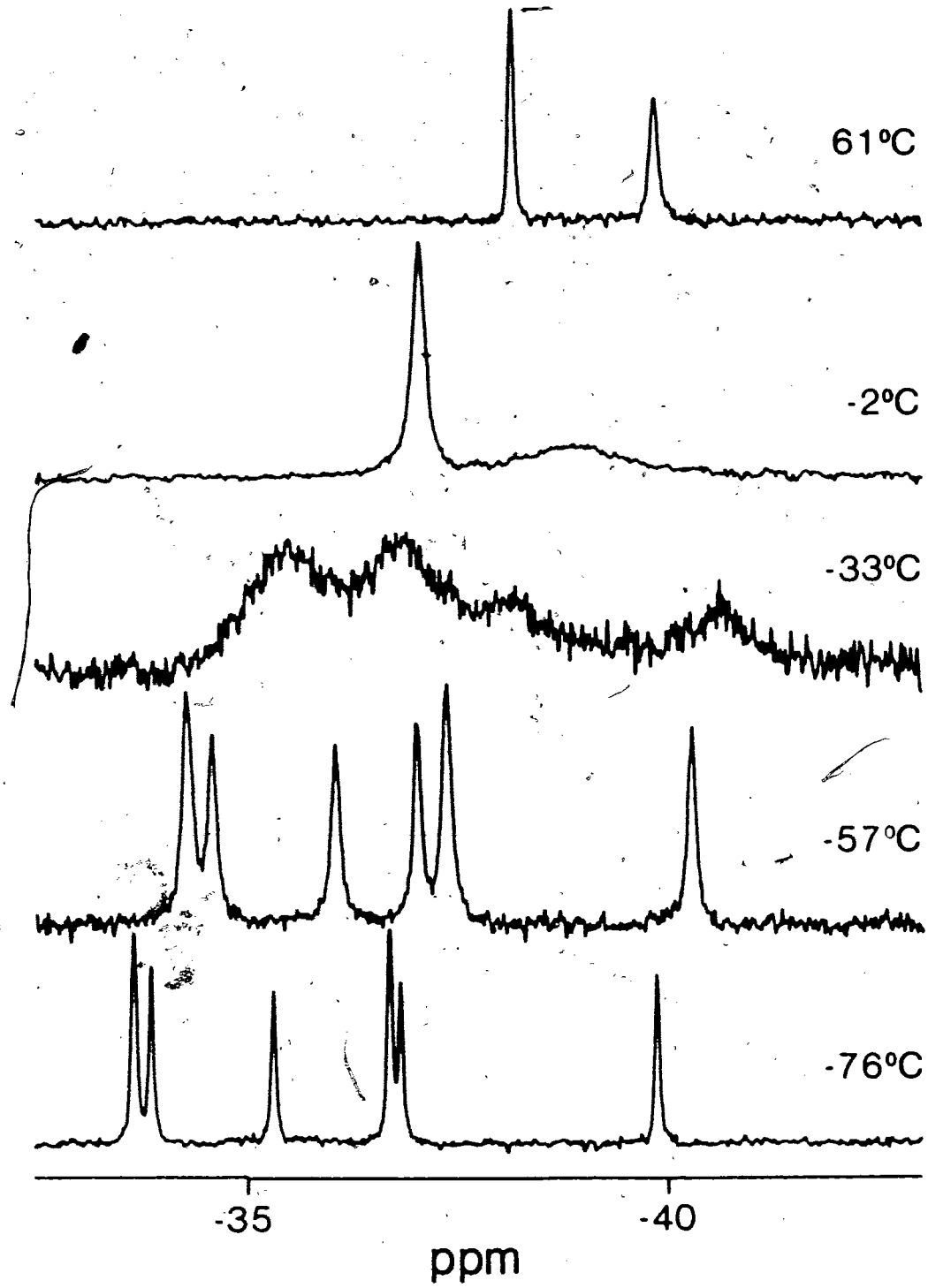

Figure 6.15 The variable temperature $^{31}P\{^{1}H\}$ NMR spectra of $Os_3[P(OCH_3)_3]_4(CO)_8$ in toluene-d_8 measured at 162.0 MHz.

added $P(OCH_3)_3$ remained sharp over the full temperature range, ruling out an intermolecular phosphite exchange.

The simplest process which can account for these spectral changes, and the one we favour, is a simultaneous set of trigonal twists of the four $Os(CO)_3P(OCH_3)_3$ units in the two isomers **6f** and **6g**. Although there is no requirement that the individual polytopal rearrangements occur at the same rate, the concurrent onset of line broadening for the six resonances in the slow exchange region argues that the rates are, within experimental detection, equal.

Although this basic site exchange mechanism can rationalize the spectral behaviour at low temperatures, an explanation of the fast exchange limit $^{31}P\{^1H\}$ NMR spectrum requires a more detailed analysis. Again the question of whether the proposed trigonal twist processes, within each isomer, are synchronous or asynchronous must be addressed. The observed $^{31}P\{^1H\}$ NMR results in the fast exchange limit demonstrate that the former cannot be the case, at least at higher temperatures. Synchronous trigonal twist processes (within each isomer) would result in the two equilibria shown schematically on page 303. Two averaged $^{31}P\{^1H\}$ NMR resonances for **each** of the two isomers would be predicted. The experimental observation of only two equally intense signals in the fast exchange region is consistent with an asynchronous trigonal twist mechanism involving all four $Os(CO)_3P(OCH_3)_3$ moieties in **6f** and **6g**.

Additional evidence in support of this dynamic process was obtained by considering averaged chemical shifts. Again, it was necessary to prepare plots of δ versus temperature for each $^{31}P\{^{1}H\}$ NMR resonance (using data from at or near the slow exchange limit) and extrapolate into the fast exchange region. Utilizing these plots and assuming the equilibrium constant between **6f** and **6g** remains unchanged over the required temperature range, the weighted average chemical shifts based on the proposed exchange process and the various assignment possibilities in figure 6.14 were calculated. Comparing these results to the experimental values at -6, 0, and +6 °C (data measured at 40.5 MHz), there is agreement within experimental error for two different permutational sets. These differ only in

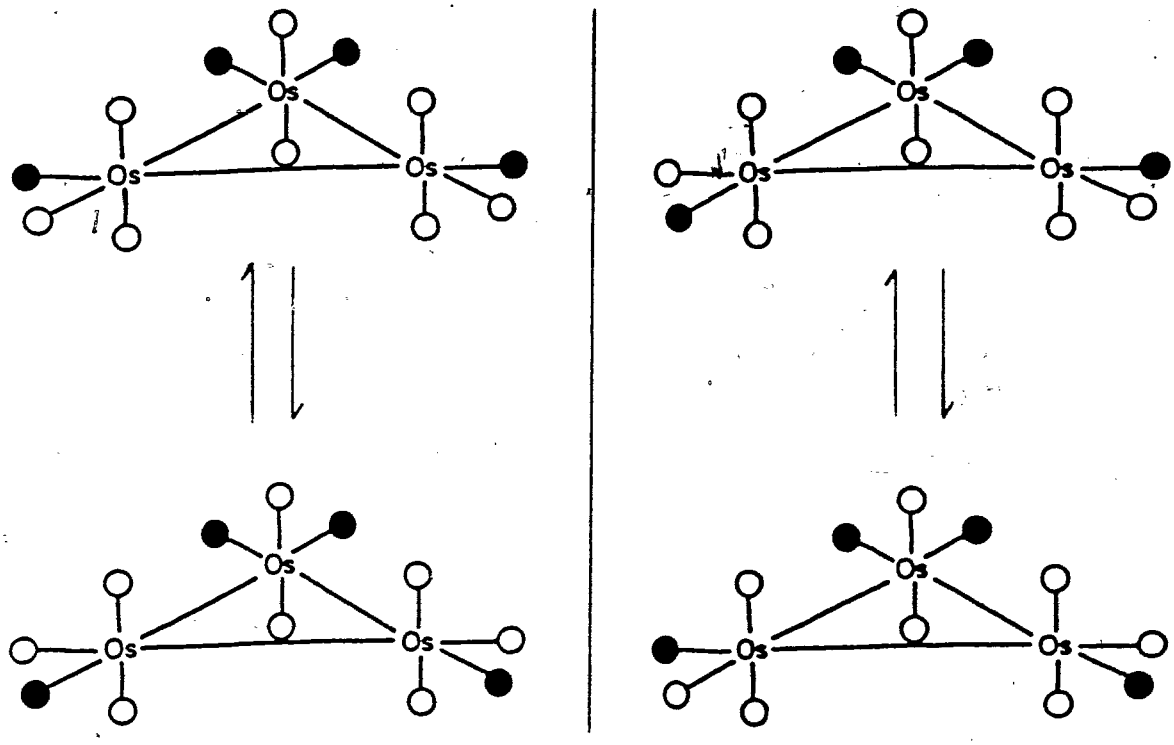

the pairwise assignment within isomer **6f** and are shown on page 305. This result lends considerable support to the proposed dynamic mechanism.

The variable temperature ^{13}C NMR data for $Os_3[P(OCH_3)_3]_4(CO)_8$ is completely consonant with isomers **6f** and **6g** and the previously proposed exchange mechanism. In addition, the effects of a lower energy process, not detectable by $^{31}P\{^1H\}$ NMR spectroscopy, are observed.

Several ^{13}C NMR spectra of $Os_3[P(OCH_3)_3]_4(CO)_8$ in toluene-d_8, over the temperature range -83 to -65 °C, are shown in figure 6.16 (see experimental section, chapter 2, for details of ^{13}CO enrichment). Consider the spectrum at -83 °C. The two low field signals appear as unresolved triplets; the analogous spectrum measured at 25.18 MHz clearly shows these resonances to be resolved triplets, with J_{PC}= 11.0, 11.6 Hz (low and high field, respectively). The most intense signal in the -83 °C spectrum at 100.6 MHz is broad with asymmetric satellites while the resonance at higher field appears as a doublet (J_{PC}= 6.4 Hz). The intensities of the seven observable resonances, from low to high field, are 4:3:10:4:2:3:2.

The ^{13}C NMR chemical shifts of the carbonyl ligands (at or near the slow exchange limit) in $Os_3[P(OCH_3)_3]_x(CO)_{12-x}$ (x= 1,3,5,6) are shown in table 6.1, grouped according to position (axial/equatorial) and degree of phosphite substitution on the attached osmium atom. Note the well-defined regions in which the

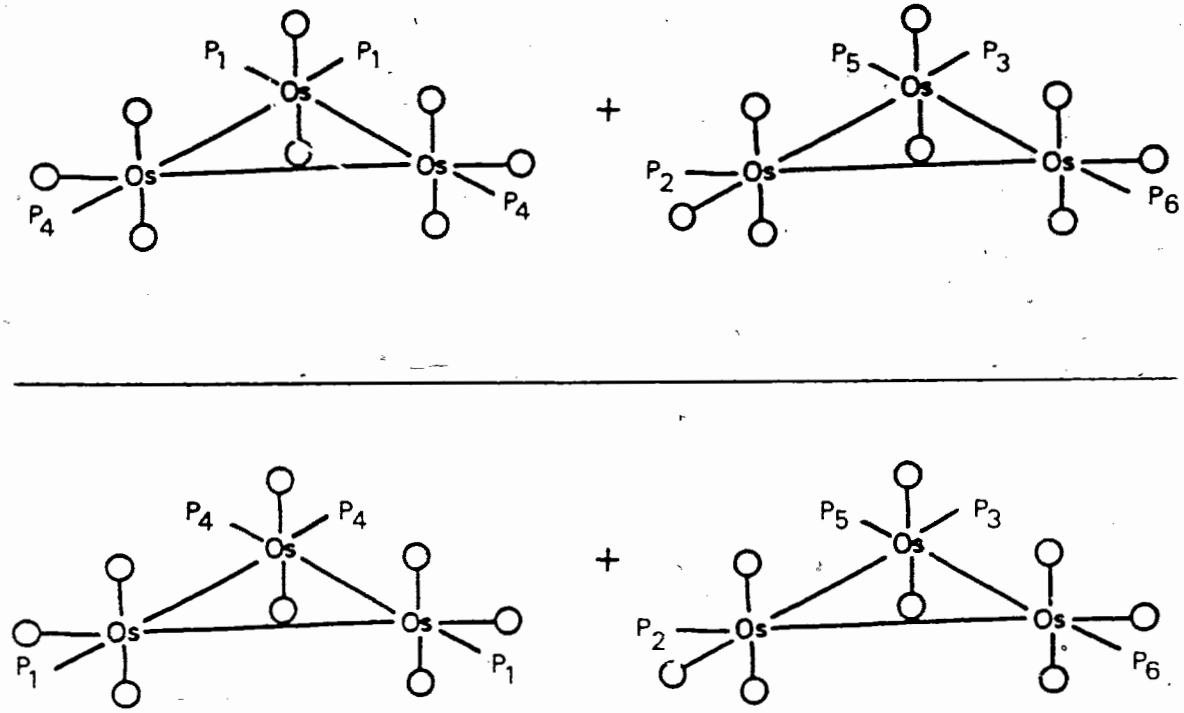

signals due to the various types of axial carbonyl groups occur. The potential utility of this phenomenon was touched on earlier and the combined data for the four complexes in table 6.1 reinforces the point.

Using the integration ratios, the chemical shift data in table 6.1, and assuming one degeneracy (the most intense signal), the ^{13}CO resonances for **6f** and **6g** may be readily assigned as illustrated in figure 6.17 (see also figure 6.16). While only pairwise designations for F/H and D/E are possible, this is not intrinsic to the following arguments regarding the site exchange mechanism.

^{13}C NMR chemical shifts of various carbonyl groups (*)

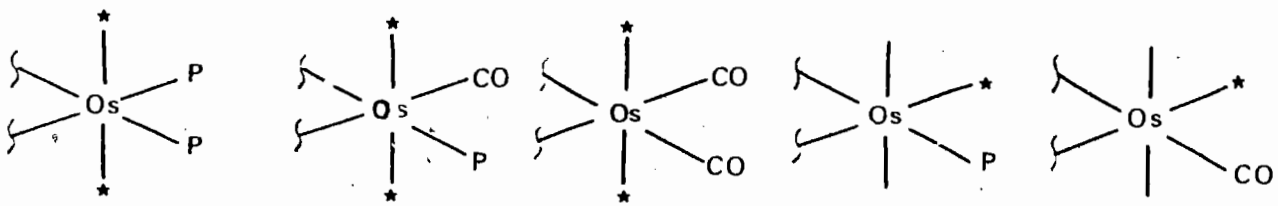

Compounds					
$Os_3[P(OCH_3)_3]_3(CO)_9$	203.4				
$Os_3[P(OCH_3)_3]_2(CO)_{10}$	199.7 199.2	194.1		179.2	
$Os_3[P(OCH_3)_3]_1(CO)_{11}$		193.3		179.9	
$Os_3[P(OCH_3)_3](CO)_{11}$		189.7	185.1 184.2	176.0	174.5 172.9 171.8 170.8

Table 6.1 ^{13}C NMR chemical shifts of the carbonyl ligands in $Os_3[P(OCH_3)_3]_x(CO)_{12-x}$ (x= 1,3,5,6).

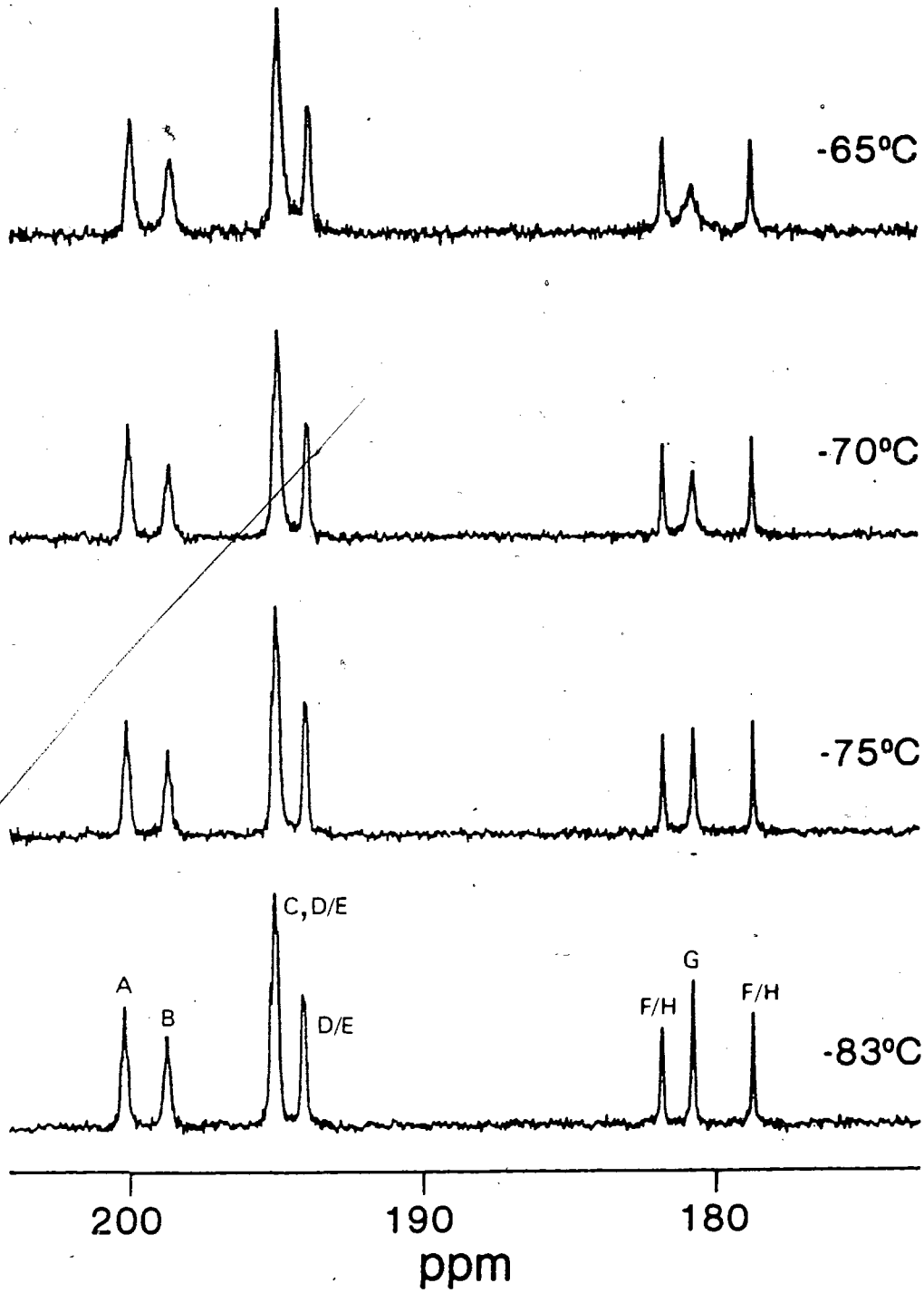

Figure 6.16 Several low temperature ^{13}C NMR spectra of $Os_3[P(OCH_3)_3]_4(^{13}CO)_8$ in toluene-d_8 measured at 100.6 MHz.

The effects of the lowest energy dynamic process occurring for $Os_3[P(OCH_3)_3]_4(CO)_8$ may be observed in the low temperature ^{13}C NMR spectra in figure 6.16. Resonance G starts to broaden at -75 °C while the degenerate signal loses its satellites and is reduced in height relative to the unbroadened signals; this latter observation is more apparent on the full size spectrum. At -65 °C, resonance G has become quite broad while the degenerate signal has lost considerable intensity and appears quite wide near the baseline.

An axial-equatorial merry-go-round process, occurring in the indicated plane of isomer **6f** (see figure 6.17), is the only reasonable mechanism which is capable of explaining these spectral changes. Over the temperature range where the effects of this process first become apparent in the ^{13}C NMR spectra (-83 to -75 °C), the resonances in the $^{31}P\{^1H\}$ NMR spectra remain unbroadened. This result is, of course, expected; the axial-equatorial merry-go-round site exchange does not involve a phosphite ligand and leaves the magnetic environment of the ^{31}P nuclei unaltered before and after the exchange. It is noted that this is the only allowed plane for this cyclic permutation in either of the two isomers. In fact, the occurrence of such an exchange at a temperature where the $^{31}P\{^1H\}$ NMR signals are unchanged is indirect evidence supporting the choice of isomer **6f** rather than **6g** (vide supra), since the latter has no allowed planes with respect to the axial-equatorial merry-go-round process.

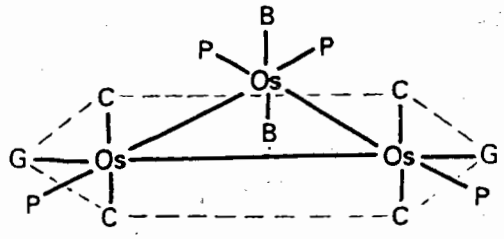

6f

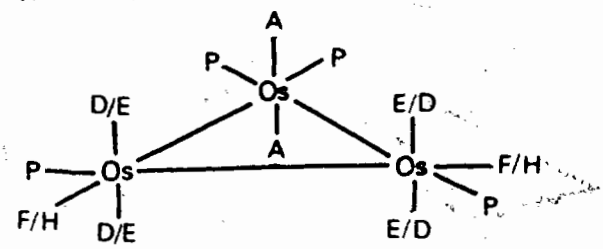

6g

Figure 6.17 Schematic representation showing assignment of the carbonyl ligands for the two isomers of $Os_3[P(OCH_3)_3]_4(CO)_8$.

The line shape for the two ^{13}CO resonances involved in the axial-equatorial merry-go-round was calculated. A consideration of figures 6.16 and 6.17 shows that the low field resonance (due to the axial carbonyl groups C) is obscured by a signal degeneracy. The portion of the calculated line shape due to the equatorial carbonyls (G) was matched to an experimental spectrum in the intermediate exchange region (-65 °C); at higher temperatures, collapse of the balance of the ^{13}C signals due to a higher energy process (vide infra) made accurate comparisons impractical. The portion of the calculated line shape due to resonance G (k= 60±4 sec^{-1}) and the matching experimental spectrum (at T= 208±2 °K) were in good agreement. A free energy of activation was calculated based on this rate and temperature data: $\Delta G^{\ddagger}$= 10.3±0.4 kcal mol^{-1} at 208 °K.

The effects of a higher energy exchange may be observed in the ^{13}C NMR spectra of $Os_3[P(OCH_3)_3]_4(CO)_8$ over the whole temperature range. These are shown in figure 6.18. The spectrum at -65 °C shows all the remaining resonances start to broaden at

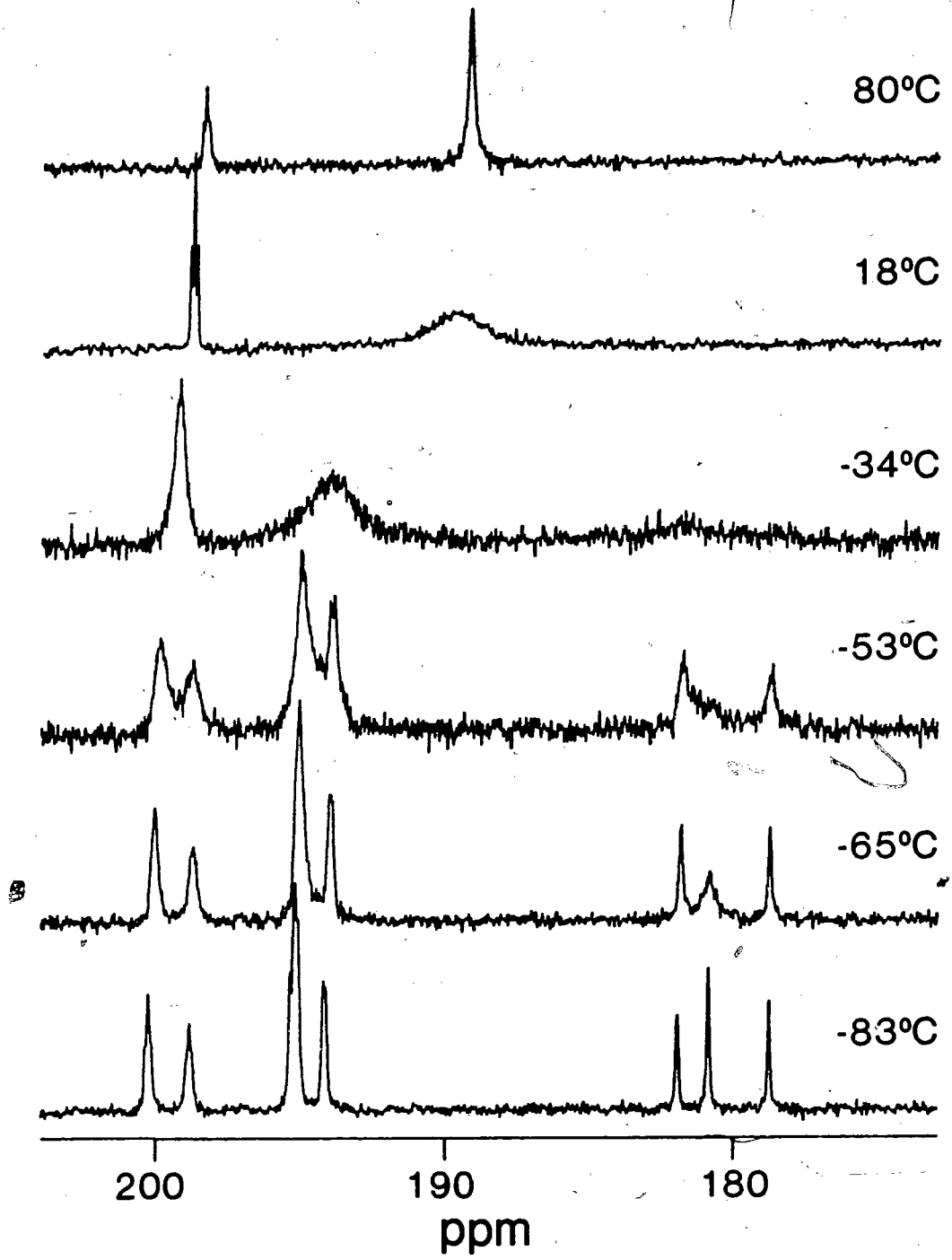

Figure 6.18 The variable temperature ^{13}C NMR spectra of $Os_3[P(OCH_3)_3]_4(CO)_8$ in toluene-d_8 measured at 100.6 MHz.

qualitatively the same rate. As the temperature is increased, the two low field triplets coalesce into a single triplet (J_{PC}= 11.2 Hz) while the remaining signals totally collapse and reappear as a singlet at 80 °C. The relative intensities of the resulting two resonances are 1:3, respectively. These spectral changes are completely consonant with the operation of a simultaneous, asynchronous set of trigonal twist processes (as previously proposed to explain the $^{31}P\{^1H\}$ NMR results) coupled with the lower energy axial-equatorial exchange. An examination of figures 6.15 and 6.16 shows that ^{13}C line broadening due to the higher energy exchange process occurs at qualitatively the same temperature as does signal broadening in the $^{31}P\{^1H\}$ NMR spectrum (~-60 °C). This result suggests that the same process is responsible for the respective changes to both sets of spectra.

An examination of **6f** and **6g** shows that this set of processes would cause averaging of the two ^{13}CO triplets to a single triplet and separate averaging of the remaining ^{13}CO resonances to a single signal. The line shape for the portion of the ^{13}C NMR spectrum containing the two triplets was calculated based on the proposed synchronous trigonal twist mechanism. This calculated line shape was matched to an experimental spectrum in the intermediate exchange region (-45 °C). The agreement between the simulated and observed data was good. The rate constant for this simulated spectrum (k= 300±5 sec^{-1}) was used to compute a free energy of activation value at the temperature of the

experimental spectrum (T= 228±2 °K): $\Delta G^{\ddagger}$= 10.6±0.4 kcal mol^{-1}.

Added evidence for the proposed mechanism comes from the averaged values of the ^{13}C chemical shifts for the carbonyl groups in $Os_3[P(OCH_3)_3]_4(CO)_8$. Plots of δ versus temperature were prepared, and in contrast to the phosphorus case, $d\delta^{13}C/dT$ was found to be approximately constant at or near the slow exchange limit. This was then used to obtain ^{13}C chemical shifts in the fast exchange region. Once again, the approximation that the equilibrium constant between **6f** and **6g** remained constant over the temperature range of interest was made. Operating under these assumptions the weighted average ^{13}C chemical shifts at 80 °C (as required by the proposed mechanism) were calculated. These values, 198.02 and 189.15 ppm, are in excellent agreement with the experimental values, 198.36 and 189.14 ppm, especially in light of the assumptions used for the calculated quantities.

The ^1H NMR spectra are also in accord with the propounded trigonal twist process. At -78 °C, the ^1H NMR spectrum of $Os_3[P(OCH_3)_3]_4(CO)_8$ in toluene-d_8 shows at least 4 sets of doublets (J~ 11-12 Hz) centred at δ 3.42 ppm. These results do not correspond to the slow exchange limit and the broad signals overlap. The analogous spectrum measured at 25 °C consists of two doublets (J_{PH}= 11.8, 12.2 Hz) of identical intensity, indicative of two magnetically unique ^{31}P (and thus ^1H) sites; the details of this argument are given in the discussion for $Os_3[P(OCH_3)_3]_5(CO)_7$.

The results for $Os_3[P(OCH_3)_3]_4(CO)_8$ may be summarized as follows. The nuclear magnetic resonance data, in the slow exchange limit, are consistent with the existence of two isomers in solution (i.e. **6f** and **6g**). The temperature dependent ^1H, ^{13}C, and $^{31}P\{^1H\}$ NMR spectra may be fully explained by two distinct dynamic processes. The effects of the one with the lowest energy are consonant with an axial-equatorial merry-go-round site exchange, occurring in the only allowed plane of the two isomers (i.e. in **6f**). For the second nonrigid process in $Os_3[P(OCH_3)_3]_4(CO)_8$, the evidence strongly supports the contention that there is set of simultaneous and asynchronous trigonal twist site exchanges operating. This overall process involves all four $Os[P(OCH_3)_3](CO)_3$ units of isomers **6f** and **6g**.

6.2.6 $Os_3[P(OCH_3)_3]_2(CO)_{10}$

The solution structures of $Os_3[P(OCH_3)_3]_2(CO)_{10}$, in the slow exchange limit, are readily deduced from the low temperature $^{31}P\{^1H\}$ NMR data. The spectrum of the disubstituted triosmium complex measured at -59 °C in toluene/toluene-d_8 (40.5 MHz) features three resonances. Two are doublets with identical coupling constants (J_{PP}= 1.9 Hz) while the other is a singlet. Clearly, more than one isomer is present in solution at this temperature. The four possible equatorially substituted isomers are schematically represented in the following figure.

Isomer **6m** may be eliminated on the basis of its inability (barring bridging phosphite intermediates) to undergo

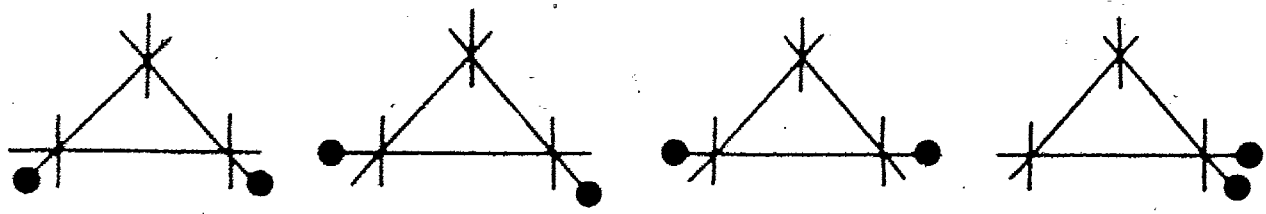

6l 6k 6j 6m

interconversion with any of the other three isomers (vide infra). The three $^{31}P\{^1H\}$ NMR signals dictate that isomer 6k must be present (two magnetically inequivalent ^{31}P nuclei) and based on steric arguments, the second isomer present is chosen as 6j. Although an accidental degeneracy of the ^{31}P NMR resonances in 6j and 6l could mask the presence of all three isomers, this possibility is precluded by the ^{13}C NMR data in the slow exchange limit (vide infra).

The only reasonable explanation for the small splittings shown by the two resonances of 6k is that they are due to a $^3J_{PP}$ coupling. This *cis* three bond coupling between magnetically inequivalent ^{31}P nuclei was not observed for $Os_3[P(OCH_3)_3]_x(CO)_{12-x}$ (x= 4,5). The single lines in the $^{31}P\{^1H\}$ NMR spectra of these complexes (in the slow exchange limit), however, are considerably broader (~8 Hz) than a corresponding line in the analogous spectrum of $Os_3[P(OCH_3)_3]_2(CO)_{10}$ (~3 Hz). This could be due to small *cis*-$^3J_{PP}$ couplings, broadening the resonances in the former. Signals due to free $P(OCH_3)_3$ have line widths of 1.5-2 Hz in both sets of spectra.

The temperature dependence of the $^{31}P\{^{1}H\}$ NMR spectra for $Os_3[P(OCH_3)_3]_2(CO)_{10}$ in toluene/toluene-d_8 is relatively uncomplicated. At approximately -20 °C, the three resonances begin to broaden at qualitatively the same rate and are close to coalescence at 30 °C. The spectrum at 79 °C features a single signal. The resonance due to added $P(OCH_3)_3$ remains sharp over this temperature range. The simplest process which can rationalize these spectral changes is identical to that proposed for $Os_3[P(OCH_3)_3]_4(CO)_8$: a simultaneous and asynchronous set of trigonal twists by the four $Os[P(OCH_3)_3](CO)_3$ moieties in the two isomers **6j** and **6k**. The observation of only a single $^{31}P\{^{1}H\}$ NMR resonance for $Os_3[P(OCH_3)_3]_2(CO)_{10}$ in the fast exchange limit precludes the possibility of single polytopal rearrangements and synchronous trigonal twist motions for either of the two isomers. This proposed dynamic process is strongly supported by the results of calculations on weighted average chemical shifts in the fast exchange region. Again, plots of $\delta^{31}P$ versus temperature were prepared for the three resonances of $Os_3[P(OCH_3)_3]_2(CO)_{10}$ from data at or near the slow exchange limit. These curves were only slightly non-linear and allowed reasonably accurate extrapolations of chemical shifts into the regions of interest. The invariance of the equilibrium constant between isomers **6j** and **6k** over the required temperature range was assumed, and values of the weighted average chemical shift at both 63 and 79 °C were calculated (based on the proposed mechanism). These and the corresponding experimental results are in excellent agreement (see table 6.2).

Temp. (°C)	δ_{calc} (ppm)	δ_{expt} (ppm)
63	-42.04±.05	-42.08±.02
79	-42.15±.06	-42.22±.02

Table 6.2 Calculated and experimental values for the $^{31}P\{^{1}H\}$ NMR chemical shifts of $Os_3[P(OCH_3)_3]_2(CO)_{10}$ in the fast exchange region.

The line shape for the $^{31}P\{^{1}H\}$ NMR spectrum of $Os_3[P(OCH_3)_3]_2(CO)_{10}$ was calculated based on the mechanism just proposed. This calculated line shape was matched to an experimental spectrum in the intermediate exchange region (17 °C). These two spectra are shown in figure 7.2 of appendix 2; it may be observed that the argeement between the calculated and observed spectra is excellent. The rate constant for the simulated spectrum (k= 31±1 sec^{-1}) was used to calculate a free energy of activation value at the temperature of the experimental spectrum (T= 290±2 °K): $\Delta G^{\ddagger}$= 15.0±0.4 kcal mol^{-1}.

The variable temperature ^{13}C NMR data for $Os_3[P(OCH_3)_3]_2(CO)_{10}$, while more complex than the analogous $^{31}P\{^{1}H\}$ NMR results, is completely consistent with the proposed mechanism. In addition, the ^{13}C spectra reveal the existence of lower energy dynamic processes. Several ^{13}C NMR spectra of $Os_3[P(OCH_3)_3]_2(CO)_{10}$ in toluene-d_8, over the temperature range -66 to -24 °C, are shown in figure 6.20. Consider the spectrum at -66 °C. The two resonances at lowest field appear as doublets, with

J_{PC} = 10.8, 11.7 Hz for the low and high field signals, respectively. The relative intensities of the 10 observable resonances, from low to high field, are 32:55:11:32:16:11:16:16:11:16.

Utilizing table 6.1 (with the data for $Os_3[P(OCH_3)_3]_4(CO)_8$ added) and the intensity data, the assignment of the ^{13}C NMR signals to the various carbonyl ligands of isomers **6j** and **6k** is straightforward. The results are presented in figures 6.19 and 6.20. These assignments assume one degeneracy; the more intense doublet is comprised of two overlapping doublets (one due to each isomer), completely consonant with the intensity data. The individual designation of the A/B pair and the pairwise specification of the H/I and F/K pairs are based on the proposed exchange process (vide infra). The validity of the succeeding argument does not require more specific assignments within the pairwise designations in isomers **6j** and **6k**.

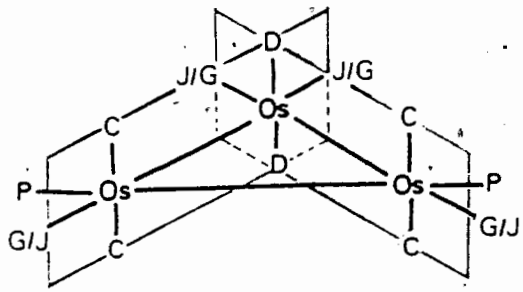

6j

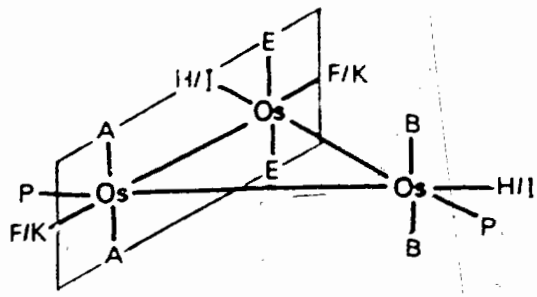

6k

Figure 6.19 Schematic representation showing assignment of the carbonyl ligands for the two isomers of $Os_3[P(OCH_3)_3]_2(CO)_{10}$.

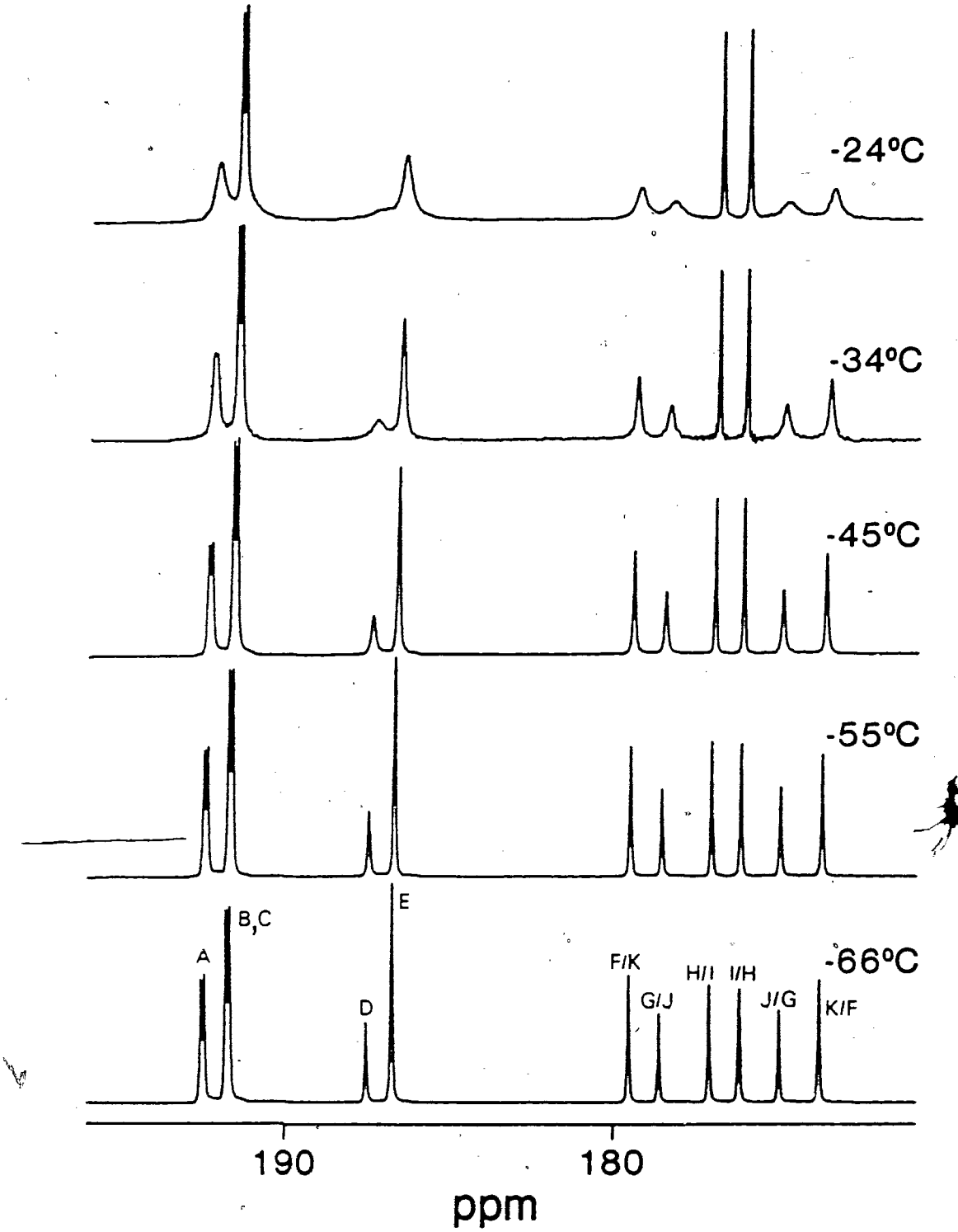

Figure 6.20 Several low temperature ^{13}C NMR spectra of $Os_3[P(OCH_3)_3]_2(^{13}CO)_{10}$ in toluene-d_8 (100.6 MHz).

The effects of the first stage of fluxionality in $Os_3[P(OCH_3)_3]_2(CO)_{10}$ may be observed in the ^{13}C NMR spectra of figure 6.20. Over this temperature range, four equatorial and three axial resonances start to broaden and collapse. In addition, the more intense doublet clearly loses intensity with respect to the two remaining equatorial signals, resulting in an approximate relative signal ratio of 2:1:1, respectively, at -24 °C. In light of the previously discussed degeneracy, the ^{13}C NMR spectra clearly show the broadening of four axial (A,C,D,E) and four equatorial resonances (F,G,J,K).

This behaviour is readily interpreted in terms of the onset of axial-equatorial merry-go-round processes, occurring in each of the three allowed planes in isomers **6j** and **6k** (see figure 6.19). Such a mechanism would leave the $P(OCH_3)_3$ ligands in unaltered positions. The resonances in the $^{31}P\{^1H\}$ NMR spectra of $Os_3[P(OCH_3)_3]_2(CO)_{10}$ remain unbroadened over this temperature range; in fact, there is no apparent broadening of the $^{31}P\{^1H\}$ NMR spectrum up to -20 °C. The difference between this temperature and that at which signal broadening becomes apparent in figure 6.20 (~-60 °C) effectively rules out the previously discussed set of trigonal twists as the sole source of the ^{13}C spectral changes shown in figure 6.20.

It should be noted that there are several reasonable site exchange processes within the two isomers. In addition to the one just mentioned, some examples are as follows: a purely equatorial merry-go-round (**6k** only, see figure 6.3), a

synchronous or asynchronous mutual trigonal twist of $Os[P(OCH_3)_3](CO)_3$ moieties, an individual trigonal twist of any one such group, a trigonal or tetragonal rotation of an $Os(CO)_4$ portion of **6j** or **6k**, and compatible combinations of the above. A careful analysis of all physically reasonable possibilities shows that only the axial-equatorial merry-go-round process, occurring in the three allowed planes, is completely consonant with the ^{13}C NMR signal intensities, the variable temperature $^{31}P\{^1H\}$ NMR data, and the information in table 6.1.

The apparent simultaneous onset of the three individual cyclic permutations requires some discussion. Such an occurrence is not required, and indeed a careful examination of the full scale ^{13}C NMR spectra indicates that this is not precisely the case.

The existence of vertical plane of symmetry in **6j** implies that the activation energies for the two planar exchanges within this isomer would be equal. Examining the expanded ^{13}C NMR spectra over the temperature range in figure 6.20, resonances J and G appear to broaden at the same rate (as required) while resonance C is obscured by the degeneracy. The signal due to the axial carbonyl groups of the $Os(CO)_4$ unit in **6j** (i.e. D), however, is observed to broaden considerably more rapidly than resonances J and G. This is, of course, just the behaviour anticipated. The site which gives rise to resonance D is common to both the allowed planes in **6j** and the rate of exchange for this position would be the sum of the rates appropriate to the

two processes.

The plane in which the axial-equatorial merry-go-round process occurs for isomer **6k** is distinct from either allowed plane in **6j**, and there is no requirement that site exchange within the former happen with the same rate as within the latter pair. A careful examination of detailed ^{13}C NMR spectra measured between -66 and -24 °C shows a clear difference between the broadening line widths of resonances F,K and J,G; at -24 °C, the line widths of J and G are approximately 1.5 times larger than those of F and K.

A consideration of figures 6.19 and 6.20 shows that all of the ^{13}CO resonances of the single allowed plane in isomer **6k** are clearly resolved. The line shape of the ^{13}C spectrum due to these resonances (based on an axial-equatorial merry-go-round process) was calculated. The calculated line shape was matched to the observed spectrum at -13 °C; these two spectra are shown in figure 7.3 in appendix 2. The simulated and experimental spectra are in excellent agreement when the effect of the other ^{13}CO resonances in the latter data are taken into account. The rate constant of the calculated line shape ($k = 120 \pm 4$ sec^{-1}) was used to calculate a value of $\Delta G^{\ddagger}$ at the temperature of the observed spectrum ($T = 260 \pm 2$ °K): $\Delta G^{\ddagger} = 12.7 \pm 0.4$ kcal mol^{-1}.

The symmetry of isomer **6j** (see figure 6.19) dictates that the axial-equatorial exchanges in both allowed planes occur at the same rate. The two planar permutations are coupled (via the

carbonyls giving rise to resonance D) which leads to a ten site exchange problem. A line shape due to this exchange was calculated and matched to the observed ^{13}C spectrum at -13 °C. The matching process was less accurate than for isomer **6k**; resonance C is part of a signal degeneracy while resonance B is extremely broad and obscured by signal A (see figures 6.19 and 6.20). The best fit of the calculated line shape to the observed spectrum was for k= 200±15 sec^{-1}. This allowed calculation of the following free energy of activation value (T= 260±2 °K): $\Delta G^{\ddagger}$= 12.4±0.5 kcal mol^{-1}.

The two values of $\Delta G^{\ddagger}$ for the axial-equatorial merry-go-round exchanges in isomers **6j** and **6k** are equal within experimental error.

The fact that the Os_3P_2 skeletons of isomers **6j** and **6k** remain distinct during the planar cyclic permutations implies that the weighted average chemical shifts for the two isomers need not be the same. The high temperature limiting spectrum due to the axial-equatorial merry-go-round processes was not observed due to the onset of a higher energy exchange (vide infra). Before the effects of the latter became apparent, however, the former process resulted in a very broad signal at δ 185±1. Assuming the equilibrium constant between **6j** and **6k** to be unchanged from its value at -66 °C, and extrapolating from plots of δ versus temperature for the various ^{13}C resonances, values for the weighted average chemical shifts of the two isomers were calculated. The results, 184.1±0.2 ppm and 184.5±0.2 ppm for **6j**

and **6k** respectively, agree reasonably well with the experimental observation of a very broad signal at 185±1 ppm.

The full variable temperature ^{13}C NMR spectra of $Os_3[P(OCH_3)_3]_2(^{13}CO)_{10}$ (see experimental section, chapter 2, for details of ^{13}CO enrichment) are presented in figure 6.21, where the spectral consequences of a second stage of fluxionality may be observed. At approximately -20 °C (spectrum not shown) the three previously unchanged resonances begin to broaden; at -3 °C, they are observed to have broadened considerably. These resonances collapse along with the nearly coalesced signal due to the first set of nonrigid processes as the temperature is increased.These signals reappear as a single broad resonance at 87 °C. This behaviour is consistent with the effects of the simultaneous and asynchronous trigonal twist processes within **6j** and **6k**, proposed earlier from $^{31}P\{^1H\}$ NMR evidence, superimposed upon the spectral changes due to the three axial-equatorial site exchanges. These two overlayed processes would result in complete exchange of all carbonyl ligands and consequent observation of a single, averaged ^{13}C NMR resonance.

The temperature at which the remaining three ^{13}CO resonances of $Os_3[P(OCH_3)_3]_2(CO)_{10}$ start to broaden (~-20 °C) is qualitatively the same as that observed for the onset of signal broadening in the $^{31}P\{^1H\}$ NMR spectrum of this complex. This result supports the contention that the same process is responsible for both the spectral changes just described.

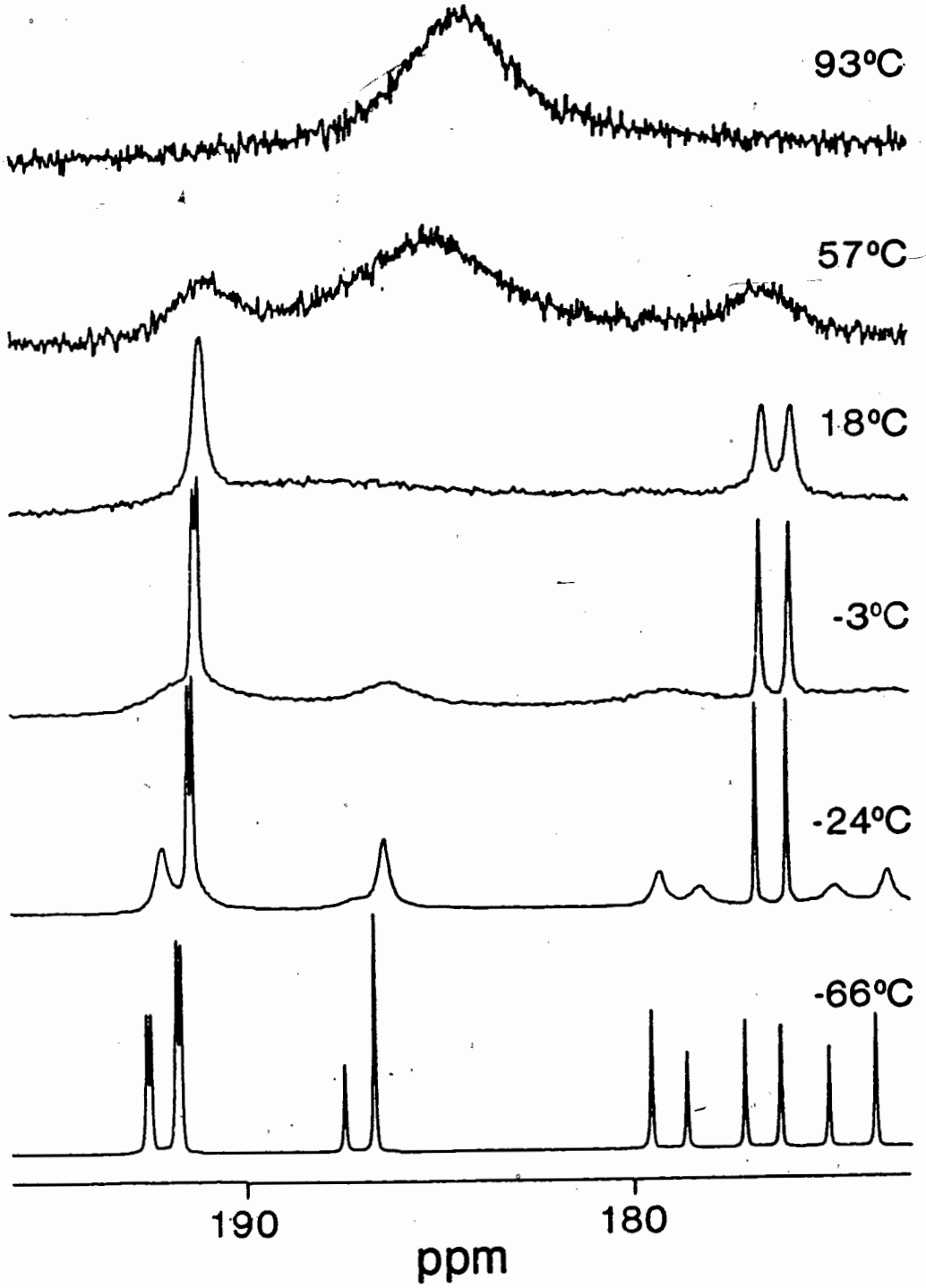

Figure 6.21 Variable temperature ^{13}C NMR spectra of $Os_3[P(OCH_3)_3]_2(^{13}CO)_{10}$ in toluene-d_8 (100.6 MHz).

Utilizing methods and assumptions completely analogous to those previously discussed, the value of this weighted average chemical shift at 87 °C was calculated to be 183.8±0.2 ppm. When compared to the experimentally determined chemical shift at this temperature, 184.3±0.3 ppm, the agreement is very close considering the assumptions used. This agreement represents further evidence in support of the proposed nonrigid processes.

The ^1H NMR spectra of $Os_3[P(OCH_3)_3]_2(CO)_{10}$, measured in the slow and fast exchange regions, are completely consistent with the previous results and proposals. At -47 °C, the spectrum in toluene-d_8 exhibits three doublets (J_{PH}= 12.4, 12.4, 12.3 Hz), in accord with isomers **6j** and **6k**. The analogous spectrum measured in the fast exchange regime (51 °C) features one doublet (J= 12.2 Hz), consonant with a single, averaged magnetic environment for the protons in $Os_3[P(OCH_3)_3]_2(CO)_{10}$.

In summary, the variable temperature ^1H, ^{13}C and $^{31}P\{^1H\}$ NMR data lead to the following conclusions regarding $Os_3[P(OCH_3)_3]_2(CO)_{10}$. In the slow exchange limit, this complex exists as 2 isomers (**6j** and **6k**) in solution. The spectral changes with increasing temperature may be fully explained by two successive and distinct dynamic processes. The effects of the one with the lowest energy are consistent with a set of axial-equatorial merry-go-round site exchanges, occurring in the three allowed planes of the two isomers. Although the evidence suggests that the two planar exchanges in isomer **6j** have a different activation energy than that associated with the

exchange in **6k**, the data does not allow calculation of a meaningful difference. The higher energy dynamic process causes spectral changes completely in accord with a set of simultaneous and asynchronous trigonal twist exchanges occurring in both **6j** and **6k**.

6.3 Discussion

In table 6.3 the calculated $\Delta G^{\ddagger}$ values for the various nonrigid processes in the series $Os_3[P(OCH_3)_3]_x(CO)_{12-x}$ (x= 1-6) are tabulated, along with the rate constants and temperatures used in the calculations. One feature of this table is immediately apparent: the free energies of activation for the axial-equatorial merry-go-round processes in $Os_3[P(OCH_3)_3]_x(CO)_{12-x}$ (x= 1,2,4) decrease as x increases.

This observation is closely linked to the conclusions drawn from the variable temperature ^{13}C behaviour of $Os_3[PEt_3]_x(CO)_{12-x}$ (x= 1,2) in toluene [111]. Both these complexes underwent selective site exchange of axial and equatorial carbonyl ligands at relatively low temperatures. This was attributed to the axial-equatorial merry-go-round process proposed in this thesis. The proposal that a phosphine had a labilizing influence on an osmium atom, causing adjacent carbonyls to take up bridging positions at low temperatures, was proffered. This hypothesis was based on the fact that $Os_3(CO)_{12}$ does not show coalescence of the axial and equatorial ^{13}CO

Compound	k (sec^{-1})	Temp. (°C)	$\Delta G^{\ddagger}$ (kcal mol^{-1})
AX/EQ MERRY-GO-ROUND			
$Os_3[P(OCH_3)_3](CO)_{11}$	230±5	20±2	14.0±0.4
	50±2	20±2	14.9±0.4
$Os_3[P(OCH_3)_3]_2(CO)_{10}$	200±15	-13±2	12.4±0.5
	120±4	-13±2	12.7±0.4
$Os_3[P(OCH_3)_3]_4(CO)_8$	60±4	-65±2	10.3±0.4
TRIGONAL TWIST			
$Os_3[P(OCH_3)_3]_2(CO)_{10}$	31±1	17±2	15.0±0.4
$Os_3[P(OCH_3)_3]_3(CO)_9$	40±2	-2±2	13.8±0.4
$Os_3[P(OCH_3)_3]_4(CO)_8$	300±5	-45±2	10.6±0.4
$Os_3[P(OCH_3)_3]_5(CO)_7$	40±2	-20±2	12.9±0.4

Table 6.3 Calculated free energies of activation for the various nonrigid processes in $Os_3[P(OCH_3)_3]_x(CO)_{12-x}$ (x= 1-5). Included are the rate constants and temperatures used in the calculations.

resonances until 70 °C [141], as opposed to 0 and -20 °C for the analogous processes in $Os_3[PEt_3]_x(CO)_{12-x}$ (x= 1,2), respectively. It is felt that the data presented in this thesis allows the analysis of this phenomenon in considerable depth.

Consider the parent $Os_3(CO)_{12}$. It has been proven that site exchange between the axial and equatorial carbonyl ligands is

not localized and all CO groups have access to the three osmium atoms [145]. In light of this evidence and the results for $Os_3[P(OCH_3)_3]_x(CO)_{12-x}$ (x= 1,2,4) and $Os_3[PEt_3]_x(CO)_{12-x}$ (x= 1,2) [111], the only physically reasonable mechanism for axial-equatorial carbonyl site exchange in $Os_3(CO)_{12}$ is the merry-go-round process.

The variable temperature ^{13}C NMR evidence for $Os_3[P(OCH_3)_3](CO)_{11}$ (below 20 °C) is completely consistent with with the operation of two individual merry-go-round processes. The one with the highest energy involves a plane lacking an attached, but non-coplanar, $P(OCH_3)_3$ ligand *trans* to a Os-Os bond (see figure 6.11). The cyclic permutation with the lowest free energy of activation occurs in a plane which has a phosphite group in this position. Both fluxional processes have a lower $\Delta G^{\ddagger}$ than that associated with the analogous exchange in $Os_3(CO)_{12}$ (>16 kcal mol^{-1}) [169].

Consider the case of $Os_3[P(OCH_3)_3]_2(CO)_{10}$. Carbonyls in three separate planes of the two isomers are capable of undergoing the cyclic permutation (see figure 6.19); the two planes within **6j** are equivalent by symmetry. Recall that the calculation of a meaningfully different $\Delta G^{\ddagger}$ value for this process (within the two planes of **6j**) relative to that for the single allowed plane of isomer **6k** was not possible. Each of these three planes has one $P(OCH_3)_3$ ligand in a non-planar position *trans* to a metal-metal bond, plus another phosphite group on the non-planar Os atom. The axial-equatorial

merry-go-round site exchanges which occur within these planes have lower free energies of activation than the two analogous processes in $Os_3[P(OCH_3)_3](CO)_{11}$.

Finally, focus on $Os_3[P(OCH_3)_3]_4(CO)_8$. The only allowed plane for the cyclic permutation has both the non-planar *trans* positions occupied by $P(OCH_3)_3$ ligands (see figure 6.17). In addition, **6f** has two phosphite ligands on the non-planar metal atom. This isomer has four $P(OCH_3)_3$ ligands in total and the $\Delta G^{\ddagger}$ for the axial-equatorial merry-go-round process is ~2 kcal mol^{-1} less than the corresponding value for $Os_3[P(OCH_3)_3]_2(CO)_{10}$.

Collectively, these results suggest the existence of some relationships between the presence of $P(OCH_3)_3$ ligands and the free energies of activation for the cyclic carbonyl site exchanges in $Os_3[P(OCH_3)_3]_x(CO)_{12-x}$ (x= 1,2,4). As already observed, an increase in the number of phosphite ligands bonded to the Os_3 framework causes a decrease in $\Delta G^{\ddagger}$ for the nonrigid process(es) within the allowed planes. In addition, the proximity of the $P(OCH_3)_3$ to the plane in question appears to have an effect. For example, the energy barrier for the process in plane A of $Os_3[P(OCH_3)_3](CO)_{11}$ (with one directly attached phosphite ligand) is lower than that for the cyclic permutation in plane B, with the lone $P(OCH_3)_3$ group bonded to the non-planar osmium atom (see figure 6.11). The unique allowed plane in $Os_3[P(OCH_3)_3]_4(CO)_8$ (figure 6.17) has $P(OCH_3)_3$ ligands in both the non-planar, *trans* positions (plus two on the extraneous Os atom): the axial-equatorial merry-go-round site

exchange in this plane occurs with a considerably lower $\Delta G^{\ddagger}$ than for $Os_3[P(OCH_3)_3]_2(CO)_{10}$, which lacks the two additional phosphite groups. Unfortunately, the large uncertainties in the free energies of activation (see table 6.3) preclude a more detailed analysis of the relative influence that number and proximity of $P(OCH_3)_3$ ligands play in the axial-equatorial exchange process.

The question arises as to why the presence of phosphite groups affects the barrier to nonrigidity; the effect might be sterically or electronically transmitted. Some experimental data regarding the question of steric effects is available. The x-ray crystal structures of $Os_3(CO)_{12}$ [137] and $Os_3[P(OCH_3)_3](CO)_{11}$ [109] yield some pertinent information regarding bond angles; the substitution of $P(OCH_3)_3$ for an equatorial carbonyl ligand causes suprisingly small changes in bond angles within the equatorial plane and between axial carbonyl groups and the triosmium plane. Consider the solid state structure of $Fe_3(CO)_{12}$ [143,167], shown schematically as **6n**. It represents the idealized structure of the intermediate in the axial-equatorial merry-go-round process (see figure 6.1). The formation of **6n** from the non-bridged structure **6o**, representing the pseudo-D_{3h} symmetry of $Os_3(CO)_{12}$ and substituted derivatives, would cause severe changes in bond angles for the carbonyl groups marked a and b. If the phosphite-induced lowering in energy of the planar cyclic permutation was steric in nature, one might anticipate the introduction of $P(OCH_3)_3$ to cause some structural changes

towards that shown in **6n**. The lack of such a reorientation of carbonyl ligands upon substitution of $P(OCH_3)_3$ for CO in $Os_3(CO)_{12}$ argues against a major role for steric effects in the variation of $\Delta G^{\ddagger}$ for the axial-equatorial merry-go-round process in $Os_3[P(OCH_3)_3]_x(CO)_{12-x}$ (x= 1,2,4). Similarly, a detailed examination of bond angle data from the x-ray structures of $Ru_3(CO)_{12}$ [170], $Ru_3[PPh_3](CO)_{11}$ [171], and $Ru_3[P(OCH_3)_3]_2(CO)_{10}$ [110] reveals only small changes as the group V donor ligand substitution is increased. These arguments are based, of course, on the assumption that one may use solid state x-ray data to infer properties of molecules in solution.

A qualitative consideration of coordination about the planar Os atoms in the bridged (**6n**) and non-bridged (**6o**) forms of the axial-equatorial merry-go-round process is informative. In the unbridged structure both osmium atoms in the allowed plane are six coordinate while the formation of the bridged intermediate causes a unit increase in coordination number. Based on this argument, the introduction of a $P(OCH_3)_3$ ligand into a non-planar site attached to an osmium atom in an allowed plane should increase the steric pressure at that metal centre in the intermediate, thus increasing the $\Delta G^{\ddagger}$ for the cyclic permutation

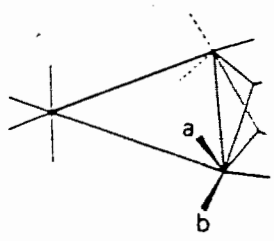

6n

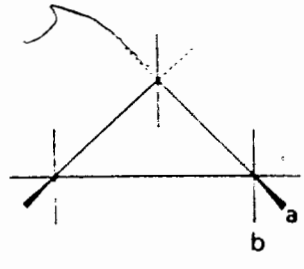

6o

process. That this prediction is contrary to the experimental results is further evidence that the variation in activation barrier with phosphite substitution for the axial-equatorial merry-go-round process is not sterically transmitted.

The observation that a phosphite ligand directly attached to (but not contained in) an allowed plane causes a greater effect than one on the non-planar Os centre may qualitatively be explained in electronic terms. The better σ-donor and poorer π-acceptor properties of $P(OCH_3)_3$ relative to CO would increase the electron density on the complex upon phosphite substitution. One might expect the consequent effects to be felt most strongly in the general area of phosphite coordination, i.e. an adjacent allowed plane. A more quantitative explanation would require molecular orbital calculations for both the complexes in question and a model for the intermediate (i.e. $Fe_3(CO)_{12}$). In addition, a more detailed understanding of the electronic nature of the axial-equatorial merry-go-round process would be helpful. Further studies of the type just reported would allow a more comprehensive assessment of the factors involved. The preparation and variable temperature ^{13}C NMR investigation of complexes such as $Os_3[PR_3](CO)_{11}$ and $Os_3[P(OR)_3](CO)_{11}$ (R= alkyl and aryl) (where the electronic and steric properties of the phosphorus donor ligand were varied in a controlled manner) would undoubtedly shed more light on the relative magnitude of steric and electronic effects.

The suggestion has been made, based on rather limited experimental observations of the variable temperature ^{13}C NMR behaviour of $HM_3(CO)_9[C_2C(CH_3)_3]$ (M= Ru, Os) and $M_3(CO)_{12}$ (M= Ru, Os), that ligand charge donor ability is of primary importance in determining the barrier to axial-equatorial exchange of carbonyl groups [142]. In addition, temperature dependent ^1H and ^{13}C NMR studies of $H_2Os_3(CO)_{10}L$ (L= various phosphines and phosphites) were interpreted as implying that the effects of L on activation barriers to carbonyl and hydride exchange were steric and electronic in nature [157]. The results of these two studies, however, are only indirectly related to the present work; both the structures and dynamic processes in the two cases are considerably different.

Let us now examine the results regarding the trigonal twist site exchange for the series $Os_3[P(OCH_3)_3]_x(CO)_{12-x}$ (x= 1-6). The changes in the $\Delta G^{\ddagger}$ values (table 6.3) for this process with increasing phosphite substitution do not parallel the findings for the axial-equatorial merry-go-round mechanism: a decrease for x= 2,3,4 is followed by an increase in the free energy of activation for $Os_3[P(OCH_3)_3]_5(CO)_7$. This result is not entirely unanticipated. The values of $\Delta G^{\ddagger}$ for the cyclic permutations occurring in the complexes $Os_3[P(OCH_3)_3]_x(CO)_{12-x}$ (x= 1,2,4) could be compared directly since the mechanistic details were essentially the same. This is not the case for the trigonal twist process; a single such site exchange was proposed for $Os_3[P(OCH_3)_3]_5(CO)_7$, three exchanges transpiring synchronously

were operating for $Os_3[P(OCH_3)_3]_3(CO)_9$, while the di- and tetrasubstituted triosmium complexes featured pairs of asynchronous trigonal twist permutations occurring within each of two isomers. The interactional details resulting from such a differential coupling of several single processes are not clear and simple, comprehensive predictions are precluded.

The results for $Os_3[P(OCH_3)_3]_2(CO)_{10}$ and $Os_3[P(OCH_3)_3]_4(CO)_8$ may be confidently compared, as they share a similar nonrigid process. The difference between the two lies in the nature of the metal-ligand group not involved in the trigonal twist site exchange: an $Os(CO)_4$ group for $Os_3[P(OCH_3)_3]_2(CO)_{10}$ and an $Os[P(OCH_3)_3]_2(CO)_2$ moiety for the tetrasubstituted complex. The free energy of activation for the process in question is ~4 kcal mol^{-1} less in the latter. This relatively large difference may be steric or electronic in origin. The near total lack of theoretical or experimental information regarding this type of complex, from either point of view, inhibits a more detailed analysis.

Clearly, a more comprehensive examination of this system is required in advance of firmer conclusions. The relative ease of preparation for $Os_3[P(OCH_3)_3]_x(CO)_{12-x}$ (x= 1-6) suggests that analogues, utilizing phosphines and phosphites of varying cone angles and basicity, are synthetically accessible. A judicious variation of these ligand properties would undoubtedly allow increased insight into the relative importance of steric and electronic factors with respect to the trigonal twist process.

Some general statements regarding the ligand exchange processes in $Os_3[P(OCH_3)_3]_x(CO)_{12-x}$ (x= 1-6) are warranted. The variable temperature NMR evidence has strongly implicated the trigonal twist process as a common mechanism for carbonyl and phosphite site exchange in this series. It is noted, however, that it does not intrinsically possess the lowest energy. Where a suitable plane exists for the axial-equatorial merry-go-round to operate, it will occur first. In the members of $Os_3[P(OCH_3)_3]_x(CO)_{12-x}$ where there are no allowed planes (i.e. x= 3,5), the trigonal twist is the only process which occurs. Recall the experimental results for $Os_3[P(OCH_3)_3](CO)_{11}$. Three distinct phases of fluxionality were observed, the two with the lowest energy completely consistent with axial-equatorial merry-go-round exchanges. The third fluxional process, which involved the carbonyl ligand not involved in the previous two processes, could not be unequivocally assigned to a specific mechanism. In light of the previous discussion, it appears likely that the trigonal twist process is responsible for this final dynamic phase in $Os_3[P(OCH_3)_3](CO)_{11}$.

It is informative to contrast the present results with those found for similar complexes. The variable temperature ^{13}C NMR study of $Os_3[PEt_3]_x(CO)_{12-x}$ (x= 1-3) [111] has been mentioned several times in this discussion. The results for x= 1,2 are not identical to those observed for $Os_3[P(OCH_3)_3](CO)_{11}$ and $Os_3[P(OCH_3)_3]_2(CO)_{10}$. For the case of the monosubstituted PEt_3 complex, only a single axial-equatorial merry-go-round site

exchange, with approximately the same coalescence temperature as the lowest energy process in $Os_3[P(OCH_3)_3](CO)_{11}$, was suggested. A second stage of fluxionality, characterized by complete collapse of all signals to a single resonance, was observed with a T_c of approximately 40 °C. This latter result was attributed only to a breakdown in the rigidity of the phosphine. As previously discussed, the overall results for $Os_3[P(OCH_3)_3]_x(CO)_{12-x}$ (x= 1-6) suggest that the final stage of fluxionality for $Os_3[P(OCH_3)_3](CO)_{11}$ is due to an individual trigonal twist site exchange. It is reasonable to assign the highest energy exchange process in $Os_3[PEt_3](CO)_{11}$ to the same source. The report of only one axial-equatorial merry-go-round site exchange for $Os_3[PEt_3](CO)_{11}$, as opposed to two such exchanges for $Os_3[P(OCH_3)_3](CO)_{11}$, is not simply rationalized on the basis of available information.

There are also significant differences between $Os_3[P(OCH_3)_3]_2(CO)_{10}$ and $Os_3[PEt_3]_2(CO)_{10}$. In the low temperature limit (-60 °C), the triethyl phosphine complex existed in solution as a single isomer as determined by ^{13}C NMR spectroscopy. The spectrum of this isomer (corresponding structurally to **6k** on page 314) suffered two distinct phases of fluxionality, consistent with the action of a single axial-equatorial merry-go-round site exchange and a subsequent process causing coalescence of all other carbonyl resonances. These results for $Os_3[PEt_3]_2(CO)_{10}$ are, of course, in sharp contrast to those found for the trimethyl phosphite analogue:

isomers **6j** and **6k** were observed for $Os_3[P(OCH_3)_3]_2(CO)_{10}$ at low temperature. In addition, axial-equatorial carbonyl exchanges by cyclic permutations in three distinct planes (two equivalent by symmetry) were observed. These processes possessed lower activation energies than that of the final process: a simultaneous and asynchronous trigonal twist exchange of the four $Os[P(OCH_3)_3](CO)_3$ moieties in **6j** and **6k**. Again, a simple rationalization for the contrasting behaviour of $Os_3[PEt_3]_2(CO)_{10}$ and $Os_3[P(OCH_3)_3]_2(CO)_{10}$ is not immediately apparent. A detailed study of the complexes $Os_3[PR_3]_x(CO)_{12-x}$ and $Os_3[P(OR)_3]_x(CO)_{12-x}$ (R= alkyl and aryl; x= 1,2) could allow a more detailed picture of the factors influencing the number of isomers observed and the nature of the exchange processes occurring.

The differences in behaviour between $Os_3[PEt_3]_x(CO)_{12-x}$ and $Os_3[P(OCH_3)_3]_x(CO)_{12-x}$ (x= 1,2) are not mirrored for the trisubstituted derivatives. Both $Os_3[P(OCH_3)_3]_3(CO)_9$ and $Os_3[PEt_3]_3(CO)_9$ exhibit two resonances in the slow exchange limiting ^{13}C NMR spectrum; these two pairs of signals undergo broadening and coalescence at approximately the same temperature (0-20 °C) to produce a single signal. This result, in concert with the present findings, implies that $Os_3[PEt_3]_3(CO)_9$ has a static solution structure analogous to **6e** (as stated by the original authors [111]) and undergoes axial-equatorial carbonyl site exchange by the synchronous trigonal twist of three equivalent $Os[PEt_3](CO)_3$ groups (as proposed for

$Os_3[P(OCH_3)_3]_3(CO)_9$).

The complex 1,2-$\{Os_3[PMe_2Ph]_2(CO)_{10}\}$ has been prepared and studied by variable temperature ^{13}C and $^{31}P\{^1H\}$ NMR methods [107,108]. The slow exchange limit $^{31}P\{^1H\}$ NMR spectrum showed a mixture of two isomers, assigned to structures **6p** and **6q**. The low temperature ^{13}C NMR spectrum did not clearly reveal the resonances due to the minor isomer (**6p**). At -10 °C, the $^{31}P\{^1H\}$ NMR signals due to the two isomers were observed to broaden at different rates (major isomer more rapidly) and coalesce to a single resonance above 80 °C. The authors claimed that the interchange of the PMe_2Ph ligands within **6q** did not occur primarily by interconversion of **6p** and **6q**, and quoted line shape analysis results that gave the rate of PMe_2Ph exchange within **6q** as 20 times faster than interconversion between the two isomers. It was claimed that a simultaneous and coupled turnstile rotation at the two substituted Os atoms of **6q** (which would cause exchange of the two magnetically inequivalent ^{31}P nuclei)

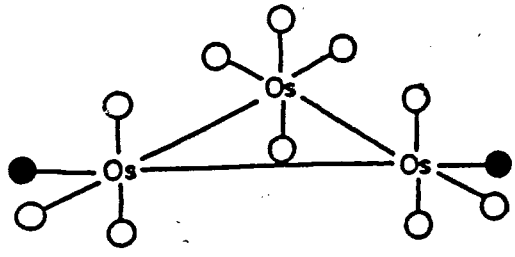

6p

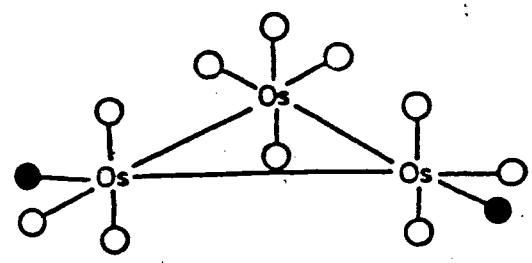

6q

●=PMe_2Ph ○=CO

was faster than rotation at a single osmium atom. The latter would lead to isomer **6p**. These results and their interpretation are in contrast to the findings for $Os_3[P(OCH_3)_3]_2(CO)_{10}$, where the three $^{31}P\{^1H\}$ NMR signals broadened at the same rate, and a simultaneous but asynchronous set of trigonal twist processes within both isomers was proposed.

A careful examination of the experimental data for 1,2-$\{Os_3[P(CH_3)_2C_6H_5]_2(CO)_{10}\}$, however, appears to indicate that it exchanges in much the same manner as $Os_3[P(OCH_3)_3]_2(CO)_{10}$. At very slow exchange rates we propose that isomer **6q** undergoes a synchronous trigonal twist process involving the two phosphine ligands, causing small amounts of signal broadening while the resonance due to **6p** is unaffected. This is as stated by the authors. However, this process is rapidly followed by the onset of an asynchronous set of such exchanges for all four $Os[P(CH_3)_2C_6H_5](CO)_3$ moieties of **6p** and **6q** (as for $Os_3[P(OCH_3)_3]_2(CO)_{10}$), those for the minor isomer being slightly slower. That the synchronous or coupled nature of the two trigonal twists in isomer **6q** must be broken may be simply ascertained: if uncoupling did not occur, one would not expect a single resonance in the fast exchange limit. This situation is similar to that shown on page 303 (change the $Os[P(OCH_3)_3]_2(CO)_2$ units to $Os(CO)_4$). The entrance of isomer **6p** into the averaging process must also be accounted for. If the two trigonal twist processes in this isomer were synchronous, again one would not expect a single resonance in the high temperature limiting

$^{31}P\{^{1}H\}$ NMR spectrum. If one or the other localized exchange occurred individually, isomer **6q** would necessarily be formed. Clearly, the individual site exchanges occurring at each $Os[P(CH_3)_2C_6H_5](CO)_3$ group of **6p** and **6q** must be asynchronous (except at very slow exchange rates) to explain the observed NMR behaviour.

A variable temperature ^{13}C and $^{31}P\{^{1}H\}$ NMR investigation of 1,2,3-$\{Os_3[P(OCH_3)_3](PPh_3)_2[CO]_9\}$ has been undertaken [107]. The low temperature limiting spectra and the temperature dependent spectral changes were completely consistent with the structure **6r** undergoing a simultaneous and synchronous set of trigonal twist processes, as proposed for $Os_3[P(OCH_3)_3]_3(CO)_9$ and $Os_3[PEt_3]_3(CO)_9$.

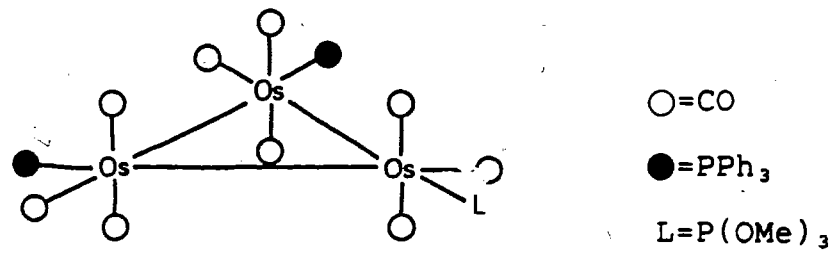

6r

An alternate view of stereochemical nonrigidity in metal clusters has recently been advanced in the literature. In this approach the CO ligands of metal clusters are regarded as spheres of radius 3.02 angstroms; these are packed so as to leave a sufficiently large polyhedral cavity to accommodate the

metal core [133]. Fluxionality is thought of as the result of a reorientation of the metal cluster within the ligand polyhedra. There is some experimental support for the contention that only small changes in metal-metal bond lengths or ligand separations are required for this type of dynamic behaviour [110,133,172].

It is difficult to imagine such a process accounting for the stereochemical nonrigidity in the series $Os_3[P(OCH_3)_3]_x(CO)_{12-x}$ (x= 1-6). The different ^{31}P and ^{13}C magnetic environments arise because of the **relative** positions of the ligands with respect to **one another**. Resonances broaden and collapse when the ligand nuclei which give rise to them undergo chemical exchange between magnetically inequivalent sites. As these sites exist by virtue of relative ligand orientation, it would appear reasonable that major reorientations of the ligands with respect to one another would be required to rationalize the observed temperature dependent spectral changes for these complexes.

The use of selected ^{13}C chemical shift data for carbonyl ligands in the $Os_3[P(OCH_3)_3]_x(CO)_{12-x}$ series to aid in spectral assignments of other members has been commented upon. The information in table 6.4 gives the ^{13}CO chemical shifts (at or near the slow exchange limit) for all members of the series in terms of the axial/equatorial position and degree of phosphite substitution on the attached Os atom.

For this series of complexes, there are three general types of axial carbonyl environments, corresponding to coordination in

an $Os(CO)_4$, $Os[P(OCH_3)_3](CO)_3$, or $Os[P(OCH_3)_3]_2(CO)_2$ moiety. The chemical shift ranges of the carbonyl ligands in these three groups are mutually exclusive. The equatorial carbonyl ligands may exist in either of two general environments, with a phosphite or carbonyl in the other equatorial position of the same osmium atom. By analogy to the situation for the axial ligands, one might expect an equatorial carbonyl group to exhibit a chemical shift further downfield when *cis* to a $P(OCH_3)_3$. For the mono- and disubstituted triosmium complexes, an assignment consistent with this expectation and the proposed fluxional processes is possible; the results are shown in table 6.4. These two chemical shift ranges are virtually mutually exclusive. This detailed division of the ^{13}CO chemical shifts into distinct regions has obvious utility if the phenomenon is general.

The ^{13}C NMR chemical shift data for $Os_3[PEt_3]_x(CO)_{12-x}$ (x= 1-3) [111], organized as previously described, are shown in table 6.5. With the exception of a single value, these chemical shifts also fall into discrete groups. This result suggests that the findings for $Os_3[P(OCH_3)_3]_x(CO)_{12-x}$ (x= 1-6) could be more general, at least within a related set of complexes. The often difficult task of assigning resonances in the ^{13}C NMR spectrum could be significantly aided by this type of analysis.

^{13}C NMR chemical shifts of various carbonyl groups (*) (ppm)

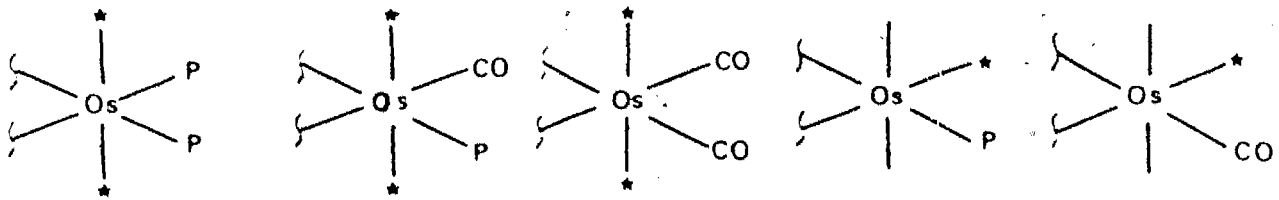

Compounds					
$Os_3[P(OCH_3)_3]_4(CO)_8$	203.4				
$Os_3[P(OCH_3)_3]_3(CO)_9$	199.7	194.1			
	199.2				
$Os_3[P(OCH_3)_3]_2(CO)_{10}$	200.2	195.1		181.9	
	198.8	194.1		180.8	
				178.7	
$Os_3[P(OCH_3)_3](CO)_{11}$		189.7		179.9	
$Os_3[P(OCH_3)_3]_2(CO)_9$		192.5	187.5	179.6	176.2
		191.7	186.7	178.7	175.0
				177.1	173.9
$Os_3[P(OCH_3)_3](CO)_{10}$		189.8	185.1	176.0	174.5
			184.2		172.9
					171.8
					170.8

Table 6.4 ^{13}C NMR chemical shifts of the carbonyl ligands in $Os_3[P(OCH_3)_3]_x(CO)_{12-x}$ (x= 1-6) in the slow exchange limit

^{13}C NMR chemical shifts of various carbonyl groups (*) (ppm)

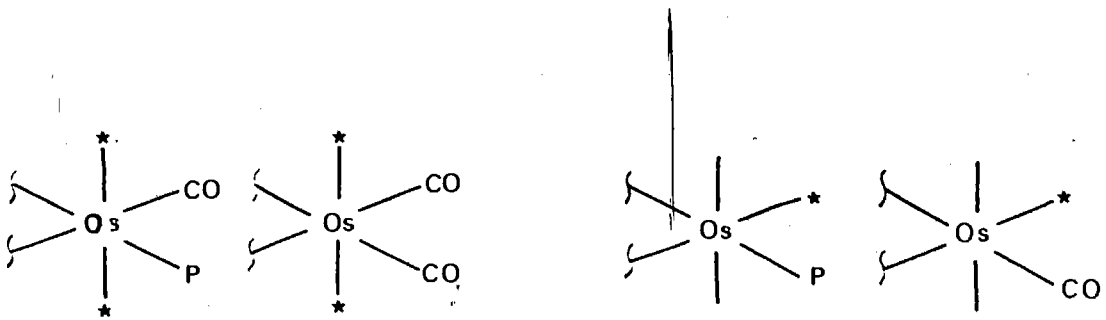

Compounds				
$Os_3[PEt_3](CO)_{11}$	194.1	186.3	176.8	178.8
		184.4		173.8
				172.8
				170.4
$Os_3[PEt_3]_2(CO)_{10}$	197.2	187.8	183.8	178.9
	196.2		180.9	174.2
$Os_3[PEt_3]_3(CO)_9$	199.4		186.4	

Table 6.5 ^{13}C NMR chemical shifts of the carbonyl ligands in $Os_3[PEt_3]_x(CO)_{12-x}$ (x= 1-3) in the slow exchange limit.

APPENDIX 1

On the following page is a plot of $^{31}P\{^{1}H\}$ NMR chemical shift versus temperature for one of the resonances of $Os_3[P(OCH_3)_3]_5(CO)_7$ in toluene. The plotted points (i.e. +) correspond to data taken at or near the slow exchange limit region. These points were then extrapolated to higher temperatures, where chemical exchange broadening precluded observation of the individual resonances. This is an example of the plots used extensively in chapter 6 to calculate weighted average chemical shifts in the fast exchange region.

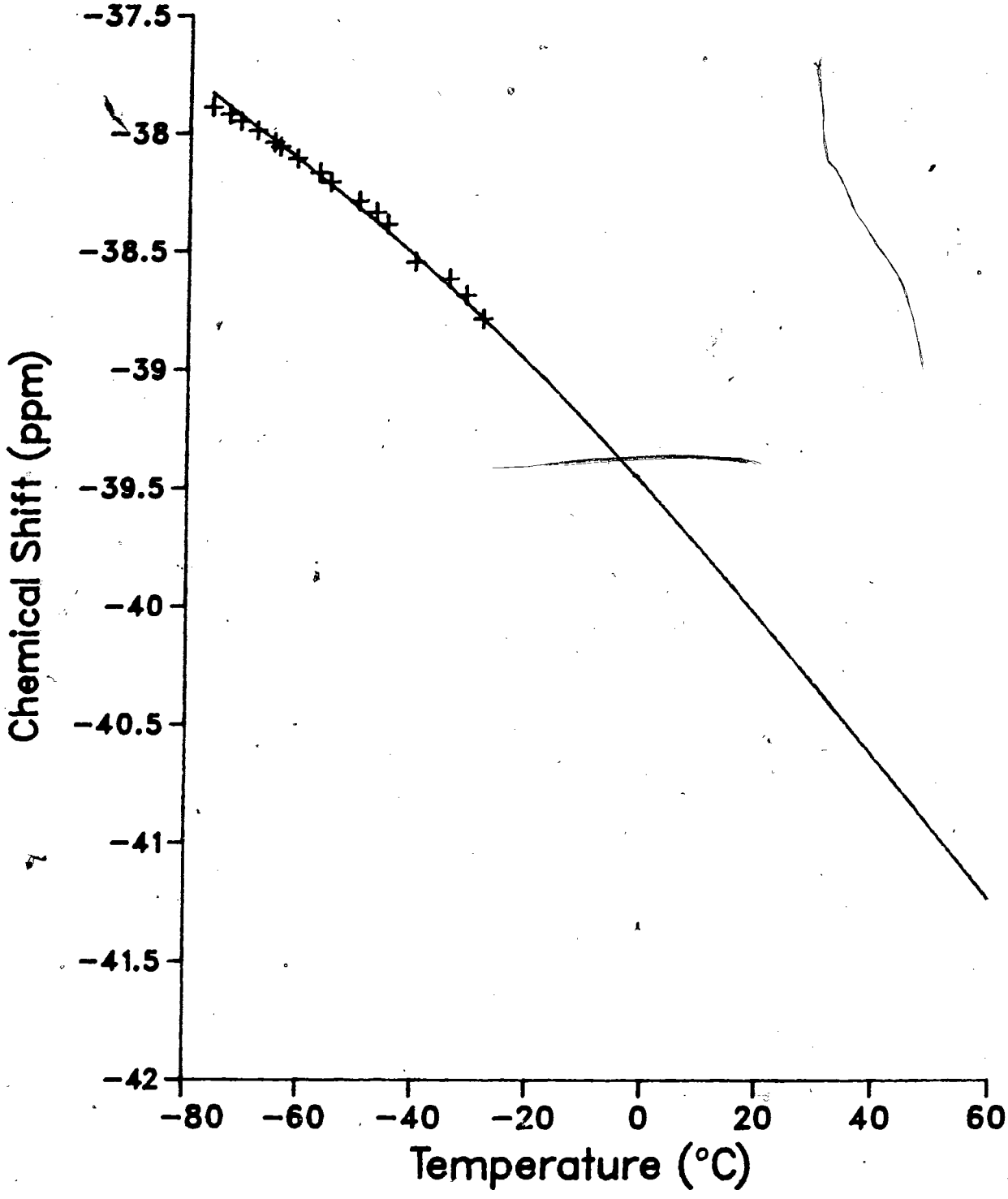

Appendix 1 A plot of $^{31}P\{^{1}H\}$ NMR chemical shift versus temperature for one of the resonances of $Os_3[P(OCH_3)_3]_5(CO)_7$.

APPENDIX 2: APPROXIMATIONS USED TO CALCULATE ACTIVATION PARAMETERS IN CHAPTERS 2 AND 6

Dynamic NMR spectroscopy deals with the effect of chemical exchange processes on NMR spectra. The most accurate method for obtaining the activation parameters associated with a chemical exchange (i.e. $\Delta G^{\ddagger}$, $\Delta H^{\ddagger}$, $\Delta S^{\ddagger}$) is a complete band shape analysis. The density matrix approach has become the most widely used method to calculate line shapes for chemically exchanging systems [173,174]. When these calculated line shapes are matched with the experimental spectra, a set of exchange rate constants at specific temperatures are obtained. The Eyring equation (in the form of equation 1) may then be used to calculate the activation parameters for the chemical exchange. An uncertainty in $\Delta G^{\ddagger}$ of ±0.04 kcal mol^{-1} (or less) may be achieved using this method [175].

$$\ln(k/T) = \Delta H^{\ddagger}/T - \Delta S^{\ddagger}/R + \ln(\kappa k_b/h) \qquad 1$$

In equation 1, k is the first order rate constant for the exchange, T is the temperature (°K), k_b is the Boltzmann constant, h is Planck's constant, and κ is the transmission coefficient. The transmission coefficient is the fraction of all reacting molecules reaching the transition state that proceed to deactivated product molecules. This coefficient is often taken as unity, although some authors use a value of 0.5 in cases where 2 equivalent transition states are separated by one or

more energy minima [176].

A complete band shape analysis yields a set of k versus T data and allows determination of both $\Delta H^{\ddagger}$ and $\Delta S^{\ddagger}$ for the exchange. One may also calculate a single k at some temperature T and use the Eyring equation (in the form of equation 2) to calculate a $\Delta G^{\ddagger}$ value for the exchange at that temperature T.

$$\Delta G^{\ddagger} = -RT\ln[(hk)(k_b T\kappa)^{-1}] \qquad 2$$

It may be shown that the standard deviation in $\Delta G^{\ddagger}$, as calculated from equation 2, is given by equation 3.

$$\Delta\Delta G^{\ddagger} = RT\{[\frac{\Delta T}{T}(\ln[k_b T/hk] + 1)]^2 + (\frac{\Delta k}{k})^2\}^{1/2} \qquad 3$$

In this equation, ΔT and Δk are the uncertainties in the temperature and the rate constant, respectively.

Rate constants at a single temperature may be determined by a variety of techniques. Calculating a line shape (e.g. density matrix approach) to match an experimental spectrum at a single temperature (T) gives k at T. This process is most accurate when an observed spectrum near coalescence is chosen; the calculated line shape often changes most rapidly in this region. The closeness of fit between the calculated and observed spectra can give added evidence for or against the mechanism on which the line shape was based.

Rate constants at a single temperature may also be found by approximate methods. One of these is based on differences in bandwidths. For a single Lorentzian line exhibiting broadening due to slow site exchange (i.e. negligible signal overlap), the following equation may be shown to hold [177].

$$W = 1/\pi(k + 1/T_2) \qquad 4$$

In equation 4 W is the width at half height for the signal in question (in Hz), k is the first-order rate constant for the site exchange, and T_2 is the effective transverse relaxation time. In the slow exchange limit, $k<<1/T_2$ and the bandwidth is dominated by the transverse relaxation time. As k becomes comparable to $1/T_2$ (i.e. as slow exchange begins to occur) the line starts to broaden. The difference in W for a line in the slow exchange limit at some temperature T and the same line undergoing slow exchange at some higher temperature T' (this difference is termed ΔW) gives k at T'. These values may be used to calculate $\Delta G^{\ddagger}$ from the Eyring equation (2) at T'.

This technique was used to calculate $\Delta G^{\ddagger}$ values for the fluxional processes occurring for the $Ru[P(OCH_3)_3]_4L$ derivatives; the results are tabulated in table 7.1. Some of these values were compared to the corresponding $\Delta G^{\ddagger}$ values calculated by a complete band shape analysis (see chapter 2 for results of these comparisons).

L	T' (°K)	ΔW (Hz)	k (sec^{-1})	$\Delta G^{\ddagger}$ (Kcal/mol)
$P(OCH_2)_3CCH_3$	159	10.2	32.0	8.0
$P(OC_2H_5)_3$	165	2.0	6.3	8.9
$P(OCH(CH_3)_2)_3$	163	6.7	21.0	8.4
$P(OC_6H_5)_3$	156	0.6	1.9	9.0
PF_3	150	7.1	22.2	7.7
$P(CH_3)_3$	229	4.5	14.1	12.1
$P(CH_3)_2C_6H_5$	191	1.4	4.4	10.5
$SbMe_3$	167	1.3	4.1	9.1

Table 7.1 $\Delta G^{\ddagger}$ values for the $Ru[P(OCH_3)_3]_4L$ derivatives calculated by the approximate methods discussed in appendix 2.

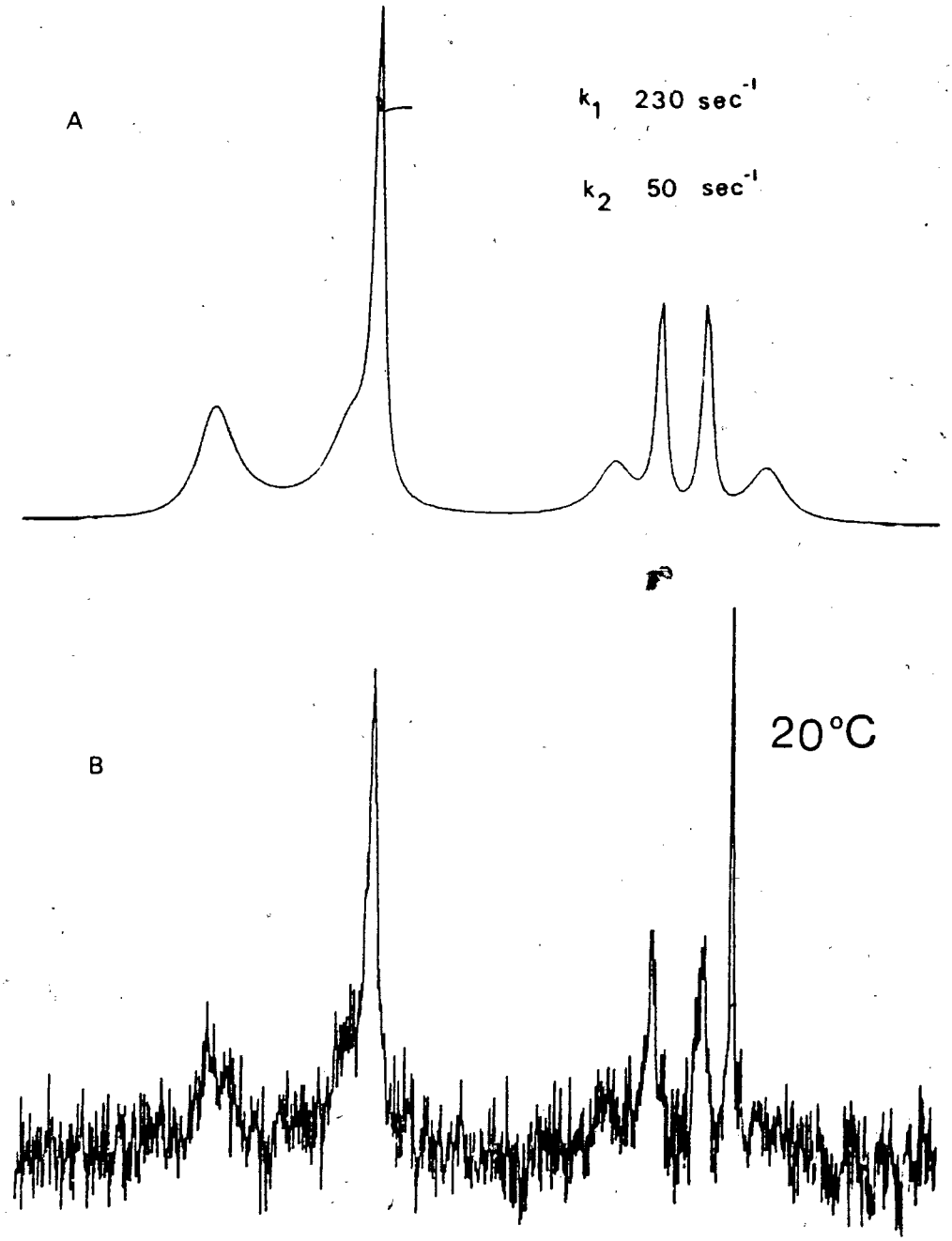

Figure 7.1 A ^{13}C NMR spectrum of $Os_3[P(OCH_3)_3](^{13}CO)_{11}$ (carbonyl region) (B) and a matching calculated spectrum (A) based on a pair of axial-equatorial merry-go-round processes (see figure 6.11 and discussion on page 288). The calculated and observed spectra are labeled with the rates and temperature, respectively.

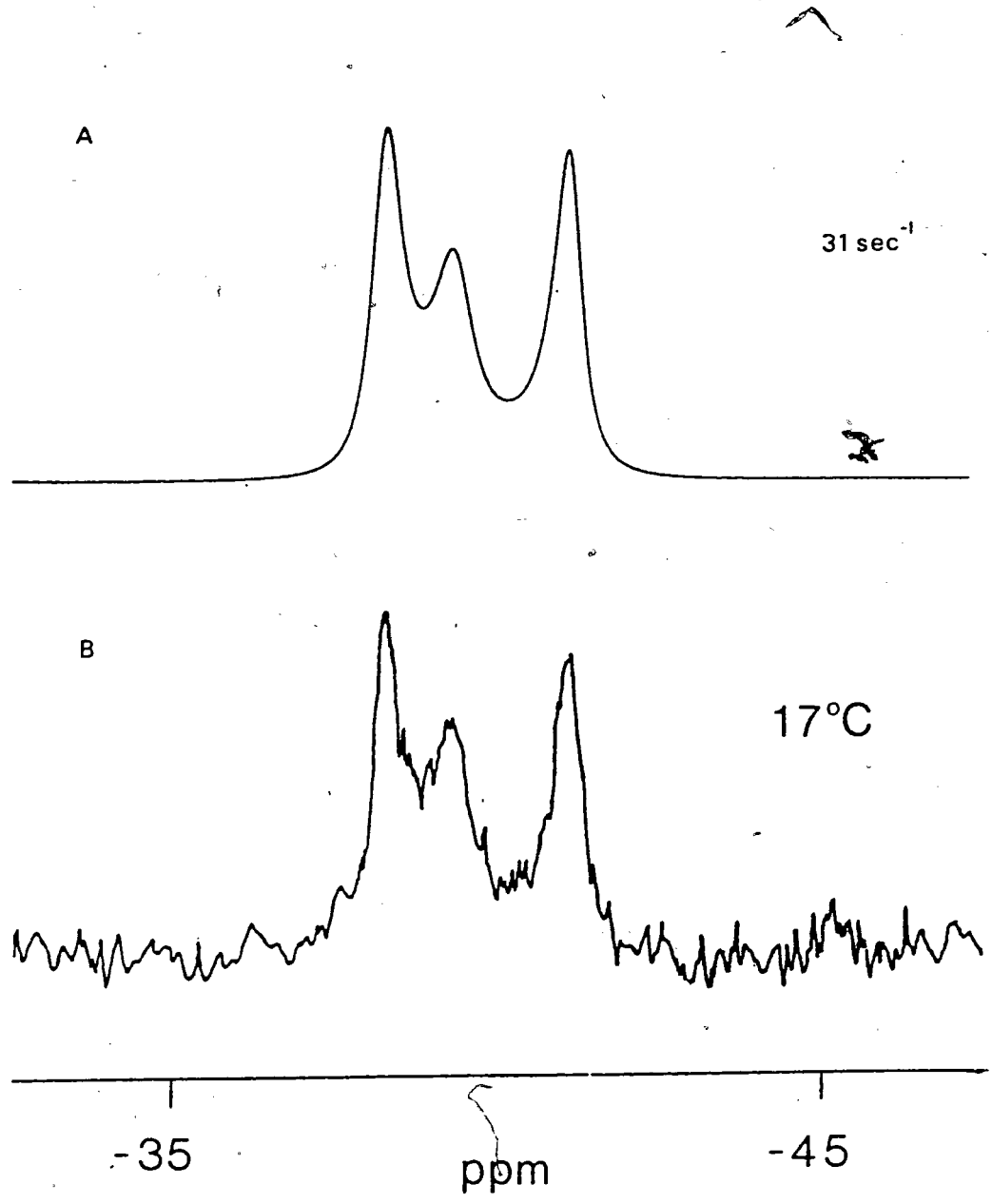

Figure 7.2 A $^{31}P\{^{1}H\}$ NMR spectrum of $Os_3[P(OCH_3)_3]_2(CO)_{10}$ (B) and a matching calculated spectrum based on a synchronous trigonal twist process (A). The calculated and observed spectra are labeled with the rate constant and temperature, respectively.

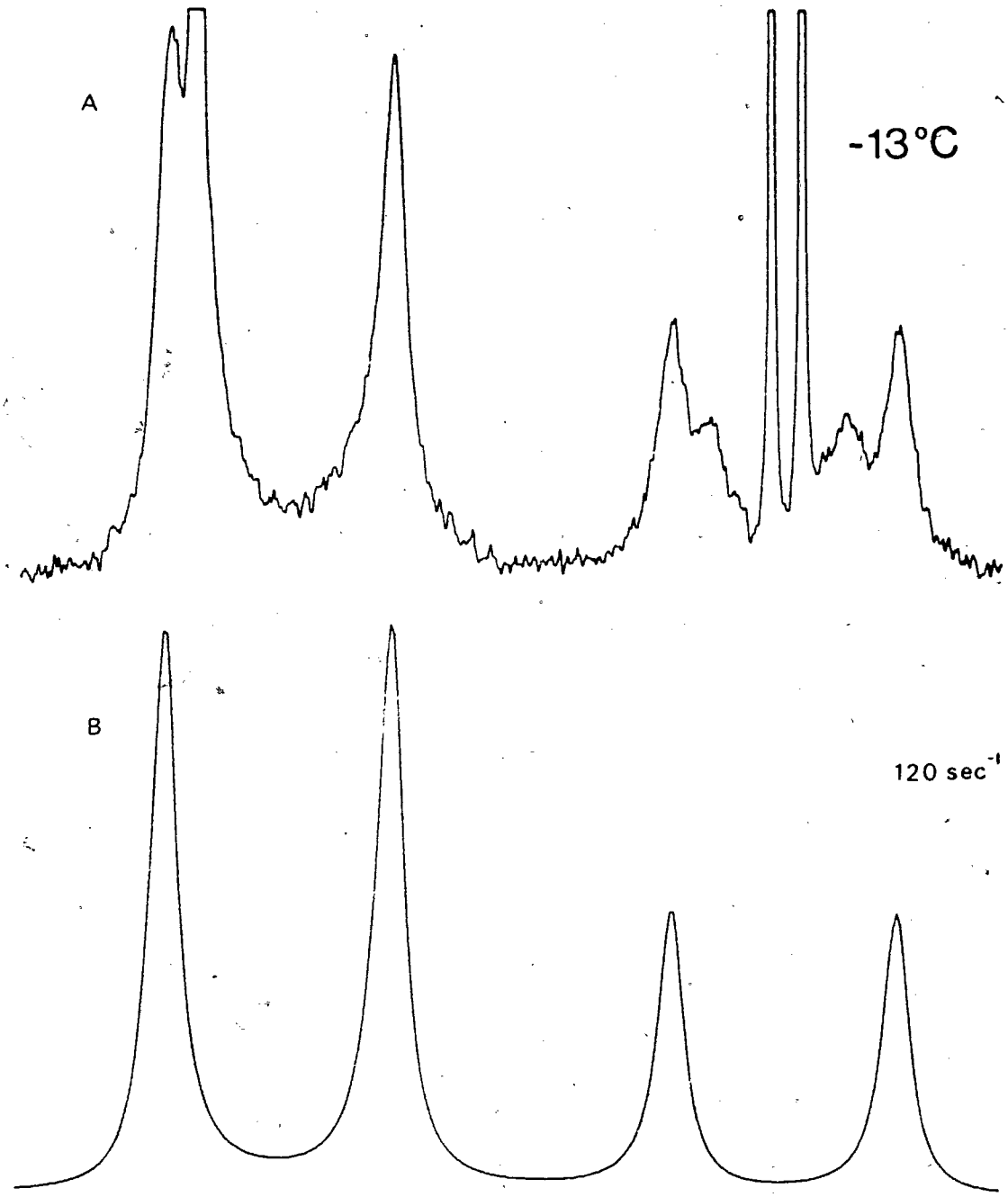

Figure 7.3 A ^{13}C NMR spectrum of $Os_3[P(OCH_3)_3]_2(^{13}CO)_{10}$ (carbonyl region) (B) and a matching calculated spectrum (A) based on an axial-equatorial merry-go-round process for isomer 6k (see chapter 6 for details). The calculated and observed spectra are labeled with the rate constant and temperature, respectively.

REFERENCES

1. Collman, J. P.; Hegedus, L. S. "Principles and Applications of Organotransition Metal Chemistry"; University Science Books: California, 1980.

2. Alyea, E. C.; Meek, D. W.; Eds. "Catalytic Aspects of Metal Phosphine Complexes", Advances in Chemistry Series (196); A.C.S.: New York, 1982.

3. Pignolet; L. H., Ed. "Homogeneous Catalysis with Metal Phosphine Complexes"; Plenum: New York, 1983.

4. Pomeroy, R. K.; Alex, R. F. *J. Chem. Soc., Chem. Commun.* 1980, 1114.

5. Alex, R. F.; Pomeroy, R. K. *Organometallics* 1982, *1*, 453.

6. English, A.; Ittel, S.; Tolman, C. A.; Meakin, P.; Jesson, J. *J. Am. Chem. Soc.* 1977, *99*, 117.

7. Cotton, F. A.; Wilkinson, G. "Advanced Inorganic Chemistry"; John Wiley and Sons: New York, 1980; pp 1217-1221.

8. Cotton, F. A.; Wilkinson, G. "Advanced Inorganic Chemistry"; John Wiley and Sons: New York, 1980; pp 87-89.

9. Orpen, A. G.; Connelly, N. G. *J. Chem. Soc., Chem. Commun.* 1985, 1310 and references therein.

10. Tolman, C. A. *J. Am. Chem. Soc.* 1970, *92*, 2956.

11. Tolman, C. A. *Chem. Rev.* 1977, *77*, 313. (a) and references therein.

12. Bartik, T.; Himmler, T.; Schulte, H. G.; Seevogel, K. *J. Organomet. Chem.* 1984, *272*, 29.

13. Mathieu, R.; Poilblanc, R. *Inorg. Chem.* 1972, *11*, 1858.

14. Choi, H.; Muetterties, E. L. *J. Am. Chem. Soc.* 1982, *104*, 153.

15. Muetterties, E. L.; Kirner, J.; Evans, W. J.; Watson, P.; Abdel-Meguid, S.; Tavanaiepour, I.; Day, V. W. *Proc. Natl. Acad. Aci. USA* 1978, *75*, 1056.

16. Choi, H.; Gavin, R.; Muetterties, E. L. *J. Chem. Soc.*,

Chem. Commun. 1979, 1085.

17. Muetterties, E. L.; Bleeke, J.; Yang, Z.-Y.; Day, V. W. *J. Am. Chem. Soc.* 1982, *104*, 2940.

18. Rakowski, M. C.; Muetterties, E. L. *J. Am. Chem. Soc.* 1977, *99*, 739.

19. Muetterties, E. L.; Hirsekorn, F. J. *J. Am. Chem. Soc.* 1974, *96*, 7920.

20. Van-Catledge, F. A.; Ittel, S.; Tolman, C. A.; Jesson, J. *J. Chem. Soc., Chem. Commun.* 1980, 254.

21. Ittel, S.; Van-Catledge, F. A.; Tolman, C. A. *Inorg. Chem.* 1985, *24*, 62.

22. Tolman, C. A.; Yarbrough, L.; Verkade, J. *Inorg. Chem.* 1977, *16*, 479.

23. Mathieu, R.; Nixon, J. *J. Chem. Soc., Chem. Commun.* 1974, 147.

24. Robinson, S. D. *J. Chem. Soc., Chem. Commun.* 1968, 521.

25. Choi, H. W.; Muetterties, E. L. *J. Am. Chem. Soc.* 1982, *104*, 153.

25a. Citations in the previous reference.

26. Harris, T. V.; Rathke, J. W.; Muetterties, E. L. *J. Am. Chem. Soc.* 1978, *100*, 6966.

27. Zecchin, S.; Schiavon, G.; Zotti, G.; Rilloni, G. *Inorg. Chim. Acta.* 1979, *34*, L267.

28. Zecchin, S.; Schiavon, G.; Zotti, G.; Rilloni, G. *Inorg. Chim. Acta.* 1976, *20*, L1.

29. George, G. N.; Klein, S.; Nixon, J. F. *Chem. Phys. Letters* 1984, *108*, 627.

30. Malatesta, L.; Cenini, S. "Zerovalent Compounds of the Metals"; Academic Press: London, 1974.

31. Kuran, W.; Musco, A. *J. Organomet. Chem.* 1972 *40*, C47.

32. Drago, R. S. "Physical Methods in Chemistry"; Saunders: Philadelphia, 1977; pp 265-267.

33. Jesson, J. P.; Meakin, P. *J. Am. Chem. Soc.* 1973 *95*, 1344.

34. Meakin, P.; Jesson, J. P. *J. Am. Chem. Soc.* 1973, *95*, 7272.

35. Meakin, P.; Jesson, J. P. *J. Am. Chem. Soc.* 1974, *96*, 5751.

36. Jesson, J. P.; Meakin, P. *J. Am. Chem. Soc.* 1974, *96*, 5760.

37. Berry, R. S. *J. Chem. Phys.* 1960, *32*, 933.

38. Citation 30 of the following reference.

39. Hoffmann, R.; Howell, J. M.; Muetterties, E. L. *J. Am. Chem. Soc.* 1972, *94*, 3047.

40. Muetterties, E. L.; Guggenberger, L. J. *J. Am. Chem. Soc.* 1974, *96*, 1748.

41. Kuhn, S.; Von Philipsborn, W. *J. Organomet. Chem.* 1977, *127*, C59.

42. Ittel, S. D.; Van-Catledge, F. A.; Jesson, J. P. *J. Am. Chem. Soc.* 1979, *101*, 3874.

43. Al-Ohaly, A.-R.; Nixon, J. F. *J. Organomet. Chem.* 1980, *202*, 297.

44. Kruczynski, L.; Martin, J. L.; Takats, J. *J. Organomet. Chem.* 1974, *80*, C9.

45. Whitesides, T. H.; Budnick, R. A. *Inorg. Chem.* 1975, *14*, 664.

46. Mills, O. S.; Robinson, G. *Acta Cryst.* 1963, *16*, 758.

47. Cotton, F. A.; Day, V. W.; Frenz, B. A.; Hardcastle, K.I.; Troup, J. M. *J. Am. Chem. Soc.* 1973, *95*, 4522.

48. Kruczynski, L.; Takats, J. *Inorg. Chem.* 1976, *15*, 3140.

49. Hails, M. J.; Mann, B. E.; Spencer, C. M. *J. Chem. Soc., Dalton Trans.* 1985, 693.

50. Alex, R. F., unpublished results from an undergraduate research project.

51. Tolman, C. A.; Seidel, W. C.; Gosser, L. W. *J. Am.*

Chem. Soc. 1974, *96*, 53.

52. Alex, R. F., unpublished results.

53. Bochmann, K.; Von Philipsborn, W. *Org. Magn. Res.* 1976, *8*, 648.

54. Pregosin, P.; Kunz, R. "^{31}P and ^{13}C NMR of Transition Metal-Phosphine Complexes"; Springer-Verlag: New York, 1979; pp 114-125.

55. Mann, B. E.; Masters, C.; Shaw, B. L.; Slade, R. M.; Stainbank, R.E. *Inorg. Nucl. Chem. Letters* 1971, *7*, 881.

55a. Sandstrom, J. "Dynamic NMR Spectroscopy"; Academic Press: New York, 1982; p 18.

56. Emsley, J. W.; Feeney, J.; Sutcliffe, L. "High Resolution Nuclear Magnetic Resonance Spectroscopy", vol. 1; Pergamon Press: Oxford, 1966; pp 365-370.

57. Marsh, R. A.; Howard, J.; Woodward, P. *J. Chem. Soc., Dalton Trans.* 1973, 778.

58. Cobbledick, R. E.; Einstein, F. W. B.; Pomeroy, R. K.; Spetch, E. R. *J. Organomet. Chem.* 1980, *195*, 77.

58a. Citations in the previous reference.

59. Johnson, B. F. G.; Raithby, P. R.; Zuccaro, C. *J. Chem. Soc., Dalton Trans.* 1980, 99.

60. Bottriel, M.; Davis, R.; Goddard, R.; Green, M.; Hughes, R. P.; Lewis, B.; Woodward, P. *J. Chem. Soc., Dalton Trans.* 1977, 1252.

61. Rossi, A. R.; Hoffmann, R. *Inorg. Chem.* 1975, *14*, 365.

62. Burdett, J. K. *Inorg. Chem.* 1976, *15*, 212.

63. Shustorovich, E. *Inorg. Chem.* 1978, *17*, 2648.

64. Cowley, A. H.; Lattman, M.; Montag, R. A.; Verkade, J. G. *Inorg. Chem.* 1984, *23*, 3378.

65. Milbrath, D. S.; Verkade, J. G. *J. Am. Chem. Soc.* 1977, *99*, 6607.

66. Lichtenberger, D. L.; Brown, T. L. *J. Am. Chem. Soc.* 1977, *99*, 8187.

67. Demuynck, J.; Strich, A.; Veillard, A. *Nouv. J. Chim.* 1977, *1*, 217.

68. Johnson, B. F. G.; Lewis, J.; Kilty, P. A.; *J. Chem. Soc. A* 1968, 2859.

69. Mantovani, A.; Cenini, S. *Inorg. Synth.* 1976, *16*, 47.

70. Rushman, P.; van Buuren, G. N.; Shiralian, M.; Pomeroy, R. K. *Organometallics* 1983, *2*, 693.

71. Heitsch, C. W.; Verkade, J. G. *Inorg. Chem.* 1962, *1*, 392.

72. Dickert, F. L.; Hellmann, S. W. *Anal. Chem.* 1980, *52*, 996.

73. Based on the comparison of this IR ν(CO) data to that observed for $Ru[P(OCH_3)_3](CO)_4$ [58,92] and $Ru[P(OCH_3)_3]_2(CO)_3$ [5].

74. Couch, D. A.; Robinson, S. D. *Inorg. Chim. Acta* 1974, *9*, 39.

75. Ittel, S. D.; English, A. D.; Tolman, C. A.; Jesson, J. P. *Inorg. Chim. Acta* 1979, *33*, 101.

76. Cole-Hamilton, D. J.; Wilkinson, G. *J. Chem. Soc., Chem Commun.* 1977, 797.

77. Anderson, R. A.; Jones, R. A.; Wilkinson, G. *J. Chem. Soc., Dalton Trans.* 1978, 446.

78. Barnard, C. F. J.; Daniels, J. A.; Mawby, R. J. *J. Chem. Soc., Dalton Trans.* 1976, 961.

79. Kramer, A.; Labinger, S.; Bradley, J.; Osborn, J.J. *Am. Chem. Soc.* 1974, *96*, 7145.

80. Labinger, J. A.; Osborn, J. A.; Colville, N. J. *Inorg. Chem.* 1980, *19*, 3236.

81. Albertin, G.; Bordignon, E. *Inorg. Chem.* 1984, *23*, 3822.

82. Emsley, J. W.; Feeney, J.; Sutcliffe, L. "High Resolution Nuclear Magnetic Resonance Spectroscopy", vol. 2; Pergamon Press: Oxford, 1966; pp 946.

83. Brown, S. D.; Colquhoun, I. J.; McFarlane, W.; Murray, M.; Salter, I. D.; Sik, V. *J. Chem. Soc., Chem. Commun.*

1986, 53.

84. Werner, H.; Gotzig, J. *Organometallics* **1983**, *2*, 547.

85. Bent, H. A. *Chem. Rev.* **1961**, *61*, 275.

86. Pregosin, P.; Kunz, R. "^{31}P and ^{13}C NMR of Transition Metal-Phosphine Complexes"; Springer-Verlag: New York, **1979**; pp 16-19.

87. Krentz, R.; Pomeroy, R. K. *Incrg. Chem.* **1985**, *24*, 2976.

88. Pregosin, P.; Kunz, R. "^{31}P and ^{13}C NMR of Transition Metal-Phosphine Complexes"; Springer-Verlag: New York, **1979**; pp 126-127.

89. Pregosin, P.; Kunz, R. "^{31}P and ^{13}C NMR of Transition Metal-Phosphine Complexes"; Springer-Verlag: New York, **1979**; pp 47-55 and references therein.

90. Emsley, J. W.; Feeney, J.; Sutcliffe, L. "High Resolution Nuclear Magnetic Resonance Spectroscopy", vol. 2; Pergamon Press: Oxford, **1966**; pp 1054-1061 and references therin.

91. Mark, V. *Mech. Mol. Migr.* **1969**, *2*, 319.

91a. Collman, J. P.; Hegedus, L. S. "Principles and Applications of Organotransition Metal Chemistry"; University Science Books: USA, **1980**; pp 210-211.

92. Martin, L. R.; Einstein, F. W. B.; Pomeroy, R. K. *Inorg. Chem.* **1985**, *24*, 2777.

93. Adams, D. M. "Metal-Ligand and Related Vibrations"; Edward Arnold: London, **1967**; pp 105-106.

94. Alex, R. F., unpublished results.

95. Grim, S. O.; Wheatland, D. A.; McFarlane, W.; *J. Am. Chem. Soc.* **1967**, *89*, 5573.

96. Genderow, D. *Acta. Crystallogr., Sect. B* **1974**, *B30*, 2798.

97. Norton, J. R.; Carter, W. J.; Kelland, J. W.; Okrasinski, S. J. *Adv. Chem. Ser.* **1978**, *167*, 13.

98. Bruce, M. I.: Cooke, M.; Green, M.; Westlake, D. J. *J. Chem. Soc. A* **1969**, 987.

99. Deeming, A. J.; Johnson, B. F. G.; Lewis, J. *J. Chem.*

Soc. A 1970, 897.

100. Clark, R. J. H.; Bradford, C. W.; Nyholm, R. S.; Bronswijk, W. V. *J. Chem. Soc. A* 1970, 2889.

101. Johnson, B. F. G.; Lewis, J.; Pippard, D. A. *J. Chem. Soc., Dalton Trans.* 1981, 407.

102. Deeming, A. J.; Johnson, B. F. G.; Lewis, J. *J. Organomet. Chem.* 1969, *17*, P40.

103. Bruce, M. I.; Kehoe, D. C.; Matisons, J. G., Nicholson, B. K.; Rieger, P. I.; Williams, M. L. *J. Chem. Soc., Chem. Commun.* 1982, 442.

104. Deeming, A. J.; Underhill, M. *J. Chem. Soc., Dalton Trans.* 1973, 2727.

105. Johnson, B. F. G.; Lewis, J.; Pippard, D. *J. Organomet. Chem.* 1978, *145*, C4.

106. Tachikawa, M.; Shapley, J. R. *J. Organomet. Chem.* 1977, *124*, C19.

107. Deeming, A. J.; Donovan-Mtunzi, S.; Kabir, S. E. *J. Organomet. Chem.* 1985, *281*, C43.

108. Deeming, A. J.; Donovan-Mtunzi, S.; Kabir, S. E.; Manning, P. J. *J. Chem. Soc., Dalton Trans.* 1985, 1037.

109. Benfield, R. E.; Johnson, B. F. G.; Raithby, P. R.; Sheldrick, G. M. *Acta Cryst.* 1978, *B34*, 666.

110. Bruce, M. I.; Matisons, J. G.; Skelton, B. W.; White, A. H. *J. Chem. Soc., Dalton Trans.* 1983, 2375.

111. Johnson, B. F. G.; Lewis, J.; Reichert, B. E.; Schorpp, K. T. *J. Chem. Soc., Dalton Trans.* 1976, 1403.

112. Alex, R. F.; Pomeroy, R. K. *J. Organomet. Chem.* 1985, *284*, 379.

113. Bradford. C. W.; Nyholm, R. S. *J. Chem. Soc., Chem. Commun.* 1967, 384.

114. Cullen, W. R.; Crow, J. P. *Inorg. Chem.* 1971, *10*, 1529.

115. Bruce, M. I.; Matisons, J. G.; Nicholson, B. K. *J. Organomet. Chem.* 1983, *247*, 321.

116. Bruce, M. I.; Shaw, G.; Stone, F. G. A. *J. Chem. Soc.,*

Dalton Trans. **1972**, 2094.

117. Bruce, M. I.; Matisons, J. G.; Patrick, J. M.; White, A. H.; Willis, A. C. *J. Chem. Soc., Dalton Trans.* **1985**, 1223.

118. Alex, R. F., unpublished results.

119. Kumar, R. *J. Organomet. Chem.* **1977**, *136*, 235.

120. Johnson, B. F. G. *Inorg. Chim. Acta* **1986**, *115*, L39.

120a. Citations in the previous reference.

121. Candin, J.; Shortland, A. C. *J. Organomet. Chem.* **1969**, *16*, 289.

122. Poe, A. J.; Twigg, M. V. *J. Chem. Soc., Dalton Trans.* **1974**, 1860.

123. Poe, A. J.; Twigg, M. V. *Inorg. Chem.* **1974**, *13*, 2982.

124. Brodie, N.; Poe, A. J.; Sekhar, V. *J. Chem. Soc., Dalton Trans.* **1985**, 1090.

125. Johnson, B. F. G.; Lewis, J.; Pippard, D. A. *J. Chem. Soc., Dalton Trans.* **1981**, 407.

126. Tripathi, J. B.; Bigorgne, M. *J. Organomet. Chem.* **1967**, *9*, 307.

127. Ginderow, D. *Acta Crystallogr. Sect. B* **1974**, *B30*, 2798.

128. Reckziegel, A.; Bigorgne, M. *J. Organomet. Chem.* **1965**, *3*, 341.

129. Stalick, J. K.; Ibers, J. A. *Inorg. Chem.* **1969**, *8*, 419.

130. Cotton, F. A.; Parish, R. V. *J. Chem. Soc.* **1960**, 1440.

131. Couch, D. A.; Robinson, S. D. *Inorg. Chim. Acta* **1974**, *9*, 39.

132. Muetterties, E. L., Ed. "Transition Metal Hydrides"; Marcel Dekker: New York, 1971; p 85.

133. Bruce, M. I.; Nicholson, B. K.; White, A. H. *J. Organomet. Chem.* **1982**, *240*, C33.

134. Rivera, A. V.; Sheldrick, G. M. *Acta Cryst.* 1978, *B34*, 3372.

135. Adams, R. D.; Golembeski, N. M. *J. Am. Chem. Soc.* 1979, *101*, 2579.

136. Bellard, S.; Raithby, P. R. *Acta Cryst.* 1980, *B36*, 705.

137. Churchill, M. R.; DeBoer, B. G. *Inorg. Chem.* 1977, *16*, 876. Corey, E. R.; Dahl, L. F. *Inorg. Chem.* 1962, *1*, 521.

138. Tyler, D. R.; Levenson, R. A.; Gray, H. B. *J. Am. Chem. Soc.* 1978, *100*, 7888.

139. Tyler, D. R.; Altobelli, M.; Gray, H. B. *J. Am. Chem. Soc.* 1980, *102*, 3022.

140. Band, E.; Muetterties, E. L. *Chem. Rev.* 1978, 639.

141. Forster, A.; Johnson, B. F. G.; Lewis, J.; Matheson, T. W.; Robinson, B. H.; Jackson, W. G. *J. Chem. Soc., Chem. Commun.* 1974, 1042.

142. Aime, S.; Gambino, D.; Milone, L.; Sappa, E.; Rosenberg, E. *Inorg. Chim. Acta* 1975, *15*, 53.

143. Cotton, F. A.; Troup, J. M. *J. Am. Chem. Soc.* 1974, *96*, 4155.

144. Cotton, F. A.; Hunter, D. L.; *Inorg. Chim. Acta* 1974, *11*, L9.

145. Koridze, A. A.; Kizas, O. A.; Astakhova, N.M.; Petrovskii, P. V.; Grishin, Y. K. *J. Chem. Soc., Chem. Commun.* 1981, 853.

146. Tachikawa, M.; Richter, S. I.; Shapley, J. R. *J. Organomet. Chem.* 1977, *128*, C9.

147. Cotton, F. A.; Hanson, B. E.; Jameison, J. D. *J. Am. Chem. Soc.* 1977, *99*, 6588.

148. Bryan, E. G.; Johnson, B. F. G.; Lewis, J. *J. Chem. Soc., Dalton Trans.* 1977, 144.

149. Aime, S.; Milone, L. *Progress in NMR Spectroscopy* 1977, *11*, 183.

150. Muetterties, E. L. *Tetrahedron* 1974, *30*, 1595.

151. Bryan, E. G.; Forster, A.; Johnson, B. F. G.; Lewis, J.; Matheson, T. W. *J. Chem. Soc., Dalton Trans.* **1978**, 196.

152. Cotton, F. A.; Hanson, B. E. *Inorg. Chem.* **1977**, *16*, 2820.

153. Koube, J. K.; Muetterties, E. L.; Thompson, M. R.; Day, V. W. *Organometallics* **1983**, *2*, 1065.

154. Johnson, B. F. G.; Lewis, J.; Mace, J. M.; Raithby, P. R.; Stevens, R. E.; Gladfelter, W. L. *Inorg. Chem.* **1984**, *23*, 1600.

155. Eady, C. R.; Jackson, W. G.; Johnson, B. F. G.; Lewis, J.; Matheson, T. W. *J. Chem. Soc., Chem. Commun.* **1975**, 958.

156. Aime, S.; Osella, D.; Milone, L.; Rosenberg, E. *J. Organomet. Chem.* **1981**, *213*, 207.

157. Keister, J. B.; Shapley, J. R. *Inorg. Chem.* **1982**, *21*, 3304.

158. Milone, L.; Aime, S.; Randall, E. W.; Rosenberg, E. *J. Chem. Soc., Chem. Commun.* **1975**, 452.

159. Geoffroy, G. L. *Accts. Chem. Res.* **1980**, *13*, 469.

160. Harris, R. K. "Nuclear Magnetic Resonance Spectroscopy", Pitman: Belfast, 1983; pp 88-89. Brevard, C.; Granger, P. "Handbook of High Resolution Multinuclear NMR"; John Wiley: New York, 1961; p 16. Lallemand, J.-Y.; Soulie, J.; Chottard, J.-C. *J. Chem. Soc., Chem. Commun.* **1980**, 436.

161. Yasufuku, K.; Yamazaki, H. *J. Organomet. Chem.* **1972**, *38*, 367.

162. Hersh, W. H.; Bergman, R. G. *J. Am. Chem. Soc.* **1981**, *103*, 6992.

163. Consider the preparation of $^{187}Os_3[P(OCH_3)_3]_x(CO)_{12-x}$ (x= 1-6) from $^{187}Os_3(CO)_{12}$ [145] by the techniques in this thesis. The retention or averaging of the ^{187}Os-^{31}P coupling constant under conditions of fast intramolecular exchange (as monitored via ^{187}Os NMR spectroscopy) would allow a definitive answer to the question of bridging phosphite intermediates for these complexes.

164. Pregosin, P.; Kunz, R. "^{31}P and ^{13}C NMR of Transition Metal-Phosphine Complexes"; Springer-Verlag: New York, 1979; p 28 and references therin.

165. Mays, M. J.; Gavens, R. D. *J. Chem. Soc., Dalton Trans.* **1980**, 911.

166. Mays, M. J.; Gavens, R. D. *J. Organomet. Chem.* **1977**, *124*, C37.

167. Wei, C. H.; Dahl, L. F. *J. Am. Chem. Soc.* **1969**, *91*, 1351.

168. Dahm, D. J.; Jacobson, R. A. *J. Am. Chem. Soc.* **1968**, *90*, 5106.

169. Estimated from data in references [141,147].

170. Mason, R.; Rae, A. I. *J. Chem. Soc. A* **1968**, 778.

171. Forbes, E. J.; Goodhand, N.; Jones, D. L.; Hamor, T. A. *J. Organomet. Chem.* **1979**, *182*, 143.

172. Benfield, R. E.; Gavens, P. D.; Johnson, B. F. G.; Mays, M. J.; Aime, S.; Milone, L.; Osella, D. *J. CHem. Soc., Dalton Trans.* **1981**, 1535.

173. Alexander, S. *J. Chem. Phys.* **1962**, *37*, 967,974.

174. Kaplan, J. I.; Fraenkel, G. "NMR of Chemically Exchanging Systems"; Academic Press: New York, 1980; pp 9-26.

175. Sandstrom, J. "Dynamic NMR Spectroscopy"; Academic Press: New York, 1982; p 97.

176. Sandstrom, J. "Dynamic NMR Spectroscopy"; Academic Press: New York, 1982; pp 93-94.

177. Sandstrom, J. "Dynamic NMR Spectroscopy"; Academic Press: New York, 1982; pp 16-17.